Institut für Nutzpflanzenwissenschaften und Ressourcenschutz

Enhancing Nitrogen Fertilisation Efficiency by Developing Novel Nitrification Inhibitors for a Greener Agriculture

Dissertation

zur Erlangung des Grades

Doctor of Philosophy (Ph.D.)

der Landwirtschaftlichen Fakultät
der Rheinischen Friedrich-Wilhelms-Universität Bonn

von
Sibel Cansu Yildirim
aus
Neunkirchen (Saar)

Bonn 2024

Referent: Prof. Dr. Nicolas Brüggemann

Korreferentin: Prof. Dr. Claudia Knief

Korreferentin: Prof. Dr. Uta Wille

Tag der mündlichen Prüfung: 12.10.2023

Angefertigt mit Genehmigung der Landwirtschaftlichen Fakultät der Universität Bonn

Enhancing Nitrogen Fertilisation Efficiency by Developing Novel Nitrification Inhibitors for a Greener Agriculture

Sibel Cansu Yildirim

ORCID: 0000-0002-1208-1210

Doctor of Philosophy

May 2023

Faculty of Science

School of Chemistry

Submitted in total fulfilment for the jointly awarded degree of Doctor of Philosophy at the University of Melbourne and the University of Bonn

Zusammenfassung

Die Nitrifikation ist ein biochemischer Prozess, der im Boden von Nitrifizierern durchgefuehrt wird. Waehrend der Nitrifikation wird Ammonium (NH_4^+) zu Nitrit (NO_2^-) und dann zu Nitrat (NO_3^-) oxidiert. Auf einem landwirtschaftlichen Feld, wo die natürlichen Ressourcen aufgrund häufiger Ernten erschöpft sind, liefern Böden nicht ausreichend N in einer pflanzenverfügbaren Form (Mineral-N, wie Nitrat (NO_3^-) und Ammonium (NH_4^+)). N ist daher ein limitierter Nährstoff und wird in enormen Mengen als N-Dünger in den Boden eingefuehrt. Während die Applikatiosnmenge an N-Dünger in 1970 noch bei 31,8 Tg lag, werden heute fast 120 Tg N in den Boden eingeführt. Aufgrund der parallel ablaufenden Nitrifikation, besteht leider keine direkte Korrelation zwischen der N-Düngungsmenge und dem Ernteertrag. Nitrifikation kann zu N-Düngerverlusten von bis zu 80% führen. Per Definition handelt es sich bei der Nitrifikation um eine Redox-Kaskade von der höchst oxidierten Form von N (NH_3) zur höchst reduzierten Form von N (NO_3^-). Die in diesem Mechanismus freigesetzten acht Elektronen liefern essentielle Energie für Bakterien und Archaea, die mit den Enzymen ausgestattet sind, um diese Reaktion durchzuführen. Die Landwirtschaft steht seit über 50 Jahren vor der Herausforderung der Überdüngung des Bodens, um den Ernteertrag sicherzustellen. Übermäßige N-Düngung ist nicht nur wirtschaftlich nicht nachhaltig, sondern führt auch zu verschiedenen Umweltproblemen. Zur Einschränkung der Nitrifikation werden synthetische Nitrifikationsinhibitoren (SNIs) über die gemeinsame Formulierung von N-Düngemitteln in den Boden eingebracht. SNIs hemmen das mikrobielle Enzym, das für die N-Umwandlung verantwortlich ist, Ammoniak-Monooxygenase (AMO), das in ammoniumoxidierenden Bakterien (AOB) und Archaea (AOA) konserviert ist und den initialen und geschwindigkeitsbestimmenden Schritt der Nitrifikation durchführt. Obwohl kommerzielle SNIs seit den 1970er Jahren auf dem Markt sind, bleibt die Stickstoffnutzungseffizienz weltweit bei 50%, aufgrund ihrer unvorhersehbaren und unzuverlässigen Leistung im Boden. Interessanterweise ist der Hemmungsmechanismus kommerzieller SNIs noch nicht vollständig verstanden. Im Rahmen dieser Doktorarbeit wurden biochemische Parameter von kommerziellen SNIs bestimmt. Darueber hinaus wurden neue SNIS synthetisiert und auf Effizienz getestet.

Abstract

Nitrogen (N) is used as a fertiliser for its essential role in building biomolecules, such as amino acids, porphyrins and nucleic acids, which directly promote plant growth.[1] Better nutrition leads to a better crop yield; this has been a central dogma in agricultural science for more than 150 years.[2] In an agricultural field, where natural resources are depleted due to frequent harvests, soils do not provide naturally sufficient N in a plant-available form (mineral-N, such as nitrate (NO_3^-) and ammonium (NH_4^+)). [3] N is, therefore, a limiting nutrient and is added in an enormous amount into the soil as N fertilisers. Whilst the application rate of N fertiliser was 31.8 Tg back in 1970,[4], today, almost 120 Tg of N is introduced into the soil.[5] Unfortunately, there is no direct correlation between N fertilisation rate and crop yield due to a competing N uptake mechanism by soil organisms known as nitrification. [6] Nitrification can lead to N fertiliser losses of up to 80%.[7] By definition, it is a redox cascade from the highest reduced form of N (NH_3) to the highest oxidised form of N (NO_3^-). The eight electrons released in the mechanism provide essential energy for bacteria and archaea equipped with the enzymes to perform this reaction.[8] Agriculture has been facing the challenge of over-fertilising soil to ensure crop yield for over 50 years now.[6] Not only is excessive N fertilisation not economically impactful, but N fertilisation also hosts various environmental problems. [9] Especially in heavily industrialised and densely populated areas, the high N application rate in soils has polluted the atmosphere with ammonia (NH_3) and nitrous oxide (N_2O), a greenhouse gas (GHG) with a warming potential approximately 300 times higher than carbon dioxide.[6]

To control microbial conversion, synthetic nitrification inhibitors (SNIs) are introduced *via* co-formulation of N fertilisers. SNIs inhibit the microbial enzyme responsible for the N conversion, namely ammonia monooxygenase (AMO) conserved in ammonia oxidising bacteria (AOB) and archaea (AOA) that perform the initial and rate-limiting step of nitrification. Whilst commercial SNIs have been on the market since the 1970s, the nitrogen use efficiency has remained 50% globally,[10] mainly due to their unpredictable and unreliable performances in soil. [10] Interestingly, the inhibition mechanism of commercial NIs has not been fully understood yet. [11, 12] Moreover, the development of new NIs has been a bottleneck in the past.

The first research chapter of this thesis investigates into the development of a rapid, accessible, and robust nitrification assay to test the efficacy of potential NI within 60 min. This essay employs AOB of the strain *Nitrosomonas europaea* and *Nitrosospira multiformis* and test their nitrification activity in the presence of a SNI. The assay summarises the most-suitable parameter for cell growth, cell harvest, inhibitor concentration and substrate concentration, as these protocols do not exist in literature. The assay was performed on 4,5-disubstituted 1,2,3-triazoles, a new class of nitrification inhibitors explored in this doctoral thesis. 16 derivatives of 4,5-disubstituted 1,2,3-triazoles were synthesised to determine their nitrification inhibitory effect in dependence on their structure. With this assay, it was found that particularly five derivates of 4,5-disubstituted 1,2,3-triazoles show a significant nitrification inhibition in comparison to uninhibited cells indeed.

The second research chapter focuses on determining the mechanism of inhibition of the existing SNIs 3,4-dimethyl-1*H*-pyrazole (DMP) and dicyandiamide (DCD), which have not been explored previously. This fundamental research is essential to understand current agricultural products and enable the design of novel NIs with more reliable performance. A series of biochemical studies were performed with DMP and DCD using *Nitrosomonas europaea* (*N. europaea*) as a model organism to identify the targeted enzyme in the nitrification enzyme cascade, binding affinity, reversibility of binding, Michaelis Menten kinetics, and toxicity. It was found that both NI act as reversible, non-mechanistic inhibitors.

Following these findings from the biochemical experiments in the previous chapter, similar experiments were performed for five derivatives of 1,4-disubstituted 1,2,3-triazoles to directly compare them to the commercial SNI. This class of SNI has recently been tested in soil incubation studies by the postdoctoral student *Bethany I. Taggert* and showed an exceptional NI in comparison to the ‘gold standard’ DMP especially observed at elevated temperatures. Biochemical parameters for this class of compounds have not been determined. Therefore, five candidates 1,4-disubstituted 1,2,3-triazoles with varying functional groups substituents in the 1-position were tested. It was found that the incorporation of functional groups is detrimental to the inhibitory effect, and with increased

lipophilicity, an increased inhibitory effect is observed. All inhibitors acted as non-competitive and reversible inhibitor.

With the detailed mechanistic knowledge of existing SNI, the fourth research chapter aims to explore the introduction of an irreversible SNI. The irreversible SNI 4-Methyl-1-(prop-2-yn-1yl)-1*H*-1,2,3-triazole (MPT) was discovered. MPT contains an alkynyl group that mimics acetylene, a known irreversible inhibitor of the AMO. Its efficacy was tested in bacterial studies and soil incubation studies with four German and one Australian soil showed that the inhibitory effect is practically pH- and soil-type independent.

Moreover, this chapter explores the effect of MPT on methanotrophic organisms. Methanotrophic organisms contain the key enzyme particulate methane monooxygenase (pMMO), which is evolutionary and structurally similar to AMO. It was found that MPT does not inhibit the methane uptake to the same extent as nitrification. Therefore, it can be concluded that MPT is an AMO-selective inhibitor.

Declaration

This is to clarify that

I. the thesis comprises only my original work towards the PhD except where indicated in the Preface;

II. due acknowledgement has been made in the text to all other material used; and

III. the thesis is less than 100 000 words in length, exclusive of tables, references and appendices.

Sibel Cansu Yildirim

May 2023

Preface

All experimental work reported herein has been conducted by the candidate Sibel C. Yildirim except where indicated. Chapter 5 includes soil mineral-N studies performed by postdoctoral researcher *Joses G. Nathanael*. Moreover, Chapter 4 includes studies performed on 1,4-disubstituted 1,2,3-triazoles, which were previously synthesised by the doctoral student *Bethany I. Taggert*. In accordance with regulations of The University of Melbourne and the Landwirtschaftlichen Fakultät der Universität Bonn, I acknowledge that portion of this work were performed in a collaborative manner (at the Bio21 Institute, The School of Chemistry and School of BioSciences at the University of Melbourne; at the Institute of Bio- and Geosciences at Forschungszentrum Jülich GmbH; and at the Landwirtschaftlichen Fakultät at the University of Bonn) as part of the joint PhD program.

Manuscripts and published articles included in this thesis related to the research questions:

Chapter 2: Yildirim, S. C.; Walker, R. M.; Roessner, U.; Wille, U. A Rapid and Inexpensive Assay for Testing the Efficiency of Potential New Synthetic Nitrification Inhibitors. *ACS Agric. Sci. Technol.* **2023**. DOI: 10.1021/acsagscitech.2c00229

Chapter 3: Yildirim, S. C.; Walker, R. M.; Roessner, U.; Wille, U. Assessing the Efficacy, Acute Toxicity, and Binding Modes of the Agricultural Nitrification Inhibitors 3,4-Dimethyl-1H-pyrazole (DMP) and Dicyandiamide (DCD) with *Nitrosomonas europaea*. *ACS Agric. Sci. Technol*. **2023**. DOI: 10.1021/acsagscitech.2c00303

Chapter 4: Yildirim, S. C.; Taggert B. I., Walker, R. M.; Roessner, U.; Wille, U. Insights into the Efficacy and Binding Mode of 1,4-Disubstituted 1,2,3-Triazoles - A New Class of Agricultural Nitrification Inhibitors. Submitted: *ACS Agric. Sci. Technol*.

Chapter 5: Yildirim, S. C.; Nathanael J. G., Frindte K., Walker, R. M.; Roessner, U.; Wille, U. 4-Methyl-1-(Prop-2-yn-1yl)-1*H*-1,2,3-Triazole (MPT): A Novel, Readily Accessible and Highly Efficient Nitrification Inhibitor for Agriculture. Submitted: *J. Agric. Food Chem.*

1. **A Rapid and Inexpensive Assay for Testing the Efficiency of Potential New Synthetic Nitrification Inhibitors**

Co-author	Contribution	
Sibel C. Yildirim	70%	Planning, execution, and analysis of experiments including writing up the paper
Robert M. Walker	5%	Induction and guidance with the experiments, comments on the paper
Ute Roessner	5%	Induction and guidance with the experiments, comments on the paper
Uta Wille	20%	Induction and guidance with the experiments, revision on the paper

2. **Assessing the Efficacy, Acute Toxicity, and Binding Modes of the Agricultural Nitrification Inhibitors 3,4-Dimethyl-1*H*-pyrazole (DMP) and Dicyandiamide (DCD) with *Nitrosomonas europaea*.**

Co-author	Contribution	
Sibel C. Yildirim	70%	Planning, execution, and analysis of experiments including writing up the paper
Robert M. Walker	5%	Induction and guidance with the experiments, comments on the paper
Ute Roessner	5%	Induction and guidance with the experiments, comments on the paper
Uta Wille	20%	Induction and guidance with the experiments, revision on the paper

3. **Insights into the Efficacy and Binding Mode of 1,4-Disubstituted 1,2,3-Triazoles - A New Class of Agricultural Nitrification Inhibitors.**

Co-author	Contribution	
Sibel C. Yildirim	70%	Planning, execution, and analysis of experiments including writing up the paper
Robert M. Walker	2.5%	Induction and guidance with the experiments, comments on the paper
Ute Roessner	2.5%	Induction and guidance with the experiments, comments on the paper
Bethany I. Taggert	5%	Provision of compounds, comments on the paper
Uta Wille	20%	Induction and guidance with the experiments, revision on the paper

4. **Methyl-1-(Prop-2-yn-1yl)-1*H*-1,2,3-Triazole (MPT): A Novel, Readily Accessible and Highly Efficient Nitrification Inhibitor for Agriculture.**

Co-author	Contribution	
Sibel C. Yildirim	70%	Planning, execution, and analysis of experiments including writing up the paper
Robert M. Walker	2%	Induction and guidance with the experiments, comments on the paper
Ute Roessner	2%	Induction and guidance with the experiments, comments on the paper
Joses N. Nathanael	2%	Mineral N soil testing, comments on the paper
Katharina Frindte	2%	Induction and guidance with the experiments, comments on the paper

Otavio Leal	2%	Induction to GC-MS experiments, comments on the paper
Claudia Knief	2%	Induction and guidance with the experiments, comments on the paper
Nicolas Brueggemann	2%	Induction and guidance with the experiments, comments on the paper
Uta Wille	16%	Induction and guidance with the experiments, revision on the draft paper

Provisional patents filed by the University of Melbourne from this work:

1. Patent assignee: The University of Melbourne; Inventors: Sibel C. Yildirim, Uta Wille, filed 02/09/2022; Application number: 2022902533

Conference abstracts and poster presentations:

1. ORCHEM 2022 Germany: Investigation in the efficacy of novel nitrification inhibitors to reduce nitrification in soil.

COVID-19 Impact Statement

COVID had a significant impact on this research. As a joint PhD project, the work was designed in an interdisciplinary project between three institutions. Therefore, the project could only be performed with the scientific input of all disciplines and requires experimental work in all institutions. The main scientific objectives of this doctoral project have been redefined several times during this period to mitigate the impact of the COVID-19 pandemic, resulting in significant shifts in the scientific focus and timeline. As a result, some key experiments that would have led to concrete scientific outcomes and high-quality publications were removed entirely or re-designed.

As a joint PhD project between the School of Chemistry of the University and the University of Bonn and Forschungszentrum Jülich in Germany, this PhD project is multidisciplinary and requires the expertise of the School of Chemistry (Unimelb), School of Biosciences (Unimelb) and School of Agriculture (UniBonn). The overall aim is to synthesise nitrification inhibitors to mitigate nitrogen fertiliser loss and reduce greenhouse gases in agriculture. At the beginning of the project (April 2019-February 2020), a library of 16 compounds were successfully synthesised and ready to be tested at the School of BioSciences; however, with the pandemic starting, these experiments were postponed as no access to the building was permitted. This led to an access prohibition and an experimental delay of 6 months. During these 6 months, the design of new nitrification inhibitors did not proceed as the initial results aimed to guide further synthesis. In addition, the still uncertain access permits required to pivot to an alternative approach that requires less time at the School of BioSciences in the case of another lockdown (which frequently happened unannounced). Therefore, the core studies shifted from plant studies to pure bacterial culture studies with ammonia-oxidising bacteria. The acquirement of microbiology and molecular biology skills was needed to master this new discipline of science with no background knowledge of the doctoral candidate. This required amendment delayed the outcome of this project for another 6 months.

Moreover, to meet the requirement of the joint PhD, it was necessary to conduct experiments in Germany. Initially, my work in Germany was aimed to commence in mid-2021 (the second year); however, due to travel restrictions, these plans had to be postponed for one year to mid-August 2022. The experiments are strictly necessary to prove the hypothesis of greenhouse gas production in agricultural systems. This experiment could not be performed at the University of Melbourne due to the lack of facilities and infrastructure.

This list summarises all disruptions in the various parts of the PhD project. These factors led to re-designing my PhD and acquiring skills in various time-intensive scientific disciplines.

- Termination of all experiments started pre-lockdown due to the complete shutdown of the University, which required re-synthesis of some compounds.
- No access to the School of Biosciences for eight months and restricted access to the Bio21 laboratories resulted in significant delays in substantial experimental flow. Soil and plant studies required to assess novel compounds could not be performed, valuable results could not be generated, and the research progress was hindered.
- Significant delays of the necessary lab consumables, such as bacterial cultures, agricultural soil collection (due to 5 km radius restriction), field visits and experiments.
- Acquirement of new scientific skills in microbiology and molecular biology to pivot restricted access at Biosciences to perform experiments also at Bio21.
- Significant reduction in productivity and increased anxiety due to isolation.
- No facilities at home that allowed to work from home peacefully due to lack of space and presence of roommates.
- Postponing significant experiment that needed to be performed in Germany for measuring the greenhouse gas emissions of the soil-plant system in the presence of suggested compounds.

Acknowledgements

Prof. Uta Wille

Thank you for your guidance, mentorship, and support in the last five years. I am amazed at what I have achieved and grown under your supervision. I thank you from the bottom of my heart for keeping me motivated and teaching me to stay curious. The highlight of my PhD studies was our weekly catch-ups; you always provided me with a safe space. I am glad that I went on this adventure with you by my side. Whatever I achieved in this journey is because you always gave me the feeling that I could achieve anything I put on my mind, and I will be forever grateful for that.

Supervisors

Thank you, Nicolas and Claudia, for letting me be a part of your group and welcoming me warmly. I have never felt that I was just a 'guest researcher' as I was part of your group from day one. Thank you for your excellent guidance throughout my research stays in Germany and beyond. Thank you, Rob, for taking the time to teach me microbiology skills. Thank you, Ute, for your great guidance, support and positive attitude.

The Wille Group

Thank you to all members (past and present): Joses, Beth, Ben, Parv, Yue, Haohan, Yifan and Fatemeh and all who visited. Thank you all for being family away from my family and making Australia feel like home.

Friends and Family

Thank you, Mom and Dad, for all the sacrifices you made for me and for showering me with love. Thank you, Dogancan and Ekin, for being the best brothers in the world. Although I am far away, you are always with me. To my best friends Cali, Muh, Ilka and Aleyna, thank you for being the craziest and funniest friends on this planet and making me laugh in times when I take life too seriously. I will never forget our student nights in Mainz, Melbourne and Seoul.

Fiancé

Thank you, my love, Faiz, for being my soul mate and best friend. Thank you for motivating me to become a better version of myself. I always feel safe and supported by you. Thank you for co-parenting the 500000 foster kittens for my emotional support during this PhD journey.

Roessner Group

The Roessner Group was my second family at the University of Melbourne. Thank you, Allene, Tannaz, Pipob, Héber, Alina and Sneha, for our great moments together and for accepting me as a group member. Thank you, Martino, for teaching me how to grow plants. You guys are exceptional, and I am so grateful I did this PhD project in collaboration with you.

Brüggemann and Knief Groups

A special thank you to the researchers in Germany who helped me complete an extraordinary amount of experiments within this short time. I would not have been able to push through this experiment marathon without your support. Thank you, Otávio, Katharina, Franz, and all Brüggemann and Knief group members, for your helpful inputs and discussions and for sharing your perfectionated protocols I could follow without significant complications.

List of symbols and abbreviations

α	alpha	BNI	biological nitrification inhibitors
Å	Ångström	bp	base pair
Ac	acetyl	Btz	benzothiazole
AMO	ammonia monooxygenase	c	centi-
amo	subunit of ammonia monooxygenase	°C	degree(s) Celcius
amoA	gene encoding subunit A of the ammonia monooxygenase	CuAAC	Cu(I)-catalysed alkyne azide cycloaddition
ANOVA	analysis of variance	CuMO	copper membrane-associated monooxygenase
AOA	ammonia oxidizing archaea	d	doublet (NMR)
AOB	ammonia oxidizing bacteria	*d*	deuterium
aq.	aqueous	Δ	delta
ARC	Australian Research Council	Da	Dalton(s)
arch	archaea	DCD	dicyandiamide
AT	allyl thoiourea	Δ	delta
ATCC	American Type Culture Collection	DCM	dichloromethane
atm	atmosphere (pressure)	dd	doublet of doublets (NMR)
ATP	adenosine triphosphate	ddd	doublet of doublet of doublets (NMR)
β	beta	DMP	3,4-dimethyl-1*H*-pyrazole
bac	bacteria	DMPP	3,4-dimethyl-1*H*-pyrazole phosphate
BCA	Bicinchoninic acid assay	DMSO	dimethyl sulfoxide

DMSZ	Deutsche Sammlung von Mikroorganismen und Zellkulturen	G°’	Gibbs free energy
DNA	deoxyribonucleic acid	GC	gas chromatography
dt	dt doublet of triplets (NMR)	GHG	greenhouse gas
dp	doublet of pentets (NMR)	GP	general procedure
dq	doublet of quartets (NMR)	h	hour(s), hexet (NMR)
dqd	doublet of quartet of doublets (NMR)	ha	hectare(s)
e^-	electon(s)	HAO	hydroxylamine oxidoreductase
eq	equation	HATS	high affinity transport systems
equiv.	equivalent(s)	hept	heptet of doublets (NMR)
ESI	electrospray ionisation	H-MPT	methyl-1-propyl-1*H*-1,2,3-triazole
Et	ethyl	HR	high resolution
ETC	electron transport chain	HSD	honestly significant difference
EWG	electron-withdrawing group	Hz	hertz (NMR)
FAO	Food and Agriculture Organization of the United Nations	$IC_{50(abs)}$	concentration of inhibitor to decrease response to 50%
eqn.	equation	IP	intellectual property
equiv.	equivalent(s)	K	Kelvin(s)
ETC	electron transport chain	K_m	Michaelis-Menten constant
EWG	electron-withdrawing group	*kobs*	pseudo-first-order rate coefficient
FAO	Food and Agriculture Organization of the United Nations	λ	wavelength
γ	gamma	L	litre(s)
g	gram(s)	LATS	low affinity transport systems

LB	Luria broth	Nitrapyrin	2-chloro-6-(trichloromethyl)pyridine
µ	micro-	NMR	nuclear magnetic resonance
m	milli-, metre(s), multiplet (NMR)	NUE	nitrogen use efficiency
M	molecular ion (HRMS), mega-, molar	*o*	ortho
m/z	mass-to-charge ratio	OD	optical density
Me	methyl	OD_{600}	optical density at 600 nm
min	minute(s)	π	pi
mol	mole(s)	p	pentet (NMR)
MPT	4-methyl-1-(prop-2-yn-1yl)-1*H*-1,2,3-triazole	*p*	para
MS	mass spectrometer	Pet.	petroleum
mol	mole(s)	Ph	phenyl
MSM	mineral salts media	$PM_{2.5}$	particulate (diameter $\leq$ 2.5 mm)
n	nano-	pMMO	particulate methane monooxygenase
NADP	nicotinamide adenine dinucleotide phosphate	*pMMO*	gene encoding particulate methane monooxygenase
NaPB	sodium phosphate buffer	ppb	parts-per-billion
NI	nitrification inhibitor	ppm	parts-per-million
N. europaea	*Nitrosomonas europaea*	ppt	parts-per-trillion
N. multiformis	*Nitrosospira multiformis*	Pr	propyl
NiR	nitrite oxireductase	q	quartet (NMR)

qPCR	quantitative polymerase chain reaction
R	R alkyl group
rpm	rotations per minute
RT	room temperature
s	second(s), singlet (NMR)
SAR	structure activity relationship
SI	supporting information
SNI	synthetic nitrification inhibitor
t	t triplet (NMR)
td	triplet of doublets (NMR)
T	terra-
THF	tetrahydrofuran
TLC	thin layer chromatography
UV /vis	ultraviolet visible region
V_{max}	maximal rate
wt.	weight

Table of Content

List of Figures

List of Tables

List of Schemes

Chapter 1: Introduction

1.1 Importance and Challenges of Nitrogen Fertilisation

Whilst plants generate their energy from oxidising glucose to carbon dioxide (CO_2) and water (H_2O) via cellular respiration, nitrogen (N) must be viewed as a central element for the production of proteins, nucleic acids, which form the living material.[13] N constitutes approximately 1.5 – 5% of a plant's dry weight, wherein 80-90% is conserved in proteins.[13] Despite the generous abundance of N_2 in the atmosphere (78%), plants are only able to take up mineral forms of N in soil, i.e., nitrate (NO_3^-) or ammonium (NH_4^+). [14] Both mineral N forms are released from organic matter via a process called mineralisation.[15] During mineralisation N bound in organic compounds and soil particles is decomposed via physical and microbiological processes.[15] The degree of mineralisation depends on the type of soil microorganisms, the chemical properties of the soil and the climate.[10] Once released, plants assimilate mineral-N through their root transporters from soil.[16] NO_3^- is the primary mineral-N form with an up to 100-1000 times higher abundance than NH_4^+ in soil, due to the short lifetime of NH_4^+ (see section 1.3).[13] N uptake rates in plants rely on the genetic predisposition and intrinsic activity of root High and Low-affinity Transport Systems (HATS and LATS).[16] HATS are active in low NO_3^- concentrations in soil (< 1 mM) and LATS are active in high concentration NO_3^- in soil. NH_4^+ is the preferred form of mineral N, as NH_4^+ can enter into amino acid synthesis directly, whereas NO_3^- must be first reduced to NH_4^+ *via* the plant enzymes nitrate and nitrite reductase.[13] A total of eight electrons is required for the reduction of NO_3^- to NH_4^+, which requires a third of the energy of the oxidation of one glucose molecule.

Due to frequent harvests, plants in agricultural fields are N deprived as the natural N release mechanisms in soils are non-sufficient and exploited. [13] As a result of the critical role of N in plant growth and the low natural supply, the management of N resources is an extremely important aspect in agricultural systems.[13] To satisfy the caloric needs of 9 billion people, the introduction of N fertiliser in a plant-available form are unavoidable.[17] N fertilisation is a substantial practice in agriculture, with an application of up to 240 kg/ha for a single harvest cycle and a global application rate of 120 Tg.[6] In comparison, the natural N pool is just 63 Tg

year^{-1} and provides only a third of the required N in agriculture.[10] N fertilisers contain NH_4^+ or the deprotonated form NH_3 as an active compound, which needs to be produced under high pressure and high-temperature conditions (Haber-Bosch Process) from gases hydrogen (H_2) and the non-reactive gas N_2. [18, 19] The N demand will undoubtedly continue to increase due to population growth, climate change and limited arable land.[9] In fact, it is predicted that N fertilisation will increase by 70-100% by 2050.[20] With introduction of excessive amounts of N fertiliser in a plant-available form, the balance of the natural ecosystems is disturbed. [9] NH_4^+, besides being a plant nutrient, is also a highly preferred substrate for microorganisms in the soil. [21] The overarching process of microbial NH_4^+ uptake is summarised in the 'N cycle' (see section 1.2),[7] which is a form of a microbial redox cascade that generates energy essential for the survival of soil microorganisms from mineral N. Therefore, a high fertilisation rate rarely results in higher crop yield but leads to the accumulation of environmental pollutants that are metabolites of the N cycle.[22]

1.2 Terrestrial Nitrogen Conversion – A Cycle?

The N cycle is a primary regulator of atmospheric and terrestrial fixed N sources. Chemically, it can be considered as the redox chemistry of N in soil and is of tremendous importance in maintaining the balance of gaseous and solid N.[6] The N cycle is not an isolated process, but instead, it is strictly linked to other cycles, such as the carbon (C) cycle and the phosphorus (P) cycle. [7] Since the beginning of industrialisation in the early 19th century, an enhanced N emission due to fossil fuel combustion and the extensive introduction of N fertiliser, in particular after the development of the Haber-Bosch process, has led to an imbalance in the N cycle.[23] Additional secondary factors, such as climate change and excessive CO_2 release, have had an undeniable impact on the N availability in both soil and the atmosphere.[24]

The N cycle consists of two main parts, N uptake and N release, which, as these two processes are driven by, are also referred to as nitrification and denitrification (**Figure 1**)**,** respectively.[22]

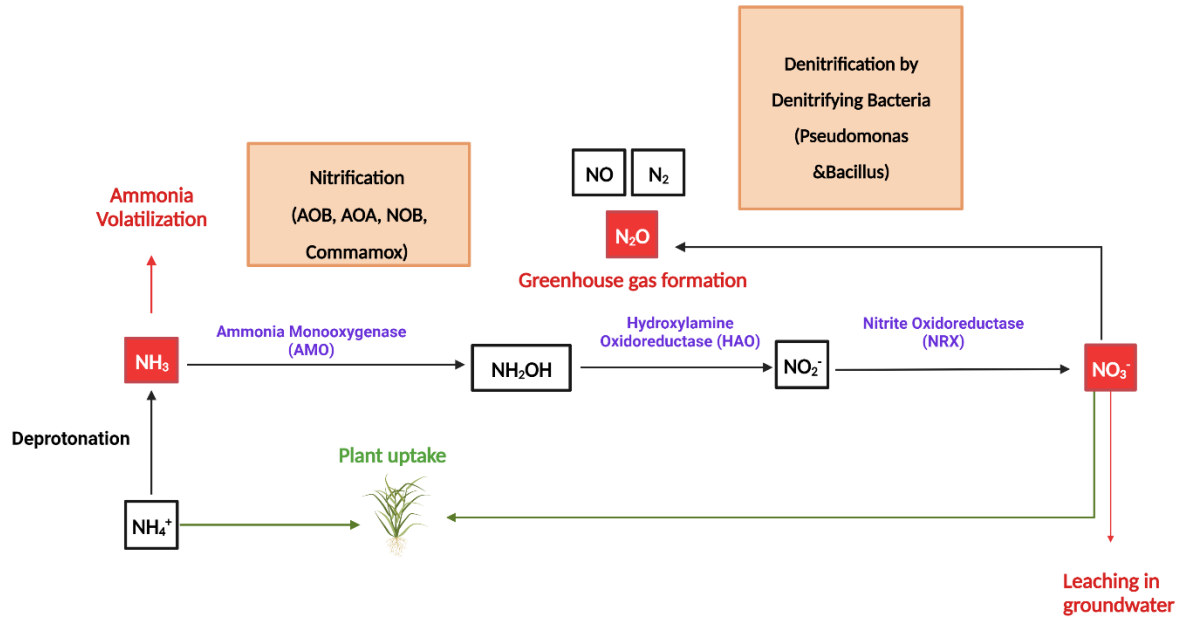

Figure 1: The terrestrial N cycle is divided into the two steps nitrification and denitrification. The metabolites indicated in red are environmental pollutants due to excessive N fertilisation. (Created with BioRender)

Nitrification starts with the introduction or release of NH_3, which can be either generated from mineralisation, microbial N-fixation or anthropogenic N fertilisation.[22] The latter is the predominant N-source in agricultural systems, with urea ($(NH_2)_2CO$; requires hydrolysis to release NH_4^+ via urease[25]) ammonium nitrate (AN; NH_4NO_3), ammonium sulphate (AS; $(NH_4)_2SO_4$) and calcium ammonium nitrate (CAN, $5Ca(NO_3)_2*NH_4NO_3*10H_2O$) being the main players. An electron release and uptake cascade are initiated once NH_3 (the deprotonated form of NH_4^+) is present in the soil. N in NH_3 has the formal oxidation number of -3, which is oxidised to +5 in NO_3^-. These eight electrons released during nitrification are essential for the survival of ammonia oxidising bacteria (AOB) and ammonia oxidising archaea (AOA), equipped with enzymes capable of performing this oxidation in exchange for gaining energy to survive. The key-player enzymes are ammonia monooxygenase (AMO) and hydroxylamine oxidoreductase (HAO) for the oxidation of $NH_3 \rightarrow NO_2^-$ and nitrite oxidoreductase (NXR) for the oxidation of $NO_3^- \rightarrow NO_2^-$. The conversion $NH_3 \rightarrow NO_2^-$ is the rate-limiting step of the N cycle, as NO_2^-- is rarely found to accumulate in the environment. The primary purpose of nitrification is the formation of nicotinamide adenine dinucleotide ($NADH^+$), an important

reductant in the generation of adenosine triphosphate (ATP).[26] In other words, NH_3 is the energy-delivering compound; and AOB and AOA can only survive in its presence.

Nitrification can positively or negatively affect N retention in a system, depending on the soil conditions and pH. Especially in alkaline soils, the deprotonation of NH_4^+ leads to the formation of a large portion of the volatile NH_3, which can be lost to the atmosphere. In this case, nitrification enables N retention by oxidising N to less volatile species.[27] However, in most cases, nitrification competes with plant N uptake. The initial step of nitrification, the oxidation of NH_3 to NH_2OH is catalysed by the copper–dependent AMO. [28]

AMO is a membrane-bound enzyme with an unknown crystal structure (see section 1.4) that is abundant in both AOA and AOB.[29] NH_2OH is immediately converted to NO_2^- by the heme-type iron-dependent enzyme HAO, which is also abundant in AOB and AOA.[8] Therefore, the oxidation product of $NH_3 \rightarrow NH_2OH$ is only a 'formal' intermediate and the overall oxidation of $NH_3 \rightarrow NO_2^-$ is considered as initial and rate-limiting step of nitrification.[8] Lastly, NO_2^- is oxidised to nitrate (NO_3^-) via the molybdenum-dependent enzyme nitrite oxidoreductase (NIR) present in nitrite oxidising bacteria (NOB). Historically, AMO and HAO were believed to be abundant in AOB and AOA, respectively, whereas NO_2^- oxidation by NXR was performed by NOB. However, recently *Comammox* were discovered that contain both AOB and NOB and can carry out the complete oxidation of NH_4^+ to NO_3^-.[30] The abundances of these species are soil type, edaphic and climate dependent.[27] The product of nitrification 'NO_3^-' is not strictly a N loss, as NO_3^- can be assimilated by plant roots (section 1.1).[16] However, as an anionic species NO_3^- has a low affinity to bind to the negatively charged soil particles and is lost through leaching in aquatic systems [10] causing accumulation and pollution in rivers and lakes (eutrophication). [31] Human and animal consumption of NO_3^- can lead to health risks, and government regulations strictly limit the amount of permitted NO_3^- in drinking water.[27] On the other hand, retained NO_3^- in the soil can be either taken up by plants or reduced to gaseous N forms, such as N_2O, N_2 and nitric oxide (NO)[32], *via* microbial denitrification processes. Excessive N fertilisation leads to anthropogenic-caused nitrous oxide (N_2O) formation, and in fact, agricultural soils account for about 50% of total global N_2O emissions. [33]

1.3 Ammonia Oxidising Bacteria

As mentioned in section 1.2, AOB are chemolithoautotrophic organisms that can be found in most aerobic environments where NH_3 is available. [27] AOB are ubiquitous in soils, freshwater and marine environments.

Most AOB fall within one taxonomic group of the β- and γ-*Proteobacteria* and are categorised into five main genera *Nitrosomonas*, *Nitrosospira*, *Nitrosococcus*, wherein *Nitrosomonas* and *Nitrosospira* (**Figure 2**) are the most predominant genus levels.[34] Pure AOB pure cultures are typically isolated by extinction via dilution methods, in which non-nitrifying bacteria gradually become extinct as the liquid media is tailored for the specific needs of AOB cultures. [35] The growth media must satisfy several requirements in order to successfully grow AOB, such as the absence of organic carbon sources, the presence of inhibitors of heterotrophic organisms (such as penicillin) and essential trace elements, for example Cu^{2+} and other metal cations. AOB are notorious for their slow growth and they form symbiosis with heterotrophic organisms. [36] As autotrophs, they rely on the energy that is released from the oxidation of NH_3 ($\Delta G^{\circ'}$ = -271 kJ mol $^{-1}$) and their organic carbon is derived from CO_2 assimilation.[34]

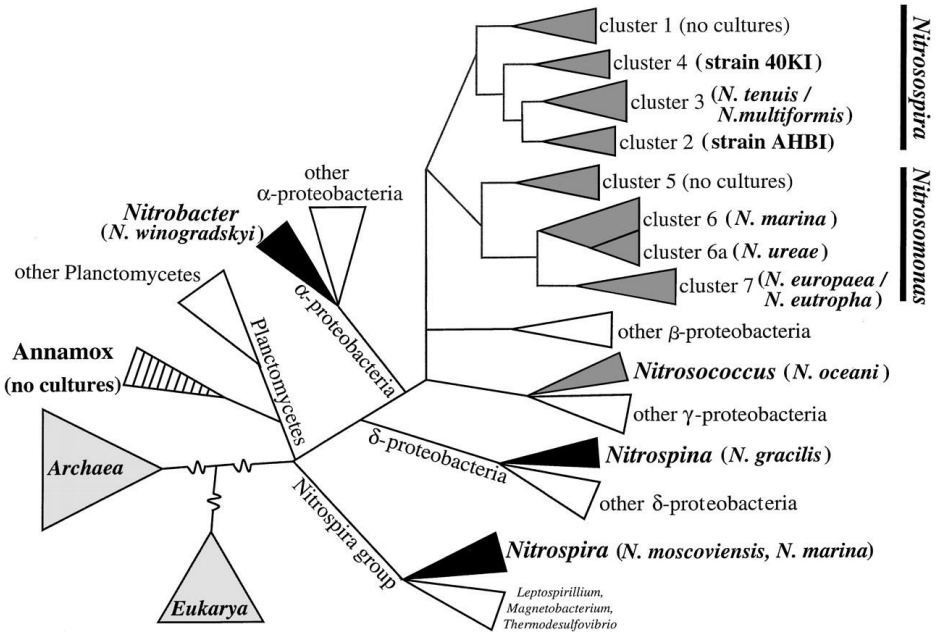

Figure 2: Phylogeny of known autotrophic nitrifiers based on 16S rRNA gene sequencing. AOB are shown in dark grey, NOB in black and anaerobic oxidisers are striped.[27]

AOB can adapt to many climatic and edaphic conditions.[8] At lower pH, NH_3 is protonated to NH_4^+ (pKa = 9.25), which is not a suitable substrate for AMO. However, some AOB have adapted to acidic conditions (pH_{KCl} < 4), such as *Nitrosospira* AHB1. [27] While AOA are the more predominant species in acidic soil, AOB also have mechanisms to cope with low pH. [37, 38] The reason for the survival of AOB/AOA in acidic soil has not been fully understood yet, as AOB cultures could not be grown in a pH = 5.5 in a laboratory setup; however, there must be a coping mechanism present in soil potentially in symbiosis with urealytic bacteria.[27] *N. europaea* is the most studied AOB due to its ability to be cultured in a laboratory environment.[39-41] However, it is not representative of the more dominant groups in soil *Nitrosospira.*[27] The complete genome sequence (2.8 Mbp) of *N. europaea* revealed about 2460 protein-encoding genes, of which the majority codes for enzymes of cellular constituents. Only a small fraction is responsible for the catabolism of compounds (such as N-oxidation). [34, 42]

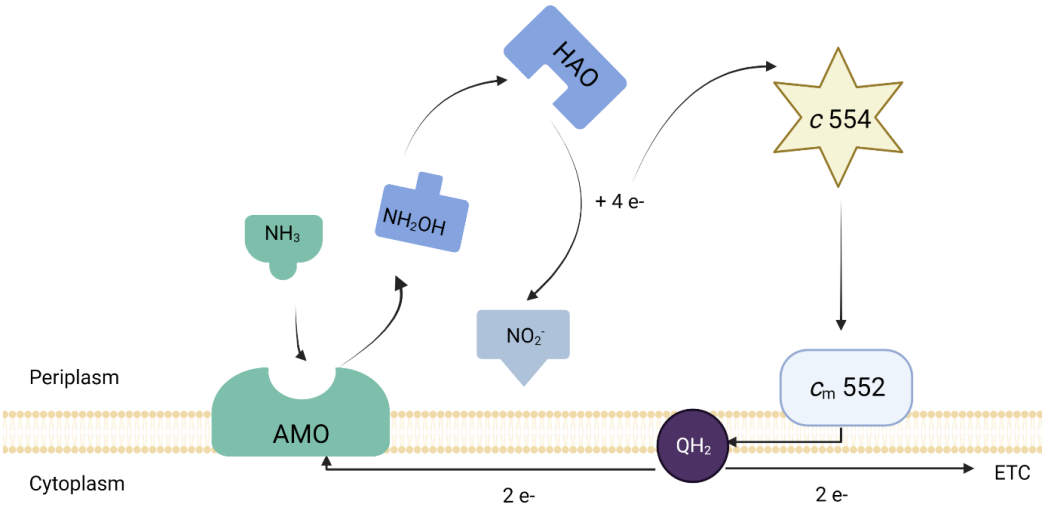

Figure 3: Membrane bound AMO oxidizes NH_3 to NH_2OH, which is further oxidized to NO_2^- by HAO. The four electrons generated during these processes are subsequently transferred to cytochrome c554, membrane cytochrome c_m552 and ubiquinone-8 (QH_2), from where two electrons are fed into the electron transport chain (ETC) and two electrons are transferred back to the AMO to deliver electrons for the reduction of oxygen.

The pathway of bioenergy generation from NH_4^+ oxidation is in several cascading steps. The AMO-catalysed oxidation of NH_3 to NH_2OH releases two electrons, which are accepted up by O_2. As the reduction $O_2 \rightarrow 2\ O^{2-}$ requires four electrons, electron deficit is generated in the first catalytic step.[8, 34] The remaining two electrons are provided by HAO, as the NH_2OH oxidation supplies a total of four electrons. The remaining two electrons are transferred to cytochrome c554, membrane cytochrome c_m552 and ubiquinone-8 (QH2).[8] HAO is, therefore, a crucial enzyme in the nitrification process that fuels the AMO reaction.[43] Thus, AMO and HAO are in proximity to each other, where AMO is located in the inner membrane facing the periplasm and HAO is a periplasmatic enzyme.

1.4 Insights into the Key Enzyme AMO

AMO, a copper membrane-associated monooxygenase (CuMO), is structurally very complex. Unfortunately, its crystal structure has not yet been successfully resolved due to difficulties cultivating CuMO-producing organisms and isolating purified active membrane-bound domains.[44] The genome of the AOB of *N. europaea* revealed that AMO most likely consists of three subunits, amoA, amoB and amoC, all of which are membrane-bound. *Nitrosomonas* spp. contain two copies of the complete *amo* operon while *Nitrosospira* spp. contain three copies, which leads to a higher activity of the latter.[45] It is believed that the subunit amoA contains the putative catalytic centre, as this subunit covalently binds acetylene (C_2H_2), resulting in inhibition of NH_3 oxidation. The irreversible binding was detected using isotope labelled acetylene ($^{14}C_2H_2$), which was found in the membrane-bound protein fraction of AOB.[45, 46] Michaelis-Menten Kinetics experiments showed that C_2H_2 is a suicide inhibitor of AMO. C_2H_2 is a competitive inhibitor of AMO, where increasing the NH_3 concentration decreases the inhibitory effect of C_2H_2 indicating that both bind on the same site of the enzyme.[47]

The size of amoA is approximately 31.990 Da.[44] The gene fragment of *amoB* predicts a polypeptide with a mass of 44.266 Da.[44, 48] Interestingly, although it is believed that amoC plays no critical role in the catalytic oxidation step of $NH_3 \rightarrow NH_2OH$, it has been shown that AOB contains *amoC* gene copies that are abundant in a higher number in the genome than the other subunits.[45] Recently, mass spectrometric approaches revealed a new subunit amoD

that also contains a copper ion in the binding site. It is believed that this subunit does not host the active centre, however, but is of importance for the entire AMO functionality.[49]
Although AOB have been discovered before AOA, AMO in archaea have been more widely studied than bacterial AMO.[50] The closest researchers ever have come to solving the crystal structure of AMO are the recent advancements in the crystal structure of the amoB site of the AOA strain *Caldus yellowstonii*.[51] An active copper site of the amoB subunit is believed to be located in the N-terminal region in the periplasm region with three histidines and the terminal amino group of the polypeptide within coordinating distance. [29] Recently, three new subunits (amoX, amoY, amoZ) that are only present in AMO of AOA have been discovered.[52] Consequently, the archaeal AMO is predicted to have six subunits instead of the three subunits in AOB. While these subunits are not believed to provide catalytic activity, it seems plausible that they play an essential role in the structural and functional integrity of the archaeal AMO complex.[52]

In summary, AMO is a structurally complex enzyme, and understanding underlying mechanisms have been challenging in the past. Ever since the discovery of AMO, researchers have grasped information on the active centre. The first and most straightforward approach is to test the substrate variety of AMO. The catalytic activity of AOB in the presence of various organic compounds, such as aromatic compounds, aliphatic alkanes, cyclic alkanes and chlorinated alkanes, was determined. Subsequent GC-MS analysis of the products was performed.[34, 40, 47, 53] **Figure 4** shows various substrates of the AMO, including linear and cyclic alkanes, alkenes, aromatic compounds, as well as NH_3.[40, 54] The main reaction is the insertion of an oxygen atom, similar to the $NH_3 \rightarrow NH_2OH$ oxidation.
AMO has a large substrate variety and can oxidise a variety of classes of organic compounds. It is to be noted that none of these compounds provide bioenergy for AOB and AOA to survive, as the subsequent enzyme HAO can only catalyse the reaction of NH_2OH to NO_2^-. However, this observation indicates that the active centre of the AMO is accessible for a large variety of compounds.

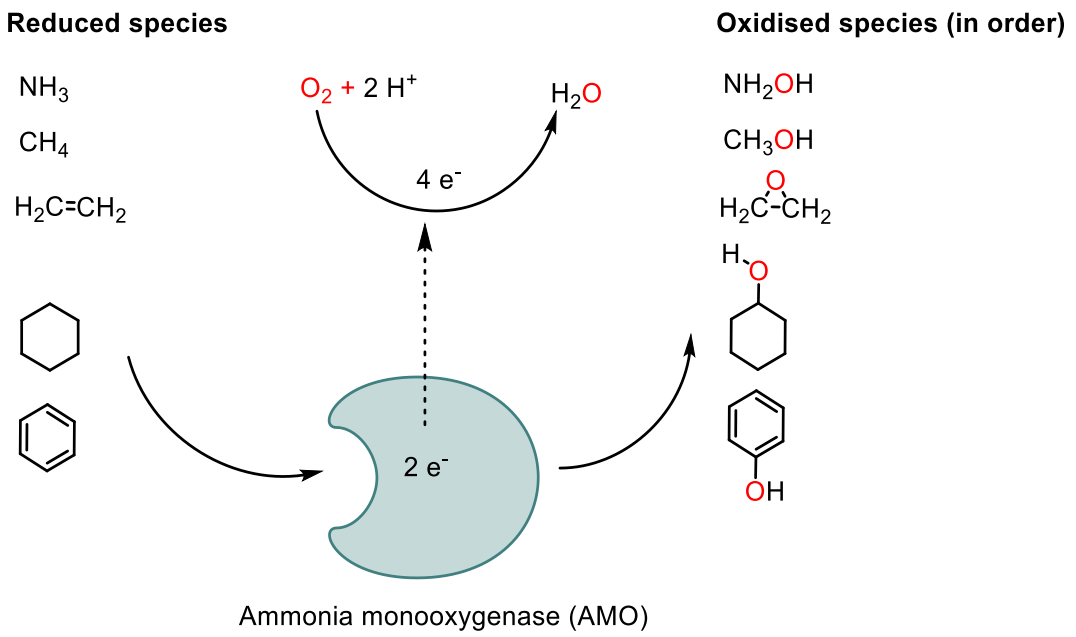

Figure 4: AMO catalyses the oxidation of a variety of different compounds, for example, ammonia, methane, ethylene, cyclohexane and benzene, which releases 2 electrons (2 e^-). Simultaneously, O_2 is reduced, which requires 4 e^-. The missing 2 e^- are provided from the set of electrons released during the subsequent oxidation processes catalyzed by HAO. [46, 54-57]

Another strategy to gain information about the catalytic centre of AMO is by comparison with similar evolutionary enzymes. The most prominent and well-studied CuMO is the particulate methane monooxygenase (pMMO) expressed by methanotrophs, representing a unique group of bacteria capable of growing using methane as a carbon source.[58] pMMO catalyses the oxidation of methane to methanol ($CH_4 \rightarrow CH_3OH$). [58] While the physiological function of AMO and pMMO differs, however, both enzymes can be considered analogues in metabolic importance and mechanistic function.[59] Interestingly, NH_3 is a substrate of pMMO, and CH_4 is a substrate of AMO, confirming the structural similarity of the active centre in these two enzymes.[59, 60] Comparison of the sequence of *pMMO* and *AMO* by Holmes *et al.* in 1995 revealed that both enzymes share a sequence of 27 kDa, suggesting that the active centre is analogous.[59] As methanotrophs and AOB have an enhanced growth of up to 5–15 times proportional to the Cu concentration in the growth media,[39] it was inferred that the active essential metabolic enzymes contain a Cu centre.[39] This presumption was confirmed in 2018 by Rosenzweig *et al.,* who solved the crystal structure of pMMO,

which is considered a scientific milestone in gaining an understanding of membrane-bound metallo-oxygenases (**Figure 5**).[29]

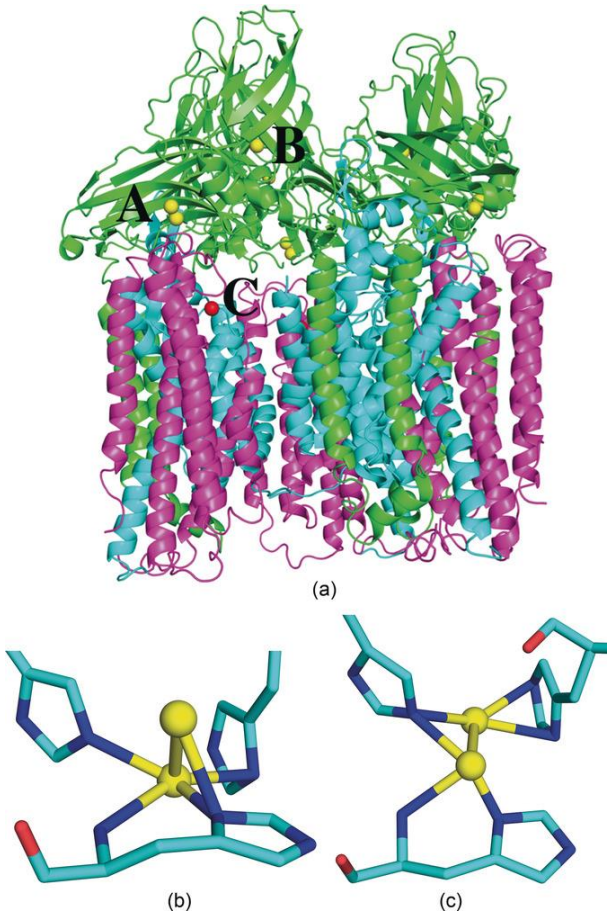

Figure 5: a) Crystal structure of pMMO: Trimeric structure of pMMO with metal sites A– C indicated (Cu ions in yellow, Zn ions in red; periplasmatic subunit pmoA, and membrane emerging pmoB and pmoC subunits in magenta, green, and cyan, respectively. The geometry of the Cu site A in protomers (b) and (c), involving three histidine residues and the amino-terminal group. Cu ions are shown as yellow balls, whereas C, N, and O atoms are shown as cyan, blue, and red sticks, respectively.[29]

Structurally, pMMO consists of a heterotrimer of which each individual comprises a single pmoA, pmoB and pmoC (similar to amoA, amoB and amoC respectively) gene fragment (**Figure 5**).[58] Rosenzweig *et al.* predicted a dinuclear and a mononuclear copper site in the soluble periplasmic parts of the pmoB subunit and a monomeric Zn site in the pmoC subunit within the membrane that binds only one Cu atom. The resolution of the crystal structure of 2.8 Å did not provide information about the location and composition of the pMMO active

site. Later, a crystal structure was reported at a slightly improved resolution, not supporting the previously suggested dinuclear copper site.[61] It also showed Cu ions in the pmoA region, modelled as mononuclear in two protomers and dinuclear in one protomer. In addition, it showed a Zn^{2+} ion in the pmoC unit.[61] The pmoB unit is believed to play an essential role in the catalytic activity and consists of two cupredoxin-like domains connected by two transmembrane helices and a long linker region.[61]

The importance of Cu in the catalytic process of AMO was further supported by experiments involving allyl thiourea (AT), where nitrification inhibition was observed.[62] AMO was inactivated, although no traces of inhibition *via* the oxidation of AT were found. [62] With a sulfur atom (**Figure 7**, indicated in blue), AT clearly distinguishes from the substrates shown in **Figure 4**; therefore, it was believed that AT acts as a ligand that coordinates to the Cu centre of the AMO (chelator), as shown in the crystal structure of the pMMO for histidine and Cu (**Figure 5b**).[62] Overall, it can be concluded that AMO is a membrane-bound enzyme with a large variety of substrates suitable for oxidation; Cu plays an essential role in the catalytic transformation. Moreover, the evolutionary similarity of the AMO and pMMO can be taken as a guideline for designing AMO inhibitors that mimic the histidine residues (**Figure 5**) bound to the Cu centres.

1.5 Biological Nitrification Inhibitors (BNIs)

Although there are uncertainties about the structure of the AMO, biological compounds excreted by plants have been detected that inactivate AMO.[63, 64] Plants have a mechanism that prevents excessive nitrification through the secretion of biological nitrification inhibitors (BNIs). The inhibitory effect of BNIs was observed by monitoring the growth of an engineered strain of AOB (luminescence recombinants of *N. europaea)* or measuring metabolites like NO_2^- in a nitrification assay *in vitro*.[47, 63, 65] BNIs have been isolated from root tissue and root exudates[66] and show a large structural diversity, such as 4-hydroxycinnamate derivatives (**1**), chlorogenic acid and flavanones (**2**), lactones (**3**) and secondary alcohols (**4**) (Figure 6). [67, 68] There are many suggestions why these molecules work as nitrification inhibitors.[6, 65, 69-71]

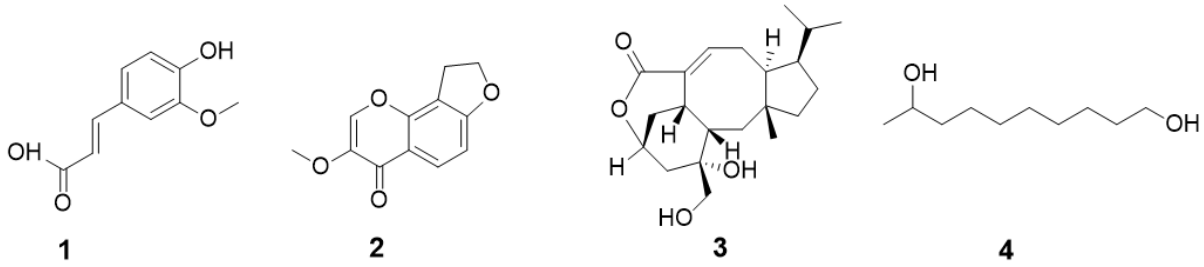

Figure 6: Examples of BNIs extracted from root tissue and exudates: methyl ferulate (**1**), dihydrokaranjin (**2**), brachialactone (**3**), and 1,9-decandiol (**4**).[6]

The BNIs shown here are hydrophobic, electron-accepting compounds and are therefore believed to inhibit both AMO and HAO.[57] It has been suggested that molecules with electron-deficient C=C double bounds, such as the a,b-unsaturated moieties in compounds **1** - **3** accept the electrons generated by the oxidation of NH_4^+ to NO_2^- instead of transferring them to cytochromes, [6] as shown in **Figure 3**. Thus, the inhibition mechanism is a disruption of the electron shuttle from HAO to cytochrome 554.[6] The fact that BNIs are hydrophobic molecules supports the importance of interaction with the membrane lipid double layer, which can be accessed more effortlessly by lipophilic compounds than by charged or hydrophilic compounds. [72] Another theory is that BNIs mimic substrates of AMO and HAO. A prominent example of substrate inhibition is 1,9-decandiol (**4**), which lacks electron-accepting properties, but two free hydroxyl groups could mimic NH_2OH, and the lipophilicity could contribute to facilitating the coordination of the binding site in the HAO.[70] BNIs are not in the scope of this thesis and will not be further discussed.

1.6 Synthetic Nitrification Inhibitors (SNIs)

To improve N management in agricultural systems, N fertilisers can be amended with nitrification inhibitors (NI). As mentioned in section 1.4, the putative active centre in AMO contains Cu^{2+} coordinated to histidine residues; hence, by inhibiting the rate-limiting enzyme AMO the residence time of N-fertiliser, specifically NH_3, in soil should be increased. Therefore, since 1962 companies such as DOW and BASF SE developed synthetic nitrification

inhibitors (SNIs) that inhibit AMO,[73, 74] which are a substantial additive to N fertilisers ranging from application rates of 0.5-5 kg ha^{-1}. [4] [73] At the time when SNIs were first developed, only a fraction of the now available information on AMO was available, and two classes of inhibitors were known: 1) substrates of AMO that cannot be further oxidized by HAO (section 1.3); 2) chelators like AT (section 1.4) that contain one or more heteroatoms that can (reversibly) coordinate to a copper centre residing in the AMO (**5**, Figure 7).[46, 62]

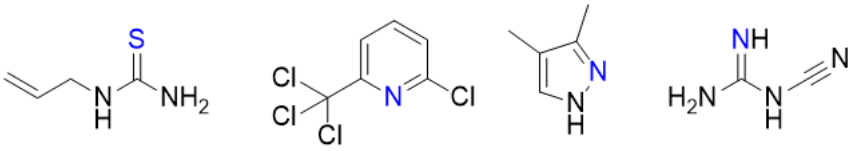

5 **6** **7** **8**

Figure 7: Chelators of AMO: allyl thiourea (**5**) and synthetic nitrification inhibitors: Nitrapyrin (**6**), 3,4-dimethyl pyrazole (DMP, **7**) and dicyandiamide (DCD, **8**).

The first SNI developed was 2-chloro-6-(trichloromethyl)pyridine (**6**) marketed as Nitrapyrin® by DOW Chemical Company.[75] Nitrapyrin is a substituted pyridine, that can bind *via* its N atom to metal centres.[76-78], such as Cu^{2+} (Figure 7 indicated in blue). 20 years later, dicyandiamide (DCD) was introduced in Europe but is now mainly used in New Zealand.[73] As revealed by the crystal structure, DCD can bind to Cu^{2+} through electron donating imino-N coordination (Figure 7 indicated in blue).[79] The most prominent SNI is 3,4-dimethyl -1*H*-pyrazole (DMP), commonly applied in agricultural systems as the phosphate salt to reduce its volatility and increase binding to soil particles (DMPP or ENTEC®). DMP principally contains two electron-donating N atoms, that can coordinate to metal ions. The crystal structure of four DMP molecules coordinating to Cu^{2+} in an octagonal geometry however showed that only one N (Figure 7 indicated in blue) coordinates to Cu^{2+}.[80] DMPP has a higher inhibitory effect and requires a lower application rate (up to 10x) than DCD and Nitrapyrin (0.5-1.5 kg DMPP ha^{-1}).

1.7 Why Are Still New SNI Needed?

Although SNIs were introduced to the market in the 1960s, the NUE remained notoriously poor. Globally, only 50% of the introduced N fertilisers end up in the plant biomass.[66] The

remainder is lost to the environment *via* NH_3 volatilisation, NO_3^- leaching or are lost to the atmosphere as N_2, N_2O and NO (Chapter 1.2).[10] Agricultural practises are increasingly becoming more expensive, with up to 140 Euro N fertiliser cost for a single corn production cycle at an application rate of 240 kg N ha^{-1}.[6]

One major factor for low NUEs is that the currently available SNI are ineffective in many soil types.[31, 81, 82] Soil can be characterised by various parameters, such as composition (sand, silt, clay), the content of the elements, such as N, O, P, and pH.[83] The composition can determine the water holding capacity (WHC), pore size and aeration of the soil, which is crucial for microbial processes and activity.[23] The content of the elements can give information on the natural predisposition and fertility of the soil. The pH can influence the NH_3 volatilisation rate, as in alkaline soil the volatilisation is enhanced (Chapter 1.2).[10] Moreover, all these factors can also influence the performance of an SNI. For example, DMP (or DMPP, respectively), has shown in various field studies unreliable efficacies in improving crop yield in neutral European soil, [84-87] but has poor efficacy in acidic soil in dry climates,[73, 82] where the nitrification inhibitory effect decreased from 45% to 39% and 23% at 10 °C, 15 °C, and 25 °C, respectively. [88] Even more concerning is the level of unpredictability that DMPP has shown in field studies, where no effect in hot-dry climates of Australia was found, clearly revealing that new solutions for these types of agricultural systems are needed.[82, 89, 90] Replacing one SNI with another is also not as straightforward as one would assume. DCD has shown to be 10 times less effective in the field and bacterial studies, making it less economical.[91] Moreover, DCD is polar and water-soluble and thus can leach into groundwater. Indeed, DCD was detected in dairy products in New Zealand. [92] Nitrapyrin is highly volatile and needs to be introduced as a gas, which makes the handling unpractical and limits its application to the cooler autumn and winter cropping cycles.[74, 75] Moreover, Nitrapyrin has shown bactericidal properties, which limits its application rate.[74, 93]

All these aspects undoubtedly indicate that new SNIs need to be developed. With the currently available knowledge about AMO, it is surprising that the development of new SNIs is still a bottleneck. There are several mechanisms by which AMO could be inhibited:

- Substrates of AMO that cannot be converted by HAO and stop the electron transfer cascade between these two enzymes.

- Mechanistic inhibitors that can irreversibly inhibit AMO through formation of covalent bonds, for example compounds with an alkyne moiety, similar to C_2H_2, but are non-hazardous.
- Lipophilic compounds that can be readily reduced and inhibit the electron flow between AMO and HOA, similar to BNIs.
- Small organic molecules with chelating properties.

In addition, new SNIs need to be non-toxic to the environment, have a good stability in various climate and edaphic conditions, and can be produced cheaply and at scale. Although the prediction of a successful SNI candidate is not possible, their value in agriculture will be tremendous once identified. Mitigating N losses includes lower fertilisation rates, less environmental pollution and preservation of biodiversity.[22]

1.8 Scope of this Thesis

This thesis will endeavour to address the following question:

"Without structural knowledge of the AMO, can better performing SNIs be developed?"

With the lack of structural information about the rate-limiting enzyme AMO the design of novel and more promising SNIs seems like an ambitious and vague aim. As outlined before, with a 50-70% fertiliser loss, N-fertilisers are doomed to remain inefficient and the need for better SNIs to mitigate N loss is obvious. Current SNIs are unpredictable and soil and climate-dependent. The more general question is whether improving current solutions without synthesising thousands of compounds and testing them in multiple soil incubation studies is feasible. To answer this question, a bottom-up approach is employed to assess SNIs more efficiently and to design and develop new SNIs based on the knowledge of the flaws in the existing compounds.

1.8.1 Chapter 2 Outline: Nitrification Assay Development with the AOB *N. europaea* and *N. multiformis* with 4,5-Disubstituted 1,2,3-Triazoles

Chapter 2 is split into two sections. Firstly, 4,5-disubstituted 1,2,3-triazoles are proposed as a new class of accessible SNI. 16 derivatives of 4,5-disubstituted 1,2,3-triazoles were synthesised with varying substitution patterns, including aliphatic, aromatic and hetero-aromatic substituted 1,2,3-triazoles. In the second part, microbiological work is performed, in which the nitrification inhibitory effect of these 4,5-disubstituted 1,2,3-triazoles was tested with pure bacterial cultures of AOB. Due to the lack of factual information in the literature, the isolation, purification and cultivation of AOB is reported in this chapter.

Moreover, an accessible, rapid and reproducible nitrification assay was developed that enables to test multiple compounds in parallel for their nitrification inhibitory properties to identify promising SNIs. The assay contains elements that challenge inhibitor-enzyme

binding, such as elevated temperature and increased pH, to mimic field conditions. However, the main purpose behind developing of the assay protocol is to keep it simple, fast and efficient, and the parameters are chosen to be performed by a non-microbiologist with minimal resources.

1.8.2 Chapter 3 Outline: Assessing the Efficacy, Acute Toxicity and Binding Modes of the Agricultural Nitrification Inhibitors 3,4-Dimethyl-1*H*-Pyrazole (DMP) and Dicyandiamide (DCD) With *N. europaea*

This chapter builds on Chapter 2. As this doctoral project aims to improve the performance of existing SNIs, an in-depth study with *N. europaea* as a representative AOB and the two commercial SNIs DMP and DCD was performed to get a deeper understanding of the biochemical parameter of existing SNIs. The study included intense microbiological studies to identify the targeted enzyme in the AMO and HAO oxidation cascade and the relative inhibitory effect of both SNIs. Furthermore, binding studies that include Michaelis-Menten Kinetics, reversibility of binding and real-time O_2 uptake kinetic studies were performed for the first time to get a detailed understanding of the mode of action of the current SNI.

1.8.3 Chapter 4 Outline: Insights into the Inhibitory Effect of 1,4-Disubstituted 1,2,3-Triazoles: A New Class of Agricultural Nitrification Inhibitors

The microbiological tests from Chapter 3 were performed with 1,4-disubstituted 1,2,3-triazoles, a new class of SNIs developed by the doctoral student *Bethany I. Taggert*. 1,4-disubstituted 1,2,3-triazoles are structurally similar to 4,5-disubstituted 1,2,3-triazoles and

have already shown excellent properties in soil. However, their mode of inhibition has never been determined with pure bacterial cultures of AOB. Therefore, an in-depth study with AOB was performed with a scope of five 1,4-disubstituted 1,2,3-triazoles with five varying substitution patterns and functional groups to identify the correlation between functional group, lipophilicity and substitution pattern with inhibitory activity. This chapter aims to connect SAR studies with the assay to compare soil incubation studies with AOB studies.

1.8.4 Chapter 5 Outline: 4-Methyl-1-(Prop-2-yn-1yl) -1*H*-1,2,3-Triazole (MPT): A Novel, Readily Accessible and Highly Efficient Nitrification Inhibitor for Agriculture

In this chapter, the attempt to inhibit the AMO irreversibly is made. Current SNIs act in a similar mode by reversibly inhibiting AMO. Therefore, it was explored whether an irreversible inhibition could overcome the soil and climate-dependent performance issues of the current SNIs entail. The synthesised compound MPT belongs to the class of 1,4-disubstituted 1,2,3-triazoles. The biochemical parameters of MPT were determined.

Moreover, MPT is the only inhibitor tested in soil incubation studies in the scope of this doctoral thesis, due to its unique mode of inhibition. During a 21-day experiment, the GHG N_2O production rate was measured to determine the efficacy of MPT to reduce nitrification in four German soil with ranging pH from 4.5─7.8. Moreover, quantitative real-time polymerase chain reaction (qPCR) studies were performed to determine the effect of MPT on the nitrifier community. In addition, due to the evolutionary similarity between AMO and pMMO, the effect of MPT was tested on the latter. Methanotrophic organisms play an essential role in scavenging the GHG CH_4, and their inhibition would be a negative outcome for MPT. To analyse the effect, CH_4 uptake data were analysed parallel to the GHG experiment in Chapter 5. Moreover, *pMMO* qPCR was performed to quantify the gene abundancies of methanotrophic organisms.

Chapter 2: Development of a Bacterial Assay for the Rapid Screening of new Nitrification Inhibitors (publication based)

2.1 Introduction

In Chapter 1.2, the main steps of nitrification were discussed. The key and rate-limiting step is the oxidation of NH_3 → NH_2OH, which is performed by AMO.[8] The subsequent oxidation of NH_2OH → NO_2^- is carried out by HAO.[8] Both enzymes are conserved in AOB. The lifetime of NO_2^- in soil is short due to the rapid oxidation of NO_2^- to NO_3^- catalysed by the enzyme NXR present in NOB.[27] Thus, loss of the substrate of nitrification (NH_4^+) and accumulation of the product of nitrification (NO_3^-) after fertilisation can give insight into the degree of nitrification in soil.[94] Conversely, when determining the efficacy of new nitrification inhibitors, both NH_4^+ and NO_3^- are key indicators to measure the nitrification inhibitory rate. The efficacy of 1,4-disubstituted 1,2,3-triazoles by Taggert *et al.* was tested in soil incubation studies over 21-28 days.[94] Mineral-N (NO_3^- and NH_4^+) was extracted from the soil periodically and quantified via Segmented Flow Analysis (SFA).[94] Figure 8 shows an exemplary mineral N profile of uninhibited soil ($(NH_4)_2SO_4$ application rate 100 mg N kg^{-1} soil (fertiliser)) and a DMP-inhibited acidic soil (pH 5.9) that contains the fertiliser in addition to the commercial inhibitor at an application rate of 5 mol% of applied N. Experimental details can be found in SI-4 (Method 3.9 Mineral-N Retention in an Australian Soil (Soil A)).

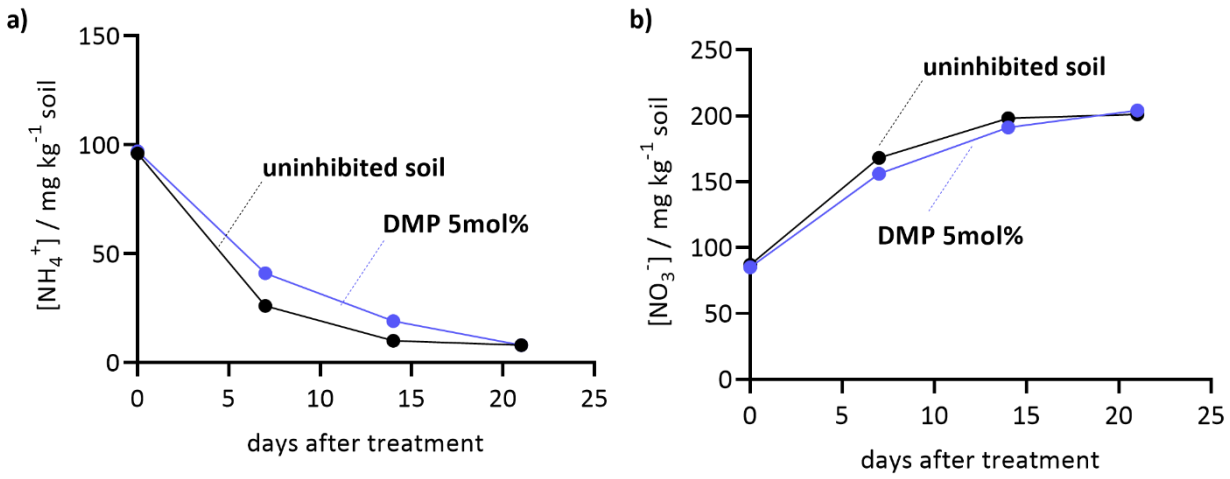

Figure 8: Measured NH_4^+-N (A) and NO_3^--N (B) concentrations over 21 days in an Australian soil (pH = 5.9) incubated at 25 °C. Detailed soil specifications are listed in SI-4 Table 4. $(NH_4)_2SO_4$ was used at an application rate of 100 mg kg^{-1} soil. DMP application rate was 5 mol% of applied N. Each concentration profile was obtained from three biological replicates.

DMP shows a delayed NH_4^+ loss compared to the 'uninhibited soil', as the NH_4^+ concentration is a direct response to the inhibition of AMO in soil microorganisms.[94] With this method inhibitor treatments can be compared within each other and/or compared to the 'gold standard' DMP with various soils and at different soil incubation studies to determine edaphic-dependent performances.

On the flip side, the soil incubations are 21-28 days, and the subsequent analysis *via* SFA is both time-consuming and expensive. Moreover, the space required for the microcosm soil incubations is also a factor that needs to be considered and becomes limiting when the number of tested inhibitors is high and multiple soils are tested at the same time with at least three replicates. Soil is a complex matrix and a mixture of various microorganisms,[95] which can be a disadvantage if one is also interested in gaining insight into the underlying biochemical processes, in this case, the mechanism of inhibition.

Therefore, the first research chapter of this doctoral thesis is dedicated to the development of a rapid screening to test the performance of SNIs and to identify the most promising compounds that can subsequently be tested in more time-demanding soil incubations. Nitrification is instantaneous that starts immediately after the addition of NH_3. However, in

soil, the rate of nitrification is controlled by the migration of NH_4^+/NH_3 as well as the SNI, which depends on the soil's physical properties.[96] Bacterial studies have been used previously to assess nitrification rate by AOB. Such setup is convenient as, due to the lack of the complex soil matrix, nitrification occurs more rapidly in pure bacterial cultures than in soil,[65] Formation of NO_2^- can be readily analysed through the colorimetric "Griess test" that is specific for NO_2^- and leads to the formation of a pink azo dye (**12**), which can be quantified photometrically at 540 nm (**Figure 9**) .[65, 97] Chemically, the colorimetric reaction is initiated by the reaction of the sulfonamide (**9**) and NO_2^- to form the diazonium salt (**10**). Subsequent azo-coupling with *N*-(1-naphthyl)ethylenediamine (**11**) gives the azo dye **12**, which can be quantified through its absorption at 540 nm. The commercially available Griess Reagent is a ready-to-use mix that contains both compounds and catalytic amounts of phosphoric acid (5 v/v%) to perform the reaction by simply adding the reagent to an NO_2^- containing liquid.

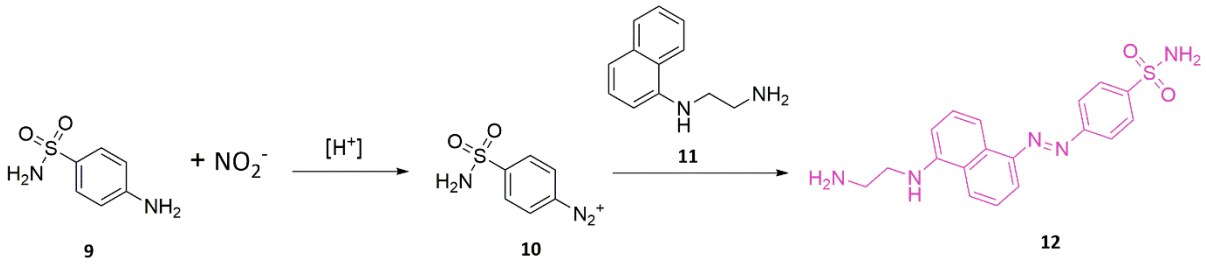

Figure 9: Reaction of Griess Reagent with NO_2^- (i.e., formed by AOB upon addition of NH_3).

As NO_2^- is the product of the AMO/HAO cascade, the concentration of NO_2^- of inhibited and uninhibited AOB can be directly compared. Due to the lack of NOB in the system, the subsequent oxidation from NO_2^- to NO_3^- is negligible. By testing the performance of potential SNI with pure bacterial cultures, the following aspects are beneficial:

- ✓ Bacterial assays can give a rapid 'inhibition' or 'no inhibition' signal in a much shorter time than soil incubation studies (minutes versus weeks);
- ✓ Bacterial assays are cheaper, need less space and can be performed under controlled conditions;
- ✓ Bacterial assays can give insight into important biochemical parameter, i.e., binding mode, mechanism of inhibition as well as toxicity.

Although these factors aid in the development and optimisation of new SNIs, soil incubation studies are still crucial. Bacterial studies represent more 'an ideal world', and soil-dependent factors and performances of SNI are neglected.

- Bacterial assays are an 'ideal world scenario' and disregard soil-dependent performance factors of potential SNIs;
- Pure bacterial studies are not always translatable to soil;
- AOA are not commercially available;

Therefore, a pipeline is suggested, in which the AOB assay is the first phase where new molecules are screened for their properties as SNI. If they show NI properties, they progress to the next phases with increasing complexity, consisting of soil incubation studies, plant studies and other agronomical studies. The advantage is that compounds that do not perform well in the assay, will not be included in soil incubation studies, and valuable resources can be saved. To make the test more representative, two strains of AOB, i.e., *N. europaea* and *N. multiformis* were employed (see Chapter 1.3). AOA are not included because they are very difficult to cultivate and are not commercially available.[47]

Surprisingly, no readily available assay protocol was reported that provided detailed information about i) cell concentration in the assay; ii) growth condition of AOB; iii) adequate inhibitor concentration vs. substrate concentration; and iv) how to screen water-insoluble inhibitors that would enable rapid and reproducible performance of the assay. Therefore, this publication comprises the optimisation of the cell growth conditions, the establishment of optimal concentration ranges for inhibitors and N-source, and the identification of compatible co-solvents to enable screening of even lipophilic organic compounds. The assay was optimized using the commercial inhibitor DMP and validated for the newly developed 4,5-disubstituted 1,2,3-triazoles.

2.1.1 Scope of Tested SNI

Apart from the commercial NIs, no structures were shown in the publication as they are still in the process of potential IP protection by the University of Melbourne. The tested

compounds were 4,5-disubstituted 1,2,3-triazoles, which were designed and synthesized in this doctoral work. Structurally, 4,5-disubstituted 1,2,3-triazoles contain one pyrrole-like N and two pyridine-like N indicated in green and blue, respectively in **Figure 10**).[98] Pyrrole-like N (indicated in green in

Figure 10) are not basic as its lone electron pair contributes to the aromatic p-system.[98] In contrast, pyridine-like N (indicated in blue in

Figure 10) have the lone pair in an sp^2 orbital that is orthogonal to the aromatic p-system and can therefore act as a weak base (pKa = 5.5).[98] In comparison, pyrazoles (like DMP) contain one pyrrole-like and one pyridine-like N (indicated in green and blue in DMP, respectively; **Figure 10**).

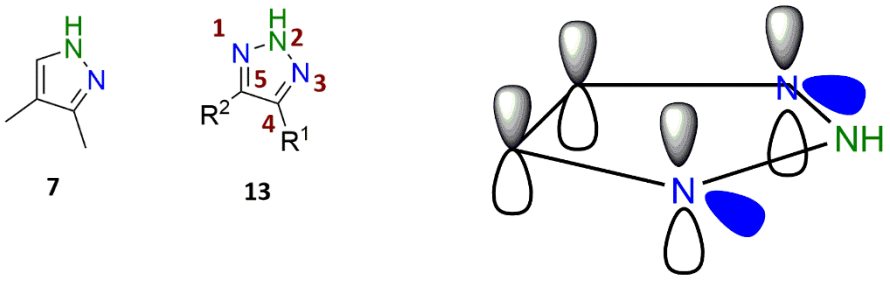

Figure 10: a) Chemistry of N in the commercial NI DMP (**7**) in comparison to the suggested new NI scaffold 3,4-disubstituted 1,2,3-triazoles (**13**). Pyrrole-like N are indicated in green. Pyridine-like N are indicated in blue. b) side view of the triazole scaffold in **13** of the π orbitals in the aromatic five-membered ring (black) and lone electron pair in orthogonal sp^2 orbital (blue). The orbitals for the pyrrole-like N (green) are not indicated for clarity.

Thus, compared to DMP, the two nucleophile N (pyrrole-like N) in 4,5-disubstituted 1,2,3-triazoles are expected to increase the probability of binding to metal centres, such as the Cu^{2+} centre in AMO (see Chapter 1.4). Furthermore, disubstituted 1,2,3-triazoles are easier synthetically accessible than pyrazoles (synthesis shown in **Figure 11**).[99]

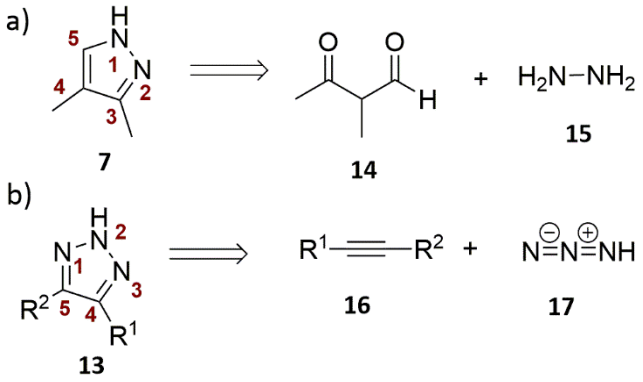

Figure 11: Retrosynthesis of a) DMP (**7**) via a 1,3-dicarbonyl (**14**) substrate and hydrazine (**15**); and b) 4,5-disubstituted 1,2,3-triazoles (**13**) are accessed via *Huisgen Sharpless* click chemistry involving an alkyne (**16**) hydrazoic acid (**17**).

Pyrazoles, such as DMP, are generally synthesised *via* Knorr-type reactions involving a 1,3-dicarbonyl (**14**) and hydrazine (**15**). The 1,3-dicarbonyl is available through a Claisen ester condensation (not shown in **Figure 11**). Any modification of the substitution pattern at positions 3, 4 and 5 of the pyrazole requires synthesis of the respective 1,3-dicarbonyl compound. On the other hand, 4,5-disubstituted 1,2,3-triazoles can be synthesised through a 1,3-dipolar cycloaddition of a 1,3-dipole (azide, **17**) and a dipolephile (alkyne, **16**). To afford *N*-unsubstituted 1,2,3-triazoles, hydrazoic acid (HN_3) would be required as the dipole. Unfortunately, because HN_3 is extremely toxic (comparable to hydrocyanic acid), explosive and has a low boiling point (39 °C), this high-energy material has not found any practical application in triazole synthesis so far.

An alternative chemical pathway to 4,5-disubstituted 1,2,3-triazoles that avoids HN_3 has been recently developed by Chai *et al.* (**Scheme 1**) [100]. The 1,3-dipolar cycloaddition step is carried out using a Julia Reagent, an aldehyde and sodium azide.

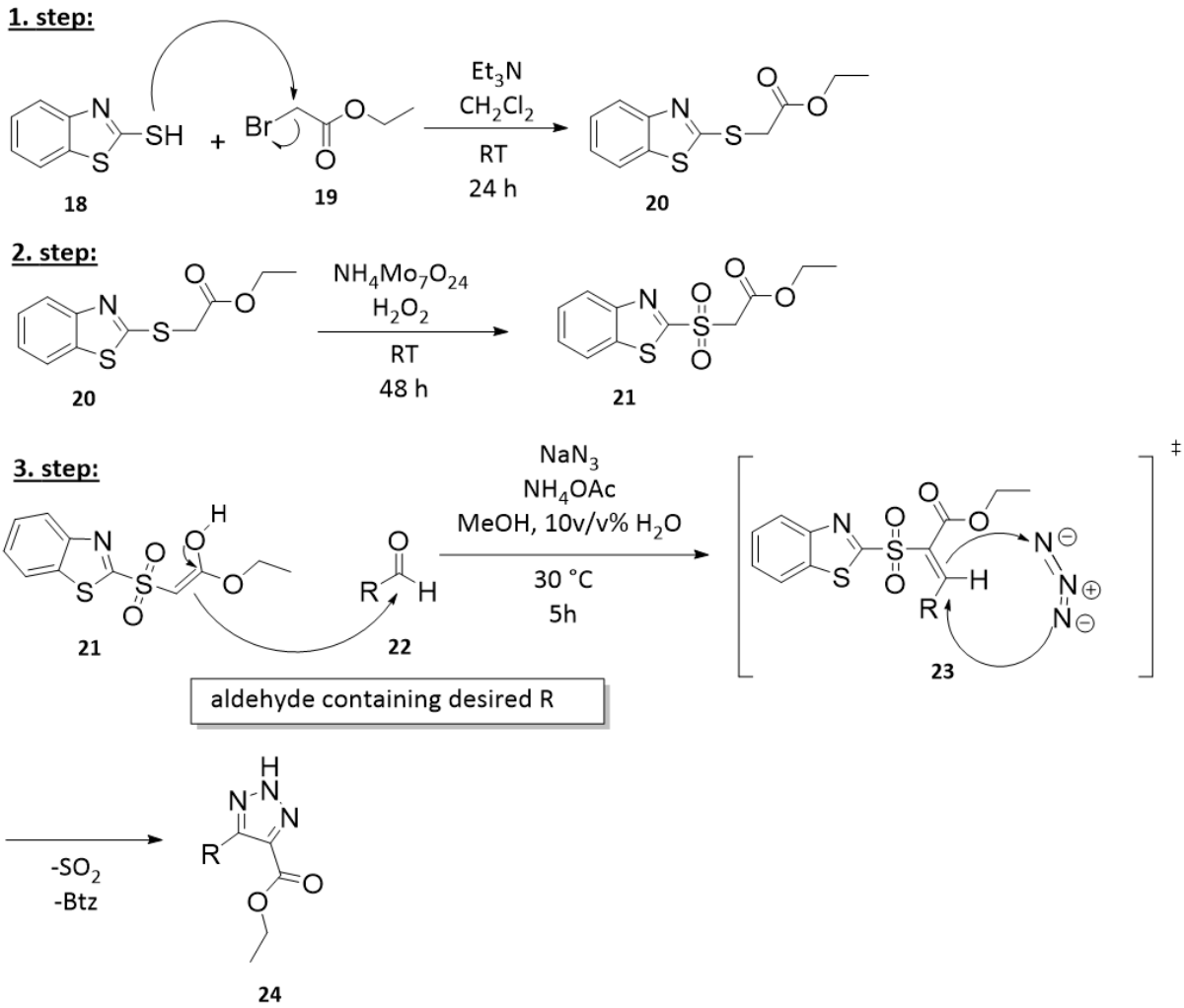

Scheme 1: Three-step synthesis of 4,5-disubstituted 1,2,3-triazoles of type **24**.[100] Starting material is mercaptobenzothiazole (**18**), which undergoes an S_N2 reaction with the α-bromo ester (**19**) to form ethyl 2-(benzothiazol-2-ylthio)acetate (**20**), followed by oxidation with ammonium molybdate and hydrogen peroxide to form the Julia reagent **21**. In step 3 the Julia reagent undergoes a Knoevenagel reaction with the desired aldehyde **22**, which is followed by a 1,3-dipolar cycloaddition involving an azide anion to give the desired 11ethyl-1,2,3 triazole-4-carboxylate derivative **24**.

The first reaction is a traditional S_N2 reaction of mercaptobenzothiazole (**18**) with *α*-bromo ethyl acetate (**19**) resulting in a quantitative yield of ethyl 2-(benzothiazol-2-ylthio) acetate (**20**)**.** The second step involves oxidation of the thio-S to a sulfonyl-S with hydrogen peroxide and ammonium molybdate to give the Julia reagent **21**.[101] The third step of the synthesis consists of a one-pot reaction where first condensation of the Julia reagent (which reacts in

its enol form) with the aldehyde (**22**) occurs, followed by the 1,3-dipolar cycloaddition of the Knoevenagel product **23** with the azide anion (N_3^-).[100, 101]

2.1.2 Synthesis of 3,4-Disubstituted 1,2,3-triazoles

The compounds tested in the publication contained an ester functional group in position 4 of the triazole scaffold (ethyl-1,2,3 triazole-4-carboxylate derivatives, see **Figure 12**) as an ester moiety should increase the lipophilicity and interaction with the bio-membrane, similar to the BNI brachialactone (**3**) (**Figure 6**).[6] Moreover, an ester group can be easily chemically modified if desired (see Chapter 2.3).

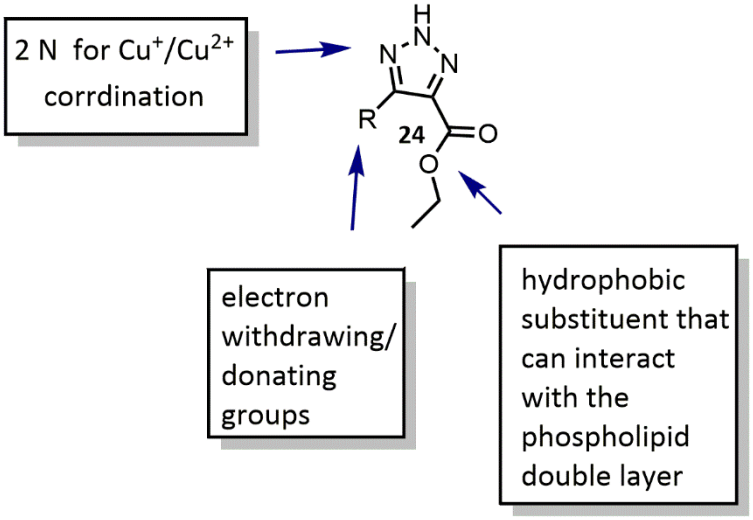

Figure 12: Potential binding of proposed 4,5-disubstituted 1,2,3-triazoles (**24**) inhibitors sites in the AMO active site.

Different substituents in position 5 of the ethyl-1,2,3 triazole-4-carboxylate scaffold were incorporated following GP1 (see Chapter 7.1.1). The substituents in position 5 can be categorised into three classes: 1. aliphatic and alicyclic, 2. aromatic and 3. heteroaromatic. The main aim was to screen for substitution patterns showing high nitrification inhibition. Therefore, a total of 16 4,5-disubstituted 1,2,3-triazoles were synthesised and tested.

2.1.2.1 Aliphatic-substituted Ethyl-1,2,3 Triazole-4-Carboxylate Derivatives

As aliphatic moieties have been shown to be oxidised to alcohols by AMO (**Figure 4**), the incorporation of an aliphatic substituent could increase the probability of inhibiting nitrification. A total of five aliphatic substituted ethyl-1,2,3 triazole-4-carboxylate derivatives were synthesised, including ethyl-, iso-propyl-, propyl-, pentyl- and cyclohexyl- substituted ethyl-1,2,3 triazole-4-carboxylate (**Figure 13**).

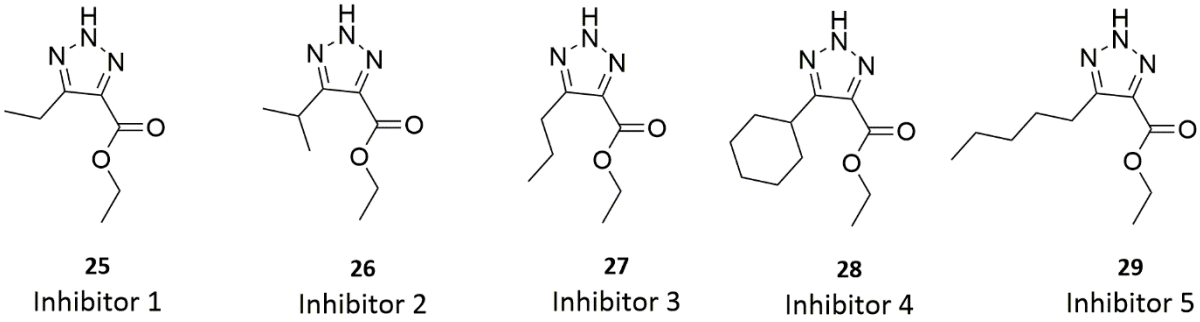

Figure 13: Position 5 aliphatic-substituted ethyl-1,2,3 triazole-4-carboxylate derivatives.

2.1.2.2 Aromatic-substituted Ethyl-1,2,3 Triazole-4-Carboxylate Derivatives

Aromatic compounds, such as benzene, have also been shown to be oxidised by AMO (**Figure 4**). A selection of 1,2,3-triazoles that contain aromatic substituents in position 5 were synthesised (**Figure 14**). The scope of aromatic substituents included halogen-, cyano-, nitro- and methoxy-substituted 1,2,3 triazole 4-carboxylate derivatives.

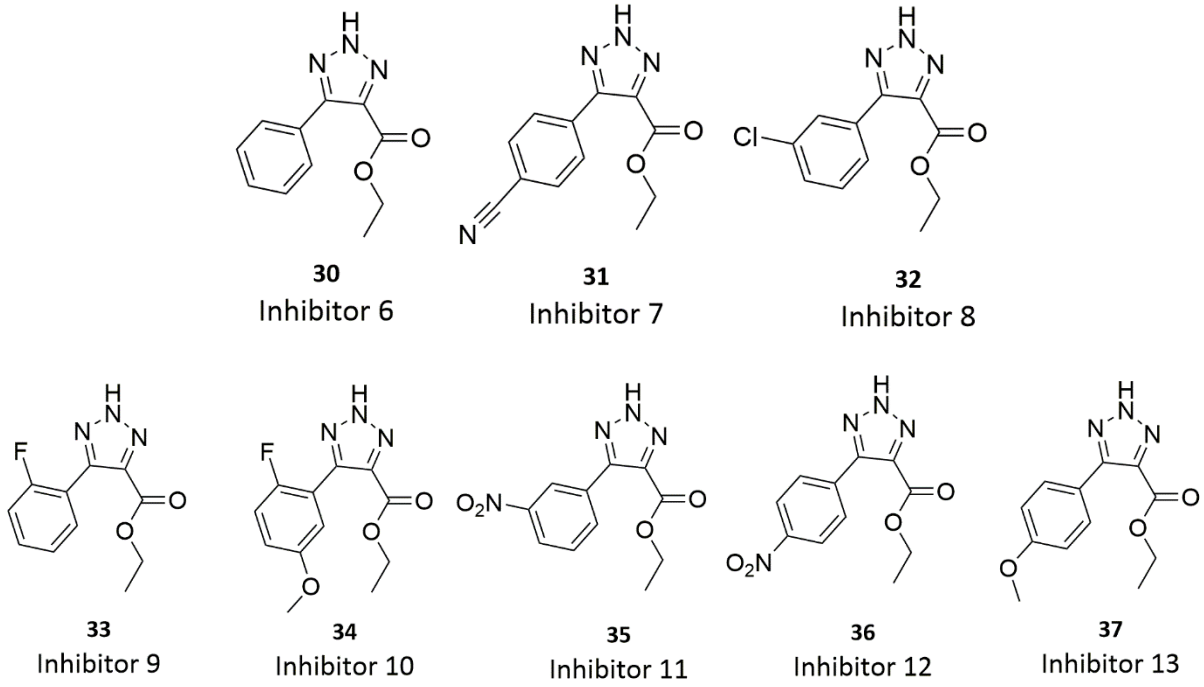

Figure 14: Position 5 aromatic-substituted ethyl-1,2,3 triazole-4-carboxylate derivatives.

2.1.2.3 **Heteroaromatic-substituted Ethyl-1,2,3 Triazole-4-Carboxylate Derivatives**

Heteroaromatic compounds could potentially inhibit the AMO by coordinating with the metal centre to form a bidentate ligand. Heteroaromatic-substituted 1,2,3-triazoles were also of interest as the heteroatoms *N* and *S* could potentially also bind to the Cu^{2+} centre of the AMO. Three heteroaromatic substituted ethyl-1,2,3 triazole-4-carboxylate derivatives were synthesised, two containing a pyridine substituent (**39** and **40**) and a thiophene moiety in 5 position of the ethyl-1,2,3 triazole-4-carboxylate scaffold (**38**) (**Figure 15**).

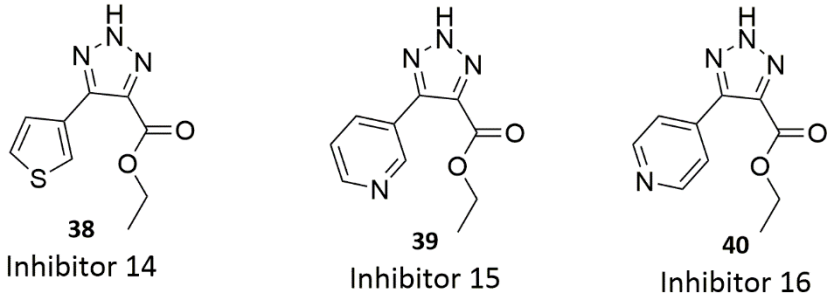

Figure 15: Position 5 heteroaromatic-substituted ethyl-1,2,3 triazole-4-carboxylate derivatives.

2.2 Rapid and Inexpensive Assay for Testing the Efficiency of Potential New SNI (publication)

ACS AGRICULTURAL SCIENCE & TECHNOLOGY

pubs.acs.org/acsagscitech Article

Rapid and Inexpensive Assay for Testing the Efficiency of Potential New Synthetic Nitrification Inhibitors

Sibel C. Yildirim, Robert M. Walker, Ute Roessner, and Uta Wille*

Cite This: *ACS Agric. Sci. Technol.* 2023, 3, 260−269 Read Online

ACCESS | Metrics & More | Article Recommendations | Supporting Information

ABSTRACT: The microbial conversion of ammonia to nitrite in soils involves three enzymatic steps. Nitrification inhibitors (NIs) are designed to inhibit ammonia monooxygenase (AMO), the enzyme performing the initial oxidation of ammonia to hydroxylamine, to mitigate excessive nitrogen fertilizer losses in agricultural systems. Because the efficiency of the current commercial NIs is highly unreliable, novel, better performing compounds need to be developed. Previously, time-consuming soil incubation studies were required as the first step to test new potential NIs. We present here a simple and cost-efficient colorimetric assay that has been developed for the rapid assessment of the efficiency of new synthetic NIs to identify the most promising compounds for subsequent soil studies. This protocol enables screening of the inhibitor activity of multiple compounds at the same time with high reproducibility and can be manipulated to determine pH and temperature-dependent effects on NIs.

KEYWORDS: *ammonia monooxygenase, ammonia oxidizers, high-throughput assay, nitrification, nitrification inhibitors*

1. INTRODUCTION

Society faces a significant challenge in providing food for an ever-growing population. According to estimates, the annual crop production needs to increase by almost 40% by 2050 to meet food needs.[1] It is common practice to use nitrogen (N) fertilizers in agricultural systems to maximize crop yield;[2−4] however, since the 1980s, the N use efficiencies (NUEs) have remained at only around 50% globally.[5−8] Ammonia (NH_3) volatilization and leaching of nitrate (NO_3^-) are major pathways for unwanted N losses from the plant/soil system, causing damaging eutrophication of surface waters and groundwater pollution. In addition, nitrification−denitrification processes can lead to the emission of the very potent greenhouse gas nitrous oxide (N_2O) into the atmosphere.

NUEs can be increased by using fertilizers amended with nitrification inhibitors (NIs).[9,10] These additives inhibit nitrifying microorganisms in the soil, such as ammonia oxidizing bacteria (AOB), that are responsible for the conversion of NH_3 to NO_3^- *via* hydroxylamine (NH_2OH), nitric oxide (NO), and nitrite (NO_2^-), thereby increasing the residence time of ammonium (NH_4^+) and reducing undesired N losses.[11−14] AOB are ubiquitous, and NIs are designed to target ammonia monooxygenase (AMO),[15,16] the key enzyme in the nitrification process, which is responsible for the initial (and rate determining) transformation $NH_3 \rightarrow NH_2OH$.[17]

Only three NIs are currently commercially used: dicyandiamide (DCD, AlzChem AG), 2-chloro-6-(trichloromethyl)-pyridine (nitrapyrin or N−Serve, Dow Chemical Co.), and 3,4-dimethyl pyrazole phosphate (DMPP or ENTEC, BASF AG) (Figure 1).[18−22] The active species in DMPP is 3,4-dimethyl pyrazole (DMP, Figure 1), but to reduce its volatility, DMP is commonly applied in agricultural systems as the phosphate salt.

The inhibitory activity of these NIs in soils depends on several factors, such as edaphic conditions, climate, and agricultural practices and varies between 4 and 8 weeks.[19,23] DMPP is the most promising commercial NI to date; however, its performance is highly variable for reasons not well understood, resulting in unreliable fertilization rates and unwanted nitrogen loss. To reliably increase NUEs in the future and reduce the adverse environmental impact of N fertilization, the development of new, more efficient nitrification inhibitor compounds is required.[24−26]

Identification of new NIs could be facilitated by performing enzymatic studies. Unfortunately, as a membrane-bound enzyme, AMO loses its activity upon isolation so that the active site's exact structure remains unknown to date.[27,28] However, it is known that copper(II) ions (Cu^{2+}) are present in the catalytic center, which bind to N atoms in adjacent histidine residues.[29−32]

Recently, we have reported substituted 1,2,3-triazoles as a new class of NIs.[33] This framework can be rapidly synthesized from readily available starting materials,[33,34] enabling access to an extensive array of compounds with different substitution patterns to allow structure−activity relationship (SAR) studies. Existing testing methods for NI activity involve time-consuming soil incubations as the first step, which is not feasible for screening large libraries of compounds. Alternative methods, for example, the segmented flow analysis to determine the NO_2^- concentration, are both costly and time-

Received: August 26, 2022
Revised: January 20, 2023
Accepted: January 27, 2023
Published: February 20, 2023

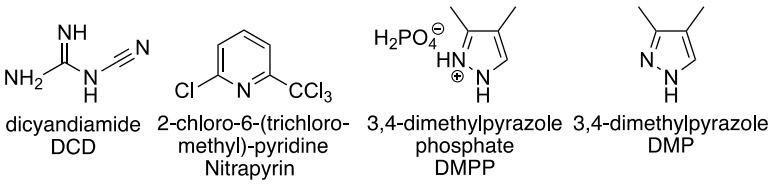

Figure 1. Commercially available nitrification inhibitors (NIs).

consuming,[35,36] whereas measurements of oxygen consumption, which have been used to determine oxygenase activity, require specialized instrumentation and are also not suitable for high-throughput screening.[37,38]

There is a pressing need for an assay that allows to rapidly test the activity of a library of new compounds to speed up the development of more efficient NIs. The assay should not only be fast but also robust and easy to set up so that the person synthesizing the inhibitor compounds (usually a synthetic organic chemist) could ideally perform the assay without having to acquire in-depth microbiological skills first. Several assays are already available that enable monitoring of nitrification processes. For example, a bioluminescence assay with *Nitrosomonas europaea* (*N. europaea*) has been developed for the detection of nitrification inhibition in wastewater[39] or to monitor biological nitrification inhibition (BNI).[40] However, this method requires DNA manipulation, which needs specialized training and equipment. Grundlitz and Dahlhammar developed a *Nitrosomonas*-based assay to determine nitrification inhibition in wastewater-treatment plants,[41] which uses the Berthelot reaction[42] to monitor the consumption of NH_3 over several hours. In this work, we present a fast, robust, and readily accessible colorimetric assay that uses the Griess reaction[43] to determine the amount of NO_2^- formed. Our assay has been developed using *N. europaea* and *Nitrospira multiformis* (*N. multiformis*) cultures and requires only minimal instrumentation. This assay is based on the recently reported assay by O'Sullivan et al., which was developed to assess BNI activity but requires monitoring of nitrification over a 9 h time window.[44] Our assay enables screening of nitrification inhibition of an extensive library of both hydrophilic and lipophilic compounds at the same time within only 60 min. The assay can be executed at different temperatures and pH and can be also used to determine the IC_{50} values and the mode of inhibition (*i.e.*, reversible or irreversible), which allows identification of the most promising inhibitors that could subsequently be further tested in more elaborate soil incubation, glass house, and field studies.

2. MATERIALS AND METHODS

2.1. Chemicals. The potential NIs explored in this work had a heteroaromatic framework possessing aliphatic or aromatic substituents, which were prepared from starting materials obtained from Sigma-Aldrich. The Griess reagent was obtained from Sigma-Aldrich and the Gram stain kit from Merck. DMP (3,4-dimethyl-1*H*-pyrazole) and DCD were supplied by Incitec Pivot Ltd., Australia. *N. multiformis* was isolated from an aquarium kit mixture as described below. *N. europaea* (ATCC19718) was purchased from the American Type Culture Collection.

2.2. Cell Preparation. *2.2.1. Isolating Ammonia Oxidizing Bacteria (AOB).* *N. multiformis* was isolated from an aquarium kit mixture (Aquasonic, BIO-NATURE STANDARD) through the extinction via a dilution method, as reported by Utåker et al.[45] Cultures were grown at 26 °C and 120 rpm in 12 tubes (polycarbonate) in subsequent dilutions of inoculum/media of 1:1000. Purification of AOB was achieved using the highest dilution level of most probable number tubes in liquid ammonium medium (German Collection of Microorganisms and Cell Cultures GmbH (DMSZ), 1583. MEDIUM FOR AMMONIA OXIDIZING BACTERIA), as indicated by acidification (phenol red) and NO_2^- production (determined via the Griess reagent).[46] The DMSZ medium contained (per L of Milli-Q water) NH_4Cl (535 mg), KH_2PO_4 (54 mg), KCl (74 mg), $MgSO_4 \times 7\ H_2O$ (49 mg), $CaCl_2 \times 2\ H_2O$ (147 mg), and NaCl (584 mg), in which 1 mL of trace element solution and 2 mL of phenol red solution were added. The trace element solution contained (per 975 mL of Milli-Q water) 1 M HCl (25 mL), $MnSO_4 \times 4\ H_2O$ (45 mg), H_3BO_3 (49 mg), $ZnSO_4 \times 7\ H_2O$ (43 mg), $(NH_4)_6Mo_7O_{24} \times 4\ H_2O$ (37 mg), $FeSO_4 \times 7\ H_2O$ (973 mg), and $CuSO_4 \times 5\ H_2O$ (25 mg). The stock phenol red solution contained 50 mg of phenol red in 100 mL of water and was used over three months. The pH was adjusted to pH 7.8 using a sterile aqueous $NaHCO_3$ (10%) solution. The cultures were checked regularly for heterotrophic contamination by inoculation on 100% strength Luria broth (LB) plates containing 15 g L^{-1} technical grade agar (BD Difco Agar, Technical, Fisher Scientific). Further contamination through air was prevented by reinoculation to sealed vessels. After several successful subcultures (at least 10), cells were harvested and analyzed through 16S rRNA sequencing.

2.2.2. Growing AOB. AOB were grown for 3−5 d in amber-colored Duran glass bottles (1 L volume, base-treated, for example, with Extran, and autoclaved) containing 600 mL of mineral salt media (MSM, see below) at 100 rpm and 30 °C in the dark. The slightly loose cap was sealed with an O_2 permeable membrane to ensure aeration (Breathe-Easy sealing membrane, Sigma-Aldrich). The MSM media contained the main bulk medium and consisted of K_2HPO_4 (2.27 g L^{-1}), KH_2PO_4 (0.95 g L^{-1}), and $(NH_4)_2SO_4$ (0.67 g L^{-1}). The pH was adjusted to 7.0 (appropriate for growing AOB[47]). This bulk medium is autoclavable and can be stored in the dark at 4 °C for up to six months. To 1 L of the bulk medium, 2 mL of a filter-sterilized (0.2 μm millipore filter) solution of metals was added: Na_2EDTA (6.37 g L^{-1}), $ZnSO_4 \times 7\ H_2O$ (1.0 g L^{-1}), $CaCl_2 \times 2\ H_2O$ (0.5 g L^{-1}), $FeSO_4 \times 7\ H_2O$ (2.5 g L^{-1}), $NaMoO_4 \times 2\ H_2O$ (0.1 g L^{-1}), $CuSO_4 \times 5\ H_2O$ (0.1 g L^{-1}), $CoCl_2 \times 6\ H_2O$ (0.2 g L^{-1}), $MnSO_4 \times H_2O$ (0.52 g L^{-1}), and $MgSO_4 \times 7\ H_2O$ (60.0 g L^{-1}). The filter-sterilized metal solution can be kept in the dark for up to one year. To this media solution, 1 v/v% of aqueous Na_2CO_3 (50 g L^{-1}) was added aseptically as a carbon source[48,49] at the start of the cell culturing process. Both *N. europaea* and *N. multiformis* grow successfully in this medium.

2.2.3. Standard Protocol for Harvesting Cells. When showing turbidity and reaching an OD_{600} of 0.1, which corresponds to the mid-exponential growth phase and an NO_2^- production of approximately 800 μM (determined by Griess assay), cells were harvested by filtration (in 200 mL batches) through nucleopore 0.2 μm membrane filters (Rowe Scientific, mixed cellulose esters (MCE)). The cells were washed with sodium phosphate buffer (NaPB, 0.1 M, 2 × 100 mL, pH = 7.5) containing magnesium sulfate (0.2 mM). The filter paper with the cells was transferred into a sterile 50 mL tube, and the cells were washed off by resuspending in NaPB (15 mL), followed by 5 s of vortexing (Ratek, Australia) and 3 s of sonication (Vevor, Australia). The inoculum had an OD_{600} of 0.9−1.2, which was diluted to OD_{600} = 0.03 and stored at 4 °C until used for the assay (cells could be stored for up to 24 h without losing activity).

2.2.4. Cell Preparation for the Nitrification Assay at pH = 8.0. Cells were harvested according to Section 2.2.3, except that they were

https://doi.org/10.1021/acsagscitech.2c00229
ACS Agric. Sci. Technol. 2023, 3, 260−269

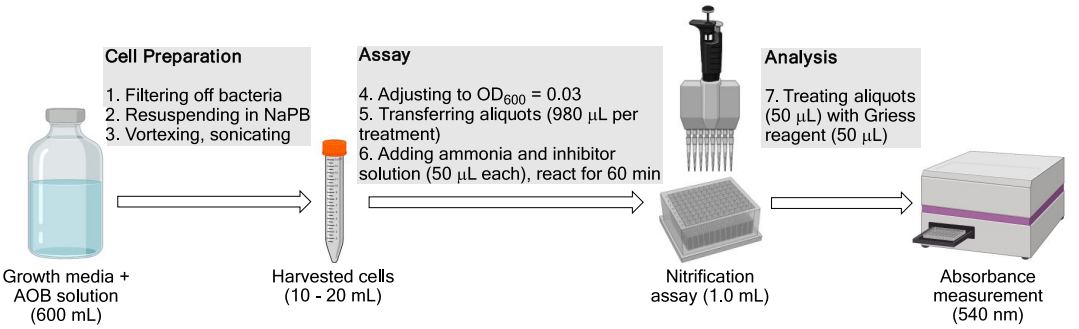

Figure 2. Schematic overview of the nitrification assay protocol developed in this work. Bacteria in 600 mL of growth media were grown in a 1 L Duran glass bottle. The assay was performed in a 96-well plate at the desired pH and temperature for 60 min. An aliquot of 50 μL was transferred to a 96-well spectrophotometric plate, 50 μL of Griess reagent was added, and the absorbance at 540 nm was measured. NaPB = sodium phosphate buffer (Figure made with BioRender).

washed with NaPB with a pH of 8. The membrane filter paper was then cut aseptically into two equal pieces. One piece was resuspended in NaPB at pH = 8, and the second half was suspended in the standard NaPB at pH = 7.5 to allow for running inhibitor tests at pH = 7.5 simultaneously as a control experiment.

2.2.5. Cell Preparation for the Nitrification Assay at 38 °C. Cells were harvested according to Section 2.2.3. The membrane filter paper was then cut aseptically into two equal pieces to allow simultaneous conduction of inhibitor tests at 38 and at 30 °C as a control experiment. Cells needed to be equilibrated for 10 min at the respective temperature to assure homogeneous temperature distribution during the assay.

2.3. Nitrification Assay and Analysis. *2.3.1. Standard Assay Protocol.* In a deep 96-well plate (2 mL capacity), 980 μL of the bacterial inoculum (OD_{600} = 0.03 in NaPB at pH 7.5 was added to the inhibitor (10 μL, 30 mmol L^{-1} in DMSO), and the solutions were mixed thoroughly and preincubated in the dark for 5 min at 100 rpm and at 30 °C (Ratek, Australia). $(NH_4)_2SO_4$ (10 μL, 150 mM, from a prepared sterile solution containing 19.8 g L^{-1} $(NH_4)_2SO_4$ in Milli-Q water) was then added using a multichannel pipette. The plate was covered with an O_2 permeable membrane to ensure aeration (Breathe-Easy sealing membrane, Sigma-Aldrich) and incubated in the dark for 60 min at 30 °C and 100 rpm. Nitrification was stopped by adding an excess of DMP (10 μmol L^{-1}, 30 mM; the final concentration of DMP in the solution was 0.27 mM, which was 45 times higher than the determined IC_{50abs} value). An aliquot of the reaction solution (50 μL) was transferred to a 96-well spectrophotometric plate (Greiner Cellstar, polystyrene) to which 50 μL of Griess reagent was added. The color was allowed to develop for 15 min at room temperature, and the absorbance was measured at 540 nm (Clariostar BMG Labtech, Australia) (schematic details are shown in Figure 2). Each assay was accompanied by control treatments to determine the 0 and 100% NO_2^- signals. The percentage inhibition was calculated according to eq 1 from the NO_2^- production of the cells in NaPB with 1 v/v% dimethyl sulfoxide (i) without any additive ("untreated cells": 0% signal), (ii) with $[NH_4^+]$ = 3 mM ("uninhibited cells": 100% signal), and (iii) with $[NH_4^+]$ = 3 mM and [inhibitor] = 0.3 mM (10 mol % of $[NH_4^+]$, 'inhibited cells').

$$\%\ \text{inhibition} = \left[1 - \frac{[NO_2^-]_{\text{inhibited cells}} - [NO_2^-]_{\text{untreated cells}}}{[NO_2^-]_{\text{uninhibited cells}} - [NO_2^-]_{\text{untreated cells}}}\right] \times 100 \quad (1)$$

2.3.2. Screening of Organic Cosolvents. Cells were harvested according to Section 2.2.3. In a deep 96-well plate (2 mL capacity), 10 μL of the respective solvent (*i.e.*, dimethyl sulfoxide (DMSO), methanol, ethanol, 1-propanol, acetone, acetonitrile, ethyl acetate, sulfolane and glycolic acids) was mixed thoroughly with 980 μL of the bacterial inoculum (OD_{600} = 0.03 in NaPB at pH 7.5) and preincubated in the dark for 5 min at 100 rpm and 30 °C. The inhibition assays were performed as described in Section 2.3.1.

2.3.3. Photometric Determination of the Solubility of Inhibitor Compounds. Two solutions with 30 and 300 mM of inhibitor in DMSO were prepared. The 1 v/v% mixture consisted of 990 μL of NaPB buffer (pH 7.5) and 10 μL of the 30 mM inhibitor solution. The 0.1 v/v% mixture was made from 999 μL of NaPB and 1 μL of the 300 mM inhibitor solution. UV/vis spectra (in the range of 200–650 nm) were recorded and corrected by the blank spectra that contained only NaPB with 1 v/v% DMSO or 0.1 v/v% DMSO, respectively.

Four concentrations of inhibitor 4 were prepared in DMSO (30, 50, 100, and 300 mM). The 1 v/v% mixture consisted of 990 μL of NaPB and 10 μL of a 30, 50, 100, and 300 mM inhibitor solution. Full spectra were measured and deducted by the blank spectra containing only NaPB in 1 v/v% DMSO.

2.3.4. Determination of IC_{50} Values. The assay was performed according to Section 2.3.1 using *N. europaea* as an AMO source. DMP was tested at concentrations of 6 mmol L^{-1}, 0.6 mmol L^{-1}, 0.3 mmol L^{-1}, 0.15 mmol L^{-1}, 75 μmol L^{-1}, 37.5 μmol L^{-1}, 18.8 μmol L^{-1}, 9.4 μmol L^{-1}, 4.7 μmol L^{-1}, 2.3 μmol L^{-1}, and 1.2 μmol L^{-1}; for DCD, 6 mmol L^{-1}, 3.0 mmol L^{-1}, 1.5 mmol L^{-1}, 0.75 mmol L^{-1}, 0.38 mmol L^{-1}, 0.18 mmol L^{-1}, 94 μmol L^{-1}, 47 μmol L^{-1}, 23 μmol L^{-1}, and 12 μmol L^{-1}; and for Inhibitor 4, 3.0 mmol L^{-1}, 1.5 mmol L^{-1}, 0.6 mmol L^{-1}, 0.3 mmol L^{-1}, 0.15 mmol L^{-1}, 50 μmol L^{-1}, and 25 μmol L^{-1}. The inhibitor concentration at which the inhibition was 50% (IC_{50abs}) was determined by fitting the $\log_{10}$ of the concentration (in μmol L^{-1}) against the response. IC_{50abs} was obtained by normalizing the response against cells in NaPB with 1 v/v% DMSO and $[NH_4^+]$ = 3 mM (uninhibited cells; 100% signal) and cells in NaPB with 1 v/v% DMSO without additives (untreated cells; 0% signal). The curves were plotted with GraphPad prism (version 9.0) to determine IC_{50abs} via a variable slope fit (three parameters).

2.4. Statistics. Statistical analysis was performed with the software package Minitab 18[50] using $P < 0.05$ as the level of statistical significance. All results were reported as mean ± standard error of the mean. In addition, significances among three treatments were compared by the least significant difference $P < 0.05$ level using one-way ANOVA.

3. RESULTS AND DISCUSSION

While many protocols for growing and isolating AOB have been developed, their focus has mainly been on enabling the identification of substrates for this enzyme and exploring the mechanism of their transformation.[51−54] As all of these experimental setups require specialized equipment and extensive training in microbiology, these assays are essentially inaccessible for other scientists who aim to develop more efficient NIs and require a rapid screening tool to identify potential new inhibitors from large libraries of compounds.

https://doi.org/10.1021/acsagscitech.2c00229
ACS Agric. Sci. Technol. 2023, 3, 260−269

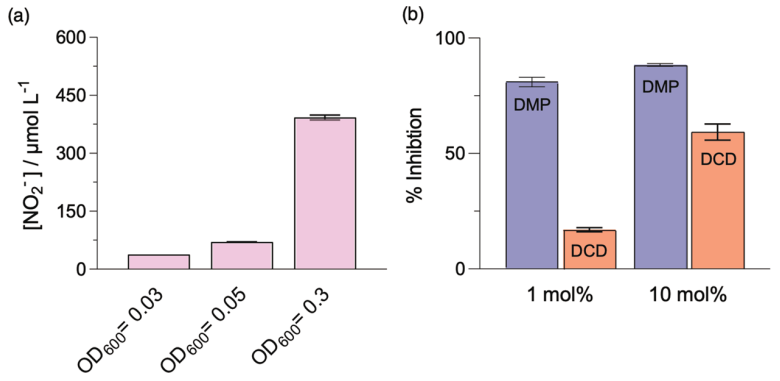

Figure 3. (a) Effect of the *N. europaea* cell concentration (represented as OD_{600}) on the NO_2^- production after 60 min of inoculation. (b) Nitrification inhibition of *N. europaea* by DMP and DCD at two different concentrations after 60 min of inoculation (OD_{600} = 0.03). The inoculations were performed with $[NH_4^+]$ = 3 mM in NaPB (pH = 7.5) at 30 °C and 100 rpm in the dark. [DMP] and [DCD] in panel (b) were 0.03 mM and 0.3 mM (1 and 10 mol % of $[NH_4^+]$), respectively. Standard errors were calculated from three biological replicates and three technical replicates.

One overarching assay requirement was that its setup and data analysis should be simple, robust, and fast. Because of the ubiquitousness of AOB, the inhibitory activity of the various new compounds needs to be assessed with different AOBs. We have used *N. europaea*, which was purchased as a pure bacterial culture, and *N. multiformis*, which was cultured and isolated from an aquarium starter kit. The inhibitory activity was determined from the production of NO_2^- through the colorimetric reaction with the Griess reagent, which leads to the formation of a pink-colored azo dye with an absorption maximum at λ = 540 nm. Figure 2 shows the assay protocol developed in this work.

In the following, we will first describe the cultivation and growth of AOB and the development of the assay, followed by the optimization and validation of the assay using commercial NIs and an evaluation of the performance of a selection of potential new NIs.

3.1. Cultivating and Growing AOB. *3.1.1. Isolating N. multiformis Bacterial Cells from an Aquarium Starter Kit.* *N. multiformis* was isolated from an aquarium kit mixture (Aquasonic, BIO-NATURE STANDARD) through the extinction via a dilution method, as reported by Utåker et al.[45] As AOB can form partnerships with other microbes, which challenges their isolation,[55] the cultures were checked regularly for heterotrophic contamination by inoculating an aliquot of bacterial solution on solid heterotrophic media (details are given in Section 2.2.1). Further contamination through air was prevented by reinoculation to sealed vessels. Unfortunately, a Gram-positive contaminant was persistent, which was eliminated by inoculating the growth medium containing the mixed culture with penicillin (5000 U, 1000× diluted), which specifically targets Gram-positive bacteria. After repeated subculturing (five times), the complete elimination of the contaminant was confirmed by light microscopy using the Gram-staining procedure following the manufacturer's guidelines. After at least 10 successful subculturing cycles, cells were harvested and analyzed by comparing the partial sequence of the 16S rRNA gene against the NCBI 16S database.

3.1.2. Growing AOB. Growing AOB can be challenging as these bacteria are not only prone to microbial contamination but also sensitive to temperature changes and light exposure.[56] Frozen stock cultures were prepared from 10% glycerol solutions (stock solutions with a higher glycerol content could not be revived). The cells were regularly monitored for contaminants by inoculating on heterotrophic media, such as full-strength Luria broth (LB) agar on which the autotrophic AOB cannot grow. Thus, any growth indicates the presence of heterotrophic impurities, and the solution needs to be discarded (this point was generally reached after the 20th subculture).

The bacterial growth was monitored daily by measuring $[NO_2^-]$ through the Griess reaction. Subculturing was initiated when the solution became turbid and reached an optical density of OD_{600} = 0.1 ± 0.005, corresponding to $[NO_2^-]$ of 800 ± 50 μM, which is in the mid-exponential growth phase (after three to five days). The subcultures containing 10 mL of inoculum were transferred to 600 mL of a freshly prepared MSM growth medium. The assay cell concentrations were determined *via* their optical density at 600 nm (OD_{600}), which is proportional to the protein concentration and reproducible when the cells were harvested after 3 d as described in Section 2.2.3. (see Section 2, Table S2, and Figures S3 and S4 in the SI).

3.2. Assay Development. *3.2.1. Optimizing the Conditions.* The assay depends on three interrelated variables, which required optimization to ensure reproducible performance: (i) AOB cell concentration, (ii) NH_4^+ concentration, and (iii) inhibitor concentration. The cell concentration needed to be sufficiently high to observe the formation of NO_2^-, whereas a too high concentration of active cells could mask the inhibitory effect. Likewise, $[NH_4^+]$ needed to be in a range that ensured a detectable production of NO_2^-. Finally, the inhibitor concentration had to be at a level that clearly enabled differentiation of the inhibitory activity of different (potential) NIs without completely inhibiting nitrification. These three concentration variables were optimized such that the colorimetric $[NO_2^-]$ determination could be performed directly without diluting the sample, as this would require additional time. It should be noted that the linear absorbance/concentration section of the Griess reagent can vary depending on the supplier and can be determined via a standard curve.

All initial screening experiments were performed with *N. europaea*. To assess the NO_2^- production as a function of cell concentration, the concentrated inoculum obtained from the cell harvesting process was diluted to create samples with

https://doi.org/10.1021/acsagscitech.2c00229
ACS Agric. Sci. Technol. 2023, 3, 260−269

different cell concentrations, as characterized by OD_{600} values of 0.3, 0.05, and 0.03. Each of these samples was pipetted in triplicates into a 96-well plate. $(NH_4)_2SO_4$ (from a stock solution containing 150 mM in NaPB at pH 7.5) was added in 1 v/v% to each sample using a multichannel pipette to ensure simultaneous addition in each well, as the nitrification process commences immediately after NH_4^+ is supplied. The final $[NH_4^+]$ in each well was 3 mM, which was close to $[NH_4^+]$ in the MSM and close to the enzyme saturation point (Table S3). The well plate was covered with a breathable membrane and incubated in the dark for 60 min at 30 °C and 100 rpm. Nitrification was stopped by adding an excess of DMP, after which an aliquot was transferred to a 96-well spectrophotometric plate, and the Griess reagent was added. The color was allowed to develop for 15 min at room temperature, and the respective absorbance was measured at 540 nm.

Figure 3a shows that, under these conditions, the NO_2^- production was linearly proportional to OD_{600} and, therefore, the cell concentration. Thus, for the sample with OD_{600} = 0.3, $[NO_2^-]$ was 392.3 ± 7.7 μmol L^{-1}. For the 6-fold diluted sample with OD_{600} = 0.05, $[NO_2^-]$ was with 70.1 ± 1.0 μmol L^{-1}, about one-sixth, whereas the 10-fold diluted sample with OD_{600} = 0.03 showed only one about a tenth of NO_2^- production (42.9 ± 1.8 μmol L^{-1}).

It should be noted that the most concentrated sample (OD_{600} = 0.3) needed to be diluted before the reaction with the Griess reagent, as otherwise the amount of NO_2^- produced in the undiluted sample was outside the linear absorbance/concentration behavior. Pleasingly, with a cell concentration of OD_{600} = 0.03, not only a distinct and reproducible amount of NO_2^- was produced after 60 min but the same cell concentration could also be used for assays with *N. multiformis*, which is more reactive than *N. europaea*.[38] Indeed, under otherwise identical conditions, *N. multiformis* at OD_{600} = 0.03 produced 62.5 ± 0.2 μmol L^{-1}, 50% more of NO_2^- than *N. europaea* (Table S4), clearly confirming the sensitivity of the assay setup.

The commercial NIs DMP and DCD were used to identify the optimum inhibitor concentration that was sufficiently sensitive to reveal the known different inhibitory performance of DMP and DCD without completely inhibiting nitrification, and which could subsequently be used to assess new NI compounds. Figure 3b shows the results of an assay performed with *N. europaea* and [DMP] or [DCD] = 0.03 mM (1 mol % of NH_4^+). The % inhibition was calculated according to eq 1. Under these conditions, nitrification inhibition by DMP was 81.4 ± 2.9%, which is very high, whereas that by DCD was considerably lower (16.9 ± 1.3%) (P < 0.005 for both compounds). Using a 10-fold higher inhibitor concentration (0.3 mM, 10 mol % of $[NH_4^+]$), the % inhibition by DMP increased slightly by about 10% to 88 ± 0.8%, suggesting that enzyme saturation with DMP was nearly reached. The inhibition by DCD increased by a factor of about 3.5 to 59.3 ± 5.0%, which not only confirms that higher application rates of DCD are required to achieve considerable nitrification inhibition[44,57,58] but also demonstrates the sensitivity of our assay.

3.2.2. Optimizing the Assay for Water-Insoluble NIs. Both DCD and DMP are water-soluble NIs, which is advantageous for the aqueous assay conditions. However, a high water-solubility is not necessarily beneficial for agricultural applications since the NI could leach into the groundwater, as is the case with DCD.[59] Increasing the lipophilicity of the inhibitor compounds to some extent could potentially increase their retention in soils. However, the reproducibility of the assays was significantly hampered by a low solubility of some of the newly synthesized compounds in the aqueous buffer, and we therefore explored whether the solubility could be increased by adding a small amount of an organic cosolvent without negatively impacting on the AMO activity.

Analysis of the UV/vis absorbance revealed that the new inhibitor compounds could be completely dissolved in NaPB with 1 v/v% of dimethyl sulfoxide (DMSO), methanol, ethanol, 2-propanol, and 1-butanol, acetone, acetonitrile, ethyl acetate, and sulfolane and glycolic acids (details are provided in "Optimizing the Assay for Water-Insoluble NIs" in the SI).

As hydrophobic organic solvents can accumulate in cell membranes leading to their disruption,[60] the toxicity of the organic cosolvents for the bacterial cells was assessed by determining the amount of NO_2^- produced using *N. europaea* in NaPB containing 1 v/v% of the cosolvent relative to that produced by the bacteria in pure NaPB. The data in Figure 4

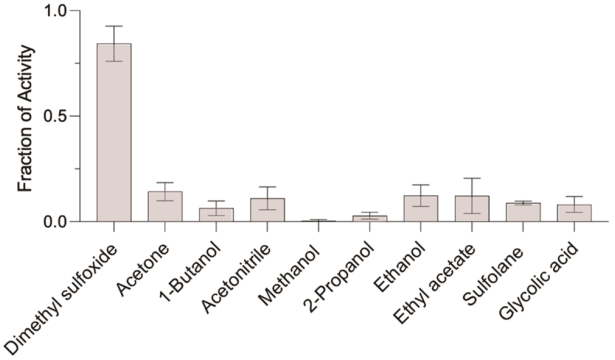

Figure 4. Effect of various organic solvents (1 v/v%) on the NO_2^- production, determined from a pure culture of *N. europaea* in NaPB at pH = 7.5 ($[NH_4^+]$ = 3 mM, 30 °C, 100 rpm in the dark). The fraction of activity was determined from the NO_2^- production in NaPB with 1 v/v% cosolvent relative to that in the absence of the cosolvent. Standard errors were calculated from three replicates.

reveal that 1 v/v% of DMSO was the only cosolvent that kept the cells almost fully functioning, as revealed by the NO_2^- production, which decreased by only 16% in comparison to the aqueous solution. All other cosolvents led to a dramatic reduction of the NO_2^- production, indicating that, at a concentration of 1 v/v%, these solvents are detrimental to the functioning of the bacteria. The nearly complete inhibition of *N. europaea* in the case of methanol as a cosolvent could be rationalized by the fact that methanol is a known substrate for AMO, which undergoes oxidation to formaldehyde.[61]

3.3. Screening of Inhibitors. The optimized assay conditions were used to screen the performance of 16 potential NIs, all of which possessed a heterocyclic framework with different substituents (aromatic and aliphatic motifs), as shown in Table 1. It should be noted that the intention of these experiments was not to identify the best inhibitor compounds from this pool but to demonstrate the sensitivity of the assay to tease out the impact of structural variations on the inhibitory activity.

3.3.1. Standard Conditions. The assay was performed with *N. europaea* at pH = 7.5 and 30 °C with the inhibitors being applied at 0.3 mM (10 mol % of $[NH_4^+]$). The percentage

https://doi.org/10.1021/acsagscitech.2c00229
ACS Agric. Sci. Technol. 2023, 3, 260−269

Table 1. Overview of the NI Structures Tested in the Assay

inhibitor ID	structure
inhibitors 1−5	1,2,3-triazoles with linear, branched and cyclic alkyl (C2−C6) substituents
inhibitors 6−13	1,2,3-triazoles substituted with aromatic rings
inhibitors 14−16	1,2,3-triazoles substituted with heteroaromatic rings

inhibition was calculated according to eq 1. Detailed data are provided in Table S5.

Figure 5 reveals that, of the set of compounds tested, those possessing aromatic substituents exhibit the highest inhibitory

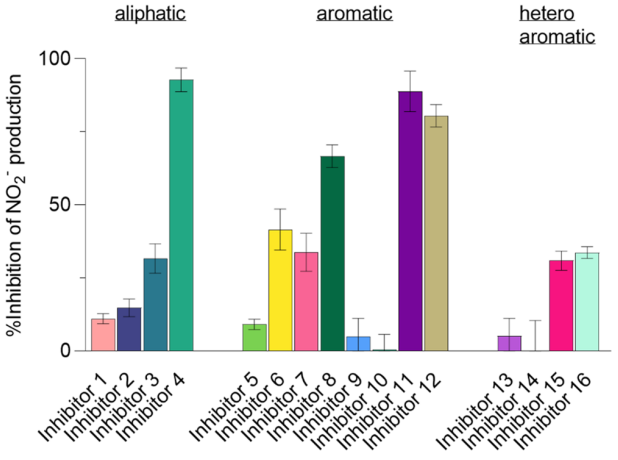

Figure 5. Effect of the potential NI structure on the nitrification inhibition, determined using *N. europaea*. The incubations in NaPB with 1 v/v% DMSO were performed at pH = 7.5 and 30 °C with $[NH_4^+]$ = 3 mM and [inhibitor] = 0.3 mM (10 mol % of $[NH_4^+]$) at 100 rpm for 60 min in the dark. Standard errors were determined from three biological and three technical replicates.

effect overall, with more than half showing a % inhibition above 30%.

In comparison, all compounds with heteroaromatic substituents inhibit nitrification with less than 50% efficiency. Likewise, apart from inhibitor 4, compounds possessing aliphatic substituents are generally less-efficient nitrification inhibitors.

The best performing NIs from this screening experiment were subsequently used to compare the % inhibition in dependence of the AMO source. The data are shown in Figure 6, confirming that *N. europaea* responds to NIs with a higher sensitivity than *N. multiformis*.[44,54] For example, the % inhibition by inhibitor 8 dropped from (67 ± 6)% with *N. europaea* to (50 ± 16)% with *N. multiformis* (Table S6).

Inhibitor 4 shows a very high inhibition (92%) when *N. europaea* is used as an AMO source, whereas *N. multiformis* suggests a lower inhibitory effect of this compound than of inhibitor 8. We point out that it is not the aim of this work to explore why the inhibitory efficacy is not uniformly "scaled down" in going from *N. europaea* to *N. multiformis*, but it is obvious from our data that the assay provides a tool to detect such behavior, which could trigger further research into the mechanism of nitrification inhibition by these two AMOs.

3.3.2. Variation of the Assay Temperature. As soil conditions vary considerably, we have explored whether the

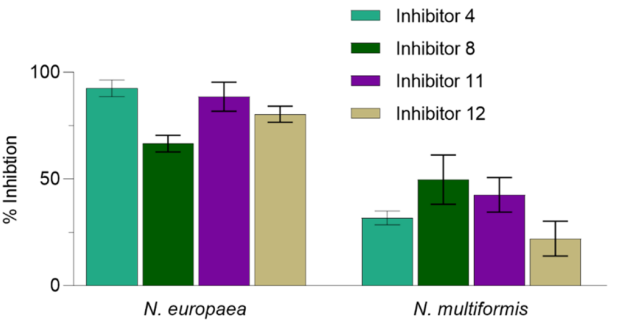

Figure 6. % Inhibition determined for inhibitors 4, 8, 11, and 12 with *N. europaea* and *N. multiformis*. Incubation in NaPB with 1 v/v% DMSO was performed at pH = 7 and 30 °C with $[NH_4^+]$ = 3 mM and [inhibitor] = 0.3 mM (10 mol % of $[NH_4^+]$) at 100 rpm for 60 min in the dark. Standard errors were determined from three biological and three technical replicates.

assay could also be performed at pH = 8 or at 38 °C. Under the assumption that the conversion of NH_3 to NO_2^- follows Arrhenius behavior, an increase of the temperature by 8° should increase the nitrification rate by about 1.6 times. Indeed, we observed that the NO_2^- production by *N. europaea* increased by 27 ± 6% at the higher temperature (Figure S5). Regarding enzyme inhibition by NIs, the higher turnover of the enzyme may provide some insight into the mode of inhibition, as reversible inhibition is affected by the enzymatic turnover, whereas irreversible inhibition is not.[37] The assay revealed that the efficacy of inhibitors 4, 11, and 12 dropped to 30−50% at 38 °C compared with 30 °C (Table 2), suggesting reversible

Table 2. Inhibition (in %) of *N. europaea* by Inhibitors 4, 8, 11, and 12 at Different Temperatures and pH[a]

conditions	inhibitor 4	inhibitor 8	inhibitor 11	inhibitor 12
standard protocol[b]	93 ± 6	68 ± 6	89 ± 9	80 ± 5
T = 38 °C[c]	30 ± 4	58 ± 2	45 ± 5	26 ± 6
pH = 8[d]	33 ± 4	60 ± 5	50 ± 3	30 ± 2

[a] $[NH_4^+]$ = 3 mM and [inhibitor] = 0.3 mM (10 mol % of $[NH_4^+]$); incubation in NaPB with 1 v/v% DMSO performed at 100 rpm for 60 min in the dark; standard errors were determined from three biological and three technical replicates. [b] 30 °C, pH = 7.5. [c] pH = 7.5. [d] 30 °C.

inhibition. On the other hand, the % inhibition by inhibitor 8, which is substituted with aromatic rings, was within error similar at both temperatures, which may indicate a more complex mode of inhibition.[62,63]

3.3.3. Variation of Assay pH. It has been shown that NH_3 oxidation by AMO is favored at a higher pH, mainly due to the higher NH_3 availability due to deprotonation of NH_4^+ (which cannot be oxidized by AMO). In addition, the enzyme activity of AMO is higher at pH = 7.8 than at neutral pH.[64−66] To explore whether the assay can also be used to evaluate the production of NO_2^- and its inhibition at a slightly alkaline pH, we conducted an experiment where *N. europaea* was inoculated at pH = 8.0 under otherwise identical conditions (see Section 2). Compared to the assay performed at pH = 7.5, at pH = 8, the NO_2^- production was increased by 26 ± 5% (Figure S5). It should be noted that, at pH = 6.5, no NO_2^- was produced (about 6 μM, which is the same as that without N-source), which can be rationalized by a too low $[NH_3]$ under these conditions. Furthermore, similar to the experiments at the

https://doi.org/10.1021/acsagscitech.2c00229
ACS Agric. Sci. Technol. 2023, 3, 260−269

higher temperature, the NO_2^- production dropped in the presence of inhibitors 4, 11, and 12 to 30−50% at pH = 8, whereas no significant decrease (within error) was found for inhibitor 8, supporting a different mode of inhibition as suggested above. These data clearly confirm the assay's high sensitivity that enables teasing out differences in the NO_2^- production by various inhibitor compounds under different conditions.

3.3.4. Determination of the Absolute IC_{50} (IC_{50abs}) Values. The absolute half-maximal inhibitory concentration, IC_{50abs}, is the NI concentration that reduces the total NO_2^- formation by AMO to 50%. While determination of NO_2^- production over 60 min gives a broader indication of the efficacy of NIs over that time window, IC_{50abs} values describe the inhibitor's efficacy at different concentrations. It should be noted that IC_{50} values are very system-sensitive, and the values reported in the literature can vary considerably, depending on the number of cells, substrate concentrations, and assay conditions.[44,57] The standard assay protocol developed in this work provides a unique opportunity to produce IC_{50} data that allow comparison of the performance of a large number of different inhibitor compounds.

The IC_{50abs} values were determined for inhibitor 8, DCD, and DMP (we did not explore DMPP, as the acidic anion could potentially impact on the inhibition by decreasing the pH and lowering the ammonia availability).[57] *N. europaea* was used as an AMO source, which was inoculated at different inhibitor concentrations, and the production of NO_2^- was measured according to Section 2.3.1. The data are shown in Figure 7, which reveal IC_{50abs} values for inhibitor 8, DCD, and DMP of 147.5, 106.8, and 6.6 μM, respectively.

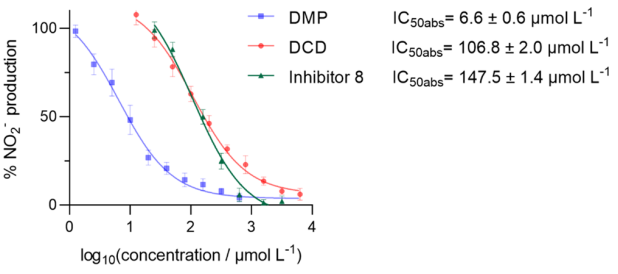

Figure 7. Function of the % NO_2^- production against the logarithmic concentration of DMP, DCD, and inhibitor 8 and the obtained IC_{50abs} values. Standard errors were determined from three biological and three technical replicates.

Compared to the % inhibition determined at 10 mol % for inhibitor 8, DCD, and DMP of 68%, 59%, and 88%, respectively (see Figure 3b and Table 2), only for DMP, the IC_{50abs} and % inhibition values correlate in that DMP is the best performing NI in this set. On the other hand, the IC_{50abs} values suggest a better performance of DCD than inhibitor 8, which contradicts the data from the % inhibition studies at 10 mol % of $[NH_4^+]$. As Figure 7 reveals, in contrast to both DCD and DMP, the efficiency of inhibitor 8 decreases significantly at lower concentrations, which leads to a higher IC_{50abs} value. Thus, the determination of IC_{50abs} values provides a useful tool to obtain information about the most useful application rate of NIs with regard to inhibitory activity.

To conclude, designing new NIs can be a vague target as AMO's crystal structure is unknown. We have developed an accessible, cheap, and fast screening assay using two different sources of AMO, which can be readily performed by people with rudimentary microbiology skills. Our assay can be used to rapidly test the inhibitory activity of multiple compounds (both hydrophilic and lipophilic) at the same time, which could significantly accelerate the development of new NIs, as molecular frameworks with promising inhibitory behavior can be identified in just one hour. These candidates can subsequently be evaluated in more time-demanding (and expensive) soil incubation and field studies and further improved through chemical modifications in an iterative process.

■ ASSOCIATED CONTENT

Supporting Information

The Supporting Information is available free of charge at https://pubs.acs.org/doi/10.1021/acsagscitech.2c00229.

Supplementary information about the optimization of the assay for water-insoluble NIs (Figures S1 and S2 and Table S1); optical density (350−650 nm range) of *N. europaea* in NaPB (pH 7.5) at different dilutions of a bacterial subculture (Supplementary Figure S3); optical density of *N. europaea* in NaPB (pH 7.5) at 600 nm as a function of protein concentrations (Figure S4); NO_2^- production by *N. europaea* in NaPB at different pH and temperatures (Figure S5); correlation between the OD_{600} and formation of NO_2^- during culturing of *N. europaea* in mineral salt media (MSM) over three days (Supplementary Table S2); NO_2^- production after inoculating *N. europaea* (OD_{600} = 0.03) with different $[NH_4^+]$ (Table S3); NO_2^- production after inoculating *N. multiformis* (OD_{600} = 0.03) with NH_4^+ (Table S4); inhibition of NO_2^- formation after inoculating *N. europaea* (OD_{600} = 0.03) with inhibitor compounds 1−16 (Table S5); inhibition of NO_2^- formation after inoculating *N. multiformis* (OD_{600} = 0.03) with selected inhibitor compounds (Table S6) (PDF)

■ AUTHOR INFORMATION

Corresponding Author

Uta Wille − *School of Chemistry, The University of Melbourne, Parkville, Victoria 3010, Australia;* orcid.org/0000-0003-1756-5449; Phone: +61 3 8344 2425; Email: uwille@unimelb.edu.au

Authors

Sibel C. Yildirim − *School of Chemistry, The University of Melbourne, Parkville, Victoria 3010, Australia;* orcid.org/0000-0002-1208-1210

Robert M. Walker − *School of BioSciences, The University of Melbourne, Parkville, Victoria 3010, Australia;* orcid.org/0000-0002-2064-4546

Ute Roessner − *School of BioSciences, The University of Melbourne, Parkville, Victoria 3010, Australia; Research School of Biology, The Australian National University, Acton, Australian Capital Territory 2600, Australia;* orcid.org/0000-0002-6482-2615

Complete contact information is available at: https://pubs.acs.org/10.1021/acsagscitech.2c00229

Author Contributions

S.C.Y. performed the experiments, processed the experimental data, and performed the analysis. R.W., U.R., and U.W.

designed, planned, and supervised the work. All authors aided in interpreting the results. S.C.Y. and U.W. wrote the manuscript and designed the figures with input of all authors.

Funding

This work was supported by the Australian Research Council through the "ARC Research Hub for Smart Fertilizers" (IH200100023) and the Discovery Project "Connecting soil nitrogen and plant uptake for greener agriculture" (DP200101162).

Notes

The authors declare no competing financial interest.

■ ACKNOWLEDGMENTS

The authors thank Sneha Gupta, Michelle Watt, Claudia Knief, and Nicolas Brüggemann for helpful discussions. Support by the Bio21 Institute's Magnetic Resonance and the Mass Spectrometry and Proteomics Facility (MSPF), Melbourne University, is gratefully acknowledged.

■ ABBREVIATIONS USED

AMO − ammonia monooxygenase
ANOVA − analysis of variance
AOB − ammonia oxidizing bacteria
ATCC − American Type Culture Collection
DCD − dicyandiamide
DMP − 3,4-dimethyl[1H]pyrazole
DMPP − 3,4-dimethyl pyrazole phosphate
DMSO − dimethyl sulfoxide
DMSZ − Deutsche Sammlung von Mikroorganismen und Zellkulturen
IC_{50abs} − concentration of inhibitor to decrease response to 50%
LB − Luria broth
MSM − mineral salt media
NaPB − sodium phosphate buffer
NI − nitrification inhibitor
N. europaea − *Nitrosomonas europaea*
N. multiformis − *Nitrospira multiformis*
NUE − nitrogen use efficiency
OD − optical density
OD_{600} − optical density at 600 nm
rpm − rotations per minute
SAR − structure−activity relationship
SI −supporting information
UV/vis − ultraviolet−visible region

■ REFERENCES

(1) Tester, M.; Langridge, P. Breeding Technologies to Increase Crop Production in a Changing World. *Science* **2010**, *327*, 818−822.
(2) Xu, L.; Chen, H.; Xu, J.; Yang, J.; Li, X.; Liu, M.; Jiao, J.; Hu, F.; Li, H. Nitrogen Transformation and Plant Growth in Response to Different Urea-Application Methods and the Addition of DMPP. *J. Plant Nutr. Soil Sci.* **2014**, *177*, 271−277.
(3) Anas, M.; Liao, F.; Verma, K. K.; Sawar, M. A.; Mahmood, A.; Chen, Z.-L.; Li, Q.; Zeng, X.-P.; Liu, Y.; Li, Y.-R. Fate of Nitrogen in Agriculture and Environment: Agronomic, Eco-Physiological and Molecular Approaches to Improve Nitrogen Use Efficiency. *Biol. Res.* **2020**, *53*, 47.
(4) Mustafa, A.; Athar, F.; Khan, I.; Chattha, M. U.; Nawaz, M.; Shah, A. N.; Mahmood, A.; Batool, M.; Aslam, M. T.; Jaremko, M.; Abdelsalam, N. R.; Ghareeb, R. Y.; Hassan, M. U. Improving Crop Productivity and Nitrogen Use Efficiency Using Sulfur and Zinc-Coated Urea: A Review. *Front. Plant Sci.* **2022**, *13*, No. 942384.
(5) Chen, D.; Suter, H.; Islam, A.; Edis, R.; Freney, J.; Walker, C. Prospects of Improving Efficiency of Fertiliser Nitrogen in Australian Agriculture: A Review of Enhanced Efficiency Fertilisers. *Soil Res.* **2008**, *46*, 289−301.
(6) Sharma, L. K.; Bali, S. K. A Review of Methods to Improve Nitrogen Use Efficiency in Agriculture. *Sustainability* **2018**, *10*, 51.
(7) Hirel, B.; Tétu, T.; Lea, P. J.; Dubois, F. Improving Nitrogen Use Efficiency in Crops for Sustainable Agriculture. *Sustainability* **2011**, *3*, 1452−1485.
(8) Lassaletta, L.; Billen, G.; Grizzetti, B.; Anglade, J.; Garnier, J. 50 Year Trends in Nitrogen Use Efficiency of World Cropping Systems: The Relationship Between Yield and Nitrogen Input to Cropland. *Environ. Res. Lett.* **2014**, *9*, No. 105011.
(9) Guo, C.; Wang, H.; Zou, D.; Wang, D.; Han, X. A Novel Amended Nitrification Inhibitor Confers an Enhanced Suppression Role in the Nitrification of Ammonium in Soil. *J. Soils Sediments* **2022**, *22*, 831−843.
(10) Cui, L.; Li, D.; Wu, Z.; Xue, Y.; Xiao, F.; Gong, P.; Zhang, L.; Song, Y.; Yu, C.; Du, Y.; Li, Y.; Zheng, Y. Effects of Combined Nitrification Inhibitors on Soil Nitrification, Maize Yield and Nitrogen Use Efficiency in Three Agricultural Soils. *PLoS One* **2022**, *17*, No. e0272935.
(11) Coskun, D.; Britto, D. T.; Shi, W.; Kronzucker, H. J. Nitrogen Transformations in Modern Agriculture and the Role of Biological Nitrification Inhibition. *Nature Plants* **2017**, *3*, 17074.
(12) Zerulla, W.; Barth, T.; Dressel, J.; Erhardt, K.; Horchler von Locquenghien, K.; Pasda, G.; Rädle, M.; Wissemeier, A. 3,4-Dimethylpyrazole Phosphate (DMPP) − A New Nitrification Inhibitor for Agriculture and Horticulture. *Biol. Fertil. Soils* **2001**, *34*, 79−84.
(13) Corrochano-Monsalve, M.; González-Murua, C.; Bozal-Leorri, A.; Lezama, L.; Artetxe, B. Mechanism of Action of Nitrification Inhibitors Based on Dimethylpyrazole: A Matter of Chelation. *Sci. Tot. Environ.* **2021**, *752*, No. 141885.
(14) Caranto, J. D.; Lancaster, K. M. Nitric Oxide is an Obligate Bacterial Nitrification Intermediate Produced by Hydroxylamine Oxidoreductase. *Proc. Natl. Acad. Sci. U.S.A.* **2017**, *114*, 8217−8222.
(15) Bozal-Leorri, A.; Corrochano-Monsalve, M.; Vega-Mas, I.; Aparicio-Tejo, P.; Gonzalez-Murua, C.; Marino, D. Evidences Towards Deciphering the Mode of Action of Dimethylpyrazole-Based Nitrification Inhibitors in Soil and Pure Cultures of *Nitrosomonas europaea*. *Chem. Biol. Technol. Agric.* **2022**, *9*, 56.
(16) Yildirim, S. C.; Walker, R. M.; Roessner, U.; Wille, U. Assessing the Efficacy, Acute Toxicity and Binding Modes of the Agricultural Nitrification Inhibitors 3,4-Dimethyl-1*H*-Pyrazole (DMP) and Dicyandiamide (DCD) With *Nitrosomonas europaea Agric. Sci. Technol.* 2023, DOI: 10.1021/acsagscitech.2c00303.
(17) Monteiro, M.; Séneca, J.; Magalhães, C. The History of Aerobic Ammonia Oxidizers: From the First Discoveries to Today. *J. Microbiol.* **2014**, *52*, 537−547.
(18) Chen, Q.; Qi, L.; Bi, Q.; Dai, P.; Sun, D.; Sun, C.; Liu, W.; Lu, L.; Ni, W.; Lin, X. Comparative Effects of 3,4-Dimethylpyrazole Phosphate (DMPP) and Dicyandiamide (DCD) on Ammonia-Oxidizing Bacteria and Archaea in a Vegetable Soil. *Appl. Microbiol. Biotechnol.* **2015**, *99*, 477−487.
(19) Dougherty, W. J.; Collins, D.; Van Zwieten, L.; Rowlings, D. W. Nitrification (DMPP) and Urease (NBPT) Inhibitors had no Effect on Pasture Yield, Nitrous Oxide Emissions, or Nitrate Leaching Under Irrigation in a hot-dry Climate. *Soil Res.* **2016**, *54*, 675−683.
(20) Gilsanz, C.; Báez, D.; Misselbrook, T. H.; Dhanoa, M. S.; Cárdenas, L. M. Development of Emission Factors and Efficiency of Two Nitrification Inhibitors, DCD and DMPP. *Agric. Ecosyst. Environ.* **2016**, *216*, 1−8.
(21) Wolt, J. D. A Meta-Evaluation of Nitrapyrin Agronomic and Environmental Effectiveness With Emphasis on Corn Production in the Midwestern USA. *Nutr. Cycl. Agroecosys.* **2004**, *69*, 23−41.
(22) Hall, G. H. Measurement of Nitrification Rates in Lake Sediments: Comparison of the Nitrification Inhibitors Nitrapyrin and Allylthiourea. *Microb. Ecol.* **1984**, *10*, 25−36.

(23) Nauer, P. A.; Fest, B. J.; Visser, L.; Arndt, S. K. On-Farm Trial on the Effectiveness of the Nitrification Inhibitor DMPP Indicates no Benefits Under Commercial Australian Farming Practices. *Agric. Ecosyst. Environ.* **2018**, *253*, 82−89.
(24) Newbould, P. The Use of Nitrogen fertiliser in Agriculture. Where do we go Practically and Ecologically? *Plant Soil* **1989**, *115*, 297−311.
(25) Wendeborn, S. The Chemistry, Biology, and Modulation of Ammonium Nitrification in Soil. *Angew. Chem., Int. Ed.* **2020**, *59*, 2182−2202.
(26) Lam, S. K.; Wille, U.; Hu, H.-W.; Caruso, F.; Mumford, K.; Liang, X.; Pan, B.; Malcolm, B.; Roessner, U.; Suter, H.; Stevens, G.; Walker, C.; Tang, C.; He, J.-Z.; Chen, D. Next-Generation Enhanced-Efficiency Fertilizers for Sustained Food Security. *Nat. Food* **2022**, *3*, 575−580.
(27) Hooper, A. B.; Vannelli, T.; Bergmann, D. J.; Arciero, D. M. Enzymology of the Oxidation of Ammonia to Nitrite by Bacteria. *Antonie van Leeuwenhoek* **1997**, *71*, 59−67.
(28) Moir, J. W. B.; Crossman, L. C.; Spiro, S.; Richardson, D. J. The Purification of Ammonia Monooxygenase From *Paracoccus denitrificans*. *FEBS Lett.* **1996**, *387*, 71−74.
(29) Lieberman, R. L.; Rosenzweig, A. C. Crystal Structure of a Membrane-Bound Metalloenzyme that Catalyses the Biological Oxidation of Methane. *Nature* **2005**, *434*, 177−182.
(30) Lieberman, R. L.; Rosenzweig, A. C. The Quest for the Particulate Methane Monooxygenase Active Site. *Dalton Trans.* **2005**, 3390−3396.
(31) Balasubramanian, R.; Smith, S. M.; Rawat, S.; Yatsunyk, L. A.; Stemmler, T. L.; Rosenzweig, A. C. Oxidation of Methane by a Biological Dicopper Centre. *Nature* **2010**, *465*, 115−119.
(32) Arp, D. J.; Sayavedra-Soto, L. A.; Hommes, N. G. Molecular Biology and Biochemistry of Ammonia Oxidation by *Nitrosomonas europaea*. *Arch. Microbiol.* **2002**, *178*, 250−255.
(33) Taggert, B. I.; Walker, C.; Chen, D.; Wille, U. Substituted 1, 2, 3-Triazoles: A New Class of Nitrification Inhibitors. *Sci. Rep.* **2021**, *11*, No. 149080.
(34) Clark, P. R.; Williams, G. D.; Hayes, J. F.; Tomkinson, N. C. A Scalable Metal-, Azide-, and Halogen-Free Method for the Preparation of Triazoles. *Angew. Chem., Int. Ed.* **2020**, *59*, 6740−6744.
(35) Li, C.; Hu, H.-W.; Chen, Q.-L.; Chen, D.; He, J.-Z. Comammox Nitrospira Play an Active Role in Nitrification of Agricultural Soils Amended With Nitrogen Fertilizers. *Soil Biol. Biochem.* **2019**, *138*, No. 107609.
(36) Lam, S. K.; Suter, H.; Bai, M.; Walker, C.; Davies, R.; Mosier, A. R.; Chen, D. Using Urease and Nitrification Inhibitors to Decrease Ammonia and Nitrous Oxide Emissions and Improve Productivity in a Subtropical Pasture. *Sci. Tot. Environ.* **2018**, *644*, 1531−1535.
(37) Hyman, M. R.; Wood, P. M. Ethylene Oxidation by *Nitrosomonas europaea*. *Arch. Microbiol.* **1984**, *137*, 155−158.
(38) Hyman, M. R.; Sansome-Smith, A. W.; Shears, J. H.; Wood, P. M. A Kinetic Study of Benzene Oxidation to Phenol by Whole Cells of *Nitrosomonas europaea* and Evidence for the Further Oxidation of Phenol to Hydroquinone. *Arch. Microbiol.* **1985**, *143*, 302−306.
(39) Iizumi, T.; Mizumoto, M.; Nakamura, K. A Bioluminescence Assay Using *Nitrosomonas europaea* for Rapid and Sensitive Detection of Nitrification Inhibitors. *Appl. Environ. Microbiol.* **1998**, *64*, 3656−3662.
(40) Subbarao, G. V.; Nakahara, K.; Hurtado, M. P.; Ono, H.; Moreta, D. E.; Salcedo, A. F.; Yoshibashi, A. T.; Ishikawa, T.; Ishitani, M.; Ohnishi-Kameyama, M.; Yoshida, M.; Rondon, M.; Rao, I. M.; Lascano, C. E.; Berry, W. L.; Ito, O. Evidence for Biological Nitrification Inhibition in *Brachiaria* Pastures. *Proc. Natl. Acad. Sci. U.S.A.* **2009**, *106*, 17302−17307.
(41) Grunditz, C.; Dalhammar, G. Development of Nitrification Inhibition Assays Using Pure Cultures of *Nitrosomonas* and *Nitrobacter*. *Water Res.* **2001**, *35*, 433−440.
(42) Berthelot, M. Violet d'Aniline. *Rep. Chim. Appl.* **1859**, *1*, 284.
(43) Griess, P. Bemerkungen zu der Abhandlung der HH. Weselky und Benedikt über einige Azoverbindungen. *Ber. Dtsch. Chem. Ges.* **1879**, *12*, 426−428.
(44) O'Sullivan, C. A.; Duncan, E. G.; Whisson, K.; Treble, K.; Ward, P. R.; Roper, M. M. A Colourimetric Microplate Assay for Simple, High Throughput Assessment of Synthetic and Biological Nitrification Inhibitors. *Plant Soil* **2017**, *413*, 275−287.
(45) Utåker, J. B.; Bakken, L.; Jiang, Q. Q.; Nes, I. F. Phylogenetic Analysis of Seven New Isolates of Ammonia-Oxidizing Bacteria Based on 16S rRNA Gene Sequences. *Syst. Appl. Microbiol.* **1995**, *18*, 549−559.
(46) Naghdi, M.; Cledon, M.; Brar, S. K.; Ramirez, A. A. Nitrification of Vegetable Waste Using Nitrifying Bacteria. *Ecol. Eng.* **2018**, *121*, 83−88.
(47) Antoniou, P.; Hamilton, J.; Koopman, B.; Jain, R.; Holloway, B.; Lyberatos, G.; Svoronos, S. A. Effect of Temperature and pH on the Effective Maximum Specific Growth Rate of Nitrifying Bacteria. *Water Res.* **1990**, *24*, 97−101.
(48) Coleman, N. V.; Mattes, T. E.; Gossett, J. M.; Spain, J. C. Biodegradation of *cis*-Dichloroethene as the Sole Carbon Source by a *β*-Proteobacterium. *Appl. Environ. Microbiol.* **2002**, *68*, 2726−2730.
(49) Hartmans, S.; Kaptein, A.; Tramper, J.; de Bont, J. A. M. Characterization of a Mycobacterium sp. and a Xanthobacter sp. for the Removal of Vinyl Chloride and 1,2-Dichloroethane From Waste Gases. *Appl. Microbiol. Biotechnol.* **1992**, *37*, 796−801.
(50) Minitab, LLC, 2021. *Minitab*, available at https:/www.minitab.com.
(51) Juliette, L. Y.; Hyman, M. R.; Arp, D. J. Inhibition of Ammonia Oxidation in *Nitrosomonas europaea* by Sulfur Compounds: Thioethers are Oxidized to Sulfoxides by Ammonia Monooxygenase. *Appl. Environ. Microbiol.* **1993**, *59*, 3718−3727.
(52) Rasche, M. E.; Hyman, M. R.; Arp, D. J. Factors Limiting Aliphatic Chlorocarbon Degradation by Nitrosomonas europaea: Cometabolic Inactivation of Ammonia Monooxygenase and Substrate Specificity. *Appl. Environ. Microbiol.* **1991**, *57*, 2986.
(53) Rasche, M. E.; Hicks, R. E.; Hyman, M. R.; Arp, D. J. Oxidation of Monohalogenated Ethanes and n-Chlorinated Alkanes by Whole Cells of *Nitrosomonas europaea*. *J. Bacteriol.* **1990**, *172*, 5368−5373.
(54) Wright, C. L.; Schatteman, A.; Crombie, A. T.; Murrell, J. C.; Lehtovirta-Morley, L. E.; Stams, A. J. M. Inhibition of Ammonia Monooxygenase from Ammonia-Oxidizing Archaea by Linear and Aromatic Alkynes. *Appl. Environ. Microbiol.* **2020**, *86*, e02388−19.
(55) Sedlacek, C. J.; Nielsen, S.; Greis, K. D.; Haffey, W. D.; Revsbech, N. P.; Ticak, T.; Laanbroek, H. J.; Bollmann, A.; Vieille, C. Effects of Bacterial Community Members on the Proteome of the Ammonia-Oxidizing Bacterium *Nitrosomonas* sp. Strain Is79. *Appl. Environ. Microbiol.* **2016**, *82*, 4776−4788.
(56) Bollmann, A.; French, E.; Laanbroek, H. J. Isolation, Cultivation, and Characterization of Ammonia-Oxidizing Bacteria and Archaea Adapted to Low Ammonium Concentrations. In *Methods in Enzymology*, Klotz, M. G., Ed.; Academic Press, 2011; Vol. *486*, pp 55−88.
(57) Subbarao, G. V.; Nakahara, K.; Ishikawa, T.; Ono, H.; Yoshida, M.; Yoshihashi, T.; Zhu, Y.; Zakir, H. A. K. M.; Deshpande, S. P.; Hash, C. T.; Sahrawat, K. L. Biological Nitrification Inhibition (BNI) Activity in Sorghum and its Characterization. *Plant Soil* **2013**, *366*, 243−259.
(58) Subbarao, G. V.; Ishikawa, T.; Ito, O.; Nakahara, K.; Wang, H. Y.; Berry, W. L. A Bioluminescence Assay to Detect Nitrification Inhibitors Released From Plant Roots: A Case Study with *Brachiaria humidicola*. *Plant Soil* **2006**, *288*, 101−112.
(59) Lin, X.; Hasi, W.-L.-J.; Lou, X.-T.; Han, S.-q.-g.-w.; Lin, D.-Y.; Lu, Z.-W. Direct and Quantitative Detection of Dicyandiamide (DCD) in Milk Using Surface-Enhanced Raman Spectroscopy. *Anal. Methods* **2015**, *7*, 3869−3875.
(60) Isken, S.; de Bont, J. A. M. Bacteria Tolerant to Organic Solvents. *Extremophiles* **1998**, *2*, 229−238.

(61) Voysey, P. A.; Wood, P. M. Methanol and Formaldehyde Oxidation by an Autotrophic Nitrifying Bacterium. *Microbiology* **1987**, *133*, 283−290.
(62) Keener, W. K.; Arp, D. J. Transformations of Aromatic Compounds by *Nitrosomonas europaea*. *Appl. Environ. Microbiol.* **1994**, *60*, 1914−1920.
(63) Vannelli, T.; Logan, M.; Arciero, D. M.; Hooper, A. B. Degradation of Halogenated Aliphatic Compounds by the Ammonia-Oxidizing Bacterium *Nitrosomonas europaea*. *Appl. Environ. Microbiol.* **1990**, *56*, 1169−1171.
(64) Azov, Y.; Goldman Joel, C. Free Ammonia Inhibition of Algal Photosynthesis in Intensive Cultures. *Appl. Environ. Microbiol.* **1982**, *43*, 735−739.
(65) Groeneweg, J.; Sellner, B.; Tappe, W. Ammonia Oxidation in *Nitrosomonas* at NH_3 Concentrations Near k_m: Effects of pH and Temperature. *Water Res.* **1994**, *28*, 2561−2566.
(66) Stein, L. Y. Insights into the Physiology of Ammonia-Oxidizing Microorganisms. *Curr. Opin. Chem. Biol.* **2019**, *49*, 9−15.

2.3 Modifications on Ethyl-1,2,3 Triazole-4-Carboxylate Derivatives

2.3.1 Introduction

In the publication, only the position 5 of the ethyl-1,2,3 triazole-4-carboxylate scaffold (**24**) was alternated in order to enable direct comparison of the performance in dependence of this substituent. Not included in the publication were triazoles with a 'fixed' substituent in position 5 but with varying substituents in position 4. The ester moiety in position 4 can be readily modified to obtain a carboxylic acid (**41**), alcohol (**42**), allyl ester (**43**) and nitrile (**44**), and keeping position 5 as a phenyl group, as aromatic substituted ethyl-1,2,3 triazole-4-carboxylate derivatives showed the highest inhibitory effect (Chapter 2.2, **Figure 5**). The compounds **41**-**44** were tested with *N. europaea* as model organism following the 'nitrification assay' procedure as reported in Chapter 2.2 (**section 2.3**). Synthetic details of ester hydrolysis (compound **41**), ester reduction (compound **42**), the esterification (**43** can be found in Chapter 7.2. Compound **44** was synthesised with an alternative one-pot reaction that is described in Chapter 7.1.2 *via* GP-2.

2.3.2 Results and discussion

Inhibitor 6 (compound **30**), which is the ester derivative of the 5-phenyl 1,2,3-triazoles listed in **Table 1**, showed a percent inhibition of 42 ± 10% with *N. europaea* (Chapter 2.2, **Figure 5**). When replacing the ester in **30** by a carboxylic acid to give **41**, the inhibitory effect dropped to approximately half, whereas conversion to the alcohol **42** reduced the percent inhibition to 27 ± 4. The allyl ester **43** had only about one third of the inhibitory activity of **30** (Table 1). These data clearly show that the ester has a functional advantage in comaprison to carboxylic acids, alcohols and allyl esters. Interstingly, when the ester group was replaced by a nitrile (**44**), a quantitative inhibition of nitrification was observed. As the nitrile group is also present in DCD, which is considered to act as a metal chelator, the increased inhibitory effect is not unexpected.

Table 1: Inhibition (in %) of *N. multiformis* after treatment with differently substituted 4,5-disubstituted 1,2,3-triazoles, determined from the NO_2^- production.[a]

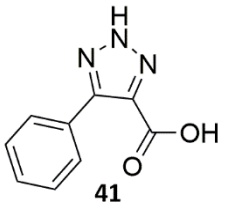

41

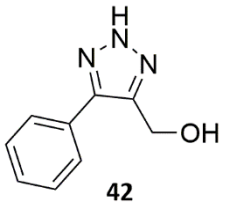

42

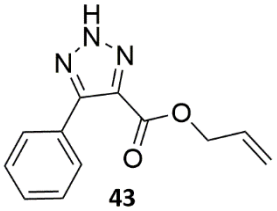

43

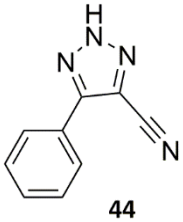

44

Compound	**% Inhibition** ***N. europaea***
41	19 ± 3
42	27 ± 4
43	10 ± 5
44	100 ± 6

[a]Incubations were performed following 'nitrification assay' Chapter 2.2, section 2.3' in NaPB with 1v/v% DMSO at pH = 7.5 and 30°C with [inhibitor] = 0.3 mM (10 mol% of N-source), $[NH_4^+]$ = 3 mM at 100 rpm for 60 min in the dark. Standard errors were determined from three biological and three technical replicates, n=3).

2.3.3 Conclusion

This chapter summarises two components that are essential to answer the scientific question. In the first section, a rapid, accessible and robust nitrification assay was developed with pure cultures of *N. europaea* and *N. multiformis*; and secondly, 4,5-disubstituted 1,2,3-triazoles are introduced as a new class of SNI. The assay was designed to facilitate bacterial cell growth and harvest, enable the use of co-solvents to increase solubility of less hydrophilic compounds and the assay protocol itself, as literature procedures were not suitable for testing large libraries of SNI by a non-skilled person of the art.

The assay was used to test 16 different ethyl-1,2,3 triazole-4-carboxylate derivatives. Ethyl-1,2,3 triazole-4-carboxylate derivatives with aromatic rings at position 5 showed a higher nitrification inhibition than aliphatic-substituted ethyl-1,2,3 triazole-4-carboxylate derivates. A heterocyclic-substituted ethyl-1,2,3 triazole-4-carboxylate derivatives did not show increased inhibitory effect. Furthermore, the ester group in ethyl 5-phenyl-1,2,3-triazole-4-carboxylate was modified to a carboxylic acid (**41**), alcohol (**42**), an allyl ester (**43**) and a nitrile (**44**) group to determine the binding affinity of the ester group. Only the latter showed an increased percent inhibition with quantitative inhibition at 10 mol% application rate and was amongst the best performing 4,5-disubstituted 1,2,3-triazoles.

In conclusion, 4,5-disubstituted 1,2,3-triazoles show nitrification inhibitory properties *in vivo*. The compounds that showed promising results and will be excessively tested in soil incubation studies to determine their effect on mineral-N transformations. Planned future experiments will include pH-dependent soil incubation studies, plant studies and ecotoxicology studies to determine nitrification inhibition in varying soils overall, their ability to increase crop yield, stability in soil and toxicity. As large-scale agronomy studies for 4,5-disubstituted 1,2,3-triazoles are out of the scope of this doctoral project, they will be performed by the ARC Hub for Smart Fertilisers in cooperation with the commercial partner Incitec Pivot Australia.

Chapter 3: Assessing the Efficacy, Acute Toxicity and Binding Modes of the Agricultural Nitrification Inhibitors 3,4-Dimethyl-1*H*-Pyrazole (DMP) and Dicyandiamide (DCD) With *N. europaea* (publication-based)

3.1 Introduction

In Chapter 2, a robust 60-min nitrification assay was presented to test the efficacy of new SNI with AOB. 4,5-disubstituted 1,2,3-triazoles were explored as a class of small organic molecules with chelating properties, such as the commercial inhibitors DMP and DCD. Both commercial SNI have been on the market for more than 20 years and have shown in various field studies to reduce nitrification to some extent. [73, 102] As shown in the results in Chapter 2.2, Inhibitor 4 (compound **28**), inhibitor 8 (**32**), inhibitor 11 (**35**) and inhibitor 12 (**36**) showed a higher percentage inhibition than DCD. However, inhibitor 8 (**32**), inhibitor 11 (**35**) and inhibitor 12 (**36**) showed up to 60% reduced percentage inhibition when the system was challenged with higher temperatures or a higher pH. Eventually, only inhibitor 4 (**28**) showed the highest binding affinity as its efficacy remained constant when the system was challenged. Whilst inhibitor 4 (**28**) is to be tested in soil incubation studies, it became increasingly clear that the protocol of testing the inhibitors at an increased temperature, higher pH, and $IC_{50(app)}$ add dimensions to elucidate the binding behavior/strength of SNI. In other words, the standard assay is a one-dimensional approach limited to simply 'screening' SNI. A high %inhibition is not always sufficient, as for instance, DMP showed the highest %inhibition and $IC_{50(app)}$ but still remains unable to solve the global N crisis. To predict the performance of SNI, (Chapter 2.2, section 2.3), it became increasingly clear that there was a lack of fundamental knowledge of the current SNI DMP and DCD. Controversially, pure bacterial studies to determine biochemical inhibitory parameters with DMP and DCD have never been performed.

Therefore, the experiments in this Chapter are aimed at obtaining understanding of the biochemical parameter of DMP and DCD. In a series of bacterial experiments with the model organism *N. europaea*, firstly, the targeted enzyme of the AMO and HAO cascade (see Chapter 1.3) was determined. Secondly, the reversibility of the binding was determined by following Chapter 3.2 (section 2.3.3) to determine the mode of inhibition. Thirdly, the binding mode was determined *via* Michaelis-Menten kinetics experiments, in which the effect of the inhibitor was challenged against ascending NH_3 concentration (Chapter 3.2, section 2.3.4). Fourthly, for the first time, real-time oxygen respiration of AOB in the presence of DMP and DCD was measured via an oxygen-selective electrode (Clark-type electrode) to analyse real-time kinetic data (Chapter 3.2, section 2.3.2). And lastly, their relative toxicity was quantified via a bacterial viability stain (Chapter 3.2, section 2.3.5). The aim of this fundamental Chapter was to generate a baseline for future SNIs and potentially to identify aspects in which current SNI underperform.

3.2 Assessing the Efficacy, Acute Toxicity, and Binding Modes of the commercial SNIs DMP and DCD (publication)

ACS AGRICULTURAL SCIENCE & TECHNOLOGY

pubs.acs.org/acsagscitech Article

Assessing the Efficacy, Acute Toxicity, and Binding Modes of the Agricultural Nitrification Inhibitors 3,4-Dimethyl-1*H*-pyrazole (DMP) and Dicyandiamide (DCD) with *Nitrosomonas europaea*

Sibel C. Yildirim, Robert M. Walker, Ute Roessner, and Uta Wille*

Cite This: *ACS Agric. Sci. Technol.* 2023, 3, 222−231 Read Online

ACCESS | Metrics & More | Article Recommendations | Supporting Information

ABSTRACT: Nitrification inhibitors have been coformulated with nitrogen fertilizers since the 1970s to modulate the microbiological conversion of nitrogen in agricultural soils. 3,4-Dimethyl-1*H*-pyrazole (DMP) and dicyandiamide (DCD) are currently the most used commercial nitrification inhibitors, but their mode of action is not well understood. This work seeks to fill this void by assessing for the first time in detail their mechanism of inhibition, efficacy, and acute toxicity with pure cell cultures of *Nitrosomonas europaea*. Bacterial assays based on the quantification of the nitrite (NO_2^-) production showed that both inhibitors reversibly target ammonia monooxygenase (AMO), which catalyzes the first step of the nitrification process. Michaelis−Menten kinetics suggest that both DMP and DCD act as uncompetitive inhibitors. Real-time measurements of the oxygen (O_2) consumption confirmed the nonmechanistic mode of inhibition and showed that DMP reduced the O_2 uptake rate by AMO much more at considerably lower concentrations than DCD, in line with the lower inhibitory efficiency of the latter. Acute toxicity tests revealed that DCD has a 10% higher toxicity than DMP when comparing treatments at the same inhibition efficacy (*i.e.*, DMP at 10 ppm, DCD at 100 ppm), indicating that the inhibition of the nitrification process cannot simply be achieved by increasing the inhibitor concentration. The methods presented in this study could assist the development of more reliable nitrification inhibitors in the future.

KEYWORDS: *ammonia monooxygenase, bacterial assay, dicyandiamide, 3,4-dimethyl-1H-pyrazole, inhibition mechanism, nitrification inhibitor*

1. INTRODUCTION

To meet the food demand of an ever-growing population, the Food and Agriculture Organization of the United Nations (FAO) has predicted that, from 2016 to 2022, a 5% increase in nitrogen (N) fertilization from 106 to 112 Tg is required.[1] However, since the 1980s, the N use efficiencies (NUEs) have remained at only around 50% globally.[2,3] The remaining 50% are lost from the soil through abiotic and biotic pathways, including volatilization of ammonia (NH_3), which is a precursor of particulate matter ($PM_{2.5}$), and nitrate (NO_3^-) leaching that causes damaging surface water eutrophication and groundwater pollution.[4−6] In addition, microbiological denitrification reduces NO_3^- to nitrous oxide (N_2O) and nitric oxide (NO).[7] N_2O has a 300 times higher global warming potential than CO_2, and mitigation of N losses in agriculture has become an important target for reducing the greenhouse gas (GHG) footprint.[6]

One strategy to improve N management in agricultural soils is to amend N fertilizers with nitrification inhibitors (NIs).[8,9] Nitrification is caused by ammonia-oxidizing bacteria (AOB) and ammonia-oxidizing archaea (AOA). NIs are small synthetic molecules that are designed to inhibit ammonia monooxygenase (AMO), a multimeric transmembrane enzyme, which is conserved in both AOB and AOA[10−12] and catalyzes the rate-limiting first oxidation step NH_3 → hydroxylamine (NH_2OH).[13,14] Subsequently, NH_2OH is converted to nitrite (NO_2^-) by the enzyme hydroxylamine oxidoreductase (HAO),[15] followed by the rapid oxidation to NO_3^-, the end-product of the nitrification process, which is catalyzed by nitrite oxidase (NXR) present in, for example in species from the genus *Nitrobacter* and *Nitrospira*. In fact, some species of *Nitrospira* are capable of catalyzing the oxidation from NH_3 to NO_3^- (complete ammonia oxidizers, comammox).[16] Furthermore, recent studies have revealed that nitrification can also directly lead to the formation of NO and N_2O.[17−21] Thus, by inhibiting AMO, the residence time of NH_3 in soils should be increased, which in turn should reduce N losses through NO_3^- leaching and emission of gaseous N compounds produced through both nitrification and denitrification processes. While the crystal structure of AMO remains to be resolved, the evolutionally similar and recently crystallized methane monooxygenase (MMO) has provided some information on the active center in AMO, suggesting that a cupredoxin-like unit could be involved in the oxidation steps.[10,22−24]

Received: November 1, 2022
Revised: January 6, 2023
Accepted: January 9, 2023
Published: January 25, 2023

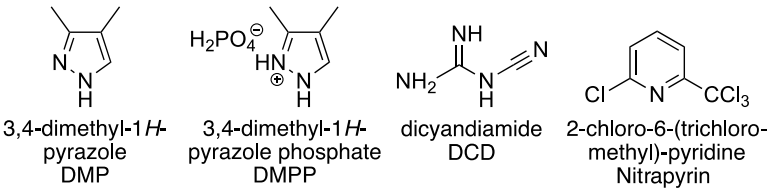

Figure 1. Commercially Available Nitrification Inhibitors (NIs).

Generally, NIs can be categorized into mechanism-based and non-mechanism-based enzyme inhibitors, such as chelators that coordinate to a metal center in the enzyme's active site without inducing a chemical change.[13] In contrast, mechanism-based inhibitors are converted in the active site to products that inactivate the enzyme, for example, through the formation of covalent bonds. Consequently, the recovery of the activity of nitrifying bacteria requires *de novo* synthesis of AMO. One prominent example for a mechanism-based NI is the gas acetylene (C_2H_4),[25,26] but the high flammability and reactivity prohibit its use in agriculture.

Currently commercially available NIs are 3,4-dimethyl-1*H*-pyrazole (DMP), which is commonly applied in agricultural systems as the phosphate salt to reduce its volatility (DMPP or ENTEC, BASF AG), dicyandiamide (DCD, AlzChem AG), and 2-chloro-6-(trichloromethyl)-pyridine (nitrapyrin or N−Serve, Dow Chemical Co.) (Figure 1).

Various *in vitro* studies have demonstrated that DMPP reduces nitrification rates; however, field studies revealed that its efficacy strongly depends on the agroecosystem.[27−33] DCD, which is widely applied in New Zealand, has been shown to reduce N_2O emissions but is prone to leaching and has been detected in dairy products.[34−36] Nitrapyrin is highly volatile and is the most intensively studied NI regarding its mode of action.[37,38] It has been classified as a metal chelator,[39] although product analyses indicate that nitrapyrin could also act as a mechanism-based enzyme inhibitor.[37]

Despite their widespread use, only very few detailed mechanistic studies are available for DMP (or DMPP, respectively) and DCD. Recently, the crystal structure of six DMP molecules coordinating to a Cu^{2+} center was solved, demonstrating the ligand-binding ability of DMP.[40] However, a recent study with DMPP suggests that its inhibitory capacity is not linked to chelation with Cu^{2+}.[41] DCD has also been categorized as a metal chelator[12,42−44] and been proposed to act as a competitive inhibitor for AMO.[21] However, because of the many remaining unknowns of the detailed mode of action of these two NIs, in this work, we have performed a comparative study of DMP (as the active component in DMPP) and DCD using assays with pure bacterial cultures of *Nitrosomonas europaea* to determine for the first time important biochemical parameter in the absence of the complex matrix of soil experiments. This study provides crucial insight into the binding mode, efficacy, and acute toxicity of these two commercial NIs, which could help to understand their variable performance in the field and support the development of guidelines to aid the design of next-generation NIs with improved and more consistent performance.

2. MATERIALS AND METHODS

2.1. Chemicals. DMP (3,4-dimethyl-1*H*-pyrazole) was supplied by Incitec Pivot Ltd., Australia. DCD (dicyandiamide) and Griess reagent (modified) were purchased from Sigma-Aldrich. Sodium dithionite ($Na_2S_2O_4$) was obtained from ChemSupply Australia. All aqueous solutions were prepared in Milli-Q water. *N. europaea* (ATCC19718) was purchased from the American Type Culture Collection.

2.2. Cell Preparation. *2.2.1. Growing N. europaea Protocol.* AOB were grown for 3−5 d in Duran glass bottles containing 600 mL of mineral salt media (MSM, see below) at 100 rpm and 30 °C in the dark. The slightly loose cap was sealed with an O_2 permeable membrane to ensure aeration (Breathe-Easy sealing membrane, Sigma-Aldrich). The MSM constituted the main bulk medium and consisted of dipotassium hydrogen phosphate (K_2HPO_4; 2.27 g L^{-1}), potassium dihydrogen phosphate (KH_2PO_4; 0.95 g L^{-1}), and ammonium sulfate ($(NH_4)_2SO_4$; 0.67 g L^{-1}). The pH was adjusted to 7.0. To 1 L of the bulk medium, 2 mL of a filter-sterilized (0.2 μm millipore filter) solution of metals was added: disodium ethylenediamine tetraacetate (Na_2EDTA; 6.37 g L^{-1}), zinc sulfate heptahydrate ($ZnSO_4 \times 7\ H_2O$; 1.0 g L^{-1}), calcium chloride dihydrate ($CaCl_2 \times 2\ H_2O$; 0.5 g L^{-1}), iron(II) sulfate heptahydrate ($FeSO_4 \times 7\ H_2O$; 2.5 g L^{-1}), sodium molybdate dihydrate ($NaMoO_4 \times 2\ H_2O$; 0.1 g L^{-1}), copper(II) sulfate pentahydrate ($CuSO_4 \times 5\ H_2O$; 0.1 g L^{-1}), cobalt(II) chloride hexahydrate ($CoCl_2 \times 6\ H_2O$; 0.2 g L^{-1}), manganese(II) sulfate monohydrate ($MnSO_4 \times H_2O$; 0.52 g L^{-1}), and magnesium sulfate heptahydrate ($MgSO_4 \times 7\ H_2O$; 60.0 g L^{-1}). To this media solution, 1v/v% of aqueous sodium carbonate (Na_2CO_3; 50 g L^{-1}) was added aseptically as a carbon source.

2.2.2. Harvesting Cell Protocol. After 3−5 d of incubation, the turbid cultures were harvested at an OD_{600} of approximately 0.1, which represented the mid-exponential growth phase and an NO_2^- production of approximately 800 μM (determined by Griess assay), cells were harvested by filtration onto 0.2 μm membrane filters (Rowe Scientific, mixed cellulose esters (MCEs)). The cells were washed with sodium phosphate buffer (NaPB, pH = 7.5, 0.1 M, 2 × 100 mL) containing $MgSO_4$ (0.2 mM). The filter paper with the cells was transferred into a sterile 50 mL tube, and the cells were washed off by resuspending in NaPB (15 mL), followed by 5 s of vortexing (Ratek, Australia) and 3 s of sonication (Vevor, Australia). The initial inoculum OD_{600}, which was between 0.9 and 1.2, was adjusted to a final OD_{600} of 0.03 and stored at 4 °C until used for the assay. Cells could be stored for up to 24 h without losing activity.

2.3. Nitrification Assay and Analysis. *2.3.1. Standard Assay Protocol.* In a deep 96-well plate (2 mL capacity), 980 μL of the bacterial inoculum (OD_{600} = 0.03 in NaPB at pH 7.5) was added to the inhibitor (10 μL of a 30 or 3 mmol L^{-1} stock solution, respectively), and the solutions were mixed thoroughly and preincubated in the dark for 5 min at 30 °C and 100 rpm (Ratek, Australia). $(NH_4)_2SO_4$ (10 μL, 150 mM, from a sterile solution containing 19.8 g L^{-1} of $(NH_4)_2SO_4$ in Milli-Q water) was then added. In experiments in which the NH_2OH-dependent activity was measured, $(NH_4)_2SO_4$ was replaced by equimolar amounts of NH_2OH. The plate was covered with an O_2 permeable membrane to ensure aeration (Breathe-Easy sealing membrane, Sigma-Aldrich) and incubated in the dark for 30, 60, or 90 min at 30 °C and 100 rpm. The nitrification process was stopped by adding an excess of DMP (10 μmol L^{-1}, 30 mM; the final concentration of DMP in the solution was 0.27 mM, which was considerably higher than the IC_{50abs} value of 6.6 μM determined previously).[45] An aliquot of the reaction solution (50 μL) was transferred to a 96-well spectrophotometric plate (Greiner Cellstar, polystyrene) to which 50 μL of Griess reagent was added. The color was allowed to develop for 15 min at room temperature, and the absorbance was measured at 540 nm (Clariostar

https://doi.org/10.1021/acsagscitech.2c00303
ACS Agric. Sci. Technol. 2023, 3, 222−231

BMG Labtech, Australia). Each assay was accompanied by control treatments to determine the 0 and 100% NO_2^- signals. The percentage inhibition was calculated according to eq 1 from the NO_2^- production of the cells in NaPB (i) without additives ("untreated cells"; 0% signal), (ii) with $[NH_4^+]$ = 3 mM ("uninhibited cells"; 100% signal), and (iii) with $[NH_4^+]$ = 3 mM and [inhibitor] = 0.3 mM (10 mol % of $[NH_4^+]$; "inhibited cells").

$$\%\ \text{inhibition} = \left[1 - \frac{[NO_2^-]_{\text{inhibited cells}} - [NO_2^-]_{\text{untreated cells}}}{[NO_2^-]_{\text{uninhibited cells}} - [NO_2^-]_{\text{untreated cells}}}\right] \times 100 \quad (1)$$

2.3.2. O_2 Consumption Measurements. O_2 consumption rates of cell suspensions of *N. europaea* were measured using a Clark-type oxygen electrode (Rank Brothers, Cambridge, U.K.) mounted in a water-jacketed electrode chamber (3 mL capacity) that was connected to a recirculating cooler (Lauda, Austria). The data were recorded using a Data-trax (World Precision Instruments, UK) sensor data collection system. All measurements were taken at 20 °C and 1 mL final reaction solution volume (the lower temperature, compared to the other experiments in this study that were performed at 30 °C, was required here to increase signal stability). The polarizing voltage was set to 0.6 V. To calibrate the oxygen signal, an excess (approximately 50 mg) of $Na_2S_2O_4$ was added to 1 mL of Milli-Q water to chemically remove dissolved O_2. Additional O_2 flux was prevented by applying a stopper, and the residual voltage was referred to as "0% O_2". The voltage at saturated O_2 concentration ("100% O_2") was determined by measuring the voltage of the equilibrated aerated reaction system consisting of 1 mL of Milli-Q water. Sample measurements were taken as follows: The 1 mL reaction mixture, composed of 980 μL of *N. europaea* cell solution in NaPB (OD_{600} = 0.8; corresponding to approximately 468 μg L^{-1} protein) was equilibrated for 5 min in the chamber until the voltage reading was stable. The reaction was then initiated by the addition of $(NH_4)_2SO_4$ (10 μL of an aqueous 150 mM stock solution, the final concentration in the reaction solution was 3 mM), and the chamber was immediately sealed with a stopper. After 5 min of oxygen consumption (a linear rate coefficient of approximately 186 ± 63 nmol O_2 L^{-1} s^{-1} was determined), 10 μL of the inhibitor stock solution of DMP (0.012, 0.12, 0.6, 1.2 mM) or DCD (1.2, 2.0, 5.0, 10.0 mM) was added via a 10 μL Eppendorf pipette through a capillary opening, ensuring the emergence of the pipette tip in the solution. The voltage was recorded over a period of 5 min in intervals of 5 s. The trace describing the O_2 concentration after the addition of $(NH_4)_2SO_4$ against the time (initial 15−300 s) was used as the baseline O_2 consumption for the uninhibited cells, whereas the trace describing the consumption in the presence of the inhibitor (300−590 s time window) was used to determine the rate of O_2 consumption in the presence of the inhibitor. All experiments were conducted in triplicate at 20 °C under constant stirring. The voltage was converted to $[O_2]$ according to eq 2[46]

$$[O_2]_t = \frac{\text{voltage (sample)}_t - \text{voltage (0\% O}_2\text{)}}{\text{voltage (100\% O}_2\text{)} - \text{voltage (0\% O}_2\text{)}} \times 280\ \mu\text{M} \quad (2)$$

2.3.3. Activity Recovery Assay. Cells were harvested according to the description in the Harvesting Cell Protocol section. The bacterial solution was adjusted to OD_{600} = 0.8 (~468 μg L^{-1} protein), and 980 μL aliquots were transferred to 1.5 mL centrifuge tubes (Eppendorf, polypropylene). The inhibitor (10 μL of a stock solution of 150 mM in Milli-Q water) was added, and after equilibrating for 5 min, $(NH_4)_2SO_4$ (10 μL of a stock solution of 150 mM in Milli-Q water) was added using a multichannel pipette to ensure simultaneous addition in each tube. The tubes were incubated in a temperature-regulated rotary incubator (Ratek, Australia) for 30 min at 30 °C and 100 rpm in the dark. A 50 μL aliquot was then transferred to a 96-well plate (Greiner Cellstar, polystyrene) to which 50 μL of Griess reagent was added, and the mixture was incubated for 15 min. The absorbance was measured at 540 nm (Clariostar BMG Labtech, Australia). The remaining cells were subsequently washed (3×) by alternating centrifuging (Boeco, Germany; 10,000 rpm, 10 min) and resuspending the cell pellet in NaPB (1 mL). After the final centrifuging step, the pellet was resuspended in NaPB (990 μL) and reincubated with $(NH_4)_2SO_4$ (10 μL of an aqueous 150 mM stock solution, see above), and the NO_2^- concentration was measured under the previously described conditions. Each assay was accompanied by control treatments to determine the 0 and 100% NO_2^- signals. The % activity was determined according to eq 3, where untreated cells (0% signal) denotes the NO_2^- production of the cells without additive, uninhibited cells (100% signal) denotes the NO_2^- production of cells treated with $[NH_4^+]$ = 3 mM, and inhibited cells denotes the NO_2^- production of cells treated with $[NH_4^+]$ = 3 mM and [inhibitor] = 1.5 mM. All experiments were performed in triplicate.

$$\%\ \text{activity} = \frac{[NO_2^-]_{\text{inhibited cells}} - [NO_2^-]_{\text{untreated cells}}}{[NO_2^-]_{\text{uninhibited cells}} - [NO_2^-]_{\text{untreated cells}}} \times 100 \quad (3)$$

2.3.4. Michaelis−Menten Kinetics. In a deep 96-well plate (2 mL capacity), 980 μL of the bacterial inoculum (OD_{600} = 0.03, ~18 μg L^{-1} protein in NaPB at pH 7.5) was added to DMP (10 μL from 0.75 mM and 1.5 mM stock solutions, respectively) or DCD (10 μL from 15 and 30 mM stock solutions, respectively). The solutions were mixed thoroughly and preincubated in the dark for 5 min at 100 rpm and at 30 °C (Ratek, Australia). Then, 10 μL of the respective $(NH_4)_2SO_4$ stock solution (150, 75, 5, 2.5, 1.5, 0.15 mM) was added to each well (final $[NH_4^+]$ in well: 3.0, 1.5, 0.1, 0.05, 0.03, 0.003 mM). The plate was covered with an O_2 permeable membrane to ensure aeration (Breathe-Easy sealing membrane, Sigma-Aldrich) and incubated in the dark for 60 min at 30 °C and 100 rpm. Termination of the nitrification process and determination of the NO_2^- production was performed as described in the Standard Assay Protocol section. Data analysis was performed with GraphPad Prism software, using nonlinear regression (curve fit) for Michaelis−Menten Kinetics.[47] The results used the best fit values with 95% likelihood.

2.3.5. Acute Toxicity Test. Cells were harvested according to the description in the Harvesting Cell Protocol section. The bacterial solution was adjusted to OD_{600} = 0.8 (~468 μg L^{-1} protein) and divided into 1 mL aliquots. To each well of a 24-well tissue culture plate (Greiner Cellstar, polystyrene Tissue Culture treated) was added 980 μL of bacterial solution, 10 μL of a 150 mM aqueous $(NH_4)_2SO_4$ solution, and 10 μL of either a DMP or a DCD solution with a final concentration in the well of 10 ppm (0.015 mM), 100 ppm (0.15 mM), and 1000 ppm (1.5 mM), respectively. The well plate was sealed with an O_2 permeable membrane to ensure aeration (Breathe-Easy sealing membrane, Sigma-Aldrich) and incubated in the dark for 4 h at 30 °C and 100 rpm. Cells were then transferred into a centrifuge tube and sedimented at 10,000 rpm for 10 min. The supernatant was separated, and the cells were resuspended in NaPB (pH = 7.5, 1 mL). A 5 μL aliquot was transferred into a 96-well plate, and the bacterial stain (LIVE/DEAD BacLight Bacterial Viability Kit for microscopy, Thermo Fisher Scientific) was added following the manufacturer's instructions. Then, 10 μL of the solution was transferred onto a microscopic slide (Fisher Scientific, Australia, 7.6 cm × 2.5 cm ($L \times W$), thickness 1−1.2 mm). Seven images were taken per treatment with a fluorescence microscope (Leica DM6000, Germany) using the red channel to detect dead cells (excitation: 575/30 nm (dichromatic) DC: 600; emission: 635/40 nm) and the green channel to detect live cells (excitation: 500/20 nm DC: 515; emission: 535/30 nm). The percentage of live and dead cells was calculated using eqs 4 and 5

$$\%\ \text{live} = \frac{\text{live cell count}}{\text{total cell count}} \times 100 \quad (4)$$

$$\%\ \text{dead} = \frac{\text{dead cell count}}{\text{total cell count}} \times 100 \quad (5)$$

Prior to the microscopic imaging, 50 μL of supernatant was reacted with a 50 μL Griess reagent to determine $[NO_2^-]$ following the Standard Assay Protocol section.

https://doi.org/10.1021/acsagscitech.2c00303
ACS Agric. Sci. Technol. 2023, 3, 222−231

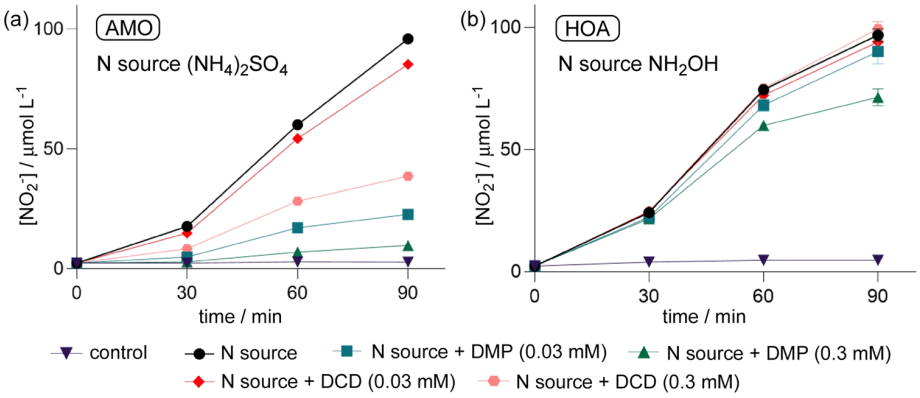

Figure 2. (a) Effect of DMP and DCD at different concentrations on the cumulative NO_2^- production after 30 min, 60 min, and 90 min of inoculation with (a) $[NH_4^+]$ = 3 mM and (b) $[NH_2OH]$ = 3 mM as N source, respectively. The inoculations were performed in NaPB (pH = 7.5) at 30 °C and 100 rpm in the dark. Standard errors were calculated from three biological replicates, each performed with three technical replicates.

2.4. Statistics. Statistical analysis was performed with GraphPad Prism software[47] using Student's *t*-test $P < 0.05$ as the level of statistical significance. All results are reported as the mean ± standard error of the mean. In addition, significances among three treatments were compared by the least significant differences $P < 0.05$ level using one-way ANOVA.

3. RESULTS AND DISCUSSION

We first identified the enzyme targeted by DMP and DCD and their mode of binding using *N. europaea* as model AOB. The analysis was performed by measuring the amount of NO_2^- produced in the absence and presence of the NI, which was determined using a recently developed assay based on the Griess reaction.[45] We then explored the mode of inhibition by measuring the Michaelis–Menten kinetics and the inhibitory efficacy by establishing the rate of NH_3 oxidation by *N. europaea*, which was obtained from O_2 consumption measurements. Analysis of the acute toxicity of both inhibitors was performed to investigate whether the lower production of NO_2^- in the presence of DMP and DCD could be due to a potential toxicity of the inhibitors for the bacteria.

3.1. Identification of the Enzyme Targeted by DMP and DCD. As outlined in the Introduction section, oxidation of NH_3 to NO_3^- occurs in several steps, where AOB are responsible for the first two steps, *i.e.*, $NH_3 \rightarrow NH_2OH \rightarrow NO_2^-$, which are catalyzed by the enzymes AMO and HAO, respectively. To explore which of these two enzymes is inhibited by DMP and DCD, we performed assays where pure cell cultures of *N. europaea* were treated in sodium phosphate buffer (NaPB) at pH 7.5 and 30 °C separately with either NH_4^+ (as substrate for AMO) or NH_2OH (as substrate for HAO) and measured the cumulative NO_2^- production over 90 min in the presence and absence of the NI. Inhibition of the enzyme should result in a lower NO_2^- production, compared to the noninhibited cell culture. The concentration of the N source (provided as $(NH_4)_2SO_4$ or NH_2OH, respectively) was 3 mM, and the inhibitors were supplied at two different concentrations (*i.e.*, 1 and 10 mol % of applied N). Figure 2 shows the production of NO_2^- over 90 min under the different conditions. Control experiments, which were performed with cells in NaPB without a N source and inhibitor, did not reveal a notable production of NO_2^-, confirming that NO_2^- resulted from the oxidation of NH_4^+ or NH_2OH, respectively. The detailed data are provided in Tables S1 and S2 in the Supporting Information (SI).

In the incubations targeting AMO (Figure 2a), uninhibited cells generated a total $[NO_2^-]$ of 17.7 µM after 30 min, corresponding to an NO_2^- production rate of about 0.5 µM min^{-1}. Over the next 60 min, the activity of AMO increased to an average NO_2^- production rate of 1.3 µM min^{-1}. Treatment with both DMP and DCD reduced the NO_2^- production when compared to the uninhibited cells; however, the inhibiting effect was generally more pronounced with DMP than with DCD at the same concentration, in agreement with literature data.[48,49] Thus, in the first 30 min, cells exposed to 0.03 and 0.3 mM of DMP produced $[NO_2^-]$ of 4.9 and 2.9 µM, respectively. Compared to the uninhibited cells, the % inhibition (calculated according to eq 1) was 83% for 0.03 mM DMP and 93% for the 10-fold higher concentration. Over the following 60 min, the % inhibition with [DMP] = 0.03 mM decreased to 74%, whereas with [DMP] = 0.3 mM, the % inhibition remained unchanged at 94%. In contrast, the inhibitory performance of DCD depended much stronger on its concentration. After 90 min, the % inhibition with [DCD] = 0.03 mM was only 11%, whereas with [DCD] = 0.3 mM, the % inhibition was 61%.

Providing NH_2OH to the cell culture enabled to study the HAO-catalyzed transformation, *i.e.*, $NH_2OH \rightarrow NO_2^-$, under exclusion of AMO. Figure 2b shows that uninhibited cells produced around the same amount of NO_2^- after 90 min as those treated with NH_4^+. Treatment of the cells with DMP at the lower concentration and with DCD at both concentrations had practically no impact on the NO_2^- production. Only when the cells were exposed to 0.3 mM of DMP, a noticeable reduction of $[NO_2^-]$ occurred, which amounted to a % inhibition of about 27% after 90 min. However, we do not believe that the lower NO_2^- production at higher [DMP] indicates HOA inhibition but is likely an indirect effect of the strong AMO inhibition. As AMO accepts two electrons from HOA that are produced during the oxidation of NH_2OH, AMO inhibition could disrupt the electron transfer chain between these two enzymes, thereby reducing HOA activity. Our finding that DMP targets AMO is in agreement with a recent study.[41]

With regards to the "fate" of both NIs in AMO, it is unlikely that they undergo conversion in the enzyme to produce a more active form, as no increase in % inhibition over time was observed. This finding suggests that both DMP and DCD are chelators (*i.e.*, non-mechanism-based enzyme inhibitors) that

https://doi.org/10.1021/acsagscitech.2c00303
ACS Agric. Sci. Technol. 2023, 3, 222–231

could coordinate to the Cu^{2+} centers in AMO through their N atoms *via* a vacant electron pair, as has been found in crystal structures of the DMP-Cu^{2+} and the DCD-Cu^{2+} complexes.[44,50] However, it cannot be excluded that the inhibitory effect of DMP and DCD could, at least in part, be due to a potential toxicity for AMO. We will explore this factor below.

3.2. Determining the Inhibition Mechanism. To gain mechanistic insight how DMP and DCD are inhibiting AMO, we studied the Michaelis–Menten kinetics by measuring the production of NO_2^- at different $[NH_4^+]$ and constant [NI]. The Michaelis constant, K_m, is the substrate concentration, [S], at which the reaction rate, v, is 50% of the maximal rate, V_{max}, and can be regarded as an inverse measure of the enzyme–substrate affinity (see eq 6).

$$v = \frac{V_{max}[S]}{K_m + [S]} \quad (6)$$

Thus, noncompetitive inhibition is characterized by a decrease of V_{max} that is independent of [S], as substrates and inhibitors are not competing for the same site in the enzyme (K_m unchanged). In contrast to this, uncompetitive inhibition shows both a decreased K_m and V_{max}, whereas competitive inhibition shows an increased K_m and an unchanged V_{max}.[51]

[DMP] and [DCD] were chosen close to their IC_{50abs} values (DMP: 6.6 μM and DCD: 0.1 mM)[45] to achieve partial inhibition (50–80%) of the NO_2^- production. Figure 3 shows

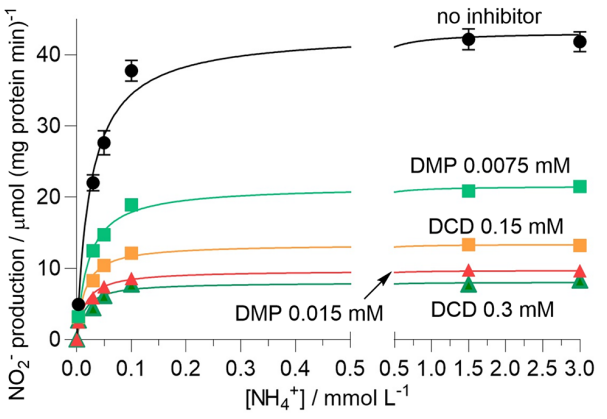

Figure 3. Effect of DMP and DCD on the NO_2^- production in the dependence of $[NH_4^+]$ after 60 min. The inoculations were performed with $[NH_4^+]$ = 0.003, 0.03, 0.05, 0.1, 1.5, and 3.0 mM in NaPB (pH = 7.5) at 30 °C and 100 rpm in the dark. Note different axis scale to include the data at higher $[NH_4^+]$. Standard errors were calculated from three biological replicates.

that the formation of NO_2^- followed Michaelis–Menten-type saturation kinetics for both inhibitors, clearly revealing that not only less NO_2^- was produced in the presence of the inhibitor but that increasing $[NH_4^+]$ beyond 1.5 mmol L^{-1} also did not have any impact on $[NO_2^-]$.

Apparent half-saturation constants for ($K_{m(app)}$) and maximum velocities ($V_{max(app)}$) in the presence/absence of DMP and DCD were calculated using the hyperbolic regression analysis (see Section 2.3.4). Note that the prefix "app" (apparent) was used as these studies were performed with bacterial cells and not with the pure enzyme. The data are shown in Table 1.

Compared to uninhibited cells, DMP and DCD reduce $V_{max(app)}$ by about 50–85%. Furthermore, $K_{m(app)}$ for both inhibitors is significantly lower ($P < 0.05$) than that for the uninhibited cells. These findings suggest that both DMP and DCD inhibit pure bacterial cultures of *N. europaea* through uncompetitive inhibition.

Although the crystal structure of AMO, particularly its active site, is unknown, simulations of bacterial AMO revealed that the enzyme contains multiple Cu^{2+}-containing subunits.[12,52] DMP and DCD could principally bind to any of these sites, depending on accessibility. However, as uncompetitive inhibitors bind to the enzyme–substrate complex to show an inhibitory effect, it is highly likely that the inhibitor binding site is near the substrate binding site.

3.3. Exploring the Reversibility of the Inhibition. Next, we explored whether the inhibition of AMO by DMP or DCD is reversible or irreversible. For these experiments, *N. europaea* cells were incubated for 30 min with 3 mM of NH_4^+ and a high concentration of DMP and DCD, respectively ([NI] = 1.5 mM), to ensure considerable inhibition, and the NO_2^- production was measured (inhibited cells). The cells were then washed several times with NaPB with the intention to remove both unbound and enzyme-bound inhibitors. After the final washing cycle, NH_4^+ was added to the cells, and the NO_2^- production was measured again after 30 min of incubation. The % activity was determined according to eq 3 (details are provided in Section 2.3.3). The data are shown in Table 2.

In the first step of the experiment, cells exposed to DMP showed an activity of about 4% (nearly quantitative inhibition due to the high [DMP] used), whereas in the case of DCD, the nitrification activity of the cells was reduced to about one-third, reconfirming that DMP is a more efficient inhibitor than DCD. After washing the cells and reincubating with NH_4^+, the activity increased to 67% for the cells previously treated with DMP and to 55% for the DCD-treated cells. The considerable recovery of enzyme activity after washing the cells, particularly in the case of DMP, suggests reversible inhibition, whereas irreversible inhibitors form covalent bonds with the enzyme,

Table 1. Michaelis–Menten Kinetics Parameter of the $[NH_4^+]$-Dependent Production of NO_2^- by *N. europaea* in the Absence and Presence of DMP and DCD, Respectively, at Different Concentrations[a]

inhibitor	concentration/mM	$V_{max(app)}$/µmol (mg protein min)$^{-1}$	$K_{m(app)}$/µM
none		43.2 ± 1.2	25.4 ± 1.8
DMP	0.0075	21.6 ± 0.2	20.5 ± 0.2
	0.015	9.7 ± 0.3	15.1 ± 1.9
DCD	0.15	13.4 ± 0.3	14.4 ± 0.7
	0.3	8.0 ± 0.3	14.4 ± 4.7

[a][NI] was selected to achieve partial inhibition of the NO_2^- production and amended according to their efficacy (see text). Standard errors were calculated from three biological replicates, each performed with three technical replicates.

https://doi.org/10.1021/acsagscitech.2c00303
ACS Agric. Sci. Technol. 2023, 3, 222–231

Table 2. Determination of the Activity of Inhibited AMO, Using Pure Cell Cultures of *N. europaea* after the Removal of the NI through Repeated Washing with NaPB.[a]

	% activity	
inhibitor	inhibited cells	after washing
DMP	4.2 ± 2.6	66.6 ± 3.3
DCD	32.6 ± 7.3	54.6 ± 13.0

[a]The inoculations were performed with $[NH_4^+]$ = 3.0 mM and [DMP] or [DCD] = 1.5 mM in NaPB (pH = 7.5) at 30 °C and 100 rpm in the dark. Standard errors were calculated from three biological replicates, each performed with three technical replicates.

requiring *de novo* synthesis of AMO to regain activity. For example, nitrifying cells exposed to the irreversible inhibitors acetylene and 1-octyne recovered their activity only after four hours.[53] Binding studies performed with nitapyrin showed that the release of the inhibitor required washing of the cells with buffer containing Cu^{2+} to "force" decomplexation of the NI from AMO.[38] In the case of DMP and DCD, however, washing the cells with buffer solution alone was sufficient to remove the inhibitors from the enzyme, suggesting that their coordination to the relevant Cu center(s) in AMO is not very strong, which could provide a rationale for the variable performance of these NIs in the field. The finding that no full recovery of activity was observed is not surprising, given the high inhibitor concentration used in this experiment, which could lead to the partial loss of cells (see below).

3.4. Determination of the Rate of NH_3 Oxidation by AMO. The rate of the NH_3 oxidation by AMO and whether NIs directly target this process can be determined through O_2 respiration measurements. As NH_3 oxidation requires equimolar O_2, the O_2 consumption (or O_2 uptake by the enzyme) is directly proportional to the NH_3 oxidation rate.[54] We measured the O_2 consumption by cell suspensions of *N. europaea* at 20 °C using a Clark-type oxygen electrode by first monitoring the decrease of $[O_2]$ in the presence of NH_4^+ (3 mM) for 5 min. The inhibitor was then added at different concentrations, the system was allowed to equilibrate for 15 s, and the O_2 decay was subsequently monitored for a further 5 min. In all measurements, NH_4^+ and O_2 were both present in excess so that the rate was only determined by the enzyme concentration (the total protein concentration was ∼ 468 μg L^{-1}, determined via a BCA assay kit). Under these conditions, the O_2 consumption should follow zero-order kinetics, and the rate coefficient, *k*, can be determined from the slope of the plot of $[O_2]$ over time. In the presence of inhibitors, NH_3 oxidation should slow down, resulting in a slower rate of O_2 consumption. It should be noted that the inhibitor concentrations were chosen such that the O_2 consumption was not completely stopped. Thus, to compensate for the lower efficacy of DCD, the latter required higher concentrations than DMP.

Figure 4a shows the O_2 consumption of cells treated with DMP, and Figure 4b shows that for DCD-treated cells.

In the initial stage of the experiment in the absence of inhibitors, the measured linear dependence of the O_2 consumption over time confirmed zero-order kinetics, revealing a rate coefficient of 186 ± 63 nmol L^{-1} s^{-1} (see Table S3 and Figure S1). The rate of O_2 consumption slowed down after the addition of the inhibitors, as would be expected for a reduced enzyme activity, but remained zero order (see Figures S2 and S3). Table 3 compiles the rate coefficients for the O_2 consumption in the absence and presence of the NIs. The data for each replicate measurement are compiled in Table S4.

Table 3. Rate Coefficient, *k*, for the O_2 Consumption by *N. europaea* in the Absence and Presence of DMP and DCD, Respectively, and the % Inhibition at the Different [NI][a]

inhibitor	concentration/mM	*k*/nmol L^{-1} s^{-1}	% Inhibition
none		186 ± 63	
DMP	0.012	199 ± 117	no inhibition
	0.12	31 ± 13	75 ± 6
	0.6	64 ± 9	65 ± 5
	1.2	56 ± 1	70 ± 1
DCD	1.2	118 ± 20	28 ± 6
	2.0	112 ± 9	40 ± 7
	5.0	68 ± 9	63 ± 5
	10.0	39 ± 9	79 ± 5

[a]Cells were treated with $[NH_4^+]$ = 3.0 mM in NaPB (pH = 7.5) at 20 °C under constant stirring in the dark. All errors are standard errors calculated from three measurements of biological replicates. % Inhibition was determined according to the following formula: 100 − [rate (with inhibitor)/rate (without inhibitor) × 100].

The zero-order behavior in the presence of DMP and DCD supports our findings from the previous sections that both NIs

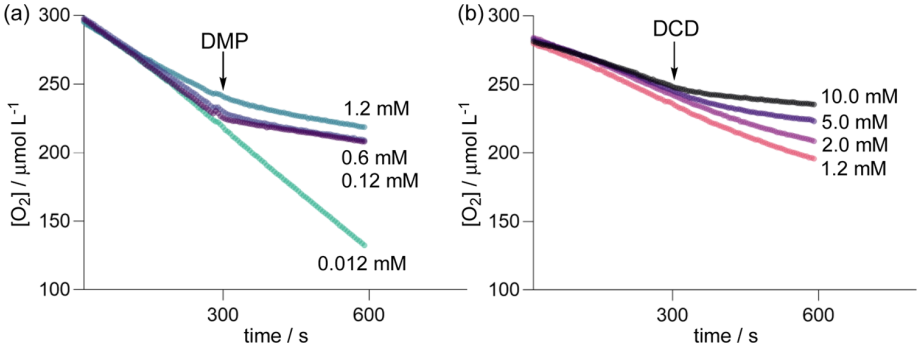

Figure 4. Measurements of the O_2 consumption by *N. europaea* in the absence and presence of (a) DMP and (b) DCD at different concentrations. The first 300 s is the rate in the absence of inhibitors. At the 300 s timepoint, the inhibitor was added (indicated with an arrow). The cells were treated with $[NH_4^+]$ = 3.0 mM at pH = 7.5 at 20 °C under constant stirring in the dark. The plot shows the mean of three measurements for each concentration; standard errors are omitted for clarity.

https://doi.org/10.1021/acsagscitech.2c00303
ACS Agric. Sci. Technol. 2023, 3, 222−231

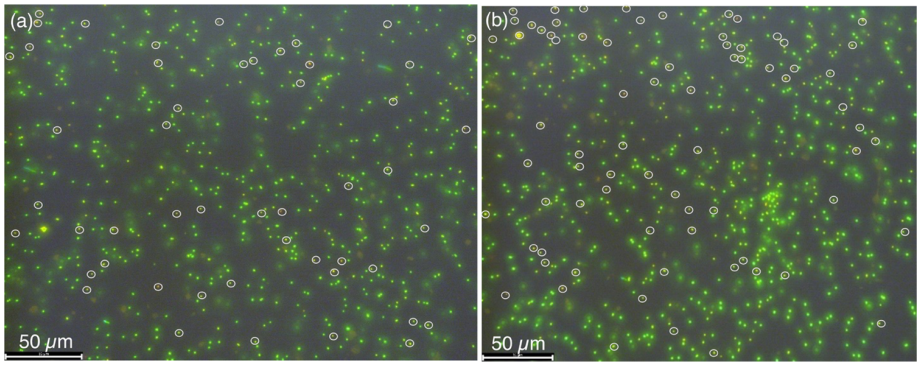

Figure 5. Microscopic images of *N. europaea* in the (a) absence of DMP and (b) presence of 10 ppm DMP. The cells were visualized with the BacLight viability stain. Channels were overlayed to show "alive" cells (green) and "dead" cells (red) in a single image. Note that the dead cells (which are in the minority) appear orange in these images, which have been circled for clarity.

are chelating agents that reversibly bind to the enzyme. In contrast, mechanism-based inhibitors, such as acetylene and phenylacetylene, bind irreversibly to the enzyme, which reduces the enzyme's "active" concentration over time and results in a first-order consumption of O_2 by the enzyme.[55,56]

Overall, cells treated with DCD consumed more O_2 than cells treated with DMP, although [DCD] was considerably higher than [DMP], clearly confirming that both inhibitors, although with different efficiency, directly impact on the ability of AMO to promote NH_3 oxidation. The % inhibition at the different [NI] could be obtained from the ratio of the rate coefficients in the presence and absence of the inhibitor, which are included in Table 3. Thus, the % inhibition by DMP was relatively constant in the concentration range 0.12−1.2 mM, averaging to 70 ± 4%. In contrast, the % inhibition by DCD was considerably more concentration-dependent, dropping from 79% for 10 mM to just 28% for 1.2 mM.

3.5. Determination of Short-Term Toxic Effects of DMP and DCD. A bacterial viability stain can provide insights of toxic effects of chemical compounds for *N. europaea*. While this method has been previously used to explore the toxicity of silver nanoparticles for *N. europaea*,[57] no such evaluation has been done for NIs.

To assess the acute toxicity of DMP and DCD for *N. europaea*, cells were incubated at 30 °C in NaPB (pH = 7.5) with $[NH_4^+]$ = 3 mM for 12 h with three different concentrations of DMP and DCD (10, 100, and 1000 ppm). Figure 5 shows two exemplary microscopic images for *N. europaea* bacterial cells without inhibitor and with [DMP] = 10 ppm. It should be noted that the incubations in the absence of inhibitor were also performed with $[NH_4^+]$ = 3 mM to avoid cell death caused by starvation. Standard errors were determined from seven microscopic images. The numbers of live/dead cells for each image are provided in Table S5.

Table 4 shows the percentage of live and dead cells (calculated using eqs 5 and 6) at the different concentrations of the NI.

At the lowest concentration (10 ppm), cell death caused by both NIs was nonsignificant compared to the control treatment. However, both inhibitors decreased the % live cells when their concentration was increased to 100 ppm, *i.e.*, 70% for DMP and 77% for DCD. With [inhibitor] = 1000 ppm, 74% of cells treated with DCD remained alive, whereas the toxicity of DMP was higher, with just 65% of the cells still alive. Parallel to the viability stain, the NO_2^- production was also measured, which showed that the higher cell death rate with increasing [DMP] correlated with a reduction of $[NO_2^-]$. In contrast, in the case of DCD, the NO_2^- production remained largely unchanged at all three concentrations (even in comparison with the control treatment), which further confirms the much lower inhibitory activity of this inhibitor.

Table 4. Acute Toxicity of DMP and DCD at Different Concentrations for Cells of *N. europaea* Determined with a Bacterial Viability Stain and Determination of the NO_2^- Production[a]

inhibitor	concentration/ppm	% live	% dead	$[NO_2^-]/\mu M$
none		96 ± 3	5 ± 3	454
DMP	10	87 ± 9	7 ± 7	338
	100[b]	70 ± 8	29 ± 5	112
	1000[b]	67 ± 5	34 ± 5	46
DCD	10	89 ± 4	10 ± 4	430
	100[b]	77 ± 15	22 ± 15	444
	1000[b]	74 ± 11	25 ± 11	445

[a]The incubations were performed in NaPB at pH = 7.5 and 30 °C with $[NH_4^+]$ = 3 mM and [inhibitor] = 10 ppm (0.015 mM), 100 ppm (0.15 mM), and 1000 ppm (1.5 mM) at 100 rpm for 12 h in the dark. Standard errors were determined from seven microscopic images. [b]Indicates significant difference in comparison to uninhibited cells ($P < 0.05$).

However, when assessing inhibitor efficiency and toxicity, it needs to be considered that an at least 10 times higher application rate of DCD would be required to achieve a nitrification inhibition comparable with DMP (see Figure 1). For example, while no significant cell death occurs [DMP] = 10 ppm, the cell death is much higher for [DCD] = 100 ppm. Therefore, increasing the application rate of DCD is not a useful approach to increase nitrification inhibition, as it would lead to increased cell death.

In conclusion, using pure cell cultures of *N. europaea*, we have shown that DMP and DCD target the first step of nitrification by inhibiting AMO. Although at higher concentrations of DMP, the NO_2^- production through NH_2OH oxidation mediated by HOA decreased too; we suggest that this reduction is an indirect effect of the strong AMO inhibition. Both inhibitors can be removed from the enzyme by washing with buffer, indicating that they act as chelating agents, which reversibly bind to the enzyme. These findings were confirmed by measuring the kinetics of the O_2 consumption by *N. europaea* in the presence of DMP and

https://doi.org/10.1021/acsagscitech.2c00303
ACS Agric. Sci. Technol. 2023, 3, 222−231

DCD, respectively. DMP reduced the O_2 uptake rate considerably more at much lower concentrations than DCD, in line with the lower inhibitory efficiency of the latter. However, the binding between enzymes and NIs is not very strong, which may, at least to some extent, explain the highly variable performance of both NIs in different soils[27−33] and could provide a potential pathway to develop more efficient and consistent NIs in the future. Furthermore, Michalis−Menten kinetics revealed that both DMP and DCD act as uncompetitive inhibitors, whereas studies of the acute toxicity suggest that increasing the application rate of the poorer-performing DCD to increase the inhibition of AMO cannot be recommended as it is associated with increased cell death. On a final note, it has been shown that temperature is also a crucial factor affecting inhibitory efficiency, as more rapid degradation of the nitrification inhibitors could occur in soils at higher temperatures.[21,58,59] In future work, we will therefore apply the bacterial assay used here to explore in detail the role of temperature on the inhibitory activity through kinetic studies.

■ ASSOCIATED CONTENT

Supporting Information

The Supporting Information is available free of charge at https://pubs.acs.org/doi/10.1021/acsagscitech.2c00303.

(Supporting Table S1) cumulative NO_2^- production by *N. europaea* with ammonium (NH_4^+) in the absence and presence of DMP and DCD over three consecutive 30-min intervals; (Table S2) cumulative NO_2^- production by *N. europaea* with hydroxylamine (NH_2OH) in the absence and presence of DMP and DCD over three consecutive 30-min intervals; (Table S3) rate coefficients, *k*, for the time-dependent O_2 consumption by *N. europaea* in the absence of NI; (Table S4) rate coefficients, *k*, for the time-dependent O_2 consumption by *N. europaea* in the presence of DMP and DCD at different concentrations; (Table S5) number of alive and dead cells of *N. europaea* in the absence and presence of DMP and DCD at different concentrations determined with a bacterial viability stain; (Supporting Figure S1) O_2 consumption by *N. europaea* as a function of time in the absence of NI; (Figure S2) O_2 consumption by *N. europaea* as a function of time after the addition of DMP at different concentrations; (Figure S3) O_2 consumption by *N. europaea* as a function of time after the addition of DCD at different concentrations (PDF)

■ AUTHOR INFORMATION

Corresponding Author

Uta Wille − *School of Chemistry, The University of Melbourne, Parkville, Victoria 3010, Australia;* orcid.org/0000-0003-1756-5449; Phone: +61 3 8344 2425; Email: uwille@unimelb.edu.au

Authors

Sibel C. Yildirim − *School of Chemistry, The University of Melbourne, Parkville, Victoria 3010, Australia;* orcid.org/0000-0002-1208-1210

Robert M. Walker − *School of BioSciences, The University of Melbourne, Parkville, Victoria 3010, Australia;* orcid.org/0000-0002-2064-4546

Ute Roessner − *School of BioSciences, The University of Melbourne, Parkville, Victoria 3010, Australia; Research School of Biology, The Australian National University, Acton, Australian Capital Territory 2600, Australia;* orcid.org/0000-0002-6482-2615

Complete contact information is available at: https://pubs.acs.org/10.1021/acsagscitech.2c00303

Author Contributions

S.C.Y. performed the experiments, processed the experimental data, and performed the analysis. R. W., U. R., and U. W. designed, planned, and supervised the work. All authors aided in interpreting the results. S. C. Y. and U. W. wrote the manuscript and designed the figures with input of all authors.

Funding

This work was supported by the Australian Research Council through the ARC Research Hub for Smart Fertilizers (IH200100023) and the Discovery Project ("Connecting soil nitrogen and plant uptake for greener agriculture", DP200101162) Schemes.

Notes

The authors declare no competing financial interest.

■ ACKNOWLEDGMENTS

The authors thank Sneha Gupta, Michelle Watt, Claudia Knief, and Nicolas Brüggemann for helpful discussions and Guy Jamesson for providing the Clark-type electrode. Support by the Bio21 Institute's Magnetic Resonance and the Mass Spectrometry and Proteomics Facility (MSPF), Melbourne University and the School of BioSciences Microscopy Unit, is gratefully acknowledged.

■ ABBREVIATIONS USED

AMO - ammonia monooxygenase
ANOVA - analysis of variance
AOA - ammonia-oxidizing archaea
AOB - ammonia-oxidizing bacteria
ATCC - American Type Culture Collection
BCA - bicinchoninic acid
DCD - dicyandiamide
DMP - 3,4-dimethyl-1*H*-pyrazole
DMPP - 3,4-dimethyl-1*H*-pyrazole phosphate
HAO - hydroxylamine oxidoreductase
FAO - Food and Agriculture Organization of the United Nations
GHG - greenhouse gas
IC_{50abs} - concentration of the inhibitor to decrease response to 50%
K_m - Michaelis−Menten constant
MSM - mineral salt media
NaPB - sodium phosphate buffer
NI - nitrification inhibitor
N. europaea - *Nitrosomonas europaea*
NUE - nitrogen use efficiency
OD - optical density
OD_{600} - optical density at 600 nm
$PM_{2.5}$ - particulate matter (diameter ≤ 2.5 μm)
ppm - parts per million
rpm - rotations per minute
SI - supporting information
UV/vis - ultraviolet−visible region
V_{max} - maximal rate

REFERENCES

(1) Food and Agriculture Organization of the United Nations (FAO). World Fertilizer Trends and Outlook to 2020. Rome, 2019. http://www.fao.org/3/ca6746en/ca6746en.pdf (Accessed September 09, 2022).

(2) Raun, W. R.; Schepers, J. S.Nitrogen Management for Improved Use Efficiency. In *Nitrogen in Agricultural Systems*; Schepers, J. S.; Raun, W. R., Eds.; 2008; pp 675−693 DOI: 10.2134/agronmonogr49.c17.

(3) Cavigelli, M. A.; Del Grosso, S. J.; Liebig, M. A.; Snyder, C. S.; Fixen, P. E.; Venterea, R. T.; Leytem, A. B.; McLain, J. E.; Watts, D. B. US Agricultural Nitrous Oxide Emissions: Context, Status, and Trends. *Front. Ecol. Environ.* **2012**, *10*, 537−546.

(4) Ladha, J. K.; Pathak, H.; Krupnik, T. J.; Six, J.; van Kessel, C.Efficiency of Fertilizer Nitrogen in Cereal Production: Retrospects and Prospects. In *Advances in Agronomy*; Academic Press, 2005; Vol. *87*, pp 85−156 DOI: 10.1016/S0065-2113(05)87003-8.

(5) Robertson, G. P.; Bruulsema, T. W.; Gehl, R. J.; Kanter, D.; Mauzerall, D. L.; Rotz, C. A.; Williams, C. O. Nitrogen−Climate Interactions in US Agriculture. *Biogeochemistry* **2013**, *114*, 41−70.

(6) Norton, J.; Ouyang, Y. Controls and Adaptive Management of Nitrification in Agricultural Soils. *Front. Microbiol.* **2019**, *10*, 1931.

(7) Jetten, M. S. M. The Microbial Nitrogen Cycle. *Environ. Microbiol.* **2008**, *10*, 2903−2909.

(8) Coskun, D.; Britto, D. T.; Shi, W.; Kronzucker, H. J. Nitrogen Transformations in Modern Agriculture and the Role of Biological Nitrification Inhibition. *Nat. Plants* **2017**, *3*, 17074.

(9) Ruser, R.; Schulz, R. The Effect of Nitrification Inhibitors on the Nitrous Oxide (N_2O) Release from Agricultural Soils—a Review. *J. Plant Nutr. Soil Sci.* **2015**, *178*, 171−188.

(10) Lawton, T. J.; Ham, J.; Sun, T.; Rosenzweig, A. C. Structural Conservation of the B Subunit in the Ammonia Monooxygenase/Particulate Methane Monooxygenase Superfamily. *Proteins* **2014**, *82*, 2263−2267.

(11) McTavish, H.; Fuchs, J. A.; Hooper, A. B. Sequence of the Gene Coding for Ammonia Monooxygenase in *Nitrosomonas europaea*. *J. Bacteriol.* **1993**, *175*, 2436.

(12) Musiani, F.; Broll, V.; Evangelisti, E.; Ciurli, S. The Model Structure of the Copper-Dependent Ammonia Monooxygenase. *J. Biol. Inorg. Chem.* **2020**, *25*, 995−1007.

(13) McCarty, G. W. Modes of Action of Nitrification Inhibitors. *Biol. Fertil. Soils* **1999**, *29*, 1−9.

(14) Hyman, M. R.; Sansome-Smith, A. W.; Shears, J. H.; Wood, P. M. A Kinetic Study of Benzene Oxidation to Phenol By Whole Cells of *Nitrosomonas europaea* and Evidence for the Further Oxidation of Phenol to Hydroquinone. *Arch. Microbiol.* **1985**, *143*, 302−306.

(15) Vajrala, N.; Martens-Habbena, W.; Sayavedra-Soto, L. A.; Schauer, A.; Bottomley, P. J.; Stahl, D. A.; Arp, D. J. Hydroxylamine as an Intermediate in Ammonia Oxidation by Globally Abundant Marine Archaea. *Proc. Natl. Acad. Sci. U.S.A.* **2013**, *110*, 1006−1011.

(16) Sun, D.; Tang, X.; Zhao, M.; Zhang, Z.; Hou, L.; Liu, M.; Wang, B.; Klümper, U.; Han, P. Distribution and Diversity of Comammox Nitrospira in Coastal Wetlands of China. *Front. Microbiol.* **2020**, *11*, No. 589268.

(17) Caranto, J. D.; Lancaster, K. M. Nitric Oxide is an Obligate Bacterial Nitrification Intermediate Produced by Hydroxylamine Oxidoreductase. *Proc. Natl. Acad. Sci. U.S.A.* **2017**, *114*, 8217−8222.

(18) Caranto, J. D.; Vilbert, A. C.; Lancaster, K. M. *Nitrosomonas europaea* Cytochrome P460 is a Direct Link Between Nitrification and Nitrous Oxide Emission. *Proc. Natl. Acad. Sci. U.S.A.* **2016**, *113*, 14704−14709.

(19) Venterea, R. T.; Rolston, D. E. Mechanisms and Kinetics of Nitric and Nitrous Oxide Production During Nitrification in Agricultural Soil. *Global Change Biol.* **2000**, *6*, 303−316.

(20) Wrage-Mönnig, N.; Horn, M. A.; Well, R.; Müller, C.; Velthof, G.; Oenema, O. The Role of Nitrifier Denitrification in the Production of Nitrous Oxide Revisited. *Soil Biol. Biochem.* **2018**, *123*, A3−A16.

(21) Venterea, R. T.; Clough, T. J.; Coulter, J. A.; Souza, E. F. C.; Breuillin-Sessoms, F.; Spokas, K. A.; Sadowsky, M. J.; Gupta, S. K.; Bronson, K. F. Temperature Alters Dicyandiamide (DCD) Efficacy for Multiple Reactive Nitrogen Species in Urea-Amended Soils: Experiments and Modeling. *Soil Biol. Biochem.* **2021**, *160*, No. 108341.

(22) Ensign, S. A.; Hyman, M. R.; Arp, D. J. *In vitro* Activation of Ammonia Monooxygenase from *Nitrosomonas europaea* by Copper. *J. Bacteriol.* **1993**, *175*, 1971−1980.

(23) Lieberman, R. L.; Rosenzweig, A. C. Crystal Structure of a Membrane-Bound Metalloenzyme that Catalyses the Biological Oxidation of Methane. *Nature* **2005**, *434*, 177−182.

(24) Cao, L.; Caldararu, O.; Rosenzweig, A. C.; Ryde, U. Quantum Refinement Does Not Support Dinuclear Copper Sites in Crystal Structures of Particulate Methane Monooxygenase. *Angew. Chem., Int. Ed.* **2018**, *57*, 162−166.

(25) Hyman, M. R.; Wood, P. M. Suicidal Inactivation and Labelling of Ammonia Monooxygenase by Acetylene. *Biochem. J.* **1985**, *227*, 719−725.

(26) Juliette, L. Y.; Hyman, M. R.; Arp, D. J. Inhibition of Ammonia Oxidation in *Nitrosomonas europaea* by Sulfur Compounds: Thioethers Are Oxidized to Sulfoxides by Ammonia Monooxygenase. *Appl. Environ. Microbiol.* **1993**, *59*, 3718−3727.

(27) Zhu, G.; Ju, X.; Zhang, J.; Müller, C.; Rees, R. M.; Thorman, R. E.; Sylvester-Bradley, R. Effects of the Nitrification Inhibitor DMPP (3,4-Dimethylpyrazole Phosphate) on Gross N Transformation Rates and N_2O Emissions. *Biol. Fertil. Soils* **2019**, *55*, 603−615.

(28) Li, H.; Liang, X.; Chen, Y.; Lian, Y.; Tian, G.; Ni, W. Effect of Nitrification Inhibitor DMPP on Nitrogen Leaching, Nitrifying Organisms, and Enzyme Activities in a Rice-Oilseed Rape Cropping System. *J. Environ. Sci.* **2008**, *20*, 149−155.

(29) Guardia, G.; Marsden, K. A.; Vallejo, A.; Jones, D. L.; Chadwick, D. R. Determining the Influence of Environmental and Edaphic Factors on the Fate of the Nitrification Inhibitors DCD and DMPP in Soil. *Sci. Total Environ.* **2018**, *624*, 1202−1212.

(30) Barrena, I.; Menéndez, S.; Correa-Galeote, D.; Vega-Mas, I.; Bedmar, E. J.; González-Murua, C.; Estavillo, J. M. Soil Water Content Modulates the Effect of the Nitrification Inhibitor 3,4-Dimethylpyrazole Phosphate (DMPP) on Nitrifying and Denitrifying Bacteria. *Geoderma* **2017**, *303*, 1−8.

(31) Koci, J.; Nelson, P. N. Tropical Dairy Pasture Yield and Nitrogen Cycling: Effect of Urea Application Rate and a Nitrification Inhibitor, DMPP. *Crop Pasture Sci.* **2016**, *67*, 766−779.

(32) Menéndez, S.; Merino, P.; Pinto, M.; González-Murua, C.; Estavillo, J. M. 3,4-Dimethylpyrazol Phosphate Effect on Nitrous Oxide, Nitric Oxide, Ammonia, and Carbon Dioxide Emissions from Grasslands. *J. Environ. Qual.* **2006**, *35*, 973−981.

(33) Dougherty, W. J.; Collins, D.; Van Zwieten, L.; Rowlings, D. W. Nitrification (DMPP) and Urease (NBPT) Inhibitors Had No Effect on Pasture Yield, Nitrous Oxide Emissions, or Nitrate Leaching under Irrigation in a Hot-Dry Climate. *Soil Res.* **2016**, *54*, 675−683.

(34) Weiske, A.; Benckiser, G.; Ottow, J. C. G. Effect of the New Nitrification Inhibitor DMPP in Comparison to DCD on Nitrous Oxide (N_2O) Emissions and Methane (CH_4) Oxidation During 3 Years of Repeated Applications in Field Experiments. *Nutr. Cycling Agroecosyst.* **2001**, *60*, 57−64.

(35) Lin, X.; Hasi, W.-L.-J.; Lou, X.-T.; Han, S.-q.-g.-w.; Lin, D.-Y.; Lu, Z.-W. Direct and Quantitative Detection of Dicyandiamide (DCD) in Milk Using Surface-Enhanced Raman Spectroscopy. *Anal. Meth.* **2015**, *7*, 3869−3875.

(36) Chen, Q.; Qi, L.; Bi, Q.; Dai, P.; Sun, D.; Sun, C.; Liu, W.; Lu, L.; Ni, W.; Lin, X. Comparative Effects of 3,4-Dimethylpyrazole Phosphate (DMPP) and Dicyandiamide (DCD) on Ammonia-Oxidizing Bacteria and Archaea in a Vegetable Soil. *Appl. Microbiol. Biotechnol.* **2015**, *99*, 477−487.

(37) Vannelli, T.; Hooper, A. B. Oxidation of Nitrapyrin to 6-Chloropicolinic Acid by the Ammonia-Oxidizing Bacterium *Nitrosomonas europaea*. *Appl. Environ. Microbiol.* **1992**, *58*, 2321−2325.

(38) Campbell, N. E. R.; Aleem, M. I. H. The Effect of 2-Chloro, 6-(Trichloromethyl) Pyridine on the Chemoautotrophic Metabolism of Nitrifying Bacteria. *Antonie van Leeuwenhoek* **1965**, *31*, 124−136.
(39) Woodward, E. E.; Edwards, T. M.; Givens, C. E.; Kolpin, D. W.; Hladik, M. L. Widespread Use of the Nitrification Inhibitor Nitrapyrin: Assessing Benefits and Costs to Agriculture, Ecosystems, and Environmental Health. *Environ. Sci. Technol.* **2021**, *55*, 1345−1353.
(40) Corrochano-Monsalve, M.; González-Murua, C.; Bozal-Leorri, A.; Lezama, L.; Artetxe, B. Mechanism of Action of Nitrification Inhibitors Based on Dimethylpyrazole: A Matter of Chelation. *Sci. Total Environ.* **2021**, *752*, No. 141885.
(41) Bozal-Leorri, A.; Corrochano-Monsalve, M.; Vega-Mas, I.; Aparicio-Tejo, P.; Gonzalez-Murua, C.; Marino, D. Evidences Towards Deciphering the Mode of Action of Dimethylpyrazole-Based Nitrification Inhibitors in Soil and Pure Cultures of Nitrosomonas europaea. *Chem. Biol. Technol. Agric.* **2022**, *9*, 56.
(42) Amberger, A. Research on Dicyandiamide as a Nitrification Inhibitor and Future Outlook. *Commun. Soil Sci. Plant Anal.* **1989**, *20*, 1933−1955.
(43) Hooper, A. B.; Terry, K. R. Specific Inhibitors of Ammonia Oxidation in *Nitrosomonas*. *J. Bacteriol.* **1973**, *115*, 480−485.
(44) Casali, L.; Feiler, T.; Heilmann, M.; Braga, D.; Emmerling, F.; Grepioni, F. Too Much Water? Not Enough? In Situ Monitoring of the Mechanochemical Reaction of Copper Salts with Dicyandiamide. *CrystEngComm* **2022**, *24*, 1292−1298.
(45) Yildirim, S. C.; Walker, R. M.; Roessner, U.; Wille, U.A Rapid and Inexpensive Assay for Testing the Efficiency of Potential New Synthetic Nitrification Inhibitors. *Submitted*.
(46) Wise, R. R.; Naylor, A. W. Calibration and Use of a Clark-Type Oxygen Electrode from 5 to 45 degrees C. *Anal. Biochem.* **1985**, *146*, 260−264.
(47) *GraphPad Prism version 9.5.0 for Windows, GraphPad Software*, San Diego, California USAwww.graphpad.com.
(48) Subbarao, G. V.; Ishikawa, T.; Ito, O.; Nakahara, K.; Wang, H. Y.; Berry, W. L. A Bioluminescence Assay to Detect Nitrification Inhibitors Released From Plant Roots: A Case Study with *Brachiaria humidicola*. *Plant Soil* **2006**, *288*, 101−112.
(49) O'Sullivan, C. A.; Duncan, E. G.; Whisson, K.; Treble, K.; Ward, P. R.; Roper, M. M. A Colourimetric Microplate Assay for Simple, High Throughput Assessment of Synthetic and Biological Nitrification Inhibitors. *Plant Soil* **2017**, *413*, 275−287.
(50) Daugherty, N. A.; Swisher, J. H. Metal Complexes of Pyrazole. *Inorg. Chem.* **1968**, *7*, 1651−1653.
(51) Delaune, K. P.; Alsayouri, K.Physiology, Noncompetitive Inhibitor. In *StatPearls Publishing [internet]*; StatPearls Publishing (accessed Oct 04, 2022).
(52) Fisher, O. S.; Kenney, G. E.; Ross, M. O.; Ro, S. Y.; Lemma, B. E.; Batelu, S.; Thomas, P. M.; Sosnowski, V. C.; DeHart, C. J.; Kelleher, N. L.; Stemmler, T. L.; Hoffman, B. M.; Rosenzweig, A. C. Characterization of a Long Overlooked Copper Protein from Methane- and Ammonia-Oxidizing Bacteria. *Nat. Commun.* **2018**, *9*, No. 4276.
(53) Wright, C. L.; Schatteman, A.; Crombie, A. T.; Murrell, J. C.; Lehtovirta-Morley, L. E.; Stams, A. J. M. Inhibition of Ammonia Monooxygenase from Ammonia-Oxidizing Archaea by Linear and Aromatic Alkynes. *Appl. Environ. Microbiol.* **2020**, *86*, e02388−02319.
(54) Arp, D. J.; Sayavedra-Soto, L. A.; Hommes, N. G. Molecular Biology and Biochemistry of Ammonia Oxidation by *Nitrosomonas europaea*. *Arch. Microbiol.* **2002**, *178*, 250−255.
(55) Keener, W. K.; Russel, S. A.; Arp, D. J. Kinetic Characterization of the Inactivation of Ammonia Monooxygenase in *Nitrosomonas europaea* by Alkyne, Aniline and Cyclopropane Derivatives. *Biochim. Biophys. Acta, Protein Struct. Mol. Enzymol.* **1998**, *1388*, 373−385.
(56) Lontoh, S.; DiSpirito, A. A.; Krema, C. L.; Whittaker, M. R.; Hooper, A. B.; Semrau, J. D. Differential Inhibition *In Vivo* of Ammonia Monooxygenase, Soluble Methane Monooxygenase and Membrane-Associated Methane Monooxygenase by Phenylacetylene. *Environ. Microbiol.* **2000**, *2*, 485−494.
(57) Arnaout, C. L.; Gunsch, C. K. Impacts of Silver Nanoparticle Coating on the Nitrification Potential of *Nitrosomonas europaea*. *Environ. Sci. Technol.* **2012**, *46*, 5387−5395.
(58) Mahmood, T.; Rehmat, A.; Asma, L.; Muhammad, S. 4-Amino-1,2,4-Triazole Can be More Effective Than Commercial Nitrification Inhibitors at High Soil Temperatures. *Soil. Res.* **2017**, *55*, 715−722.
(59) Kelliher, F. M.; Clough, T. J.; Clark, H.; Rys, G.; Sedcole, J. R. The Temperature Dependence of Dicyandiamide (DCD) Degradation in Soils: A Data Synthesis. *Soil Biol. Biochem.* **2008**, *40*, 1878−1882.

Chapter 4: Insights into the Efficacy and Binding Mode of 1,4-Disubstituted 1,2,3-Triazoles (includes submitted manuscript)

3.3 Introduction

This chapter explores the biochemical parameter of 1,4-disubstituted 1,2,3-triazoles, which have previously been described and tested in three Australian soils by Taggert *et al.* to determine soil-dependent inhibitory effect on soil via mineral-N analysis (see Chapter 2.1).[94] These experiments were aimed to provide a complete overview of fundamental knowledge of recently developed SNI and compare them with the existing SNIs DMP and DCD..

3.4 Insights into the Efficacy and Binding Mode of 1,4-Disubstituted 1,2,3-Triazoles - A New Class of Agricultural Nitrification Inhibitors (submitted manuscript)

Abstract

Recently, 1,4-disubstituted 1,2,3-triazoles have been reported as a new class of nitrification inhibitors. In this work, a bacterial assay based on the measurement of nitrite (NO_2^-) production by pure cell cultures of *Nitrosomonas europaea* and *Nitrosospira multiformis* was used to explore the mechanism of inhibition of five differently 1,4-disubstituted 1,2,3-triazoles. While polar functional groups, such as amines, esters and alkoxy residues, were detrimental to inhibiting production of NO_2^-, triazoles carrying only aliphatic substituents showed the highest inhibition of up to 98%. The observed correlation between lipophilicity and inhibitory activity suggests that more lipophilic compounds could easier access the membrane-bound ammonia monooxygenase (AMO), which catalyzes the first step of the nitrification process. Measurement of the Michaelis-Menten kinetics suggests that the disubstituted 1,2,3-triazoles studied in this work act as reversible, non-competitive inhibitors.

Real-time measurements of the oxygen (O_2) consumption showed that the O_2 uptake rate by AMO following zero order kinetics in the presence of the triazoles, confirming the non-mechanistic mode of inhibition.

Keywords

Ammonia monooxygenase, bacterial assay, 1,4-disubstituted 1,2,3-triazoles, dicyandiamide, 3,4-dimethyl-1*H*-pyrazole; inhibition mechanism; nitrification inhibitor.

1. Introduction

Estimates show that the use of nitrogen (N) fertilizers will be required to increase by 70-100% worldwide by 2050 to provide food for the constantly growing population. [1] Unfortunately, for several decades N use efficiencies (NUEs), which measure the ratio of N taken up by crops to the total applied N fertilizer, [2] have remained at only around 50% globally. [3] The remaining 50% are lost from the soil to the environment through abiotic and biotic processes. The main loss pathways are volatilization of ammonia (NH_3), which is a precursor of particulate matter ($PM_{2.5}$), and leaching of nitrate (NO_3^-), which causes water eutrophication and groundwater pollution. [4-5,6] Furthermore, denitrifying bacteria in soil can reduce NO_3^- to nitrogen gas (N_2), nitric oxide (NO) and nitrous oxide (N_2O). [7] N_2O is particularly problematic for the environment as it has a 300 times higher global warming potential than carbon dioxide (CO_2). Thus, the reduction of unwanted N losses from agricultural systems, particularly with regards to the greenhouse gas footprint, has become an important goal. [2,8,9]

One strategy to improve NUEs is to amend N fertilizers with nitrification inhibitors (NIs). [10] Urea, which is the most commonly applied N fertilizer worldwide, undergoes hydrolysis in the soil to ammonium (NH_4^+). NH_4^+ is the major N nutrient for crops but is also consumed by microbial nitrification, which is the stepwise oxidation of NH_3 to NO_3^- by ammonia-oxidizing bacteria (AOB) and ammonia-oxidizing archaea (AOA). NIs are intended to inhibit ammonia monooxygenase (AMO), which catalyzes the rate-limiting first oxidation of NH_3 to hydroxylamine (NH_2OH). [11,12] The enzyme hydroxylamine oxidoreductase (HAO) subsequently converts NH_2OH to nitrite (NO_2^-), which is followed by the rapid oxidation to NO_3^- catalyzed by nitrite oxidase (NXR) present in *Nitrobacter* spp. Thus, inhibition of AMO should increase the residence time of NH_4^+ in soil, thereby reducing N losses through NO_3^- leaching and denitrification. [10] Unfortunately, the catalytically active site of AMO is not

known, as isolation of this transmembrane enzyme, which is conserved in both AOB and AOA, [13-15] leads to loss of structure and function. However, comparison with the evolutionally similar and recently crystallized particulate methane monooxygenase (pMMO) suggests that a cupredoxin-like unit could mediate this oxidation process. [13,16-18]

Figure 1 presents the currently commercially available nitrification inhibitors 4-dimethyl-1*H*-pyrazole (DMP, which is commonly applied as the phosphate salt DMPP, ENTEC®, BASF AG), 2-chloro-6-(trichloromethyl)-pyridine (Nitrapyrin or N-Serve®, Dow Chemical Co.) and dicyandiamide (DCD, AlzChem AG). These NIs are commonly formulated with a mineral N fertilizer[10] and contain at least one N atom that could in principle coordinate to the Cu-centre in the active site of AMO to lower the enzyme's activity. [15,19]

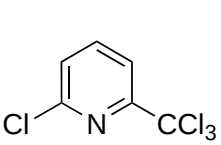

2-chloro-6-(trichloromethyl) pyridine
Nitrapyrin

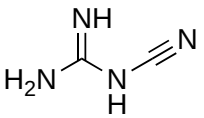

dicyandiamide
DCD

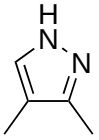

3,4-dimethyl-1*H*-pyrazole
DMP

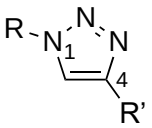

1: R = *n*-C_4H_7, R' = *n*-C_5H_9
2: R = $CH_2CO_2C_2H_5$, R' = *n*-C_4H_9
3: R = $(CH_2)_3NH_2$, R' = *n*-C_4H_9
4: R = $(CH_2)_2OCH_3$, R' = *n*-C_4H_9
5: R = $CH_2CH{=}CH_2$, R' = *n*-C_3H_7
6: R, R' = CH_3
7: R = *n*-C_4H_7, R' = *n*-C_3H_7
8: R = $CH_2CO_2C_2H_5$, R' = *n*-C_3H_7

Figure 1. The commercial NIs Nitrapyrin, DCD and DMP and 1,4-disubstituted 1,2,3-triazoles 1-8 studied in this work.

Bacterial studies with AOB have demonstrated that DMP reduces nitrification rates; however, field studies revealed that its efficacy strongly depends on the agroecosystem for reasons not well understood. [20-26] DCD is widely applied in New Zealand, where it has been shown to reduce N_2O emissions. Unfortunately, DCD is also prone to leaching and has been detected in dairy products. [27-29] Our recently studies with pure cells of *Nitrosomonas europaea* (*N. europaea*) have demonstrated that DMP and DCD both inhibit AMO reversibly through an uncompetitive mechanism. [30]

In our effort to address the challenges associated with the commercially available inhibitors, we have recently presented 1,4-disubstituted 1,2,3-triazoles as a novel class of NIs. [31]

Incubations in alkaline and neutral Australian soils performed over four weeks showed that these compounds can outperform DMP, particularly at increased temperatures. [31] Our reasoning behind the promising inhibitory potential of these compounds is based on the presence of three adjacent N atoms in the planar triazole ring, which should enhance the probability of successful binding to the Cu centres in the enzyme's active site. Furthermore, 1,2,3-triazoles are readily accessible with a large variety of substituents through Cu mediated alkyne azide click chemistry or through a metal and azide-free protocol involving a primary amine and the hydrazone of an *α*-ketoacetal, [32,33] which presents opportunities to perform structure-activity relationship (SAR) studies and design NIs tailored to specific soil conditions.

Soil incubations do not allow for the investigation of the mechanism of inhibition, which could offer insight for the further development of NIs. Therefore, in this study we present a comparative analysis of the 1,4-disubstituted 1,2,3-triazoles **1**-**5** (Figure 1) [31] by measuring biochemical parameters, such as %inhibition of the NO_2^- production, binding mode, oxygen (O_2) uptake and acute toxicity, using assays with pure bacterial cultures of *N. europaea* and *Nitrosospira multiformis* (*N. multiformis*) in the absence of the complex soil matrix. Furthermore, an evaluation of the impact of lipophilicity on inhibitory efficacy was also conducted.

2. Materials and Methods

2.1 Chemicals

The 1,4-disubstituted 1,2,3-triazoles **1**-**8** were prepared according to literature. [31] Griess reagent (listed as modified) was purchased from Sigma Aldrich. All aqueous solutions were prepared in Milli-Q water. *N. europaea* (ATCC19718) was purchased from the American Type Culture Collection**.** *N. multiformis* was isolated from an aquarium kit, as described previously. [34]

2.2 Studies with AOB

The bacterial assay, including growth and harvest of the cells, measurements of the O_2 consumption and the Michael-Menten kinetics, as well as the activity recovery assay, were conducted as previously reported. [30] All bacterial incubations were performed in sodium phosphate buffer (NaPB) with 1v/v% DMSO at pH = 7.5 and 30°C with different inhibitors and

concentrations, as indicated. Experimental details are provided in the Supporting Information (SI).

2.3 Statistics

Statistical analysis was performed from three technical and three biological replicates. Significant difference between the two treatments was determined from the NO_2^- concentration (*i.e.*, absorbance at 540 nm) using Student's t-test with a significance level of $P < 0.05$, for the assessment of the factors 'treatment' and 'enzyme source' a two-way analysis of variation (ANOVA) was performed using Šidák's multiple comparison test with a significance level of $P < 0.05$. The calculated K_m and V_{max} values for inhibited and uninhibited cells were used to determine the mode of inhibition using the Student's t-test between inhibited and uninhibited cells with a significance level of $P < 0.05$. All results are reported as mean ± standard error of the mean.

3. Results and Discussion

3.1 Identification of the Targeted Enzyme

As outlined in the Introduction, the oxidation of NH_3 to NO_2^- occurs in two steps, where AOB carry out both steps, i.e., $NH_3 \rightarrow NH_2OH \rightarrow NO_2^-$, which are catalyzed by the enzymes AMO and HAO, respectively. The performance of compounds **1**-**5**, which had alkyl, amine, ester, ether and alkene substituents, has previously been assessed in *in vitro* incubations in alkaline and neutral Australian soils. [31] To explore which of these two enzymes is targeted by inhibitors **1**-**5**, pure cell cultures of the two AOBs *N. europaea* and *N. multiformis* were separately treated in sodium phosphate buffer (NaPB) with 1v/v% dimethylsulfoxide (DMSO) at pH 7.5 and 30°C with either NH_4^+ (as the substrate for AMO) or NH_2OH (as the substrate for HAO). The NO_2^- production was determined after 60 min in the presence and absence of compounds **1**-**5** using a recently developed assay based on the Griess reaction. [34] Enzyme inhibition should reduce the NO_2^- production compared to the non-inhibited cell culture.

Figure 2 shows the percentage inhibition of NO_2^- production after 60 min, determined according to equation SI-1 (see Tables S1-S5 for the data for each replicate). Control experiments performed with cells in the absence of both N source and inhibitor compound did not reveal a notable production of NO_2^- (data not shown).

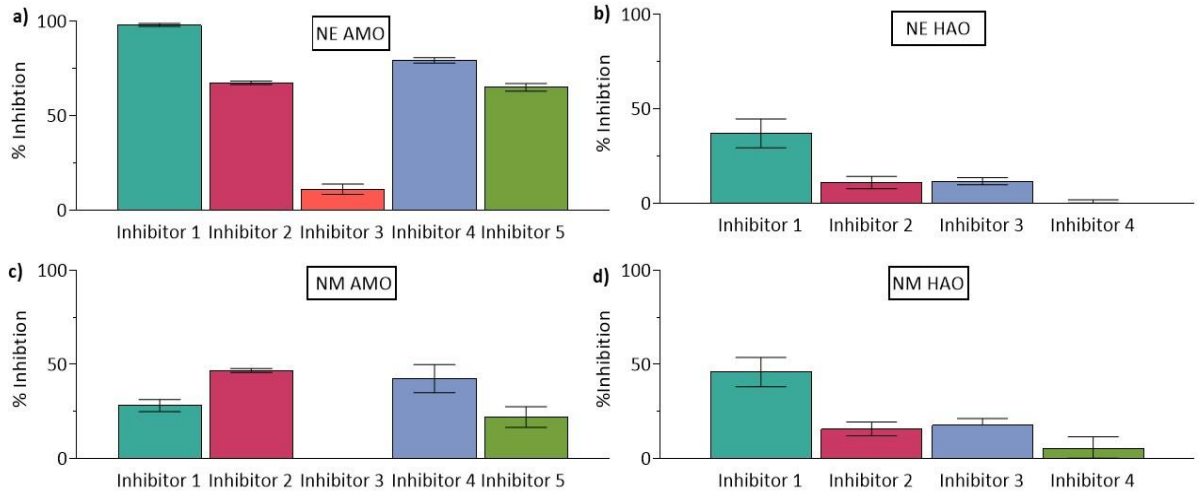

Figure 2. Identification of the enzyme targeted by inhibitors 1-5 by measuring the percentage inhibition of the NO_2^- production after 60 min of inoculation with *N. europaea* (NE) and *N. multiformis* (NM) using different N-sources. NE: (a) $[NH_4^+]$ = 3 mM; (b) $[NH_2OH]$ = 3 mM. NM: (c) $[NH_4^+]$ = 3 mM; (d) $[NH_2OH]$ = 3 mM. The inoculations were performed in NaPB (pH = 7.5) and 1v/v% DMSO at 30°C and 100 rpm in the dark. Standard errors were calculated from three biological replicates, each performed with three technical replicates.

a) Incubations targeting AMO: A nearly quantitative inhibition (98%) of the NO_2^- production by *N. europaea* was found for compound **1** (Figure 2a). Compounds **2**, **4** and **5** showed an inhibition of 67%, 78% and 65%, respectively, whereas compound **3** performed poorest with an inhibition of only 11%. Because of the higher abundance of active AMOs in *N. multiformis* compared to *N. europaea*, [35] *N. multiformis* is less sensitive to nitrification inhibitors applied at the same concentration, as has previously been shown with both DCD and the known NI allyl thiourea. [36,37] The data in Figure 2c confirm this behavior for all compounds tested here. In particular, the inhibitory activity of compound **3** vanished completely with *N. multiformis*. From these SAR studies, it can be concluded that the primary amine substituent in **3** appears to be particularly detrimental to the inhibitory activity. The generally poorer inhibitory performance of 1,2,3-triazoles with polar substituents in the assay, compared to non-polar alkyl groups, agrees with the results from the *in vitro* soil incubations with the same compounds, confirming the potential of the bacterial assay as a predictive tool for the performance of nitrification inhibitors in soil. [31]

b) Incubations targeting HAO: In the case of *N. europaea*, a drastically lower or even absent inhibitory effect was found for inhibitors **1**, **2**, **4** and **5** (Figure 2b), suggesting that AMO is the predominantly inhibited enzyme (compound **3** was not tested here, as it did not inhibit AMO). However, the observed inhibition by compounds **1**, **2** and **4** of 37%, 11% and 12%, respectively, is likely a consequence of the inhibition of AMO, as AMO and HAO are not independently acting enzymes but are interconnected through an electron transfer chain. Thus, inhibition of AMO disrupts this electron shuttle and, therefore, also prevents to some extent the oxidation $NH_2OH \rightarrow NO_2^-$, as has previously been reported for DMP. [30, 38] In the case of *N. multiformis*, a small to moderate percentage inhibition of NO_2^- production was also found (Figure 2d), which is, again, likely a consequence of AMO inhibition. One notable exception is compound **1**, where the inhibition was lower in the experiment targeting AMO than in the one targeting HOA (21% and 46 %, respectively; Figure 2c vs. 2d). It is not clear whether the N-source NH_2OH was an additional 'stressor' for HOA in the presence of compound **1**, leading to a reduced NO_2^- production. Thus, for compound **1,** the inhibitory effect for AMO and HOA of *N. multiformis* is not significantly different ($P > 0.05$).

3.2 Determining the Role of Lipophilicity on Inhibitory Activity

Compound **1**, which showed the highest percentage inhibition amongst the tested 1,4-disubstituted triazoles, should be quite lipophilic as both substituents are non-polar alkyl groups. The lipophilicity can be expressed by the partition coefficient *P* between octanol and water, according to equation 1: [39]

$$\log P_{oct/wat} = \log_{10} \frac{[compound]_{octanol}}{[compound]_{water}} \quad \text{(eqn. 1)}$$

To evaluate the importance of lipophilicity on inhibitory activity, we extended our pool of 1,4-disubstituted 1,2,3-triazoles to include compounds **6** - **8**. Compounds **6** and **7** have only alkyl substituents with shorter chain lengths than compound **1**, which should reduce their lipophilicity. Compound **8** is an analogue to the ester-containing triazole **2** but with an *n*-propyl instead of an *n*-butyl substituent. The predicted log $P_{oct/wat}$ values are included in Figure 3. [40]

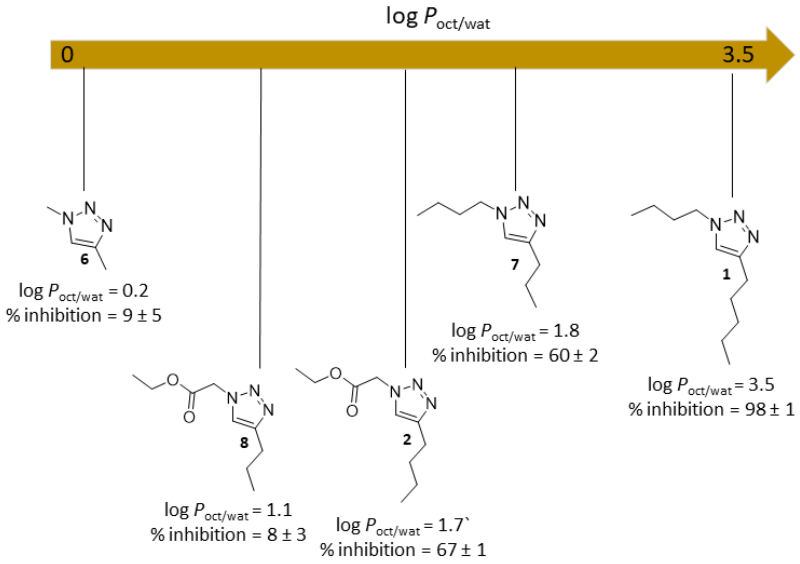

Figure 3. Correlation between log $P_{oct/wat}$ of 1,4-disubstituted 1,2,3-triazoles (predicted according to ref. [40]) and the percentage inhibition of NO_2^- production, determined with *N. europaea*. The inoculations were performed with [NH_4^+] = 3.0 mM and [NI] = 0.3 mM in NaPB (pH = 7.5) and 1v/v% DMSO at 30°C and 100 rpm in the dark. Standard errors were calculated from three biological replicates, each performed with three technical replicates.

The bacterial assay (performed with *N. europaea*) revealed for compounds **6** and **7** that shortening the alkyl chain length significantly decreased the inhibition ($P < 0.05$), dropping from 60% for compound **7**, which has *n*-butyl and *n*-propyl substituents, to just 9 % for the dimethyl substituted compound **6**. A similar trend was observed for inhibitors **2** and **8**, which have the same polar ester substituent but alkyl groups with different chain lengths. Thus, the inhibition decreases from 67% to 8% upon shortening the alkyl chain from *n*-butyl (**2**) to *n*-propyl (**8**). These data show that lipophilicity plays an important role for the inhibitory effect of 1,4-disubstituted triazoles, suggesting that a higher lipophilicity facilitates migration

through the bacterial lipid-bilayer and reaching of the binding site in the membrane-bound AMO. [41, 42]

It should be noted that, interestingly, our previous incubation studies in a neutral soil (pH = 7.3) revealed an opposite trend, where the less lipophilic compound **7** showed a higher inhibitory effect than the more lipophilic compound **1**. [31] In the bacterial assays geophysical parameter of soils that can impact on the mobility of an NI, such as soil organic content and pH, are absent. [43-45] Therefore, from a biochemical perspective, it seems that triazoles with higher lipophilicity are more effective as nitrification inhibitors as they can better access the AMO. However, their lipophilic nature may become a disadvantage in soil, as they could be adsorbed on soil constituents, thereby reducing their mobility and potentially also promoting their degradation. [43-45] We will explore these aspects in more detail in future work.

3.3 Exploring the Reversibility of the Inhibition

To explore whether compounds **1**, **2**, **4** and **5** inhibit AMO in a reversible or irreversible fashion, cells of *N*. *europaea* were incubated for 30 min with NH_4^+ and 50 mol% of the respective NI to ensure considerable inhibition, and the NO_2^- production was measured ("inhibited cells"). The cells were then thoroughly washed with NaPB to remove both unbound and enzyme-bound inhibitor. After the final washing cycle, fresh NH_4^+ was added to the cells, and NO_2^- production was measured again after 30 min of incubation. Control experiments were performed, where cells were incubated without NI ("uninhibited cells", activity = 100 %) and without both NH_4^+ and NI ("untreated cells", activity = 0 %). The

percentage activity of the inhibited cells with regards to the NO_2^- production was determined according to equation SI-2. The data are shown in Figure 4.

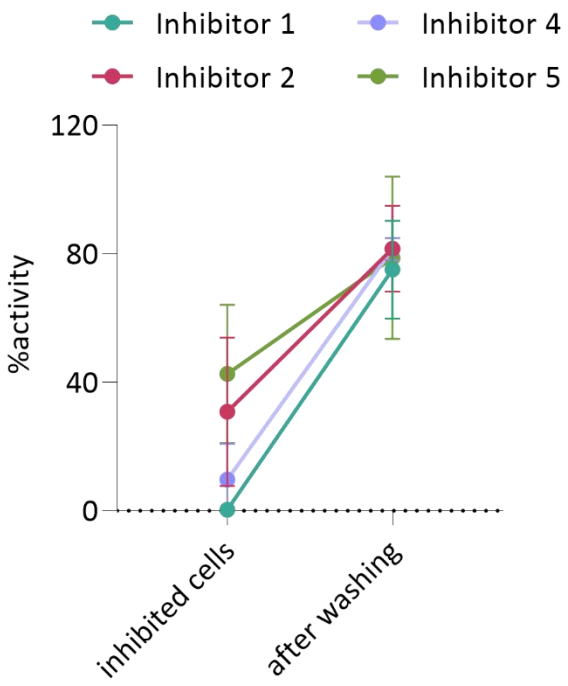

Figure 4. Determination of the activity of inhibited AMO, using pure cell cultures of *N. europaea*, and after removal of the NI through repeated washing with NaPB, followed by re-incubation with fresh NH_4^+. The inoculations were performed with [NH_4^+] = 3.0 mM (before and after washing) and [NI] = 1.5 mM in NaPB (pH = 7.5) and 1v/v% DMSO at 30°C and 100 rpm in the dark. Standard errors were calculated from three biological replicates, each performed with three technical replicates.

The inhibition of cells exposed to compound **1** was nearly quantitative (3% activity), whereas the activity of cells treated with compounds **2**, **4**, and **5** was 31%, 10% and 43%, respectively. After washing the cells and re-incubation with NH_4^+, the activity increased to about 80% regardless of the inhibitor's efficacy. The recovery of enzyme activity indicates that the inhibition is likely to be reversible, similar to previous findings for DMP and DCD. [30] The observation that complete recovery of activity did not occur is not unexpected, considering the high [NI] used in this experiment, which could cause some degree of cell loss (see Table S9 exemplary for compound **1**).

3.4 Determination of the Acute Toxicity of Compound 1

To verify that the observed inhibition of NO_2^- production inhibition in the previous experiments was not caused by a potential toxicity of these triazoles for the bacterial cells, a viability staining experiment was conducted, exemplary for compound **1**, to evaluate its acute toxicity for *N. europaea*. This inhibitor was chosen as it had the most significant impact on nitrification amongst those tested here (see Figure 2). Cells of *N. europaea* were incubated for 12 hours with NH_4^+ without (control) and with NI at two different concentrations (100 ppm and 1000 ppm). Table 2 shows the percentage of live and dead cells from each set of incubations, which were calculated according to equations SI-3 and SI-4. Standard errors were determined from seven microscopic images. The data for the individual microscopic images are provided in Table S10.

Table 2. Acute toxicity of compound **1** at two different concentrations for cells of *N. europaea* determined with a bacterial viability stain and determination of the NO_2^- production.[a]

Inhibitor	Concentration / ppm	% Live	% Dead
none	--	84 ± 5	16 ± 5
1	100	79 ± 10	21 ± 10
	1000	78 ± 5	22 ± 5

[a]The incubations were performed in NaPB and 1v/v% DMSO at pH = 7.5 and 30°C with [NH_4^+] = 3 mM, [**1**] = 100 ppm (0.15 mM, 5 mol% of applied fertilizer-N) and 1000 ppm (1.5 mM, 50 mol% of applied fertilizer-N) at 100 rpm for 12 h in the dark. Standard errors were determined from seven microscopic images.

The results indicate that, even at the high concentration of 1000 ppm, compound **1** did not cause significantly greater cell death than the control treatment ($P > 0.05$). Therefore, it is evident that the inhibitory effect of inhibitor **1** (as a representative for the triazoles studied here) can be attributed to its reversible coordination with AMO rather than enzyme inactivation due to toxicity.

3.5 Determination of $IC_{50(app)}$ Values

While NO_2^- production measurements give an indication of the performance of NIs at one concentration, determination of the half-maximal inhibitory concentration, $IC_{50(app)}$, provides a quantitative measure of the amount of NI needed to reduce the total NO_2^- production by AMO to 50% (note that the prefix 'app' (apparent) was used as the studies were performed with bacterial cells and not with the pure enzyme). Therefore, $IC_{50(app)}$ values were determined at 30°C with *N. europaea*, which was inoculated with inhibitors **1**, **2**, **4** and **5** at seven different concentrations, and the production of NO_2^- was measured (Table 3; the sigmoidal plot is shown in Figure S1).

Table 3. $IC_{50(app)}$ values for compounds **1**, **2**, **4** and **5** determined with *N. europaea*.[a]

Inhibitor	$IC_{50(app)}$ / µmol L^{-1}
1	77.2 ± 7.6
2	112.4 ± 5.2
4	82.9 ± 7.8
5	98.4 ± 4.1
DMP[b]	6.6 ± 0.6
DCD[b]	106.8 ± 2.0

[a]Cells were treated with $[NH_4^+]$ = 3.0 mM in NaPB (pH = 7.5) and 1 v/v% DMSO at 30°C under constant stirring in the dark. All errors are standard errors calculated from three measurements of biological replicates. [b]Data taken from ref. [34]

Of these four triazole-based NIs, compound **1** has the lowest $IC_{50(app)}$ value (77.2 µmol L^{-1}), whereas compound **2** has the highest (112.4 µmol L^{-1}). Compared to DCD, whose $IC_{50(app)}$ has been determined previously (106.6 µmol L^{-1}; included in the table), [30, 34] compounds **1**, **4** and **5** are more efficient NIs in the bacterial assay. On the other hand, all triazoles have a lower binding affinity to AMO than DMP ($IC_{50(app)}$ = 6.6 µmol L^{-1}).[31] However, since our previous *in vivo* soil incubations showed that 1,4-disubstituted 1,2,3-triazoles can outperform DMP,[31,34] it seems not appropriate to rely on the $IC_{50(app)}$ value determined in the absence of the soil matrix as a measure for inhibitor performance in soil. On the other hand, the $IC_{50(app)}$ values

could serve as a valuable reference for determining the appropriate ratio of inhibitor to fertilizer in fertilizer formulations.

3.6 Determining the Mechanism of Inhibition

Michaelis-Menten kinetics were performed using *N. europaea* to gain additional insight into the mechanism by which the triazoles **1**, **2**, **4** and **5** inhibit AMO. The Michaelis constant, $K_{m(app)}$, is the concentration of NH_3 at which the reaction rate, v, is 50% of the maximal rate $V_{max(app)}$ (equation 2).

$$v = \frac{V_{max(app)}\,[NH_3]}{K_{m(app)} + [NH_3]} \quad \text{(eqn. 2)}$$

Non-competitive inhibition of AMO would show an unchanged $K_{m(app)}$ and a decrease of $V_{max(app)}$ that is independent of [NI], as NH_3 and NI are not competing for the same site in the enzyme. Uncompetitive inhibition would show both a decreased $K_{m(app)}$ and $V_{max(app)}$, whereas an increased $K_{m(app)}$ and an unchanged $V_{max(app)}$ would indicate competitive inhibition. [46]

The production of NO_2^- was measured for two different [NI] (0. 15 mM and 0.3 mM) by varying [NH_4^+]. The inhibitor concentrations were chosen to partially inhibit the NO_2^- production (see $IC_{50(app)}$ values in Table 3). Figure 5 shows that the formation of NO_2^- followed Michaelis-Menten-type saturation kinetics for all compounds, clearly revealing that not only was less NO_2^- produced in the presence of the inhibitors but that increasing [NH_4^+] beyond 0.2 mmol L^{-1} did not inflate the NO_2^- production (the different NO_2^- production in the absence of NIs in Figure 5a and 5b is due to the varying activity of biological replicates).

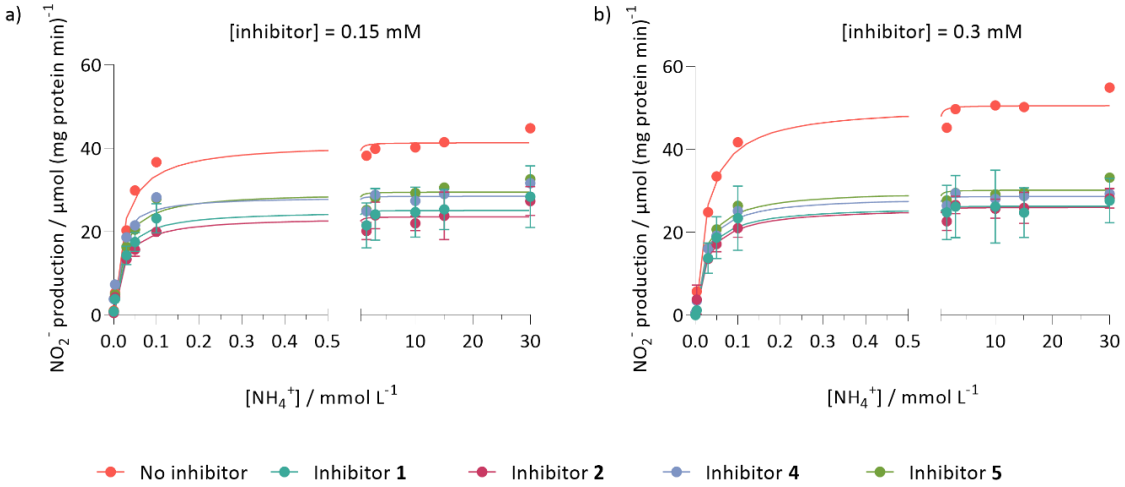

Figure 5. Effect of inhibitors 1, 2, 4 and 5 on the NO_2^- production in dependence of $[NH_4^+]$ after 60 min; a) [NI] 0.15 mM and b) NI 0.3 mM. The inoculations were performed with $[NH_4^+]$ = 0.003 mM, 0.03 mM, 0.05 mM, 0.1 mM, 1.5 mM, 3.0 mM, 10 mM, 15 mM, and 30 mM in NaPB (pH = 7.5) and 1 v/v% DMSO at 30°C and 100 rpm in the dark. Note the different axes scales to include data at higher $[NH_4^+]$. Standard errors were calculated from three biological replicates.

Hyperbolic regression analysis provided the values for $K_{m(app)}$ and $V_{max(app)}$, which are shown in Table 4.

Table 4. Michaelis-Menten kinetics parameter of the $[NH_4^+]$ dependent production of NO_2^- by *N. europaea* in the absence and presence of inhibitors 1, 2, 4 and 5 at two different concentrations.[a]

Inhibitor	**Concentration / mM**	**$V_{max(app)}$ / µmol (mg protein min)$^{-1}$**	**$K_{m(app)}$ / µM**
none[b]		41.4 ± 4.2	24.6 ± 7.6
none[c]		50.5 ± 6.5	30.2 ± 11.2
1	0.15	25.0 ± 5.6	20.6 ± 8.1
	0.3	26.6 ± 6.5	24.7 ± 5.5
2	0.15	23.5 ± 2.7	22.5 ± 6.0
	0.3	26.0 ± 2.2	25.7 ± 3.5

4	0.15	28.3 ± 10.4	14.5 ± 4.9
	0.3	28.7 ± 5.1	22.9 ± 3.8
5	0.15	29.4 ± 7.1	21.3 ± 8.1
	0.3	30.2 ± 0.5	24.1 ± 7.7

[a][NI] were chosen to achieve partial inhibition of the NO_2^- production (see text). Standard errors were calculated from three biological replicates, each performed with three technical replicates. [b]Determined from [Inhibitor] = 0.15 mM experiment. [c]Determined from [Inhibitor] = 0.3 mM experiment.

Compared to the uninhibited cells, compounds **1**, **2**, **4** and **5** reduced $V_{max(app)}$ by about 30 - 50% without having an effect on $K_{m(app)}$ ($P > 0.05$). This result indicates that these triazoles inhibit AMO in *N. europaea* through a non-competitive mechanism, *i.e*., the inhibitor reduces the activity of AMO irrespective of whether or not NH_3 is bound to the enzyme. [47] Simulations of the structure of bacterial AMO revealed that the enzyme contains multiple Cu^+/Cu^{2+}-containing subunits. [15, 48] Our finding that the inhibitory activity of these triazole-based NIs correlates with their lipophilicity (see section 3.2), although they are acting through the same mechanism, suggests that the metal sites could be more accessible for more lipophilic inhibitors. It is worth noting that the commercial NIs DMP and DCD are also reversible inhibitors, but they act through an uncompetitive mechanism and need to bind to the enzyme-substrate complex to show an inhibitory effect.[32]

3.7 Determination of the Order of NH_3 Oxidation by AMO

To verify that the triazole-based NIs studied here act as 'coordinating/chelating' compounds and not as mechanistic inhibitors, the rate of the NH_3 oxidation by AMO was determined exemplary for compounds **1**, **4** and **5** by measuring the O_2 consumption (or uptake, respectively) by the enzyme using a Clark-type oxygen electrode. As the oxidation $NH_3 \rightarrow NH_2OH$ requires equimolar amounts of O_2, the O_2 consumption is directly proportional to the NH_3 oxidation rate. [38] The inhibitor concentration was identical to that used in the reversibility test (0.15 mmol, section 3.3). Figure 6 shows the O_2 consumption by *N. europaea*, where the decay in the first 300 seconds (s) results from O_2 uptake by the enzyme

in the absence of inhibitor. At the 300 s timepoint, the inhibitor was added (indicated by an arrow), the system was allowed to equilibrate for 15 s, and the O_2 decay was subsequently monitored for another 5 min. The O_2 concentration was determined according to equation SI-5.

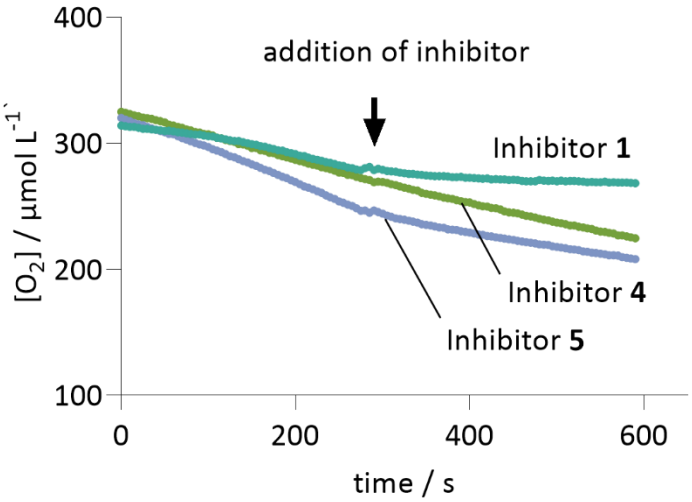

Figure 6. Measurements of the O_2 consumption by *N. europaea* in the absence and presence of compounds **1**, **4** and **5** (at 0.15 mM). The first 300 seconds (s) is the rate in the absence of inhibitor. At the 300 s timepoint (arrow) the inhibitor was added. The cells were treated with $[NH_4^+]$ = 3.0 mM at pH = 7.5 at 20°C under constant stirring in the dark. The plot shows the mean of three measurements for each inhibitor concentration; standard errors are omitted for clarity but can be obtained from the rate coefficients in Table 5.

In all experiments, both NH_4^+ and O_2 were present in excess so that the rate was only dependent on the enzyme concentration (the total protein concentration was about 468 µg L^{-1}, as determined with a BCA assay kit). In the absence of NI, the O_2 consumption should follow zero-order kinetics and the rate coefficient, k_{obs}, can be determined from the slope of the plot of $[O_2]$ vs time. In the presence of an inhibitor the rate of NH_3 oxidation and, therefore, of the O_2 consumption should slow down.

Indeed, without inhibitor the measured linear dependence of the O_2 consumption over time confirmed zero-order kinetics, revealing an average rate coefficient of 240 nmol L^{-1} s^{-1} (see Table S7 for the data of the individual measurements of this section). After addition of the inhibitors the rate of O_2 consumption slowed down. The rate coefficients, k_{obs}, for the O_2

consumption and the percentage inhibition for the three NIs, which was obtained from the ratio of the rate coefficients in the presence and absence of the inhibitor, are given in Table 5.

Table 5. Rate coefficients, k_{obs}, for the O_2 consumption by *N. europaea* in the presence of the NIs **1**, **4** and **5** and the calculated percentage inhibition.[a,b]

Inhibitor	k_{obs} / nmol L^{-1} s^{-1}	%Inhibition
none[c]	240 ± 96	--
1	30 ± 6	77 ± 3
4	199 ± 51	32 ± 7
5	194 ± 13	45 ± 2

[a]Cells were treated with [NH_4^+] = 3.0 mM and [NI] = 1.5 mM (50 mol% of applied N) in NaPB (pH = 7.5) and 1 v/v% DMSO at 20°C under constant stirring in the dark. All errors are standard errors calculated from three biological replicates. [b] %Inhibition determined according to: (1 - ($k_{\text{with inhibitor}}$ / $k_{\text{without inhibitor}}$)) x 100, using the rate data obtained for each individual experiment (provided in Table S7). [c]Average value from nine measurements.

The strongest reduction of the O_2 uptake rate by the enzyme was found for compound **1**, where k_{obs} dropped to just 30 nmol L^{-1} s^{-1}, which accounts for an inhibition of 77%. Compounds **4** and **5** were less effective with k_{obs} -values of about 200 nmol L^{-1} s^{-1}, resulting in 32% and 45% inhibition, respectively. However, for all NIs, the reaction remained zero order with an R^2 value > 0.9. Such kinetic behaviour supports our findings from the previous sections that the triazole-based NIs explored here reversibly bind to the enzyme, likely as chelating or coordinating agents. In contrast, mechanism-based inhibitors, such as acetylene or phenylacetylene, which bind irreversibly to the enzyme, reduce the enzyme's 'active' concentration over time resulting in a first-order consumption of O_2.[49,50]

To conclude, we have explored the mechanism of inhibition of the 1,4-disubstituted 1,2,3-triazoles **1**-**5**, which have recently been presented as a novel class of nitrification inhibitors.[31] Using pure cell cultures of *N. europaea and N. multiformis* and measuring the amount of NO_2^- formed revealed that the alkyl-substituted compound **1** shows the highest inhibitory effect, whereas incorporation of polar substituents is detrimental for inhibitory activity, most

notably the primary amine group in compound **3**, confirming findings from previous *in vitro* soil incubations. [31] Compounds **1**, **2**, **4** and **5** act as reversible, non-competitive inhibitors, which target AMO but do not lead to significant cell death. Our data suggest that lipophilicity is beneficial for nitrification inhibitory effects *in vivo*, whereas in the complex soil matrix a higher lipophilicity could be detrimental as adsorption processes could potentially reduce their mobility. O_2 respiration measurements exemplary performed with inhibitors **1**, **4** and **5** confirmed their non-mechanistic inhibition, which is similar to the mode of action of DMP and DCD. [30] Determination of the $IC_{50(app)}$ values revealed that 1,4-disubstituted 1,2,3-triazoles generally have a higher binding affinity to AMO than the commercial inhibitor DCD but not DMP. Given that some of these triazole-based inhibitors outperform DMP in soil incubations, the $IC_{50(app)}$ values should not be taken as an indicator for the inhibitory performance in soil but could provide useful guidelines to optimize inhibitor-fertilizer formulations

Supporting Information

Protocols for the bacterial studies. Supplementary Table S1. Inhibition of AMO NO_2^- formation after inoculating *N. europaea* with inhibitor compounds **1**-**5**; Table S2. Inhibition of HAO NO_2^- formation after inoculating *N. europaea* with inhibitor compounds **1**-**5**; Table S3. Inhibition of AMO NO_2^- formation after inoculating *N. europaea* with inhibitor compounds **1**-**5**; Table S4. Inhibition of HAO NO_2^- formation after inoculating *N. europaea* with inhibitor compounds **1**-**5**; Table S5. Calculated log $P_{oct/wat}$ values of substituted 1,2,3-triazoles; Table S6. %Inhibition in dependence of log $P_{oct/wat}$ of AMO NO_2^- formation after inoculating *N. europaea* with inhibitor compounds **6**-**8**. Table S7. Rate coefficients, k_{obs}, for the time dependent O_2 consumption by *N. europaea* in the absence and presence of NI; Table S8. Fraction of the activity of inhibited AMO, using pure cell cultures of *N*. *europaea*, and after removal of the NI through repeated washing with NaPB; Table S9. Concentration-dependent fraction of the activity of inhibited AMO with compound **1**, using pure cell cultures of *N*. *europaea*, and after removal of the NI through repeated washing with NaPB; Table S10. Number of cells alive and cells dead of *N. europaea* determined without and with treatment of compound **1** at different concentrations determined with a bacterial viability stain. Supplementary Figure S1. Function of the $\%NO_2^-$ production against the logarithmic concentration of compounds **1**, **2**, **4** and **5** and the obtained $IC_{50(abs)}$ values.

References

1. Godfray, H. C. J.; Beddington, J. R.; Crute, I. R.; Haddad, L.; Lawrence, D.; Muir, J. F.; Pretty, J.; Robinson, S.; Thomas, S. M.; Toulmin, C. Food Security: The Challenge of Feeding 9 Billion People. *Science* **2010**, *327*, 812-818. DOI: 10.1126/science.1185383

2. Raun, W. R.; Schepers, J. S. Nitrogen Management for Improved Use Efficiency. In: *Nitrogen in Agricultural Systems* (Schepers, J. S. R., W. R., eds.). **2008**, pp 675-693. DOI 10.2134/agronmonogr49.c17

3. Coskun, D.; Britto, D. T.; Shi, W.; Kronzucker, H. J. Nitrogen Transformations in Modern Agriculture and the Role of Biological Nitrification Inhibition. *Nat. Plants* **2017**, *3*, 17074. DOI: 10.1038/nplants.2017.74

4. Ladha, J. K.; Pathak, H.; J. Krupnik, T.; Six, J.; van Kessel, C. Efficiency of Fertilizer Nitrogen in Cereal Production: Retrospects and Prospects. In: *Adv. Agron.* Vol. 87; Academic Press, **2005**, pp 85-156. DOI 10.1016/S0065-2113(05)87003-8

5. Robertson, G. P.; Bruulsema, T. W.; Gehl, R. J.; Kanter, D.; Mauzerall, D. L.; Rotz, C. A.; Williams, C. O. Nitrogen–Climate Interactions in US Agriculture. *Biogeochemistry* **2013**, *114*, 41-70. DOI: 10.2307/24715091

6. Norton, J.; Ouyang, Y. Controls and Adaptive Management of Nitrification in Agricultural Soils. *Front. Microbiol.* **2019**, *10*, 1931. DOI: 10.3389/fmicb.2019.01931

7. Jetten, M. S. M. The Microbial Nitrogen Cycle. *Environ. Microbiol.* **2008**, *10*, 2903-2909. DOI: 10.1111/j.1462-2920.2008.01786.x

8. Cavigelli, M. A.; Del Grosso, S. J.; Liebig, M. A.; Snyder, C. S.; Fixen, P. E.; Venterea, R. T.; Leytem, A. B.; McLain, J. E.; Watts, D. B. US Agricultural Nitrous Oxide Emissions: Context, Status, and Trends. *Front. Ecol. Environ.* **2012**, *10*, 537-546. DOI: 10.1890/120054

9. Ruser, R.; Schulz, R. The Effect of Nitrification Inhibitors on the Nitrous Oxide (N_2O) Release from Agricultural Soils—a Review. *J. Plant Nutr. Soil Sci.* **2015**, *178*, 171-188. DOI: 10.1002/jpln.201400251

10. McCarty, G. W. Modes of Action of Nitrification Inhibitors. *Biol. Fertil. Soils* **1999**, *29*, 1-9. DOI: 10.1007/s003740050518

11. Hyman, M. R.; Sansome-Smith, A. W.; Shears, J. H.; Wood, P. M. A Kinetic Study of Benzene Oxidation to Phenol By Whole Cells of Nitrosomonas europaea and Evidence For The Further Oxidation of Phenol to Hydroquinone. *Arch. Microbiol.* **1985**, *143*, 302-306. DOI: 10.1007/BF00411254

12. Vajrala, N.; Martens-Habbena, W.; Sayavedra-Soto, L. A.; Schauer, A.; Bottomley, P. J.; Stahl, D. A.; Arp, D. J. Hydroxylamine as an Intermediate in Ammonia Oxidation by Globally Abundant Marine Archaea. *Proc. Natl. Acad. Sci.* **2013**, *110*, 1006-1011. DOI: 10.1073/pnas.1214272110

13. Lawton, T. J.; Ham, J.; Sun, T.; Rosenzweig, A. C. Structural Conservation of the B Subunit in the Ammonia Monooxygenase/Particulate Methane Monooxygenase Superfamily. *Proteins* **2014**, *82*, 2263-2267. DOI: 10.1002/prot.24535

14. McTavish, H.; Fuchs, J. A.; Hooper, A. B. Sequence of the Gene Coding for Ammonia Monooxygenase in Nitrosomonas europaea. *J. Bacteriol.* **1993**, *175*, 2436. DOI: 10.1128/jb.175.8.2436-2444.1993

15. Musiani, F.; Broll, V.; Evangelisti, E.; Ciurli, S. The Model Structure of the Copper-Dependent Ammonia Monooxygenase. *J. Biol. Inorg. Chem.* **2020**, *25*, 995-1007. DOI: 10.1007/s00775-020-01820-0

16. Ensign, S. A.; Hyman, M. R.; Arp, D. J. *In vitro* Activation of Ammonia Monooxygenase from Nitrosomonas europaea by Copper. *J. Bacteriol.* **1993**, *175*, 1971-1980. DOI: 10.1128/jb.175.7.1971-1980.1993

17. Lieberman, R. L.; Rosenzweig, A. C. Crystal structure of a membrane-bound metalloenzyme that catalyses the biological oxidation of methane. *Nature* **2005**, *434*, 177-182. DOI: 10.1038/nature03311

18. Cao, L.; Caldararu, O.; Rosenzweig, A. C.; Ryde, U. Quantum Refinement Does Not Support Dinuclear Copper Sites in Crystal Structures of Particulate Methane Monooxygenase. *Angew. Chem. Int. Ed.* **2018**, *57*, 162-166. DOI: 10.1002/anie.201708977

19. Amberger, A. Research on Dicyandiamide as a Nitrification Inhibitor and Future Outlook. *Commun. Soil Sci. Plant Anal.* **1989**, *20*, 1933-1955. DOI: 10.1080/00103628909368195

20. Zhu, G.; Ju, X.; Zhang, J.; Müller, C.; Rees, R. M.; Thorman, R. E.; Sylvester-Bradley, R. Effects of the Nitrification Inhibitor DMPP (3,4-Dimethylpyrazole Phosphate) on Gross N Transformation Rates and N_2O Emissions. *Biol. Fertil. Soils* **2019**, *55*, 603-615. DOI: 10.1007/s00374-019-01375-6

21. Li, H.; Liang, X.; Chen, Y.; Lian, Y.; Tian, G.; Ni, W. Effect of Nitrification Inhibitor DMPP on Nitrogen Leaching, Nitrifying Organisms, and Enzyme Activities in a Rice-Oilseed Rape Cropping System. *J. Environ. Sci.* **2008**, *20*, 149-155. DOI: 10.1016/S1001-0742(08)60023-6

22. Guardia, G.; Marsden, K. A.; Vallejo, A.; Jones, D. L.; Chadwick, D. R. Determining the Influence of Environmental and Edaphic Factors on the Fate of the Nitrification Inhibitors DCD and DMPP in Soil. *Sci. Total Environ.* **2018**, *624*, 1202-1212. DOI: 10.1016/j.scitotenv.2017.12.250

23. Barrena, I.; Menéndez, S.; Correa-Galeote, D.; Vega-Mas, I.; Bedmar, E. J.; González-Murua, C.; Estavillo, J. M. Soil Water Content Modulates the Effect of the Nitrification

Inhibitor 3,4-Dimethylpyrazole phosphate (DMPP) on Nitrifying and Denitrifying Bacteria. *Geoderma* **2017**, *303*, 1-8. DOI: 10.1016/j.geoderma.2017.04.022

24. Koci, J.; Nelson, P. N. Tropical Dairy Pasture Yield and Nitrogen Cycling: Effect of Urea Application Rate and A Nitrification Inhibitor, DMPP. *Crop Pasture Sci.* **2016**, *67*, 766-779. DOI: 10.1071/CP15400

25. Menéndez, S.; Merino, P.; Pinto, M.; González-Murua, C.; Estavillo, J. M. 3,4-Dimethylpyrazol Phosphate Effect on Nitrous Oxide, Nitric Oxide, Ammonia, and Carbon Dioxide Emissions from Grasslands. *J. Environ. Qual.* **2006**, *35*, 973-981. DOI: 10.2134/jeq2005.0320

26. Dougherty, W. J.; Collins, D.; Van Zwieten, L.; Rowlings, D. W. Nitrification (DMPP) and Urease (NBPT) Inhibitors Had No Effect on Pasture Yield, Nitrous Oxide Emissions, or Nitrate Leaching under Irrigation in a Hot-Dry Climate. *Soil Res.* **2016**, *54*, 675-683. DOI: 10.1071/SR15330

27. Weiske, A.; Benckiser, G.; Ottow, J. C. G. Effect of the New Nitrification Inhibitor DMPP in Comparison to DCD on Nitrous Oxide (N_2O) Emissions and Methane (CH_4) Oxidation During 3 Years of Repeated Applications in Field Experiments. *Nutr. Cycling Agroecosyst.* **2001**, *60*, 57-64. DOI: 10.1023/A:1012669500547

28. Lin, X.; Hasi, W.-L.-J.; Lou, X.-T.; Han, S.-q.-g.-w.; Lin, D.-Y.; Lu, Z.-W. Direct and Quantitative Detection of Dicyandiamide (DCD) in Milk Using Surface-Enhanced Raman Spectroscopy. *Anal. Meth.* **2015**, *7*, 3869-3875. DOI: 10.1039/C5AY00313J

29. Chen, Q.; Qi, L.; Bi, Q.; Dai, P.; Sun, D.; Sun, C.; Liu, W.; Lu, L.; Ni, W.; Lin, X. Comparative Effects of 3,4-Dimethylpyrazole Phosphate (DMPP) and Dicyandiamide (DCD) on Ammonia-

oxidizing Bacteria and Archaea in a Vegetable Soil. *Appl. Microbiol. Biotechnol.* **2015**, *99*, 477-487. DOI: 10.1007/s00253-014-6026-7

30. Yildirim, S. C.; Walker, R. M.; Roessner, U.; Wille, U. Assessing the Efficacy, Acute Toxicity, and Binding Modes of the Agricultural Nitrification Inhibitors 3,4-Dimethyl-1H-pyrazole (DMP) and Dicyandiamide (DCD) with Nitrosomonas europaea. *ACS Agric. Sci. Technol.* **2023**. DOI: 10.1021/acsagscitech.2c00303

31. Taggert, B. I.; Walker, C.; Chen, D.; Wille, U. Substituted 1, 2, 3-Triazoles: A New Class of Nitrification Inhibitors. *Sci. Rep.* **2021**, *11*, 1-12. DOI: 10.1038/s41598-021-94306-1

32. Zehnder, L. R.; Hawkins, J. M.; Sutton, S. C. One-pot, Metal-and Azide-free Synthesis of 1, 2, 3-Triazoles from α-Ketoacetals and Amines. *Synlett* **2020**, *31*, 175-178.

33. Clark, P. R.; Williams, G. D.; Hayes, J. F.; Tomkinson, N. C. A Scalable Metal-, Azide-, and Halogen-Free Method for the Preparation of Triazoles. *Angewandte Chemie International Edition* **2020**, *59*, 6740-6744. DOI: 10.1002/anie.201915944

34. Yildirim, S. C.; Walker, R. M.; Roessner, U.; Wille, U. Rapid and Inexpensive Assay for Testing the Efficiency of Potential New Synthetic Nitrification Inhibitors. *ACS Agric. Sci. Technol.* **2023**. DOI: 10.1021/acsagscitech.2c00229

35. Sayavedra-Soto, L. A.; Hommes, N. G.; Alzerreca, J. J.; Arp, D. J.; Norton, J. M.; Klotz, M. G. Transcription of the *amo*C, *amo*A and *amo*B Genes in *Nitrosomonas europaea* and *Nitrosospira sp.* NpAV. *FEMS Microbiol. Lett.* **1998**, *167*, 81-88. DOI: 10.1016/S0378-1097(98)00367-X

36. O'Sullivan, C. A.; Duncan, E. G.; Whisson, K.; Treble, K.; Ward, P. R.; Roper, M. M. A Colourimetric Microplate Assay for Simple, High Throughput Assessment of Synthetic and Biological Nitrification Inhibitors. *Plant Soil* **2017**, *413*, 275-287. DOI: 10.1007/s11104-016-3100-1

37. Subbarao, G. V.; Ishikawa, T.; Ito, O.; Nakahara, K.; Wang, H. Y.; Berry, W. L. A Bioluminescence Assay to Detect Nitrification Inhibitors Released From Plant Roots: A Case Study with Brachiaria humidicola. *Plant Soil* **2006**, *288*, 101-112. DOI: 10.1007/s11104-006-9094-3

38. Arp, D. J.; Sayavedra-Soto, L. A.; Hommes, N. G. Molecular Biology and Biochemistry of Ammonia Oxidation by Nitrosomonas europaea. *Arch. Microbiol.* **2002**, *178*, 250-255. DOI: 10.1007/s00203-002-0452-0

39. Bhal, S. K.; Kassam, K.; Peirson, I. G.; Pearl, G. M. The Rule of Five Revisited: Applying Log D in Place of Log P in Drug-Likeness Filters. *Mol. Pharmaceutics* **2007**, *4*, 556-560. DOI: 10.1021/mp0700209

40. Elsevier *Reaxys,* https://www.reaxys.com, (accessed 24.01.2023).

41. Heipieper, H. J.; Martínez, P. Toxicity of hydrocarbons to microorganisms. *Cellular Ecophysiology of Microbe: Hydrocarbon and Lipid Interactions* **2018**, *335*.

42. Sikkema, J.; de Bont, J. A.; Poolman, B. Interactions of Cyclic Hydrocarbons with Biological Membranes. *J. Biol. Chem.* **1994**, *269*, 8022-8028. DOI: 10.1016/S0021-9258(17)37154-5

43. Paszko, T.; Muszyński, P.; Materska, M.; Bojanowska, M.; Kostecka, M.; Jackowska, I. Adsorption and Degradation of Phenoxyalkanoic Acid Herbicides in Soils: A Review. *Environ. Toxicol. Chem.* **2016**, *35*, 271-286. DOI: 10.1002/etc.3212

44. dos Reis, R. R.; Sampaio, S. C.; de Melo, E. B. The Effect of Different log *P* Algorithms on The Modeling of The Soil Sorption Coefficient of Nonionic Pesticides. *Water Res.* **2013**, *47*, 5751-5759. DOI: 10.1016/j.watres.2013.06.053

45. Sidhu, P. K.; Taggert, B. I.; Chen, D.; Wille, U. Degradation of the Nitrification Inhibitor 3,4-Dimethylpyrazole Phosphate in Soils: Indication of Chemical Pathways. *ACS Agricult. Sci. & Tech.* **2021**, *1*, 540-549. DOI: 10.1021/acsagscitech.1c00150

46. Delaune, K. P.; Alsayouri, K. *Physiology, Noncompetitive Inhibitor*. In: *StatPearls Publishing [internet]*. StatPearls Publishing 2022. (accessed 2022-10-04).

47. Blat, Y. Non-Competitive Inhibition by Active Site Binders. *Chem. Biol. Drug Des.* **2010**, *75*, 535-540. DOI: 10.1111/j.1747-0285.2010.00972.x

48. O. S. Fisher; G. E. Kenney; M.O. Ross; S. Y. Ro; B. E. Lemma; S. Batelu; P. M. Thomas; V.C. Sosnowski; C. J. DeHart; N. L. Kelleher; et al. Characterization of a Long Overlooked Copper Protein From Methane- and Ammonia-Oxidizing Bacteria. *Nature Communications* **2018**, *9*, 4276. DOI: 10.1038/s41467-018-06681-5

49. Hyman, M. R.; Wood, P. M. Suicidal Inactivation and Labelling of Ammonia Monooxygenase by Acetylene. *Biochem. J.* **1985**, *227*, 719-725. DOI: 10.1042/bj2270719

50. Wright, C. L.; Schatteman, A.; Crombie, A. T.; Murrell, J. C.; Lehtovirta-Morley, L. E.; Stams, A. J. M. Inhibition of Ammonia Monooxygenase from Ammonia-Oxidizing Archaea by Linear and Aromatic Alkynes. *Appl. Environ. Microbiol.* **2020**, *86*, e02388-02319. DOI: doi:10.1128/AEM.02388-19

Chapter 5: The discovery of 4-Methyl-1-(Prop-2-yn-1yl)-1*H*-1,2,3-Triazole (MPT): A Novel, Readily Accessible and Highly Efficient Nitrification Inhibitor for Agriculture (includes submitted manuscript)

5.1 Introduction

As mentioned in Chapter 1.6, AMO inhibitors can be either reversible (non-mechanism based) or irreversible (mechanism-based). In Chapter 3 it was shown that the current SNIs DMP and DCD are reversible inhibitors that most likely bind to AMO via chelation of metal centres. Their mode of inhibition is uncompetitive, indicating that their binding site is in vicinity of the substrate binding site in the AMO. In Chapter 4, the selection of 1,4-disubstituted 1,2,3-triazoles acted as non-competitive, reversible inhibitors where increasing lipophilicity resulted in a higher inhibitory effect, suggesting that lipophilic interactions with AMO may be important. The binding site of 1,4-disubstituted 1,2,3-triazoles is most likely not the same as that of DMP and DCD. It is not clear, whether they are chelating reagents, as AMO contains multiple metal sites. Interestingly, amongst all tested SNIs, DMP showed the highest binding affinity with an $IC_{50(app)}$ of 6.6 µmol L^{-1} (Chapter 2.2, **Figure 7**), although its performance in soil remains unpredictable (see Chapter 1.7). Therefore, the scientific question raised of whether the development of a new SNI with a substantially different inhibitory mode than DMP could provide a solution to overcome the shortcomings of the current commercial SNIs. As mentioned in Chapter 1.4, C_2H_2 inhibits the AMO irreversibly through covalently binding to the AMO.[46] and it has been shown in soil incubation studies under inert atmosphere, that C_2H_2 reduces nitrification effectively for over up to 14 days. [104] Notably, C_2H_2 contains an alkynyl moiety and lacks chelating properties, which distinguishes it from all tested SNI.[46, 47] Unfortunately, C_2H_2 has no commercial use in agriculture, due to its highly flammable nature.

Therefore, it was aimed to develop a new SNI that contained an alkynyl group that mimics C_2H_2. The reported synthesis for 4,5-disubstituted 1,2,3-triazoles shown in **Scheme 1** was the

starting point of an attempt to incorporating an alkynyl substituent (**Scheme 2**). As a reminder, **Scheme 1** in Chapter 2.1.1 provided a mechanistic overview of the three steps to form the 4,5-disubstituted 1,2,3-triazoles. In the first step of the reaction is a traditional S_N2 reaction of mercaptobenzothiazole (**18**) with *α*-bromo ethyl acetate (**19**) resulted in a quantitative yield of ethyl 2-(benzothiazol-2-ylthio) acetate (**20**)**.** The second step of the synthesis comprised of an oxidation of the thioether to a sulfone with hydrogen peroxide and ammonium molybdate to form the Julia-Reagent (**21**).[101] The third step of the synthesis consists of a one-pot reaction, firstly by condensation of the Julia Reagent (**21**) with the aldehyde (**22**) *in situ*, followed by a concerted 1,3-dipolar cycloaddition (**23**) with the azide anion (N_3).[100, 101] It was intended to replace the ester by an alkynyl group. Therefore, the first of two steps of Scheme 1 remained identical by solely replacing α-bromo ethyl acetate (**19**) with equimolar amounts of propargyl bromide to form the Julia Reagent (**45**) (**Scheme 2**). Unfortunately, no traces of the 1,2,3-triazole (**46**) were detected when replacing the ester by an alkynyl group (**Scheme 2**).

a) Reaction Scheme 1:

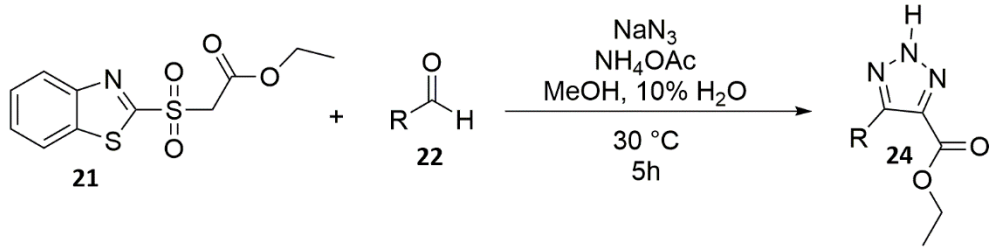

b) Proposed alkynyl inclusion (modification Scheme 1):

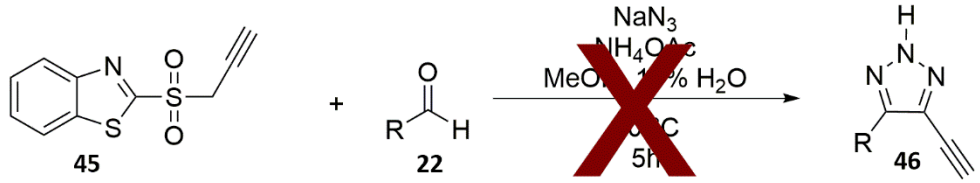

Scheme 2: a) Knoevenagel reaction occurring b) when replacing the ester group in the Julia precursor **21** with an alkynyl group (**45**) no formation of the 1,2,3-triazole (**46**) was detected.

It was suggested that for the successful performance of the Knoevenagel reaction (step 3 in **Scheme 1**) the hydrogen atom in the *α* position to the sulfonyl-group (**Scheme 3** indicated in

red) needs to be acidic. When replacing the ester with an alkynyl group the α-hydrogen is not sufficiently acidic.

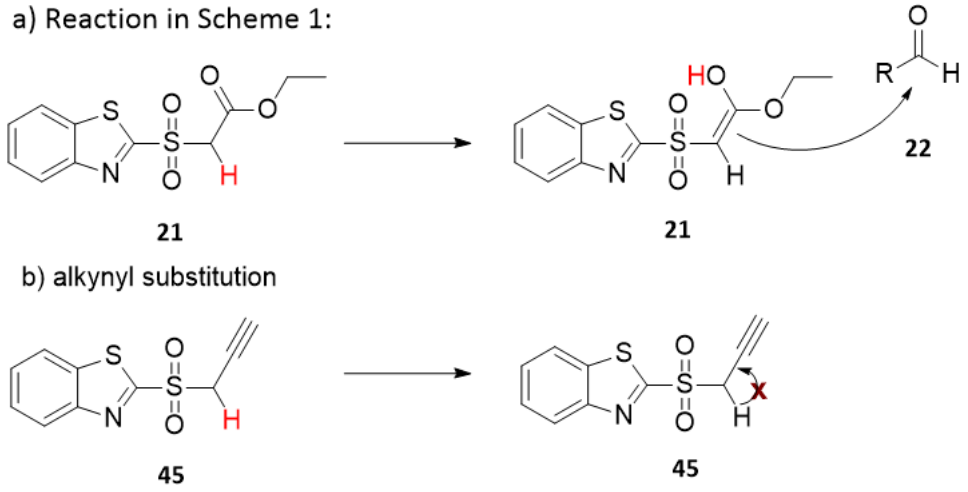

Scheme 3: Knoevenagel reaction occurring in Julia Reagent containing an ester group (compound **21**) when replacing the ester group in **21** with an alkynyl group (**45**) no reaction was observed.

Therefore, a literature search for alternative synthesis routes was performed. Recently, Clark *et al*. reported 'A Scalable Metal-, Azide-, and Halogen-Free Method for the Preparation of Triazoles', which successfully led to high-yield alkynyl substituted 1,4-disubstituted 1,2,3-triazoles (**Scheme 4b**). [105] This method was remarkable as 1,4-alkynyl- (di)substituted 1,2,3-triazoles have been challenging to synthesise in the past *via* the traditional Cu(I)-catalysed alkyne azide cycloaddition (CuAAC) ((**Scheme 4a**). Notably, alkynyl groups of type **48** are the reactants to perform the reaction, and the inclusion of two alkynyl groups (to generate alkynyl-substituted 1,2,3-triazoles) commonly leads to the formation of side products and results in low yield.[106, 107] In the procedure reported by Clark *et al*., a scope of 1.4,-disubstituted 1,2,3-triazoles was reported, which included 4-methyl-1-(prop-2-yn-1yl)-1*H*-1,2,3-triazole (shortly MPT (**54**) **Scheme 4b**). MPT contains a short propargyl group in position 1 and a methyl substituent in position 4, and was of particular interest, due to its small size of the molecule that potentially could increase the likelihood of binding to the same active site as C_2H_2. The Clark *et al.* synthesis (**Scheme 4b**) employed the reaction of the *α*-ketoacetal 1,1-dimethoxypropan-2-one (**50**) with 4-methylbenzene sulfonohydrazide (tosyl hydrazide

(**51**)) to form the hydrazone **52**, followed by the addition of propargyl amine (**53**) to yield MPT (**54**).

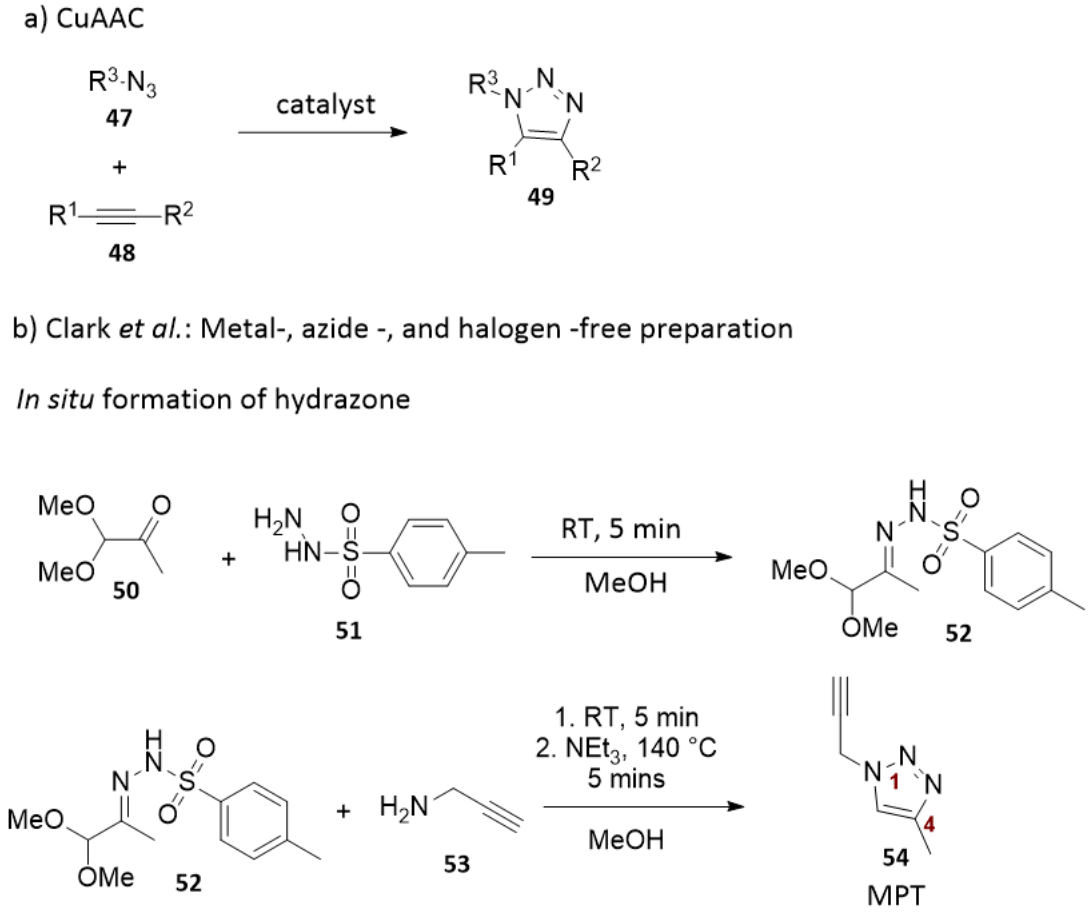

Scheme 4: a) Conventional Cu(I)-catalysed alkyne azide cycloaddition (CuAAC) and b) Clark *et al.* alternative synthesis for the synthesis of methyl-1-(prop-2-yn-1yl)-1*H*-1,2,3-triazole (MPT).

5.2 4-Methyl-1-(Prop-2-yn-1yl)-1H-1,2,3-Triazole (MPT): A Novel, Readily Accessible and Highly Efficient Nitrification Inhibitor for Agriculture (submitted manuscript)

Abstract

Nitrogen (N) fertilization in agriculture has become an environmental threat. Formation of the greenhouse gas nitrous oxide (N_2O), groundwater pollution with nitrate (NO_3^-), and river eutrophication are examples of the adverse impacts. N fertilizers can be amended with nitrification inhibitors to slow down microbial nitrification, which converts ammonia (NH_3) to NO_3^- in soils, but the often unreliable performance of the commercial inhibitors, such as 3,4-dimethylpyrazole (DMP), requires development of new compounds with consistent inhibitory efficacy. We demonstrate that 4-methyl-1-(prop-2-yn-1-yl)-1*H*-1,2,3-triazole (MPT) shows a considerably improved performance compared to DMP. Unlike DMP, MPT acts as a mechanistic, irreversible inhibitor of the key enzyme ammonia monooxygenase, resulting in retention of NH_3 and a decreased NO_3^- and N_2O production over 21 days in various agricultural soils with pH ranging from 4.7 to 7.5. Real-time quantitative polymerase chain reaction analysis revealed that MPT has an enhanced inhibitory effect on both ammonia-oxidizing bacteria and ammonia-oxidizing archaea.

Introduction

The provision of food for the constantly growing world population will require an increase of nitrogen (N) fertilizer usage by 70-100% worldwide by 2050, which is exacerbated by limited arable land and deteriorating agricultural conditions, particularly due to global warming.[1,2] Unfortunately, since several decades the N use efficiencies (NUEs) have remained at only around 50% globally.[3,4] A large fraction of N fertilizers is lost from agricultural systems through abiotic and biotic pathways, including volatilization of ammonia (NH_3), which is a precursor of particulate matter ($PM_{2.5}$), and nitrate (NO_3^-) leaching that causes surface water eutrophication and groundwater pollution.[5-7] Microbial nitrification and denitrification processes lead to the formation of the gases nitrous oxide (N_2O), nitric oxide (NO) and nitrogen (N_2).[8] N_2O has a 300 times higher global warming potential than carbon dioxide

(CO_2), and mitigation of N losses in agriculture has become an important target for reducing the greenhouse gas (GHG) footprint.[7]

To improve N management in agricultural soils, one approach is to add nitrification inhibitors (NIs) to N fertilisers.[9,10] Nitrification is carried out by ammonia-oxidizing bacteria (AOB) and ammonia-oxidizing archaea (AOA) (Figure 1a). NIs are designed to inhibit ammonia monooxygenase (AMO), a multimeric transmembrane enzyme, which is conserved in both AOB and AOA[11-13] and catalyses the rate-limiting first oxidation step of NH_3 to hydroxylamine (NH_2OH).[14,15] NH_2OH is subsequently converted to nitrite (NO_2^-) by the enzyme hydroxylamine oxidoreductase (HAO), followed by rapid oxidation to NO_3^-, the end-product of the nitrification process, which is catalysed by nitrite oxidase (NXR) present in, for example, *Nitrobacter* spp. Thus, inhibition of AMO should increase the residence time of NH_3 (or ammonium, NH_4^+, respectively) and reduce N losses from soil through NO_3^- leaching, and N_2O emissions during nitrification and denitrification. Although the crystal structure of the key enzyme AMO has not been resolved, some details about its active center have been inferred from the recently crystallized particulate methane monooxygenase (pMMO), which is evolutionally comparable to AMO. According to the pMMO findings, a cupredoxin-like unit might be involved in the oxidation process.[11,16-18]

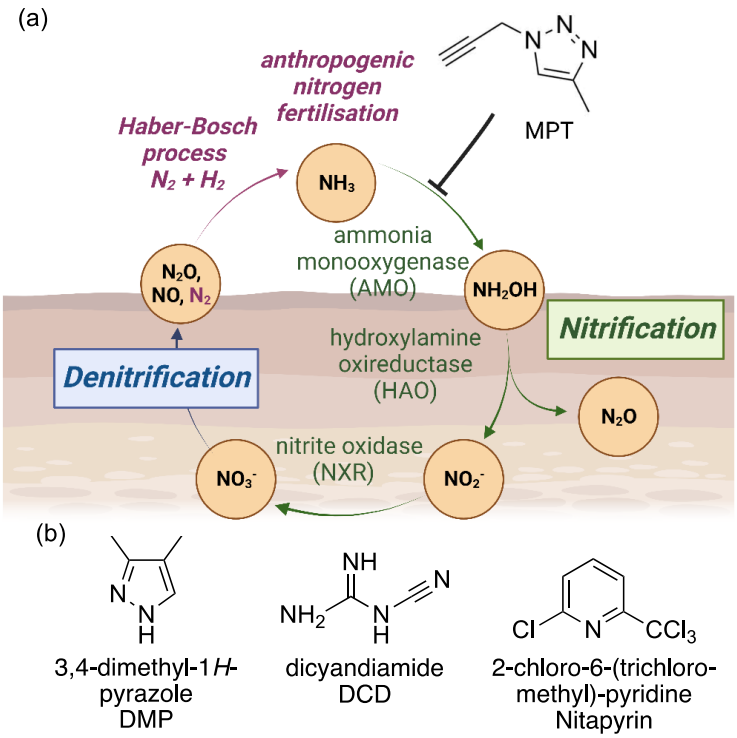

Figure 1. (a) Introduction of N fertilizer (e.g., NH_4^+ based fertilizer, including urea) into soil initiates microbial nitrification by ammonia oxidising archaea and bacteria (AOA and AOB). NH_4^+ is deprotonated in soil to NH_3 (not shown), which is oxidised to NH_2OH catalysed by ammonia monooxygenase (AMO), followed by the oxidation to NO_2^- or, under oxygen-limiting conditions, to N_2O, catalysed by hydroxylamine oxireductase (HAO), and NO_3^-, catalysed by nitrite oxidizing bacteria (NOB). Denitrifying bacteria reduce NO_3^- to gaseous N_2, N_2O and NO. N_2 is reintroduced into the N cycle as NH_3 obtained by the Haber-Bosch process through reaction of hydrogen (H_2) with N_2. MPT prevents nitrification by irreversibly inhibiting AMO, thereby increasing the residence time of NH_4^+ in soils for plant uptake and decreasing N loss through NO_3^- leaching and emission of the greenhouse gas N_2O. (b) Current commercial nitrification inhibitors. Created with Biorender.

Currently commercially available NIs are 3,4-dimethyl-1*H*-pyrazole (DMP), which is commonly applied in agricultural systems as the phosphate salt (DMPP or ENTEC®, BASF AG), dicyandiamide (DCD, AlzChem AG) and 2-chloro-6-(trichloromethyl)-pyridine (Nitrapyrin or N-Serve®, Dow Chemical Co.) (Figure 1b). Enzyme inhibitors can operate through mechanism-based or non-mechanism-based pathways.[19-21] Chelators, which (reversibly) bind to a metal centre in the enzyme's active site without causing a chemical reaction, fall into the latter

category.[14] In previous work we have found that DMP and DCD act as reversible inhibitors of AMO.[22]

In contrast, mechanism-based inhibitors operate through formation of covalent bonds with the catalytic center of the enzyme. With regards to nitrifying bacteria, recovery of their activity would require *de novo* synthesis of the enzyme. One prominent example for a mechanism-based NI is the gas acetylene,[19,23] but its high flammability and reactivity prohibits the use in agriculture.

Of the three commercial NIs, DMP is the newest product, which was introduced more than 20 years ago. However, despite the often unreliable performance of DMP, DCD and Nitrapyrin, particularly in acidic soils, no new inhibitor compounds have been developed and brought to market that reliably overcome the problems associated with any of the existing commercial NIs.[24-27]

Recently, we have shown that substituted 1,2,3-triazoles are a promising new NI class, which can outperform the current 'gold standard' DMP, especially at increased temperatures.[28] We present in this work the novel NI 4-methyl-1-(prop-2-yn-1-yl)-1*H*-1,2,3-triazole (MPT, Figure 1a), which has a different mechanism of inhibition than the existing commercial NIs. MPT exhibits outstanding inhibitory properties and has the potential to significantly reduce GHG emissions from agriculture, including acidic soils.

Materials and Methods

Chemicals

DMP (3,4-dimethyl-1*H*-pyrazole) was supplied by Incitec Pivot Ltd. Australia. Griess reagent (listed as modified) and dimethyl sulfoxide (DMSO) were purchased from Sigma Aldrich. All aqueous solutions were prepared in Milli-Q water unless stated as distilled. *N. europaea* (ATCC19718) was purchased from the American Type Culture Collection**.** *N. multiformis* was isolated from an aquarium kit as described previously.[29] 4-Methyl-1-(prop-2-yn-1-yl)-1*H*-1,2,3-triazole (MPT) and 4-methyl-1-propyl-1*H*-1,2,3-triazole (H-MPT) were synthesised according to the procedure reported by Clark *et al.*[30] The compounds NI-1-3 were provided

by Taggert *et al.* and synthesised as described.[28] Experimental details and spectroscopic data are provided in the Supporting Information (SI).

Studies with AOB

The growth and harvest of pure bacterial cell cultures, the standard activity and activity recovery assays, the measurements of the O_2 consumption and Michaelis-Menten kinetics were conducted as previously reported.[22] All bacterial incubations were performed in sodium phosphate buffer (NaPB) with 1v/v% DMSO at pH = 7.5 and 30°C with different inhibitors and concentrations, as indicated. Experimental details are provided in the SI.

Mineral-N Transformation Studies

Soil incubations to determine the loss of NH_4^+-N and production of NO_3^--N over 21 days after treatment were performed in an Australian soil (soil A; pH = 5.9, soil specifications are provided in Table S6), similar to the previously described protocol (see Supplementary Information).[28] Treatments were: (1) fertilizer only ($(NH_4)_2SO_4$), 100 mg N kg^{-1} soil; (2) fertilizer + 0.5 mol% MPT, (3) fertilizer + 2.5 mol% MPT, (4) fertilizer + 5 mol% MPT and (5) fertilizer + 5 mol% DMP, with three replicates of each treatment per time interval (n = 3).

N_2O Measurements

Soil incubations were performed with four German soils with raning pH(soils B - E) (soil specifications are provided in Table S6). Each of the three replicates consisted of 6 g of sieved soil (2 mm). The soil was air-dried after collection and pre-incubated prior to the experiment for seven days at 50% water holding capacity (WHC).[31] The soil was transferred to a gas chromatography vial (22 mL volume, clear glass, Macherey-Nagel, Germany) and compacted densely to allow 5.5 - 6.2 cm headspace. The soil in the vials was incubated for a total of 21 days at a constant temperature of 21°C with an open lid to ensure gas circulation. The control incubations contained 'untreated' soil (deionized H_2O only), 'fertilizer only' soil ($(NH_4)_2SO_4$; 50 mg kg^{-1} soil) and accompanied each measurement. $(NH_4)_2SO_4$ was applied as an aqueous solution (1 g NH_4^+ mL^{-1} H_2O) and introduced on the soil surface to mimic field conditions. Three inhibitor solutions were prepared from DMP and MPT at concentrations of 0.5 mol%, 2.5 mol% and 5 mol% of applied fertilizer-N (see Supplementary Table 7) and applied on the soil surface. The soils reached 60% WHC after the treatments had been applied and were

kept at that moisture level by periodically adding deionized water to compensate for evaporation losses.

At the day of measurement (day 1, 3, 5, 7, 14 and 21 after fertilization) the vials were closed gas-tight with a rubber septum and aluminium lid and opened again after each measurement. The N_2O emission was analysed using a gas chromatograph equipped with an electron capture detector and flame ionization detector (GC-ECD/FID; Clarus 580, Perkin Elmer).[32] Details for the calculation of the N_2O production rate are provided in the SI.

Real-Time qPCR of Bacterial and Archaeal *amoA*

Soil samples (400 mg) from the N_2O experiments after the 21-day incubation period were used to extract DNA using a NucleoSpin Soil DNA extraction kit (Macherey Nagel, Germany) according to the manufacturer's instruction. For extraction, SL1 buffer and enhancer were chosen for extraction, and DNA was finally eluted in 40 µL PCR-grade water. Real-time quantitative PCR (qPCR) of *amoA* genes was performed for the bacterial and archaeal community for each treatment with three biological and three technical replicates. The primers Arch-amoAF and Arch-amoAR were used for AOA[33], while amoA-1F and amoA-2R were used for AOB.[34] The DNA extracts were diluted 10-fold to avoid inhibitory effects. Real-time qPCR assays were performed on a Bio-Rad CFX Connect real-time PCR machine. The quantification was performed using 5.0 µL SYBR® Green Master Mix (BioRad, USA), 0.4 µL of the forward and reverse primer (10 pmol μL^{-1}), respectively; 3.2 µL PCR-H_2O and 1 µL of the 10-fold diluted DNA. The fragments of bacterial and archaeal *amoA* genes were amplified using an initial denaturation phase (2 min), followed by 40 cycles (i) at 95°C (10 s), (ii) annealing at 72°C for bacteria (1 min) and archaea (30 s), and (iii) elongation for 45 s at 57.4°C (bacteria) and 60°C (archaea). The PCR reaction runs had an efficiency between 97-111%. Standard curves were generated using serial dilutions ranging from 10^8 to 10^3 gene copies per reaction, provided as linearized plasmids that contained cloned *amoA* genes of bacteria or archaea, respectively ($R^2 > 0.8$). The correct PCR product length was verifed by obtaining a melting curve in the temperature range 65 – 95°C.

Statistics

Statistical analysis was performed with three technical (except the GC studies) and three biological replicates (n = 3). For the bacterial cell studies, NO_2^- production, $K_{m(app)}$, $V_{max(app)}$ and k_{obs} values for inhibited and uninhibited cells were determined using student's T-test with a significance level of $P < 0.05$ using GraphPad Prism version 9.5.0. Statistical analysis of the measured GC gas concentrations was performed on the calculated N_2O production rates via two-way analysis of variance (ANOVA), assessing the factors day and treatment at each time point evaluated using the Tukey HSD post-hoc test with a significance level of $P < 0.05$. All results are reported as mean values ± standard error of the mean.

Results and Discussion

MPT can be conveniently synthesized within minutes through a previously reported metal- and azide-free one-pot protocol from 1-dimethoxy propan-2-one, *N*-tosylhydrazide and propargyl amine.[30] As NIs can exhibit varying inhibitory effects on orthologous AMO enzymes,[21,35] we have used pure cultures of both *Nitrosomonas europaea* (*N. europaea*) and *Nitrosospira multiformis* (*N. multiformis*) to explore in detail the mechanism of inhibition of MPT. Incubations were performed with MPT as well as DMP (for comparison) in one Australian soil (pH 5.9) to study mineral-N transformation and in four German soils with pH levels ranging from 4.5 to 7.5 to determine N_2O production rates. Furthermore, the impact on the nitrifier community was evaluated for both MPT and DMP by quantifying the number of ammonia monooxygenase gene (*amoA*) copies following a three-week soil incubation period, using quantitative polymerase-chain reaction (qPCR) analysis.

Identification of Enzyme Targeted by MPT

As outlined in the Introduction, AOB are responsible for the first two steps of the oxidation of NH_3 to NO_3^-, i.e., $NH_3 \rightarrow NH_2OH \rightarrow NO_2^-$, which are catalysed by the enzymes AMO and HAO, respectively. To identify whether MPT targets AMO or HAO, cell cultures of *N. europaea* and *N. multiformis* were prepared separately and incubated with equimolar amounts of either NH_4^+ (as substrate for AMO) or NH_2OH (as substrate for HAO) in sodium phosphate buffer (NaPB), which contained 1v/v% dimethylsulfoxide (DMSO), at pH = 7.5. The production of NO_2^- was measured after 60 min in an assay based on the Griess reaction[29] in the presence

of MPT ('inhibited cells') and its absence ('uninhibited cells', 100% signal). A control experiment confirmed that the NO_2^- production in the absence of both N-sources and MPT was practically negligible ('untreated cells', 0% signal). The % activity of the cells was calculated according to eqn. 1:

$$\% \text{ Activity} = \left[\frac{[NO_2^-]_{\text{inhibited cells}} - [NO_2^-]_{\text{untreated cells}}}{[NO_2^-]_{\text{uninhibited cells}} - [NO_2^-]_{\text{untreated cells}}} \right] \times 100 \qquad (1)$$

Table 1 presents the % activity after 60 min (see also Tables S1 and S2).

Table 1. Activity (in %) of *N. europaea and N. multiformis* after treatment with differently substituted 1,2,3-triazoles, determined from the NO_2^- production.[a]

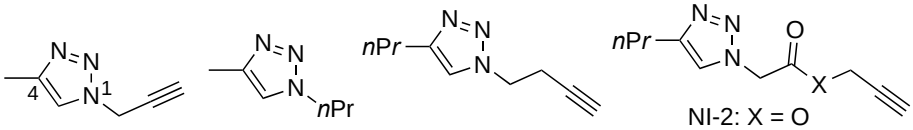

Compound	N source	% Activity	
		N. europaea	*N. multiformis*
MPT	NH_3	24 ± 5	25 ± 4
	NH_2OH	72 ± 3	67 ± 4
H-MPT	NH_3	100	100
NI-1	NH_3	79 ± 2	60 ± 1
NI-2	NH_3	51 ± 2	53 ± 2
NI-3	NH_3	93 ± 1	100

[a]Incubations were performed in NaPB with 1v/v% DMSO at pH = 7.5 and 30°C with [inhibitor] = 0.3 mM (10 mol% of N-source), $[NH_4^+]$ = 3 mM or $[NH_2OH]$ = 3 mM, at 100 rpm for 60 min in the dark. Standard errors were determined from three biological replicates, n = 3).

The data for MPT show that the activity of both *N. europaea* and *N. multiformis* cells dropped to about 25% upon treatment with NH_4^+. Interestingly, when NH_2OH was used as N-source, a reduction of the activity of both bacterial cell cultures to about 70% was found. This might suggest that MPT inhibits both AMO and HOA, as AMO-specific inhibitors would be expected

to show a minimal effect on the activity of HAO. [36] However, as AMO and HAO are not operating independently but are interconnected through an electron shuttle mechanism, it is likely that disruption of the electron transfer chain due to AMO inhibition, in this case by MPT, leads also to a partial inhibition of HAO. This proposal is supported by previous findings that hydrazine, a known AMO inhibitor, as well as DMP also decrease the activity of HAO. [22, 37]

Structure-Activity Relationship (SAR) Studies

To explore the role of the triple bond for the inhibitory activity of MPT, structure-activity relationship (SAR) studies with a series of triazoles without and with alkyne-containing substituents were performed. The data are included in Table 1 (see Table S3 for full data). H-MPT, which has a saturated propyl substituent instead of the propargyl chain, had no impact on the activity of both *N. europaea* and *N. multiformis*. NI-1, which has a propyl group at C-4 and a butynyl instead of propynyl chain, reduced the AMO activity to about 80% in both cell cultures. In NI-2 the alkynyl group was replaced by an alkynyl ester, resulting in an activity drop to about 50%, whereas the alkynyl amide substituent in NI-3 almost eradicated any inhibitory activity. These data show that the presence of an alkynyl substituent on the 1,2,3-triazole does not 'automatically' create a potent inhibitor for AMO. Additional factors, for example size, shape and polarity, are obviously also important for inhibitory activity, which will be explored further in future work.

Measurement of the Oxygen (O_2) Consumption

Acetylene has been shown to act as an irreversible AMO inhibitor.[19] As the alkyne moiety constitutes a considerable fraction of the molecular structure of MPT, we explored whether MPT might also function as an irreversible inhibitor by performing real-time kinetic measurements of the rate of O_2 consumption (or O_2 uptake, respectively) by AMO. The oxidation $NH_3 \rightarrow NH_2OH$ requires equimolar amounts of O_2, and the rate of O_2 consumption is therefore proportional to the NH_3 oxidation.[36]

The O_2 consumption by cell suspensions *of N. europaea* was measured at 20°C using a Clark-type oxygen electrode by first monitoring the decrease of [O_2] in the presence of NH_4^+ for 5 min. MPT was then added, the system was equilibrated for 15 s, and the O_2 decay was subsequently monitored for a further 5 min. In all measurements, both NH_4^+ and O_2 were

present in excess so that the O_2 uptake rate was only dependent on the enzyme concentration (the total protein concentration was ca. 468 µg L^{-1}, determined via a BCA assay kit). Thus, under these conditions the O_2 consumption by uninhibited cells should follow zero-order kinetics. [MPT] was chosen such that the O_2 consumption was not completely stopped. Figure 2 shows the recorded real-time trace of the O_2 consumption of cells before and after treatment with 0.6 mM and 1.2 mM MPT, respectively.

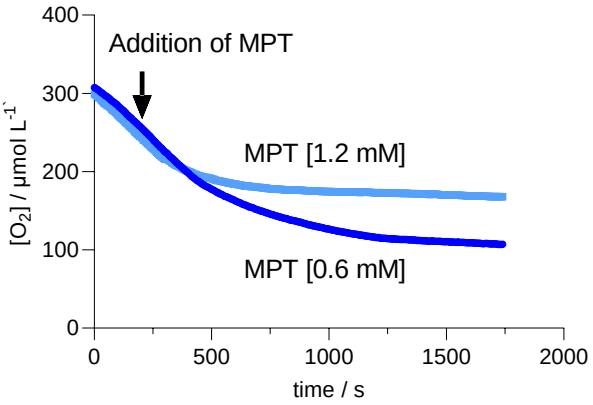

Figure 2. O_2 consumption by *N. europaea* in the absence and presence of MPT. The first 240 s show the O_2 consumption in the absence of MPT. After 255 s, MPT was added (indicated by the arrow); [MPT] = 0.6 mM (dark blue trace) and 1.2 mM (light blue trace). The cells were treated with [NH_4^+] = 3.0 mM in NaPB (pH = 7.5) with 1v/v% DMSO and 20°C under constant stirring in the dark. The plot shows the mean of three measurements for each concentration; standard errors are omitted for clarity and are provided in the *k* value of uninhibited cells.

Addition of MPT considerably slowed down O_2 consumption by *N. europaea*. Whilst uninhibited cells showed, as expected, zero-order kinetics with an average rate coefficient *k* = 275 ± 20 nmol O_2 L^{-1} s^{-1} (Figure S1 and Table S4), the decay profile after the addition of MPT changed to follow first-order kinetics. The observed rate coefficients, k_{obs}, for the O_2 consumption in the presence of MPT were determined as 2.7 x 10^{-3} s^{-1} and 4.5 x 10^{-3} s^{-1} for [MPT] = 0.6 mM and 1.2 mM, respectively (Figure S2 and Table S5).

The rate of O_2 consumption in the presence of MPT is a measure for the rate of enzyme inhibition. Thus, the observed increase of the rate of inhibition with increasing [MPT] (doubling [MPT] increased the rate of inhibition by a factor of about two in our experiment),

is indicative for a mechanistic inhibition, where the number of active enzymes declines over time. A similar observation has been made previously for the nitrification inhibitors phenylacetylene and acetylene.[19,38] This mode of inhibition is different from that of DMP and DCD, which are both non-mechanistic inhibitors, as revealed by the rate of O_2 consumption by *N. europaea*, which remained zero order in the presence of these inhibitors.[22]

Exploring the Reversibility of Enzyme Inhibition by MPT

To explore whether MPT acts as a reversible or irreversible mechanistic inhibitor, cells of *N. europaea* and *N. multiformis* were inoculated with NH_4^+ and MPT for 30 min and the AMO activity determined by measuring the NO_2^- production. The cells were subsequently thoroughly washed with NaPB in order to remove unbound and bound MPT (a high inhibitor loading of 50 mol% of applied NH_4^+-N was chosen to ensure noticeable effects), re-incubated with NH_4^+ at 30 °C for 30 min, and the NO_2^- production was measured again. Control experiments in the absence of MPT confirmed that the washing and re-incubation protocol did not impact (within error) on the NO_2^- production of both bacterial strains.

Table 2. NO_2^- production by pure cell cultures of *N. europaea* and *N. multiformis* after treatment with NH_4^+ and MPT and repeated washing with NaPB, followed by re-incubation with NH_4^+.[a]

AMO source	[MPT] / mM	NO_2^- production / nmol L^{-1} min^{-1}	
		before washing	after washing
N. europaea	--	1537 ± 512	1458 ± 255
N. europaea	1.5	379 ± 51	317 ± 73
N. multiformis	--	1314 ± 374	1777 ± 293
N. multiformis	1.5	345 ± 77	358 ± 39

[a] The inoculations were performed with $[NH_4^+]$ = 3.0 mM in NaPB (pH = 7.5) with 1 v/v% DMSO at 30°C and 100 rpm in the dark. Standard errors were calculated from three biological replicates, each performed with three technical replicates.

Thus, reversible binding of MPT to AMO would be expected to result in a recovery of the NO_2^- production activity after washing and re-incubation, approximately to the level of the uninhibited cells, as we have recently found for DMP and DCD. [22]

The data in Table 2 reveal that, compared to the uninhibited cells, the NO_2^- production drops considerably upon treatment with MPT, irrespective of the AMO orthologue. For example, before washing, *N. europaea* cells exposed to MPT produced about 379 nmol L^{-1} min^{-1} of NO_2^-, whereas uninhibited cells produced about four times more NO_2^-. After washing the MPT-treated cells and re-incubation with NH_4^+, the activity did not increase significantly ($P > 0.05$), clearly showing that MPT irreversibly inhibits AMO. Recovery of the full NO_2^- production rate requires *de novo* synthesis of AMO, which takes at least several hours, depending on the duration of exposure to the inhibitor. [21, 39]

Michaelis-Menten kinetics

Insight of the binding site of MPT in AMO was obtained by studying the Michaelis-Menten kinetics through measuring the production of NO_2^- at different [NH_4^+] and constant [MPT]. Figure 3 shows the formation of NO_2^- by uninhibited cells and cells treated with 37.5 µM and 75 µM of MPT, respectively. It should be noted that [MPT] was deliberately chosen to be below the $IC_{50(abs)}$ value of about 104 µM (determined with *N. europaea*; see Figure S3) to obtain an NO_2^- production that is 25 - 44% of that of the uninhibited cells. The Michaelis constant K_m is the substrate concentration at which the reaction rate is 50% of the maximal rate, V_{max} (see SI).

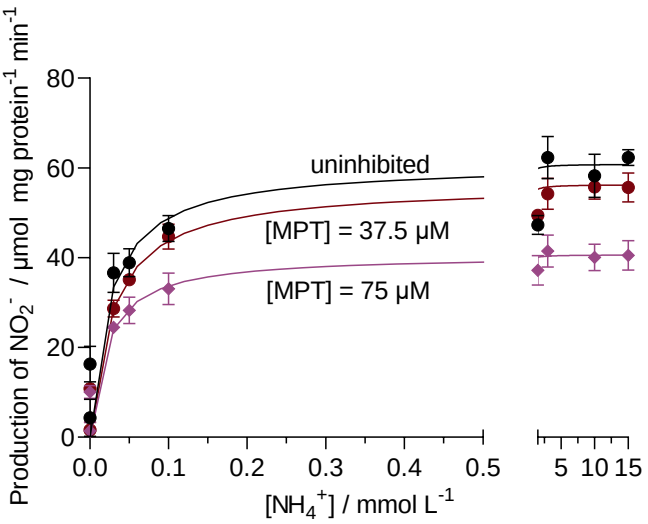

Figure 3. Effect of MPT on the NO_2^- production in dependence of [NH_4^+] after 60 min. The inoculations were performed with [NH_4^+] = 0.003 mM, 0.03 mM, 0.05 mM, 0.1 mM, 1.5 mM, 3.0 mM, 10 mM and 15 mM in NaPB (pH = 7.5) with 1v/v% DMSO at 30°C and 100 rpm in the dark. Note the different axis scale to include the data at higher [NH_4^+]. Standard errors were calculated from three biological replicates.

The Michaelis-Menten plots show saturation kinetics, where the NO_2^- production became independent of [NH_4^+] beyond 0.5 mmol L^{-1}. Furthermore, cells treated with MPT did not lead to an increased NO_2^- production even when [NH_4^+] was increased by up to four orders of magnitude. Determination of the Michaelis-Menten parameters via hyperbolic analysis revealed an unchanged value of $K_{m(app)}$, whereas $V_{max(app)}$ decreased with increasing [MPT] (the suffix 'app' indicates that these constants were determined from bacterial cells and not the purified enzyme) (Table 3).

Table 3. Michaelis-Menten kinetic parameters of the [NH_4^+]-dependent production of NO_2^- by *N. europaea* in the absence and presence of MPT at two different MPT concentrations.[a,b]

Inhibitor	Concentration / mM	$V_{max(app)}$ / µmol (mg protein min)$^{-1}$	$K_{m(app)}$ / µM
none	--	70.4 ± 7.3	29.9 ± 4.9
MPT	75 µM	39.2 ± 2.0	23.7 ± 4.0
MPT	37.5 µM	52.7 ± 2.7	30.2 ± 0.3

[a] [MPT] was chosen to achieve partial inhibition of the NO_2^- production (see text). [b] The suffix 'app' in $V_{max(app)}$ and $K_{m(app)}$ indicates that these constants were determined from bacterial cells and not the purified enzyme. Standard errors were calculated from three biological replicates, each performed with three technical replicates.

Such a behaviour is indicative for a non-competitive inhibition mode,[40] i.e., MPT is not competing with NH_3 for the same binding site in AMO. This inhibition mechanism is similar to that of phenylacetylene, whereas acetylene acts as a competitive inhibitor, which becomes less effective with increasing [NH_3]. [21] This mode of inhibition is also different from that of DMP and DCD, which are both uncompetitive inhibitors, and binding of NH_3 to the active site in AMO is essential for their inhibitory effect.[22]

Measurement of NH_4^+ and NO_3^- in Soil A

To determine the nitrification inhibitory effect of MPT *in vivo*, soil incubations were performed by measuring concentration-time profiles for NH_4^+ and NO_3^- in an acidic Australian soil (soil A, pH = 5.9) over 21 days. MPT was tested at three different concentrations (0.5 mol%, 2.5 mol% and 5 mol% of applied fertilizer-N) and compared with the commercial inhibitor DMP (5 mol% of applied fertiliser-N). The data are shown in Figure 3 (NH_4^+ and NO_3^- concentrations for all replicate runs are provided in Table S8).

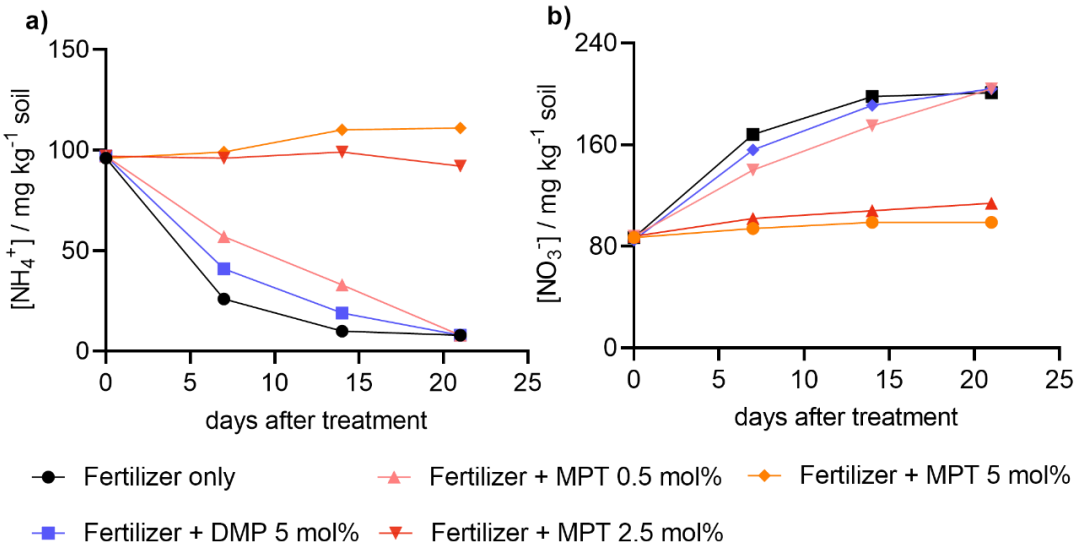

Figure 4. Mineral N-transformations in soil A (pH = 5.9). NH_4^+ (a) and NO_3^- (b) concentrations measured at different timepoints over an incubation period of 21 days at 25°C. Detailed soil specifications are listed in Table S6. $(NH_4)_2SO_4$ was used at an application rate of 100 mg N

kg^{-1} soil. Inhibitor treatments were 0.5 mol%, 2.5 mol% and 5 mol% of applied N for MPT, and 5 mol% for DMP, respectively. Each concentration profile was obtained from three replicates (n = 3).

Loss of NH_4^+ occurred rapidly without NI and with DMP, with no NH_4^+ being present any more after 21 days of incubation (Figure 3a) and quantititive formation of NO_3^- (Figure 3b). This result confirms the poor inhibitory performance of DMP in acidic soils reported in the literature.[25, 41-43]. Also, while MPT at the lowest application rate noticeably slowed down NH_4^+ loss within the first 15 days, it was not sufficiently effective to retain NH_4^+ in the soil beyond 21 days.

In contrast, MPT treatment at the higher application rates of 2.5 and 5 mol% NH_4^+ was quantitatively retained in the soil over the entire incubation period ($P < 0.001$), indicating excellent inhibitory activity. These findings were also reflected by the lack of NO_3^- production over the duration of the incubation with the two higher application rates of MPT. In fact, the inhibitory performance of MPT at the 2.5 mol% application rate was only marginally poorer than with the higher application rate of 5 mol%, clearly illustrating MPT's excellent inhibitory performance, particularly compared to the current 'gold standard' DMP.

Measurement of N_2O Formation in Soils B - E

As N_2O emissions from soils are controlled by biological nitrification-denitrification pathways, retention of NH_4^+ in the soil through the use of MPT should also reduce formation of N_2O.[10,44] Therefore, incubations were performed with four different German soils (soils B - E) with varying pH, and the N_2O production rates in the presence of MPT were compared with those measured using DMP at the same application rates (i.e., 0.5 mol%, 2.5 mol% and 5 mol% of applied fertilizer-N) as well as in the absence of NI (see Table S6 for soil specifications).

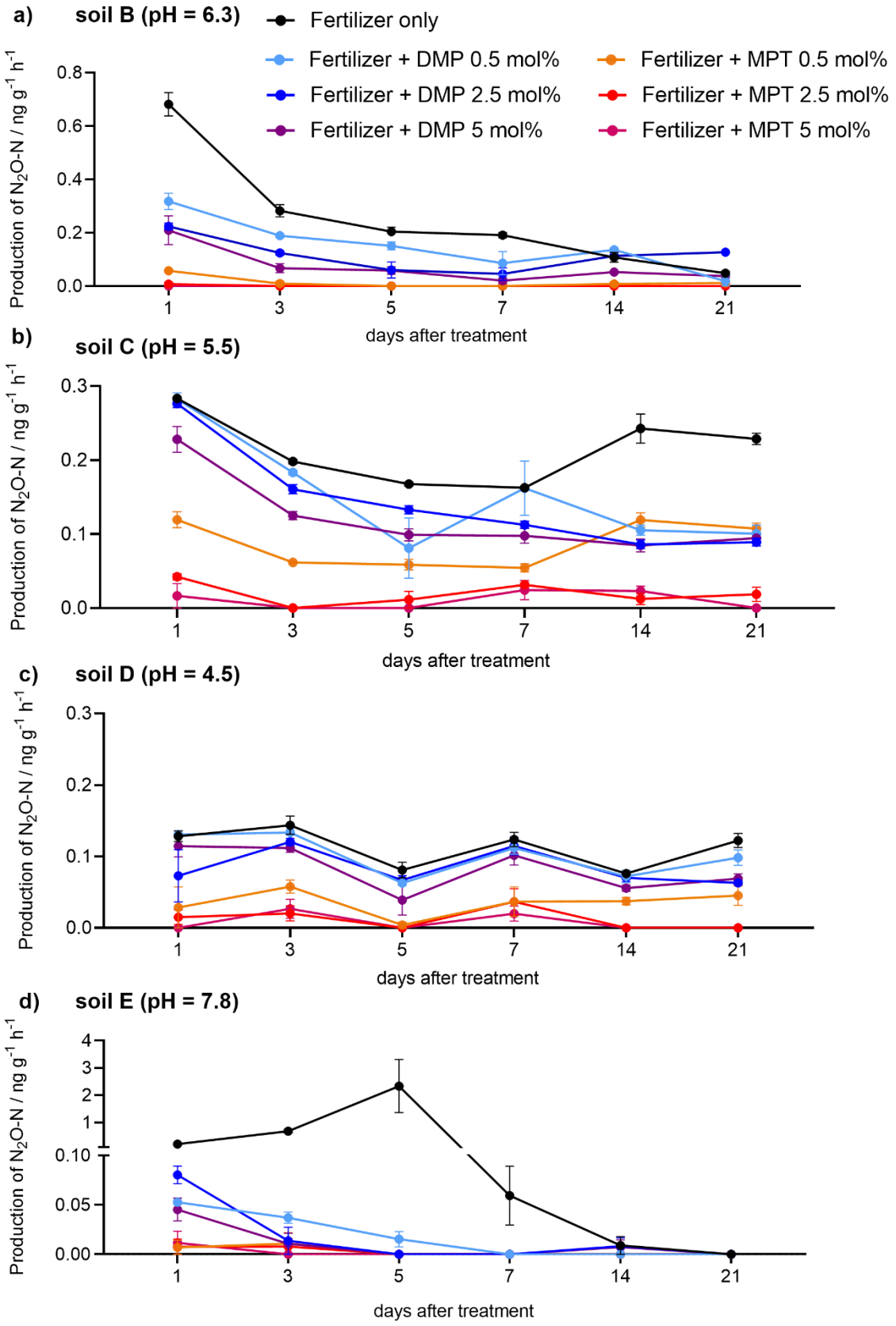

Figure 5. N_2O production rates over 21 days in soils B - E. $(NH_4)_2SO_4$ was applied as 50 mg kg^{-1} soil 'fertilizer only'. [DMP] and [MPT] were 0.5 mol%, 2.5 mol% and 5 mol% of the applied

fertilizer-N, respectively. Soil E: Note the different axis scale to include higher N_2O production rates; no N_2O production was detected beyond day 5 for DMP at 5 mol% and all MPT treatments. Data were calculated from three biological replicates (n = 3).

In the first week after fertilizer application to soil B (pH = 6.3), the N_2O production rate by the uninhibited soil was the highest with 0.68 ng g^{-1} soil h^{-1} at day 1 and 0.19 ng g^{-1} soil h^{-1} at day 7, before gradually dropping to 0.05 ng g^{-1} soil h^{-1} at day 21 (Figure 4a). This behaviour reflects the initially high N availability, which depletes over time. Compared to the uninhibited soil, treatment with DMP slowed down the N_2O formation depending on the application rate. Thus, with 0.5 mol% of DMP the N_2O production rate was with 0.32 ng g^{-1} soil h^{-1} at day 1 approximately 50% of that of the uninhibited soil. Using DMP at the higher application rates of 2.5 mol% and 5 mol%, the N_2O production rate was approximately 67% of that in the absence of the inhibitor. In contrast, soil treated with MPT produced N_2O at a rate of only 0.06 ng g^{-1}soil h^{-1} at day 1 in the case of the lowest application rate, otherwise the amount of N_2O remained below the detection limit over the duration of the experiment, clearly revealing that MPT is significantly more effective in reducing N_2O emissions than DMP.

In the more acidic soil C (pH = 5.5), the reduced amount of NH_3 available for oxidation by AMO due to protonation resulted in a much lower N_2O production rate of the uninhibited soil, compared to soil B (Figure 4b). The average rate of N_2O production remained largely unchanged over the entire 21 days, confirming that acidic soils are able to efficiently retain NH_3 as NH_4^+.[45] Soil treated with 0.5 mol% and 2.5 mol% DMP did not show a significantly reduced N_2O formation rate in the first two weeks ($P > 0.05$) compared to the uninhibited soil. Only at the highest application rate of DMP, a gradual reduction of the N_2O production rate to 0.095 ng g^{-1} soil h^{-1} at day 21 was found. In comparison, soil treated with 0.5 mol% of MPT produced about 0.12 ng h^1 of N_2O across the duration of the incubation, which is just 25% of the amount released from the uninhibited soil. At the higher MPT application rates the production of N_2O was nearly completely suppressed.

The most acidic soil (soil D, pH = 4.7) produced the lowest amount of N_2O, ranging from 0.08 to 0.14 ng g^{-1} soil h^{-1} throughout the experiment (Figure 4c). No significant difference of the N_2O production rates between the uninhibited soil and soil treated with DMP was found ($P >$

0.05). These data align with the NH_4^+/NO_3^- profiles in measured in this work (see Figure 3) and literature.[26,27,43] In contrast, soil treated with MPT at 0.5 mol% slowed down N_2O production by 60%, whereas MPT at application rates of 2.5 mol% and 5 mol% reduced the N_2O production rate to practically zero from the start of the experiment, indicating that the inhibitory performance of MPT is practically pH-independent at these concentrations.

Soil E (pH = 7.5) was collected from an agricultural recultivation site of a former opencast brown coal mine. Replanting recultivation soils is an important approach to utilising soil resources and increasing cultivated land areas.[46,47] Recultivation soils are known to maintain a low total N content over several decades.[48] This lack of N retention capacity resulted in an unusual N_2O profile in the uninhibited soil, where the N_2O production rate rapidly increased within the first five days following fertilizer application, reaching a maximum of 2.33 ng g^{-1} soil h^{-1} at day 5, before declining again to practically zero at day 14, indicating a depleted N availability (Figure 4d). Since N_2O formation correlates with the nitrification rate, this behaviour indicates a very high N nitrification/denitrification activity of this soil, which quickly adapts to N fertilization. Treatment with DMP and MPT led to a dampening of the N_2O production spike, with MPT being more effective than DMP in the first five days. Beyond that timepoint, the rate of N_2O production in the presence of either inhibitor remained extremely low.

qPCR Measurements in Soils B - E

To assess the effect of MPT and DMP on the nitrifier community in soils B - E, a quantitative analysis of the DNA *amoA* bacterial and archaeal gene copies was carried out at day 22 of the incubation for untreated soils (H_2O added only), fertilizer-only treated soils ($(NH_4)_2SO_4$), and both MPT and DMP treated soils at an application rate of 5 mol% of applied fertilizer-N. Figure 5 shows that archaea were the more abundant microorganisms in these four soils, as revealed by the *amoA* gene copies for AOB, which ranged from 1.2 - 56 x 10^5 g^{-1} wet soil, whereas the AOA *amoA* gene abundance ranged from 1.1-35 x 10^7 g^{-1} wet soil (detailed data are provided in Table S10).

No significant change in the bacterial *amoA* population was found in the untreated or fertilized soils B-D ($P > 0.05$), respectively. On the other hand, the *amoA* gene copies in soil E

increased three-fold from 5.1 x 10^5 to 1.5 x 10^6 copies g^{-1} soil upon fertilizer treatment, clearly showing a correlation between the enhanced N_2O production at the beginning of the experiment (see Figure 4d) with bacterial growth. (Figure 5a). Treatment with fertilizer and either MPT or DMP did not lead to a significant change in the bacterial *amoA* population in soils B - D compared to the untreated or fertilized soils, respectively ($P < 0.0001$). However, when soil E was treated with fertilizer and DMP or MPT, respectively, the population dropped to the value of the unfertilized soil, suggesting that both NIs inhibit the growth of AOB.

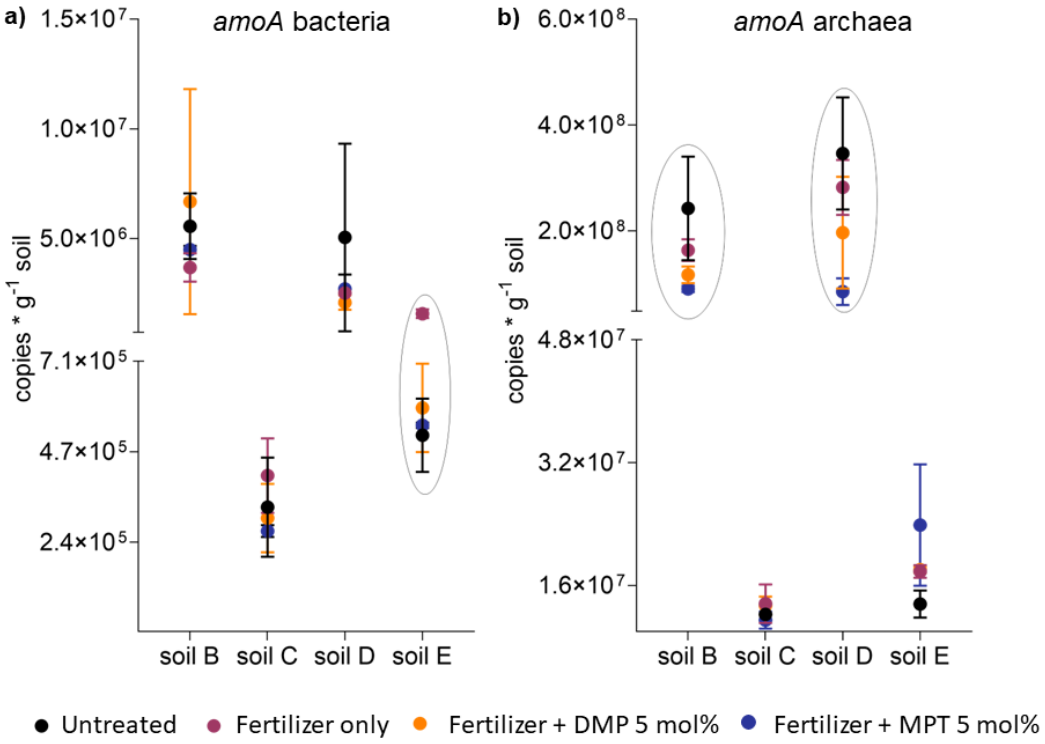

Figure 6. qPCR analysis of soils B - E. Bacterial (a) and archaeal (b) *amoA* gene copy numbers per g soil determined at day 22 of incubation in soils B (pH = 6.3), C (pH = 5.5), D (pH = 4.7) and E (pH = 7.5). 'Untreated' soil contained only deionized water as additive, 'fertilizer only' contained $(NH_4)_2SO_4$ at an application rate of 50 mg N kg^{-1} soil. The inhibitors MPT and DMP were applied at 5 mol% of applied fertilizer-N. Note the different axis scales to include the data with higher copy numbers. Each data point was calculated from three biological replicates (n = 3). Circled datasets indicate significant differences of *amoA* gene abundances ($P < 0.05$) between fertilized and inhibited fertilized soil.

The archaeal population showed a similar response to fertilization across all soils, as no increase of gene copies in fertilized compared to untreated soils was detected. On the other hand, a significant reduction of *amoA* gene copies was found in soils B and D after treatment with MPT compared to the respective untreated soils (P = 0.02). Thus, in soil B the average gene abundance dropped by 40% from 2.4 x 10^8 copies g^{-1} soil for the untreated soil to 9.1 x 10^7 copies g^{-1} soil for the MPT treated soil. In soil D the population dropped by 24% from an average of 3.5 x 10^8 copies g^{-1} soil to 8.4 x 10^7 g^{-1} soil. In contrast, no decrease of archaeal *amoA* gene copies by DMP was found in any of the soils, confirming the reported low efficacy of this inhibitor against archaeal strains. [49-51] From the finding that none of the three DMP treatments significantly reduced the N_2O emission in soil D, whereas MPT inhibited nitrification up to 100% for 21 days (Figure 4c), these data indicate an enhanced inhibitory effect of MPT on archaeal strains. It can therefore be concluded that the performance of MPT is not only independent of soil pH, but also independent of the AMO orthologue. Thus, the novel nitrification inhibitor MPT has the potential to address the triple challenge faced by agriculture, i.e., food security for a growing population, environmental protection, and climate change.

Supporting Information

Synthetic procedures for MPT and H-MPT, including spectroscopic data. Protocols of the bacterial assays and soil incubations (mineral-N transformations and N_2O measurements). Supplementary Table S1 (NH_4^+-dependent NO_2^- production after supplementing *N. europaea* and *N. multiformis* (OD_{600} = 0.03) with and MPT and H-MPT); Table S2 (NH_2OH-dependent NO_2^- production after supplementing *N. europaea* and *N. multiformis* with MPT); Table S3 (NO_2^- production after supplementing *N. europaea* and *N. multiformis* (OD_{600} = 0.03) with inhibitors NI-1-3); Table S4 (rate coefficients for the time-dependent O_2 consumption by *N. europaea* in the absence of MPT); Table S5 (rate coefficients for the inhibition of *N. europaea* by MPT at different concentrations, as determined by the O_2 consumption); Table S6 (specifications of the soils studied in this work); Table S7 (application rates of DMP and MPT and weight % of total $(NH_4)_2SO_4$ applied to soils B - E); Table S8 (soil incubation studies to determine mineral-N conversion in soil A); Table S9 (N_2O production rates for soils B-E); Table S10 (calculated gene abundances of *amoA* from bacteria and archaea). Supplementary Figure

S1 (O_2 consumption by *N. europaea* as a function of time before the addition of MPT); Figure S2 (pseudo-first order decay exponential fit of O_2 consumption by *N. europaea* as a function of time after the addition of MPT), Figure S3 (determination of the $IC_{50(abs)}$ value for MPT).

References

1. Lin, B.-L.; Sakoda, A.; Shibasaki, R; Suzuki, M. A Modelling Approach to Global Nitrate Leaching Caused by Anthropogenic Fertilisation. *Water Research* **2001**, *35*, 1961-1968. DOI: 10.1016/S0043-1354(00)00484-X

2. Godfray, H. C. J.; Beddington, J. R.; Crute, I. R.; Haddad, L.; Lawrence, D.; Muir, J. F.; Pretty, J.; Robinson, S.; Thomas, S. M.; Toulmin, C. Food Security: The Challenge of Feeding 9 Billion People. *Science* **2010**, *327*, 812-818. DOI: 10.1126/science.1185383

3. Raun, W. R.; Schepers, J. S. Nitrogen Management for Improved Use Efficiency. In: *Nitrogen in Agricultural Systems* (Schepers, J. S. R.; Raun, W. R., Eds.). **2008**, pp 675-693. DOI: 10.2134/agronmonogr49.c17

4. Cavigelli, M. A.; Del Grosso, S. J.; Liebig, M. A.; Snyder, C. S.; Fixen, P. E.; Venterea, R. T.; Leytem, A. B.; McLain, J. E.; Watts, D. B. US Agricultural Nitrous Oxide Emissions: Context, Status, and Trends. *Front. Ecol. Environ.* **2012**, *10*, 537-546. DOI: 10.1890/120054

5. Ladha, J. K.; Pathak, H.; J. Krupnik, T.; Six, J.; van Kessel, C. Efficiency of Fertilizer Nitrogen in Cereal Production: Retrospects and Prospects. In: *Adv. Agron.* Vol. 87; Academic Press, **2005**, pp 85-156. DOI 10.1016/S0065-2113(05)87003-8

6. Robertson, G. P.; Bruulsema, T. W.; Gehl, R. J.; Kanter, D.; Mauzerall, D. L.; Rotz, C. A.; Williams, C. O. Nitrogen–Climate Interactions in US Agriculture. *Biogeochemistry* **2013**, *114*, 41-70. DOI: 10.2307/24715091

7. Norton, J.; Ouyang, Y. Controls and Adaptive Management of Nitrification in Agricultural Soils. *Front. Microbiol.* **2019**, *10*, 1931. DOI: 10.3389/fmicb.2019.01931

8. Jetten, M. S. M. The Microbial Nitrogen Cycle. *Environ. Microbiol.* **2008**, *10*, 2903-2909. DOI: 10.1111/j.1462-2920.2008.01786.x

9. Coskun, D.; Britto, D. T.; Shi, W.; Kronzucker, H. J. Nitrogen Transformations in Modern Agriculture and the Role of Biological Nitrification Inhibition. *Nature Plants* **2017**, *3*, 17074. DOI: 10.1038/nplants.2017.74

10. Ruser, R.; Schulz, R. The Effect of Nitrification Inhibitors on the Nitrous Oxide (N_2O) Release from Agricultural Soils—a Review. *J. Plant Nutr. Soil Sci.* **2015**, *178*, 171-188. DOI: 10.1002/jpln.201400251

11. Lawton, T. J.; Ham, J.; Sun, T.; Rosenzweig, A. C. Structural Conservation of the B Subunit in the Ammonia Monooxygenase/Particulate Methane Monooxygenase Superfamily. *Proteins* **2014**, *82*, 2263-2267. DOI: 10.1002/prot.24535

12. McTavish, H.; Fuchs, J. A.; Hooper, A. B. Sequence of the Gene Coding for Ammonia Monooxygenase in *Nitrosomonas europaea*. *J. Bacteriol.* **1993**, *175*, 2436. DOI: 10.1128/jb.175.8.2436-2444.1993

13. Musiani, F.; Broll, V.; Evangelisti, E.; Ciurli, S. The Model Structure of the Copper-Dependent Ammonia Monooxygenase. *J. Biol. Inorg. Chem.* **2020**, *25*, 995-1007. DOI: 10.1007/s00775-020-01820-0

14. McCarty, G. W. Modes of Action of Nitrification Inhibitors. *Biol. Fertil. Soils* **1999**, *29*, 1-9. DOI: 10.1007/s003740050518

15. Hyman, M. R.; Sansome-Smith, A. W.; Shears, J. H.; Wood, P. M. A Kinetic Study of Benzene Oxidation to Phenol By Whole Cells of *Nitrosomonas europaea* and Evidence For The Further Oxidation of Phenol to Hydroquinone. *Arch. Microbiol.* **1985**, *143*, 302-306. DOI: 10.1007/BF00411254

16. Ensign, S. A.; Hyman, M. R.; Arp, D. J. *In vitro* Activation of Ammonia Monooxygenase from *Nitrosomonas europaea* by Copper. *J. Bacteriol.* **1993**, *175*, 1971-1980. DOI: 10.1128/jb.175.7.1971-1980.1993

17. Lieberman, R. L.; Rosenzweig, A. C. Crystal structure of a membrane-bound metalloenzyme that catalyses the biological oxidation of methane. *Nature* **2005**, *434*, 177-182. DOI: 10.1038/nature03311

18. Cao, L.; Caldararu, O.; Rosenzweig, A. C.; Ryde, U. Quantum Refinement Does Not Support Dinuclear Copper Sites in Crystal Structures of Particulate Methane Monooxygenase. *Angew. Chem. Int. Ed.* **2018**, *57*, 162-166. DOI: 10.1002/anie.201708977

19. Hyman, M. R.; Wood, P. M. Suicidal Inactivation and Labelling of Ammonia Monooxygenase by Acetylene. *Biochem. J.* **1985**, *227*, 719-725. DOI: 10.1042/bj2270719

20. McCarty, G. W.; Bremner, J. M. Inhibition of Nitrification in Soil by Heterocyclic Nitrogen Compounds. *Biol. Fertil. Soils* **1989**, *8*, 204-211. DOI: 10.1007/BF00266480

21. Wright, C. L.; Schatteman, A.; Crombie, A. T.; Murrell, J. C.; Lehtovirta-Morley, L. E.; Stams, A. J. M. Inhibition of Ammonia Monooxygenase from Ammonia-Oxidizing Archaea by Linear and Aromatic Alkynes. *Appl. Environ. Microbiol.* **2020**, *86*, e02388-02319. DOI: doi:10.1128/AEM.02388-19

22. Yildirim, S. C., Walker, R. M., Roessner, U. & Wille, U. Assessing the Efficacy, Acute Toxicity, and Binding Modes of the Agricultural Nitrification Inhibitors 3,4-Dimethyl-1H-pyrazole (DMP) and Dicyandiamide (DCD) with *Nitrosomonas europaea*. *ACS Agric. Sci. Technol.* **2023,** *3*, 222-231. DOI: 10.1021/acsagscitech.2c00303

23. Juliette, L. Y.; Hyman, M. R.; Arp, D. J. Inhibition of Ammonia Oxidation in *Nitrosomonas europae*a by Sulfur Compounds: Thioethers Are Oxidized to Sulfoxides by Ammonia Monooxygenase. *Appl. Environ. Microbiol.* **1993**, *59*, 3718-3727. DOI: 10.1128/aem.59.11.3718-3727.1993

24. Zerulla, W.; Barth, T.; Dressel, J.; Erhardt, K.; Horchler von Locquenghien, K.; Pasda, G.; Rädle, M.; Wissemeier, A. 3,4-Dimethylpyrazole Phosphate (DMPP) – A New Nitrification Inhibitor For Agriculture and Horticulture. *Biol. Fertil. Soils* **2001**, *34*, 79-84. DOI: 10.1007/s003740100380

25. Koci, J.; Nelson, P. N. Tropical Dairy Pasture Yield and Nitrogen Cycling: Effect of Urea Application Rate and A Nitrification Inhibitor, DMPP. *Crop Pasture Sci.* **2016**, *67*, 766-779. DOI: 10.1071/CP15400

26. Barrena, I.; Menéndez, S.; Correa-Galeote, D.; Vega-Mas, I.; Bedmar, E. J.; González-Murua, C.; Estavillo, J. M. Soil Water Content Modulates the Effect of the Nitrification Inhibitor 3,4-Dimethylpyrazole phosphate (DMPP) on Nitrifying and Denitrifying Bacteria. Geoderma **2017**, *303*, 1-8. DOI: 10.1016/j.geoderma.2017.04.022

27. Guardia, G.; Marsden, K. A.; Vallejo, A. Jones, D. L.; Chadwick, D. R. Determining the Influence of Environmental and Edaphic Factors on the Fate of the Nitrification Inhibitors DCD and DMPP in Soil. *Sci. Total Environ.* **2018**, *624*, 1202-1212. DOI: 10.1016/j.scitotenv.2017.12.250

28. Taggert, B. I.; Walker, C.; Chen, D.; Wille, U. Substituted 1, 2, 3-Triazoles: A New Class of Nitrification Inhibitors. Sci. Rep. **2021**, *11*, 1-12. DOI: 10.1038/s41598-021-94306-1

29. Yildirim, S. C.; Walker, R. M.; Roessner, U.; Wille, U. Rapid and Inexpensive Assay for Testing the Efficiency of Potential New Synthetic Nitrification Inhibitors. *ACS Agric. Sci. Technol.* **2023**, *3*, 260-269. DOI: 10.1021/acsagscitech.2c00229

30. Clark, P. R.; Williams, G. D.; Hayes, J. F.; Tomkinson, N. C. A Scalable Metal-, Azide-, and Halogen-Free Method for the Preparation of Triazoles. *Angew. Chem. Int. Ed.* **2020**, *59*, 6740-6744. DOI: 10.1002/anie.201915944

31. Li, Z.; Reichel, R.; Brüggemann, N. Effect of C:N:P stoichiometry on soil nitrous oxide emission and nitrogen retention. *J. Soil Sci. Plant Nutr.* **2021**, *184*, 520-529. DOI: 10.1002/jpln.202000416

32. Reichel, R.; Wei, J.; Islam, M. S.; Schmid, C.; Wissel, H.; Schröder, P.; Schloter, M.; Brüggemann, N. Potential of Wheat Straw, Spruce Sawdust, and Lignin as High Organic Carbon Soil Amendments to Improve Agricultural Nitrogen Retention Capacity: An Incubation Study. *Front. Plant Sci.* **2018**, *9*. DOI: 10.3389/fpls.2018.00900

33. Christopher, A. F.; Kathryn, J. R.; Beman, J. M.; Alyson, E. S.; Brian, B. O. Ubiquity and Diversity of Ammonia-Oxidizing Archaea in Water Columns and Sediments of the Ocean. *Proc. Natl. Acad. Sci.* **2005**, *102*, 14683-14688. DOI: 10.1073/pnas.0506625102

34. Rotthauwe, J. H.; Witzel; K. P.; Liesack, W. The Ammonia Monooxygenase Structural Gene *amoA* as a Functional Marker: Molecular Fine-Scale Analysis of Natural Ammonia-Oxidizing Populations. *Appl. Environ. Microbio.* **1997**, *63*, 4704-4712. DOI: 10.1128/aem.63.12.4704-4712.1997

35. O'Sullivan, C. A.; Duncan, E. G.; Whisson, K.; Treble, K.; Ward, P. R.; Roper, M. M. A Colourimetric Microplate Assay for Simple, High Throughput Assessment of Synthetic and Biological Nitrification Inhibitors. *Plant Soil* **2017**, *413*, 275-287. DOI: 10.1007/s11104-016-3100-1

36. Arp, D. J.; Sayavedra-Soto, L. A.; Hommes, N. G. Molecular Biology and Biochemistry of Ammonia Oxidation by *Nitrosomonas europaea*. *Arch. Microbiol.* **2002**, *178*, 250-255. DOI: 10.1007/s00203-002-0452-0

37. Schatteman, A., Wright, C. L., Crombie, A. T., Murrell, J. C. & Lehtovirta-Morley, L. E. Hydrazines as Substrates and Inhibitors of the Archaeal Ammonia Oxidation Pathway. *Appl. Environ. Microbiol.* **2022**, *88*, e02470-02421. DOI: 10.1128/aem.02470-21

38. Lontoh, S.; DiSpirito, A. A.; Krema, C. L.; Whittaker, M. R.; Hooper, A. B.; Semrau, J. D. Differential Inhibition In Vivo of Ammonia Monooxygenase, Soluble Methane

Monooxygenase and Membrane-Associated Methane Monooxygenase by Phenylacetylene. *Environ. Microbiol.* **2000**, *2*, 485-494. DOI: 10.1046/j.1462-2920.2000.00130.x

39. Hyman, M. R. & Arp, D. J. $^{14}C_2H_2$- and $^{14}CO_2$-Labeling Studies of the *De Novo* Synthesis of Polypeptides by *Nitrosomonas europaea* During Recovery from Acetylene and Light Inactivation of Ammonia Monooxygenase. *J. Biol. Chem.* **1992**, *267*, 1534-1545. DOI: doi.org/10.1016/S0021-9258(18)45979-0

40. Delaune, K. P. & Alsayouri, K. *Physiology, Noncompetitive Inhibitor*. In: *StatPearls Publishing [internet]*. StatPearls Publishing 2022. (accessed 2022-10-04).

41. Nauer, P. A.; Fest, B. J.; Visser, L.; Arndt, S. K. On-farm Trial on the Effectiveness of the Nitrification Inhibitor DMPP Indicates No Benefits Under Commercial Australian Farming Practices. *Agric. Ecosyst. Environ.* **2018**, *253*, 82-89. DOI: 10.1016/j.agee.2017.10.022

42. Dougherty, W. J.; Collins, D.; Van Zwieten, L.; Rowlings, D. W. Nitrification (DMPP) and Urease (NBPT) Inhibitors Had No Effect on Pasture Yield, Nitrous Oxide Emissions, or Nitrate Leaching under Irrigation in a Hot-Dry Climate. *Soil Res.* **2016**, *54*, 675-683. DOI: 10.1071/SR15330

43. Shi, X., Hu, H., He, J., Chen, D. & Suter, H. C. Effects of 3,4-Dimethylpyrazole Phosphate (DMPP) on Nitrification and the Abundance and Community Composition of Soil Ammonia Oxidizers in Three Land Uses. *Biol. Fertil. Soils* **2016**, *52*, 927-939. DOI: 10.1007/s00374-016-1131-7

44. Guzman-Bustamante, I.; Schulz, R., Müller, T.; Ruser, R. Split N Application and DMP Based Nitrification Inhibitors Mitigate N_2O Losses in a Soil Cropped With Winter Wheat. *Nutr. Cycling Agroecosyst.* **2022**, *123*, 119-135. DOI: 10.1007/s10705-022-10211-7

45. Kowalchuk, G. A.; Stephen, J. R. Ammonia-Oxidizing Bacteria: A Model for Molecular Microbial Ecology. *Ann. Rev. Microb.* **2001**, *55*, 485-529. DOI: 10.1146/annurev.micro.55.1.485

46. Roy, J.; Reichel, R.; Brüggemann, N.; Hempel, S.; Rillig, M. C. Succession of Arbuscular Mycorrhizal Fungi Along a 52-Year Agricultural Recultivation Chronosequence. *FEMS Microbiol.Ecol.* **2017**, *93*, fix102. DOI: 10.1093/femsec/fix102

47. Nii-Annang, S.; Grünewald, H.; Freese, D.; Hüttl, R. F.; Dilly, O. Microbial Activity, Organic C Accumulation and ^{13}C Abundance in Soils Under Alley Cropping Systems After 9 Years of Recultivation of Quaternary Deposits. *Biol. Fertil. Soils* **2009**, *45*, 531-538. DOI: 10.1007/s00374-009-0360-4

48. Zhao, Y.; Reichel, R.; Herbst, M.; Sun, Y.; Brüggemann, N.; Mörchen, R.; Welp, G.; Meng, F.; Bol, R. Declining Total Carbon Stocks in Carbonate-Containing Agricultural Soils Over a 62-Year Recultivation Chronosequence Under Humid Conditions. *Geoderma* **2022**, *425*, 116060. DOI: 10.1016/j.geoderma.2022.116060

49. Chen, Q.; Qi, L.; Bi, Q.; Dai, P.; Sun, D.; Sun, C.; Liu, W.; Lu, L.; Ni, W.; Lin, X. Comparative Effects of 3,4-Dimethylpyrazole Phosphate (DMPP) and Dicyandiamide (DCD) on Ammonia-Oxidizing Bacteria and Archaea in a Vegetable Soil. *Appl. Microbiol. Biotechnol.* **2015**, *99*, 477-487. DOI: 10.1007/s00253-014-6026-7

50. Bachtsevani, E.; Papazlatani, C. V.; Rousidou, C.; Lampronikou, E.; Menkissoglu-Spiroudi, U.; Nicol, G. W.; Karpouzas, D. G.; Papadopoulou, E. S. Effects of the Nitrification inhibitor 3,4-Dimethylpyrazole phosphate (DMPP) on the Activity and Diversity of the Soil Microbial Community Under Contrasting Soil pH. *Biol. Fertil. Soils* **2021**, *57*, 1117-1135. DOI: 10.1007/s00374-021-01602-z

51. Castellano-Hinojosa, A., González-López, J., Vallejo, A. & Bedmar, E. J. Effect of Urease and Nitrification Inhibitors on Ammonia Volatilization and Abundance of N-Cycling Genes in an Agricultural Soil. *J. Plant Nutr. Soil Sci.* **2020**, *183*, 99-109. DOI: 10.1002/jpln.201900038

5.3 The impact of MPT on the Activity of the Particulate Methane Monooxygenase (pMMO)

5.3.1 Introduction

As outlined in Chapter 1.4, the enzymes pMMO and the AMO are evolutionary related, which is reflected in **Figure 4**, that demonstrates the ability of the AMO oxidising the substrate of the pMMO (CH_4). [29, 51, 108] Likewise, it has been shown that the pMMO oxidises NH_3, the substrate of the AMO. [29, 51, 108] Unsurprisingly, alkynyl groups containing compounds, such as C_2H_2 and phenylacetylene, have also shown to have an effect on pMMO.[108] Methanotrophic organisms play a crucial role in the carbon (C) cycle by scavenging the GHG CH_4 . Therefore, the evaluation of a potential inhibitory effect of MPT on methanotrophic organisms was of great interest. The CH_4 uptake rate was collected and calculated from soil B, soil C, soil D and soil E in the same experimental setup from Chapter 5.2. (soil specifications can be found in SI-4 Table 6).

5.3.2 Material and Methods

5.3.2.1 **CH_4 Gas Measurements**

CH_4 gas measurements were performed simultaneously to the N_2O GHG studies from soil B-D (soil specifications can be found in SI-4 Table 6). At the day of the measurement (day 1, 3, 5, 7, 14 and 21 after fertilisation) the vials were closed gas-tight with a rubber septum and aluminum lid and opened after each measurement. The N_2O concentrations were analysed using a GC-ECD/FID (Electron Capture Detector/Flame Ionization Detector) (Claurus 580, Perkin Elmer) in intervals of 1, 5.05, 9.1 and 13 h, as described previously.[109] A linear regression slope was used to calculate CH_4-C production rates, F, according to eqn. 1,

$$F = \frac{\frac{\Delta C}{\Delta t} V T_0 M}{m T_a V_m}$$

where ΔC/Δt represents the change of the CH_4 concentration over the time intervall t in ppbv, V represents the headspace volume in L, M represents the molar mass of C in CH_4, m represents the amount of soil in g dry weight, V_m represents the molar volume of ideal gases (22.414 L mol^{-1}) at 0 °C and 101.325 kPa, corrected for the gas sampler using T_0 (273.15 K) and T_a (air temperature in K). Detailed CH_4 production rates are given in the Appendix (Table A-1).

5.3.2.2 **qPCR studies *pMMO* gene**

Soil samples (400 mg) from the CH_4/N_2O experiment after the 21-day incubation period were used to extract DNA using a NucleoSpin Soil DNA extraction kit (Macherey Nagel, Germany) according to the manufacturer's instruction. For extraction, SL1 buffer and enhancer were chosen for extraction, and DNA was finally eluted in 40 µL PCR-grade water. Real-time quantitative PCR (qPCR) of *pMMO* genes was performed for the bacterial community for each treatment with three biological and three technical replicates. The primer system 187f/650r were used. [110, 111] The DNA extracts were diluted 10-fold and the DNA amplification was monitored on a Bio-Rad CFX1000 real-time PCR machine. The quantification was performed in a total volume of 10 µL using 5.0 µL SYBR® Green Master Mix (BioRad, USA), 0.4 µL of the forward and reverse primer, respectively; 3.2 µL PCR-H_2O and 1 µL of the ten-fold diluted DNA. The fragments of bacterial *pMMO* genes were amplified using were amplified using an an initial denaturation phase (2 min), followed by 44 cycles (i) at 95 °C (10s), (ii) annealing at 59 °C (45 s), and (iii) elongation for by 45 s at 65.0 °C. Standard curves were generated using serial dilutions ranging from 10^8 to 10^3 gene copies per reaction, provided as linearized plasmids that contained cloned *pMMO* genes of bacteria ($R^2 > 0.8$). The correct PCR product length was verifed by obtaining a melting curve in the temperature range 65 – 95°C.

5.3.2.3 **Statistics**

Statistical analysis was performed with three biological replicates. Statistical analysis of the measured GC gas concentrations was performed on the calculated CH_4 production rates via two-way analysis of variance (ANOVA), assessing the factors day and treatment at each time point evaluated using the Tukey HSD post-hoc test with a significance level of $P < 0.05$. All results are reported as mean values ± standard error of the mean.

5.3.3 Results and Discussion

Amongst all tested soils, soil C showed the highest activity in methanotrophic organisms and a clear signal of methane uptake ($R^2 > 0.9$), whereas soil B, D and E did not correlate in a linear decrease of CH_4 uptake over the course of the experiment and will therefore not be included in the following discussion.

Throughout the experiment the untreated (H_2O only) soil C showed a CH_4 uptake rate with an average of 1.2 µg g^{-1} soil h^{-1}, whereas fertilised soils showed a reduced uptake rate by 50% (**Figure 16**). This is not unexpected, as NH_3 is an alternative substrate of pMMO and acts therefore as an competitive inhibitor of CH_4. [60] When comparing the uninhibited with inhibited soil treated with MPT and DMP, a significant difference (P = 0.02) was only observed from day five onwards for the highest application rate of MPT, which inhibited the uptake by 40%. All other remaining treatments showed a reduced, however, not statistically significant ($P > 0.05$) reduction of CH_4 uptake. At the highest application rate of DMP a significantly reduced CH_4-C uptake rate after 14 days onwards was found (P = 0.004). Previously, it has been reported that DMP has the reverse effect by increasing CH_4 uptake, however this was not observed in this experiment.[102, 112] As NH_3 is already a "(competitive) inhibitor" of CH_4, the effect of inhibitors was expected to add up to the NH_3 effect. Interestingly, the addition of SNI was not to the same extend as observed for N_2O (Chapter 5.2, **Figure 4**). Although it was observed that DMP at the highest concentration showed a significant inhibition at a later time point (day 17) than MPT, it can be concluded that both NI inhibit the CH_4 uptake to some extent. It is believed that the inhibition could correlate with the dependence of the N and C cycle (Chapter 1.2), especially in case of MPT, which effectively reduced the N_2O production rate up to 100% for the whole duration of the experiment. By inhibiting the nitrification, NH_3 is retained in soil; and consequently, the CH_4 uptake could have been impacted by the high NH_3 availability. The time dependent ascending inhibitory effect could be an indication for a secondary inhibitory effect rather than a primary irreversible inhibition like observed in the N_2O studies (Chapter 5.2, **Figure 4**). It can be concluded that DMP and MPT inhibited pMMO and thus CH_4 uptake not to the same extent as the AMO, given that the inhibition was time dependent and only observed at the higher concentrations of the inhibitor treatments.

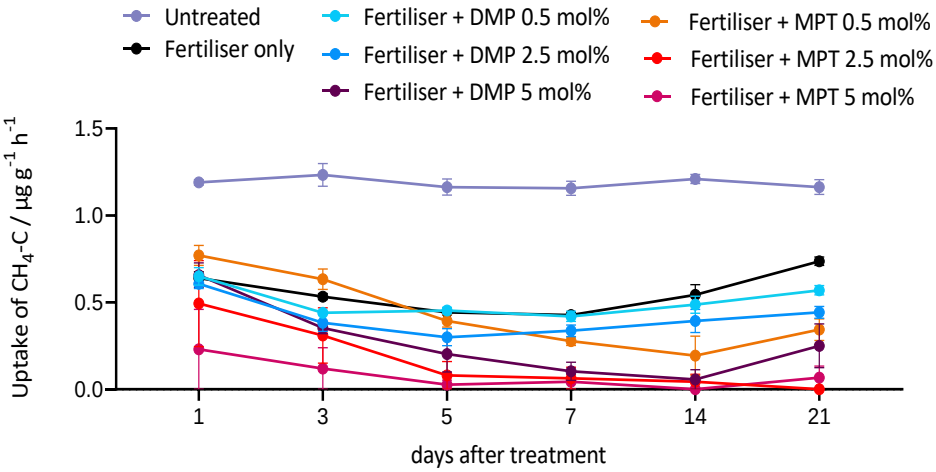

Figure 16: Calculated CH_4 uptake rates in µg g^{-1} soil h^{-1} for the days 1, 3, 5, 7, 14 and 21 of soil C (pH = 5.5) as this was the soil with the highest CH_4 uptake dynamics for soil D (specifications can be found in SI-4 Table 6). The 'untreated' soil contains only water as an 'additive'. The fertiliser treatment contained N fertiliser ($(NH_4)_2SO_4$ at an application rate of 50 mg kg^{-1} soil). Inhibitor treatments were applied at three concentrations (0.5 mol%, 2.5 mol% and 5 mol% of applied N), respectively, in addition to the fertiliser. Experimental details can be found in 'Material and Methods' in section 4. Each data bar was calculated from three biological replicates.

Similar to the *amoA* qPCR in the manuscript in Chapter 5.2, a quantitative real-time PCR with soil C was performed to determine the abundancies of the *bacterial* pMMO gene with the highest concentration of 5 mol% for DMP and MPT, which were compared with the copy numbers with untreated and uninhibited soils. As the SNI effect comes "on top" of the NH_3 inhibition, significant changes ($P < 0.05$) of the fertilised treatment were compared with the fertilised and inhibited treatments ranging an average copy number of *pMMO* genes of 6.3×10^5 - 9.2×10^5. Although the methane uptake was inhibited, the growth rate of methanotrophic was not impacted.

Table 2. Bacterial *pMMO* gene copies of the 'untreated', 'fertilised', and 'fertilised + DMP/MPT treated' soil of soil C (pH = 5.5).[a]

	Untreated	**Fertiliser only**	**DMP**	**MPT**
pMMO gene copy g^{-1} soil	$9.2 \times 10^5 \pm 5.5 \times 10^4$	$7.6 \times 10^5 \pm 4.0 \times 10^4$	$6.3 \times 10^5 \pm 4.4 \times 10^4$	$8.4 \times 10^5 \pm 9.4 \times 10^4$

[a] Detailed soil specifications are listed in SI-4 Table 6. 'Untreated' soil contained only deionized water as an 'additive'. The fertiliser treatment contained N fertiliser ($(NH_4)_2SO_4$ at an application rate of 50 mg kg^{-1} soil. Inhibitor treatments were performed for the highest application rate of 5 mol% of applied N in addition to the fertiliser to determine maximum effect. Data was obtained on day 22 of incubation. Experimental details can be found in Chapter 5.3.2. Each data bar was calculated from three technical and three biological replicates.

Although the pMMO production was inhibited, a significantly reduced copy number of methanotrophic organism was not observed. Consequently, both inhibitors seem not to inhibit methanotrophic growth, but impact their activity. As methanotrophic organisms are scavengers of atmospheric CH_4, their reduced growth could potentially have an impact on methane emissions from agricultural fields.

5.3.4 Conclusion

This sub-chapter summarised the discovery and development of the irreversible SNI MPT. Due to the evolutionary similarity of AMO and pMMO, the effect of MPT on the latter was determined via GHG studies, where it was shown that the pMMO was not inhibited to the same extent as the AMO. Thus, it appears that the pMMO inhibition is a secondary effect of AMO inhibition. The qPCR studies showed an initial effect on the nitrifier community with up to 40% reduced cell numbers of *amoA* bacteria and archaea; however, no reduced cell numbers for pMMO-containing bacteria were observed. In an agricultural field, the natural balance of soil organisms is disturbed over a prolonged time.[113] Therefore, the long-time effects of MPT on the soil population will need to be determined by soil microbiologists to understand long-term effects of MPT on the soil population.

Chapter 6: Conclusion and outlook

This doctoral thesis provided crucial scientific results to develop, test and design new SNIs. In Chapter 2, a rapid, inexpensive, and accessible assay was developed that requires minimal microbiological skills and resources to grow, harvest and assay AOB against potential new SNI. This assay enabled efficient SAR studies of SNIs and identification of the most potent structures. In total, 20 4,5-disubstituted 1,2,3-triazoles were tested with the assay, and four compounds showed promising inhibitory results. In fact, a 4-nitrile substituted 1,2,3-triazole showed quantitatively reduced nitrification. The five compounds will be fed into the pipeline of agronomy testings to determine performance in soil, plant yield, ecotoxicology and formulation.

In-depth studies with AOB were performed to determine the biochemical parameters of the commercial SNIs DMP and DCD for the first time. Not only did this provide information about the current status of currently available SNIs, but it also provided a fundamental knowledge of the 'gold standard' compounds. This information can be taken as a guideline to improve the performance of future SNI. In summary, DMP and DCD have been demonstrated to be selective inhibitors of AMO and have minimal impact on HAO activity. Their inhibition mode is uncompetitive, requiring substrate binding for the inhibitor binding. Both inhibitors have been shown to bind reversibly, as their binding was reverted when washing cells repeatedly with NaPB. In addition, the bacterial viability stain showed that DCD showed higher toxicity at increased concentrations.

1,4-Disubstituted 1,2,3-triazoles are a new class of NI reported by *Taggert* et al. Although soil incubation studies showed promising results and excellent nitrification inhibitory properties, their biochemical parameters have not been determined yet. Therefore, five 1,4-disubstituted 1,2,3-triazoles with varying functional groups in position 1 were tested similarly to DMP and DCD to determine their inhibitory efficacy with AOB. It was found that including functional groups was detrimental, and for 1,4-dialkyl substituted 1,2,3-triazoles, the inhibitory effect was proportional to the increased lipophilicity. In-depth studies with AOB

revealed that these 1,4-disubstituted 1,2,3-triazoles act as non-competitive, reversible inhibitors, which indicates that their binding site differs from DMP and DCD. Due to two adjacent N in the structure, chelating properties could not be excluded as the AMO contains various metal sites. The lipophilicity could have potentially facilitated access to the membrane-embedded metal site.

Considering the information above, a new binding mode for SNI was explored. Irreversible inhibitors are not well-studied as the only known compounds are highly-flammable (C_2H_2) or irritating and toxic (phenylacetylene). Therefore, including an alkynyl group in a heteroaromatic framework was explored. MPT was synthesised via a reported route that did not require the conventional azide, metal and halogens to form the 1,2,3-triazole scaffold. It is an easy, accessible, and economically beneficial synthesis route than the synthesis of DMP (see Chapter 2). MPT has shown the ability to inhibit AMO irreversibly. Including the alkynyl group does not automatically result in an irreversible inhibitor, as the derivative 1-(but-3-yn-1-yl)-4-propyl-1*H*-1,2,3-triazole showed no inhibitory properties. MPT has shown excellent nitrification inhibitory properties, pH independence and high stability tested in four German and one Australian soil. NH_4^+ was retained quantitively over 21 days in Australian acidic soil. The mineral-N experiment with DMP and MPT clearly showed that the SNI failed to perform in acidic soils, clearly showing the advantage of MPT. Moreover, measured N_2O production rate showed that MPT at a ten-time lower concentration than DMP had a lower N_2O production rate. Compared to fertilised-only soil, MPT-treated soil showed up to 100% suppression of N_2O production over the entire experiment (21 days).

Future work includes agronomy testing, ecotoxicology (long-term and short-term) and upscaling of the MPT production. The agronomy tests will include greenhouse studies with plants to determine root and shoot length, crop yield, grain number and rhizosphere screening. Moreover, the optimal fertiliser to MPT ratio will be determined in field experiments. MPT inhibits NH_3 uptake for at least 21 days (Chapter 5.2.4), which might result in a considerable reduction of fertiliser when applied with MPT. Moreover, chemical engineers will work on MPT + Urea coatings to design slow-release systems to ensure extended inhibitor release. Degradation studies on MPT will be performed to determine stability upon UV and extreme temperature exposure. Most importantly, to commercialise MPT, ecotoxicology studies will be outsourced by specialised (good lab practice) GLP

laboratories that certify the compatibility of MPT in terrestrial and aquatic systems. Once all these factors have been determined and have provided positive results, MPT will be commercialised and help to tackle the challenge of food production and environmental pollution in agriculture.

Chapter 7: Experimental section

Chemicals

All aldehydes, benzothiazole (C_7H_5NS), α-bromoethyl acetate ($C_4H_7BrO_2$), ammonium molybdate ($Mo_7O_{24}N_6H_{24}$), hydrogen peroxide solution 30 w/w% (H_2O_2), sodium azide (NaN_3), *L*-proline ($C_5H_9NO_2$) dimethyl sulfoxide (DMSO, $(CH_3)_2SO$), sodium sulfate (Na_2SO_4), petroleum spirits (boiling range 40 ─60°C) and deuterated chloroform (chloroform-*d*, $CDCl_3$) was purchased from Sigma Aldrich. Dichloromethane (CH_2Cl_2), ammonium acetate ($C_2H_7NO_2$), triethylamine $(C_2H_5)_3N$, ethyl acetate ($C_3H_8CO_2$), and methanol (CH_4O) was obtained from ChemSupply Australia. 1-dimethoxypropan-2-one ($C_5H_{10}O_3$), propargyl amine (C_3H_5N), propyl amine (C_3H_9N) was obtained from AKSci.

General methods

Chromatography

Preparative silica gel flash chromatography was performed using Davisil Chromatographic Silica Media LC60A 40-63 micron. The eluents were ethyl acetate (technical), cyclohexane (technical), dichloromethane (technical) and methanol (99%). Unless otherwise stated, reactions were monitored using thin layer chromatography (TLC) on commercial silica gel 60 aluminium-backed plates coated with fluorescent indicator F254, purchased from Merck. Plates were visualised using UV light (254 nm) alone or in conjunction with ninhydrin, potassium permanganate or phosphomolybdic acid stains.

NMR

NMR spectra were recorded on a Varian INOVA or Agilent instrument, with operating frequencies of 400 MHz and 500 MHz for ^{1}H NMR, and 101 MHz and 126 MHz, respectively, for ^{13}C NMR. Chemical shifts (δ) are expressed in ppm, with residual solvent peaks used as an internal reference ($CDCl_3$ ^{1}H NMR = 7.26 ppm, ^{13}C NMR = 77.16 ppm; $(CD_3)_2SO$ ^{1}H NMR = 2.50 ppm, ^{13}C NMR = 39.52 ppm). The following letters assign NMR peak multiplicities: s = singlet, d = doublet, t = triplet, p = pentet, h = hextet, m = multiplet, dd = doublet of doublets, ddd = doublet of doublet of doublets.

HRMS

High resolution mass spectra (HRMS) were collected via electrospray ionisation (ESI) mass spectrometry, using either a Thermo Scientific Exactive Plus Orbitrap mass spectrometer or a Thermo hybrid LTQ-FTICR mass spectrometer (Thermo, Bremen, Germany) as indicated. Unless otherwise indicated, all MS spectra were acquired in the Positive Ion Mode.

7.1 General Experimental Procedures

7.1.1 General Procedure 1 for the One-Pot Multicomponent Synthesis of 4,5-Disubstituted-1,2,3-Triazoles[100] (GP1)

A solution of the synthesized Julia reagent precursor **21** (1.43 g, 5 mmol.), the respective aldehyde **22** (5.5 mmol), sodium azide (0.48 g, 7.5 mmol) and ammonium acetate (0.5 mmol, 0.041 g) in methanol (10 mL, containing 5w/w% water) was stirred at 32 °C until consumption of the Julia reagent **21** was observed via HRMS (at least 4 hours). The reaction mixture was concentrated in *vacuo*. The crude oil was dissolved in ethyl acetate (50 mL), washed with water (3x 50 mL), dried over sodium sulphate, filtered, and concentrated under vacuum Purification by flash column chromatography (SiO_2, ethyl acetate/petroleum spirits 2:1) and recrystallisation from hot heptane/ethyl acetate gave the 4,5-disubstituted 1,2,3-triazole as crystalline material.

7.1.2 General Procedure 2 for the One-Pot Multicomponent Synthesis of 4,5-disubstituted-1,2,3-triazoles with *L*-proline[114] (GP2)

To a solution of ethyl bromoacetate **19** (200 mg, 1.2 mmol) in DMSO (5 mL) was added dimethyl sulfide (112 mg, 1.8 mmol), and the mixture was stirred for 5 h at room temperature. The respective aldehyde **22** (1.8 mmol), sodium azide (117 mg, 1.8 mmol) and

L-proline (14 mg, 0.12 mmol) was added. The mixture was stirred at room temperature overnight. After complete conversion the starting material **19** was observed in the HRMS, the mixture was poured into ice water (10 mL) and extracted with ethyl acetate (3x 20 mL). The combined organic layers were dried over sodium sulfate and concentrated *in vacuo*.
Purification by flash column chromatography (SiO_2, ethyl acetate/petroleum spirits 2:1) and recrystallisation from hot heptane/ethyl acetate gave the 4,5-disubstituted 1,2,3-triazole as crystalline material.

7.1.3 General Procedure 3 for the Metal-Azide-, and Halogen-Free Microwave Reaction of the Synthesis of 1,4-disubstituted-1,2,3-triazoles [114] (GP3)

1-Dimethoxypropan-2-one (**50,** 0.25 mL, 2.20 mmol) in methanol (5 mL) and 4-methylbenzenesulfonohydrazide (**51**, 388 mg, 2.08 mmol) were stirred for 10 min in a 10 mL microwave tube (Biotage®, Sweden). After complete consumption of the starting material was observed via HRMS, a primary amine (2.29 mmol) and triethylamine (0.15 mL, 2.30 mmol) were added, and the tube sealed. After 20 minutes at 120 °C and cooling to room temperature, the reaction mixture was concentrated *in vacuo* to afford an orange oil. The crude oil was extracted in a DCM and water (1:1) mixture (20 mL), and the aqueous layer was extracted additional three times with DCM. The combined organic fractions were washed with brine, dried over Na_2SO_4, concentrated *in vacuo* and purified via flash column chromatography (ethyl acetate: petroleum spirits (1:1)) to yield the desired 1,4-disubstituted 1,2,3-triazole.

7.2 Synthesised Molecules

Ethyl 2-(benzothiazol-2-ylsulfonyl) acetate (21) [101]

Ethyl bromoacetate (**19**) (2.76 mL, 25 mmol) and triethyl amine (9.7 mL) were added to a solution of 2-mercaptobenzothiazole (**18**) (3.34 mg, 20 mmol) in dichloromethane (70 mL). The reaction mixture was stirred for 14 h at room temperature under an inert atmosphere. The solvent was evaporated *in vacuo* and diethyl ethyl ether (50 mL) and water (50mL) was added. The aqueous layer was extracted two times with diethyl ethyl ether (50 mL) and dried over sodium sulphate. The ether was removed *in vacuo* to give ethyl 2-(benzothiazole2-ylthio) acetate **20** as yellow oil (quantitative yield), which was directly used in the next step upon crystallisation. Ammonium molybdate (1.05 g, 0.84 mmol) and aqueous hydrogen peroxide 30% (6.45 mL, 0.66 mmol.) were added to **20** in ethanol (25 mL) at 0 ^{o}C. The reaction mixture was stirred for 48h at room temperature and concentrated under vacuum. The crude reaction oil was dissolved in ethyl acetate (50 mL) and washed with water (2x 50 mL) and brine (2x 50 mL), dried over anhydrous sodium sulfate and concentrated *in vacuo*. Upon addition of chloroform the ethyl 2-(benzothiazol-2-ylsulfonyl) acetate (**21**) slowly crushed out as colourless needles (2.96 g, 52%). ^{1}H NMR (400 MHz, $CDCl_3$) δ 8.26 – 8.19 (m, 1H, *aromatic–H*), 8.06 – 7.98 (m, 1H, *aromatic–H*), 7.69 – 7.56 (m, 2H, *aromatic–H*), 4.56 (s, 2H, *S–CH$_2$*), 4.17 (q, *J* = 7.1 Hz, 2H, *O–CH$_2$*), 1.17 (t, *J* = 7.1 Hz, 3H, *CH$_3$*).^{13}C NMR (101 MHz, $CDCl_3$) δ 164.9 (carbonyl-C), 161.6 (aromatic-C), 152.4 (*aromatic-C*), 136.9 (*aromatic-C*), 128.2 (*aromatic-C*), 127.7 (*aromatic-C*), 125.5 (*aromatic-C*), 122.3 (*aromatic-C*), 62.7 (*aliphatic-C*), 58.7 (*aliphatic-C*), 13.7 (*aliphatic-C*). ESI-HRMS calc. for $C_{11}H_{12}NO_4S_2$ $[M+H]^+$: 286.0201; found 286.0203.

Ethyl 5-ethyl-2*H*-1,2,3-triazole-4-carboxylate (25)

Ethyl-5-ethyl-2*H*-1,2,3-triazole-4-carboxylate (**25**) was synthesised following GP1. Colourless crystals, yield: 540 mg, 63%. ^{1}H NMR (500 MHz, $CDCl_3$) δ 4.44 (q, *J* = 7.2 Hz, 2H, *aliphatic–H*), 3.07 (q, *J* = 7.6 Hz, 2H, *aliphatic–H*), 1.40 (td, *J* = 7.1, 0.8 Hz, 3H, *aliphatic–H*), 1.33 (t, *J* = 7.6 Hz, 3H, *aliphatic–H*). ^{13}C NMR (126 MHz, $CDCl_3$) δ 161.5 (*carbonyl-C)*, 148.6 (*aromatic-C)*, 134.6 (*aromatic-C)*, 61.3 (*aliphatic–C)*, 18.2 (*aliphatic–C)*, 14.2 (*aliphatic–C)*, 13.0 (*aliphatic–C)*. ESI-HRMS calc. for $C_7H_{12}N_2O_3$ $[M+H]^+$: 170.0925; found 170.0925.

Ethyl 5-isopropyl-2*H*-1,2,3-triazole-4-carboxylate (26)

Ethyl 5-isopropyl-2*H*-1,2,3-triazole-4-carboxylate (**26**) was synthesised following GP1. Colourless crystals, yield: 600 mg, 66%. Identity of the product was confirmed by comparison with literature NMR spectra.[100] ^{1}H NMR (400 MHz, $CDCl_3$) δ 4.44 (q, *J* = 7.2 Hz, 2H, *aliphatic–H*), 3.67 (p, *J* = 7.0 Hz, 1H, *aliphatic–H*), 1.41 (dd, *J* = 7.7, 6.7 Hz, 3H, *aliphatic–H*), 1.36 (dd, *J* = 7.0, 1.0 Hz, 6H, *aliphatic–H*). ^{13}C NMR (126 MHz, $CDCl_3$) δ 161.6 (*carbonyl–C*), 152.5 (broad, aromatic *C*), 134.1 (broad, *aromatic–C*), 61.1 (*C*H_2–CH_3), 24.8 (*aliphatic–C*), 21.6 (*aliphatic–C*), 14.1 (*aliphatic–C*). ESI-HRMS calc. for $C_8H_{14}N_3O_2$ $[M+H]^+$: 184.1081; found 184.1081.

Ethyl 5-propyl-2*H*-1,2,3-triazole-4-carboxylate (27)

Ethyl 5-propyl-2H-1,2,3-triazole-4-carboxylate (**27**) was synthesised following GP1 with 2 mmol limiting reagent (ethyl bromoacetate **19**) and adjusted equivalents of reactants. Colourless crystals, yield: 227 mg, 62%. ^{1}H NMR (400 MHz, $CDCl_3$) δ 4.40 (q, *J* = 7.1 Hz, 2H, *aliphatic–H*), 3.01 (t, *J* = 7.7 Hz, 2H, *aliphatic–H*), 1.72 (h, *J* = 7.4 Hz, 2H, *aliphatic–H*), 1.35 (t, *J* = 7.1 Hz, 3H, *aliphatic–H*), 0.93 (t, *J* = 7.4 Hz, 3H, CH_3). ^{13}C NMR (101 MHz, $CDCl_3$) δ 161.6 (*carbonyl-C*), 146.2 (*aromatic-C, broad peak*), 135.1 (*aromatic-C*), 61.2 (*aliphatic-C*), 26.0 (*aliphatic-C*), 22.1 (*aliphatic-C*), 14.1 (*aliphatic-C*), 13.6 (*aliphatic-C*). HRMS calc. for $C_8H_{14}N_3O_2$ $[M+H]^+$: 184.1081; found 184.1080.

Ethyl 5-cyclohexyl-2*H*-1,2,3-triazole-4-carboxylate (28)

Ethyl 5-cyclohexyl-2*H*-1,2,3-triazole-4-carboxylate (**28**) was synthesised following GP1 with 2 mmol starting material (ethyl bromoacetate **19**) and adjusted equivalents of reactants. Yellow crystals, yield: 10 mg, 2%. The low yield was due to incorrect storage of the aldehyde, which resulted in oxidation to the carboxylic acid. ^{1}H NMR (500 MHz, $CDCl_3$) δ 4.40 (tt, *J* = 11.9, 3.8 Hz, 1H, *aliphatic–H*), 4.30 (q, *J* = 7.1 Hz, 2H, *aliphatic–H*), 2.24 – 2.10 (m, 2H, *aliphatic–H*), 1.91 (dt, *J* = 14.2, 3.6 Hz, 2H, *aliphatic–H*), 1.82 – 1.64 (m, 3H, *aliphatic–H*), 1.44 (qt, *J* = 13.0, 3.5 Hz, 2H, *aliphatic–H*), 1.26 (qt, *J* = 12.9, 3.8 Hz, 1H, *aliphatic–H*), 1.25 (t, *J* = 7.1 Hz, 3H, *aliphatic–H*). ^{13}C NMR (126 MHz, $CDCl_3$) δ 161.2 (*carbonyl-C*), 129.9 (*aromatic-C*), 118.7 (*aromatic-C*), 61.3 (*aliphatic -C*), 33.6 (*aliphatic-C*), 25.2 (*aliphatic-C*), 25.1 (*aliphatic-C*), 14.4 (*aliphatic -C*), 10.9 (*aliphatic-C*). HRMS calc. for $C_{11}H_{18}N_3O_2$ $[M+H]^+$: 224.1934; found 224.1932.

Ethyl 5-pentyl-2*H*-1,2,3-triazole-4-carboxylate (29)

Ethyl 5-pentyl-2*H*-1,2,3-triazole-4-carboxylate (**29**) was synthesised following GP1 with 1 mmol staring material 2 mmol limiting reagent (ethyl bromoacetate **19**) and adjusted equivalents of reactants. Colourless crystals, yield: 206 mg, 97%. ^{1}H NMR (400 MHz, $CDCl_3$) δ 4.41 (q, *J* = 7.1 Hz, 2H, aliphatic– H), 3.03 (t, *J* = 7.8 Hz, 2H, aliphatic– H), 1.69 (dd, *J* = 10.7, 4.8 Hz, 2H, aliphatic– H), 1.36 (t, *J* = 7.1 Hz, 3H, aliphatic– H), 1.30 (h, *J* = 3.2 Hz, 4H, aliphatic– H), 0.85 (d, *J* = 6.8 Hz, 3H, aliphatic– H). ^{13}C NMR (101 MHz, $CDCl_3$) δ 161.7 (carbonyl-C), 147.2 (aromatic-C, broad), 135.1 (aromatic-C), 61.3 (aliphatic-C), 31.4 (aliphatic-C), 28.6 (aliphatic-C), 24.4 (aliphatic-C), 22.3 (aliphatic-C), 14.2 (aliphatic-C), 13.9 (aliphatic-C). HRMS calc. for $C_{10}H_{18}N_3O_2$ $[M+H]^+$: 212.1394; found 212.1394.

Ethyl 5-phenyl-2*H*-1,2,3-triazole-4-carboxylate (30)

Ethyl 5-phenyl-2*H*-1,2,3-triazole-4-carboxylate (**30**) was synthesised following GP1. Colourless crystals, yield: 781 mg, 72%. Identity of the product was confirmed by comparison with literature NMR spectra. [100] ^{1}H NMR (600 MHz, $CDCl_3$) δ 7.83 (dd, *J* = 6.6, 3.1 Hz, 2H, *aromatic–H*), 7.45 (q, *J* = 3.2, 2.7 Hz, 3H, *aromatic–H*), 4.41 (q, *J* = 7.1 Hz, 2H, *aliphatic–H*), 1.35 (t, *J* = 7.2 Hz, 3H, *aliphatic–H*). ^{13}C NMR (101 MHz, $CDCl_3$) δ 161.4 (carbonyl-C), 145.4 (aromatic-C), 134.7 (aromatic-C), 129.8 (aromatic-C), 129.6 (aromatic-C), 129.0 (aromatic-C), 128.7 (aromatic-C), 61.2 (aliphatic-C), 14.4 (aliphatic-C). ESI-HRMS calc. for $C_{11}H_{12}N_3O_2$ $[M+H]^+$: 218.0924; found 218.0923.

Ethyl 5-(4-cyanophenyl)-2*H*-1,2,3-triazole-4-carboxylate (31)

Ethyl 5-(4-cyanophenyl)-2*H*-1,2,3-triazole-4-carboxylate (**31**) was synthesised following GP1 with 2 mmol limiting reagent (ethyl bromoacetate **19**) and adjusted equivalents of reactants. Identity of the product was confirmed by comparison with literature NMR spectra. [100] Colourless crystals, yield: 185 mg, 65%. ^{1}H NMR (400 MHz, $CDCl_3$) δ 8.27 (d, *J* = 1.7 Hz, 1H, *aromatic–H*), 8.20 (dt, *J* = 7.9, 1.5 Hz, 1H, *aromatic–H*), 7.74 (dt, *J* = 7.7, 1.5 Hz, 1H, *aromatic–H*), 7.59 (t, *J* = 7.9 Hz, 1H, *aromatic–H*), 4.47 (q, *J* = 7.1 Hz, 2H, *aliphatic-H*), 1.42 (t, *J* = 7.1 Hz, 3H, *aliphatic-H*). ^{13}C NMR (101 MHz, $CDCl_3$) δ 160.3 (carbonyl-C), 146.7 (aromatic-C), 133.5 (aromatic-C), 132.9 (aromatic-C), 132.7 (aromatic-C), 130.3 (aromatic-C), 129.1 (aromatic-C), 118.4 (aromatic-C), 112.6 (aromatic-C), 62.2 (aliphatic-C), 14.1 (aliphatic-C). ESI-HRMS calc. for $C_{12}H_{11}N_4O_2$ $[M+H]^+$: 243.0877; found 243.0876.

Ethyl 5-(3-chlorophenyl)-2*H*-1,2,3-triazole-4-carboxylate (32)

Ethyl 5-(3-chlorophenyl)-2*H*-1,2,3-triazole-4-carboxylate (**32**) was synthesised following GP1 with 2 mmol starting material 2 mmol limiting reagent (ethyl bromoacetate **19**) and adjusted equivalents of reactants. Identity of the product was confirmed by comparison with

literature NMR spectra. [100] Yellow crystals, yield: 270 mg, 54%. ^{1}H NMR (400 MHz, $CDCl_3$) δ 7.89 (t, *J* = 1.8 Hz, 1H, *aromatic–H*)), 7.77 (dt, *J* = 7.2, 1.6 Hz, 1H, *aromatic–H*)), 7.46 – 7.33 (m, 2H, *aromatic–H*)), 4.45 (q, *J* = 7.1 Hz, 2H, *aliphatic–H*)), 1.38 (t, *J* = 7.1 Hz, 3H, *aliphatic–H*)). ^{13}C NMR (101 MHz, $CDCl_3$) δ 160.7 (*aromatic-C*), 146.6 (*aromatic-C*), 134.1 (*aromatic-C*), 130.2 (aromatic-C), 129.5 (*aromatic-C-broad*), 129.5 (*aromatic-C-broad*), 129.3 (*aromatic-C-broad, 2C*), 127.4 (*aromatic-C*), 62.0 (*aliphatic-C*), 14.0 (*aliphatic-C*). HRMS calc. for $C_{11}H_{11}{}^{35}ClN_3O_2$ $[M+H]^+$: 252.0534; found 252.0534.

Ethyl 5-(2-fluorophenyl)-2*H*-1,2,3-triazole-4-carboxylate (33)

Ethyl 5-(2-fluorophenyl)-2*H*-1,2,3-triazole-4-carboxylate (**33**) was synthesised following GP1 with 1 mmol starting material 2 mmol limiting reagent (ethyl bromoacetate **19**) and adjusted equivalents of reactants. Identity of the product was confirmed by comparison with literature NMR spectra. [100] Colourless crystals, yield: 91 mg, 37%. ^{1}H NMR (400 MHz, $CDCl_3$) δ 7.57 (td, *J* = 7.4, 1.8 Hz, 1H, *aromatic–H*), 7.40 (dddd, *J* = 8.3, 7.2, 5.2, 1.8 Hz, 1H, *aromatic–H*), 7.18 (td, *J* = 7.6, 1.1 Hz, 1H, *aromatic–H*), 7.11 (ddd, *J* = 9.6, 8.3, 1.1 Hz, 1H, *aromatic–H*), 4.33 (q, *J* = 7.1 Hz, 2H, *aliphatic–H*), 1.22 (t, *J* = 7.1 Hz, 3H , *aliphatic–H*). ^{13}C NMR (126 MHz, $CDCl_3$) δ 161.0 (*carbonyl-C*), 159.0 (*aromatic-C*), 141.0 (*aromatic-C*), 136.1 (*aromatic-C*), 131.5 (*aromatic-C*), 131.3 (*aromatic-C*), 124.0 (*aromatic-C*), 116.5 (*aromatic-C*), 115.7 (*aromatic-C*), 115.5 (*aromatic-C*), 61.7 (*aliphatic-C*), 13.8 (*aliphatic-C*). HRMS calc. for $C_{11}H_{11}FN_3O_2$ $[M+H]^+$: 252.0534; found 236.0835.

Ethyl 5-(2-fluoro-5-methoxyphenyl)-2*H*-1,2,3-triazole-4-carboxylate (34)

Ethyl 5-(2-fluoro-5-methoxyphenyl)-2*H*-1,2,3-triazole-4-carboxylate (**34**) was synthesised following GP1 with 1 mmol staring material 2 mmol limiting reagent (ethyl bromoacetate **19**) and adjusted equivalents of reactants. Identity of the product was confirmed by comparison with literature NMR spectra. [100] ^{1}H NMR (400 MHz, $CDCl_3$) δ 7.20 (dd, *J* = 5.8, 3.1 Hz, 1H,

aromatic–H), 7.09 (t, *J* = 9.2 Hz, 1H, *aromatic–H*), 7.01 – 6.92 (m, 1H *aromatic–H*), 4.39 (q, *J* = 7.1 Hz, 2H, *aliphatic– H*), 3.82 (s, 3H, *aliphatic– H*), 1.31 (t, *J* = 7.1 Hz, 3H, *aliphatic– H*). ^{13}C NMR (151 MHz, $CDCl_3$) δ 160.6 (*carbonyl-C*), 155.6 (*aromatic-C*), 155.4 (*aromatic-C*), 153.2 (*aromatic-C*), 117.1 (*aromatic-C*), 117.1 (*aromatic-C*), 116.4 (*aromatic-C*), 116.2 (*aromatic-C*), 115.5 (*aromatic-C*), 61.7 (*aliphatic-C*), 55.8 (*aliphatic-C*), 13.97 (*aliphatic-C*). HRMS calc. for $C_{12}H_{13}FN_3O_3$ $[M+H]^+$: 266.0936; found 266.0936.

Ethyl 5-(3-nitrophenyl)-2*H*-1,2,3-triazole-4-carboxylate (35)

Ethyl 5-(3-nitrophenyl)-2*H*-1,2,3-triazole-4-carboxylate (**35**) was synthesised following GP1 with 1 mmol staring material 2 mmol limiting reagent (ethyl bromoacetate **19**) and adjusted equivalents of reactants. Identity of the product was confirmed by comparison with literature NMR spectra. [100] Colourless crystals, yield: 240 mg, 91%. ^{1}H NMR (400 MHz, $CDCl_3$) δ 8.87 (t, *J* = 1.9 Hz, 1H, *aromatic–H*), 8.31 (dd, *J* = 8.1, 2.0 Hz, 2H, *aromatic–H*), 7.66 (t, *J* = 8.0 Hz, 1H, *aromatic–H*), 4.47 (p, *J* = 7.1 Hz, 2H, *aliphatic–H*), 1.41 (t, *J* = 7.1 Hz, 3H, *aliphatic–H*). ^{13}C NMR (101 MHz, $CDCl_3$) δ 160.3 (*carbonyl-C*), 148.1 (*aromatic-C*), 146.6 (*aromatic-C*), 135.1 (*aromatic-C*), 130.7 (*aromatic-C*), 129.3 (*aromatic-C*), 124.4 (*aromatic-C*), 124.1 (*aromatic-C*), 62.3 (*aliphatic-C)*, 14.1 (*aliphatic-C)*. HRMS calc. for $C_4H_{11}N_4O_4$ $[M+H]^+$: 263.0775; found 263.0775.

Ethyl 5-(4-nitrophenyl)-2*H*-1,2,3-triazole-4-carboxylate (36)

Ethyl 5-(4-nitrophenyl)-2*H*-1,2,3-triazole-4-carboxylate (**36**) was synthesised following GP1 with 1 mmol staring material 2 mmol limiting reagent (ethyl bromoacetate **19**) and adjusted equivalents of reactants. Identity of the product was confirmed by comparison with literature NMR spectra. [100] Colourless crystals, yield: 140 mg, 53%.^{1}H NMR (400 MHz, DMSO-d_6) δ 8.30 (d, *J* = 8.4 Hz, 2H, *aromatic–H*), 8.06 (d, *J* = 8.4 Hz, 2H, *aromatic–H*), 4.29 (q, *J* = 7.1

Hz, 2H, *aliphatic–H*), 1.24 (t, *J* = 7.1 Hz, 3H, *aliphatic–H*). ^{13}C NMR (101 MHz, DMSO-d_6) δ 160.8 (*carbonyl-C*), 148.0 (*aromatic-C*), 144.8 (*aromatic-C*), 135.9 (*aromatic-C*), 130.7 (*aromatic-C*), 123.7 (*aromatic-C*), 61.6 (*aliphatic-C*), 14.3 (*aliphatic-C*). HRMS calc. for $C_4H_{11}N_4O_4$ $[M+H]^+$: 263.0775; found 263.07756.

Ethyl 5-(4-methoxyphenyl)-2*H*-1,2,3-triazole-4-carboxylate (37)

Ethyl 5-(4-methoxyphenyl)-2H-1,2,3-triazole-4-carboxylate (**37**) was synthesised following GP1 with 1 mmol limiting reagent (ethyl bromoacetate **19**) and adjusted equivalents of reactants. Identity of the product was confirmed by comparison with literature NMR spectra. [100] Colourless crystals, yield: 178 mg, 72%. ^{1}H NMR (400 MHz, $CDCl_3$) δ 7.99 – 7.62 (m, 2H, *aromatic–H*), 7.07 – 6.83 (m, 2H, *aromatic–H*), 4.36 (q, *J* = 7.1 Hz, 2H, *aliphatic–H*), 3.82 (s, 3H, *aliphatic–H*), 1.29 (t, *J* = 7.1 Hz, 3H, *aliphatic–H*). ^{13}C NMR (101 MHz, $CDCl_3$) δ 161.3 (*carbonyl-C*), 160.8 (*aromatic-C*), 145.5 (*aromatic-C*), 133.5 (*aromatic-C*), 130.7 (*aromatic-C*), 113.9 (*aromatic-C*), 61.6 (*aliphatic-C*), 55.4 (*aliphatic-C*), 14.1 (*aliphatic-C*). HRMS calc. for $C_{12}H_{114}N_3O_3$ $[M+H]^+$: 248.1030; found 248.1030.

Ethyl 5-(thiophen-3-yl)-2*H*-1,2,3-triazole-4-carboxylate (38)

Ethyl 5-(thiophen-3-yl)-2*H*-1,2,3-triazole-4-carboxylate (**38**) was synthesised following GP1. Identity of the product was confirmed by comparison with literature NMR spectra. [100] Brown crystals, yield: 120 mg, 10%. ^{1}H NMR (400 MHz, $CDCl_3$) δ 8.32 (dd, *J* = 3.1, 1.3 Hz, 1H, *aromatic–H*), 7.72 (d, *J* = 5.0 Hz, 1H, *aromatic–H*), 7.40 (dd, *J* = 5.1, 3.1 Hz, 1H, *aromatic–H*), 4.48 (q, *J* = 7.1 Hz, 2H, *aliphatic-H*), 1.44 (t, *J* = 7.1 Hz, 3H, *CH₃*). ^{13}C NMR (151 MHz, $CDCl_3$) δ 161.0 (*carbonyl-C*), 128.2 (*aromatic-C, broad peak*), 127.7 (*aromatic-C*), 127.4 (*aromatic-C*), 125.7 (*aromatic-C*), 61.8 (*aliphatic-C*), 14.1 (*aliphatic-C*). ESI-HRMS calc. for $C_{11}H_{12}NO_4S_2$ $[M+H]^+$: 224.0494; found 224.0489.

Ethyl 5-(pyridin-3-yl)-2H-1,2,3-triazole-4-carboxylate (**39**)

Ethyl 5-(pyridin-3-yl)-2*H*-1,2,3-triazole-4-carboxylate (**39**) was synthesised following GP1 with 1 mmol staring material (ethyl bromoacetate **19**) and adjusted equivalents of reactants. Identity of the product was confirmed by comparison with literature NMR spectra. [100] Colourless crystals, yield: 72 mg, 33%. ^{1}H NMR (400 MHz, DMSO-d6) δ 9.32 – 8.79 (m, 1H, *aromatic–H*), 8.66 (dd, *J* = 4.8, 1.7 Hz, 1H, *aromatic–H*), 8.18 (dt, *J* = 8.0, 2.0 Hz, 1H, *aromatic–H*), 7.53 (ddd, *J* = 7.9, 4.9, 0.9 Hz, 1H, *aromatic–H*), 4.30 (q, *J* = 7.1 Hz, 2H, *aliphatic–H*), 1.25 (t, *J* = 7.1 Hz, 3H, *aliphatic–H*).^{13}C NMR (101 MHz, DMSO-d_6) δ 161.0 (*carbonyl-C*), 150.5 (*aromatic-C*), 149.9 (*aromatic-C*), 143.4 (*aromatic-C*), 137.1 (*aromatic-C*), 134.8 (*aromatic-C*), 126.2 (*aromatic-C*), 123.7 (*aromatic-C*), 61.4 (*aliphatic-C*), 14.4 (*aliphatic-C*). HRMS calc. for $C_{10}H_{11}N_4O_2$ $[M+H]^+$: 219.0877; found 219.0877

Ethyl 5-(pyridin-4-yl)-2*H*-1,2,3-triazole-4-carboxylate (40)

Ethyl 5-(pyridin-4-yl)-2*H*-1,2,3-triazole-4-carboxylate (**40**) was synthesised following GP1 with 1 mmol staring material (ethyl bromoacetate **19**) and adjusted equivalents of reactants. Identity of the product was confirmed by comparison with literature NMR spectra. [100] Colourless crystals, yield: 104 mg, 48%. ^{1}H NMR (400 MHz, DMSO-d_6) δ 8.31 ((m, 2H, *aromatic–H*), 7.95 – 7.63 (m, 2H, *aromatic–H*), 4.32 (q, *J* = 7.1 Hz, 2H, *aliphatic–H*), 1.27 (t, *J* = 7.1 Hz, 3H, *aliphatic–H*). ^{13}C NMR (101 MHz, DMSO-d_6) δ 160.9 (*carbonyl-C*), 150.2 (*aromatic-C*), 144.3 (*aromatic-C*), 137.0 (*aromatic-C*), 134.6 (*aromatic-C*), 123.8 (*aromatic-C*), 61.6 (*aliphatic-C*), 14.4 (*aliphatic-C*). HRMS calc. for $C_{10}H_{11}N_4O_2$ $[M+H]^+$: 219.0877; found 219.0877.

5-Phenyl-2H-1,2,3-triazole-4-carboxylic acid [118] (41)

A solution of ethyl 5-phenyl-2*H*-1,2,3-triazole-4-carboxylate (**41**) (50 mg, 0.23 mmol) was dissolved in THF (10 mL) and cooled to 0°C. An ice-cold NaOH solution (100 mg in 5 mL H_2O, 0.5 M) was added dropwise and the mixture stirred at room temperature for 24 h. 1M HCl (approximately 5 mL) was added to neutralise the reaction. The solution was extracted with ethyl acetate (3x 30 mL), the combined organic fractions dried over sodium sulfate concentrated *in vacuo*. Purification by flash chromatography (SiO_2, chloroform/methanol/triethylamine10:1:0.1) gave afford **41** as colourless powder (37 mg, 85%). ^{1}H NMR (500 MHz, Methanol-d_4) δ 7.89 – 7.74 (m, 2H, *aromatic–H*), 7.46 (t, *J* = 3.4 Hz, 3H, *aromatic–H*). ^{13}C NMR ((101 MHz, DMSO-d_6) δ 168.1 (*carbonyl-C*), 144.4 (*aromatic-C*), 135.5 (*aromatic-C*), 129.5 (*aromatic-C*), 128.7 (*aromatic-C*), 127.4 (*aromatic-C*), 61.2 (*aliphatic-C*), 14.6 (*aliphatic-C*). HRMS calc. for $C_9H_7N_3O_2$ $[M+H]^+$: 190.0611; found 190.0613.

5-Phenyl-2*H*-1,2,3-triazole-4-carbonitrile (42)

5-Phenyl-2*H*-1,2,3-triazole-4-carbonitrile (**42**) was synthesised following GP2. Yellow crystals, yield: 90 mg, 44%. ^{1}H NMR (400 MHz, DMSO-d_6) δ 7.77 (d, *J* = 6.9 Hz, 2H, *aromatic–H*), 7.51 – 7.31 (m, 3H, *aromatic–H*). ^{13}C NMR (101 MHz, DMSO-d_6) δ 173.6 (*nitrile-C)*, 162.6 (*aromatic-C*), 129.4 (*aromatic-C*), 128.7 (*aromatic-C*); triazole-C not detected. HRMS calc. for $C_9H_7N_4$ $[M+H]^+$: 171.0655; found 171.0655.

Allyl 5-phenyl-2H-1,2,3-triazole-4-carboxylate (43)

Allyl 5-phenyl-*2H*-1,2,3-triazole-4-carboxylate (**43**) was synthesised following GP2 with 6.5 mmol starting material (ethyl bromoacetate **19**) and adjusted equivalents of reactants. Colourless crystals, yield: 1.25 g, 83%. ^{1}H NMR (500 MHz, $CDCl_3$) δ 7.92 – 7.75 (m, 2H, *aromatic–H*), 7.44 (dt, *J* = 5.2, 1.8 Hz, 3H, *aromatic–H*), 6.04 – 5.85 (m, 1H, *aromatic–H*), 5.32 (dt, *J* = 17.1, 1.6 Hz, 1H, *vinylic–H*), 5.24 (dt, *J* = 10.4, 1.6 Hz, 1H, *vinylic –H*), 5.01 – 4.70 (m,

2H, *allylic–H*). ^{13}C NMR (126 MHz, $CDCl_3$) δ 160.7 (*carbonyl-C*), 146.7 (*aromatic-C*), 134.0 (*aromatic-C*), 131.3 (*aromatic-C*), 129.7 (*aromatic-C*), 129.2 (*aromatic-C*), 128.4 (*aromatic-C*), 127.7 (*vinylic-C*), 119.3 (*vinylic-C*), 66.2 (*allylic-C*). HRMS calc. for $C_{12}H_{12}N_3O_2$ $[M+H]^+$: 230.0924; found 230.0924.

(5-Phenyl-2*H*-1,2,3-triazol-4-yl)methanol [115] **(44)**

To a solution of ethyl 5-phenyl-2*H*-1,2,3-triazole-4-carboxylate (**44**) (50 mg, 0.23 mmol) in toluene (20 mL), sodium bis(2-methoxyethoxy) aluminium hydride (Red-Al® ≥ 60 w/w% in toluene; 2 mL, 0.6 mmol) was added under an inert atmosphere, and the reaction was stirred 18 h at room temperature. Water (20mL) was added, the pH of the suspension was adjusted to pH 2 with 1M HCl and extracted with ethyl acetate (3x 20 mL). The combined organic fractions were dried over sodium sulfate, concentrated and purified via silica gel chromatography (10:1 chloroform/methanol) to afford (5-phenyl-2*H*-1,2,3-triazol-4-yl)methanol (**44**) as a crystalline solid (27 mg, 67%). Identity of the product was confirmed by literature NMR spectra.[116] ^{1}H NMR (500 MHz, CD_3OD) δ 7.84 – 7.74 (m, 2H, *aromatic–H*), 7.48 (td, *J* = 7.3, 6.3, 1.4 Hz, 2H, *aromatic–H*), 7.43 – 7.36 (m, 1H, *aromatic–H*), 4.80 (s, 2H, *aliphatic–H*). ^{13}C NMR (126 MHz, DMSO-d_6) δ 130.6 (*aromatic-C, broad 2C)*, 129.3 (*aromatic-C)*, 128.5 (*aromatic-C)*, 127.4 (*aromatic-C)*, 127.1 *(aromatic-C)*, 54.1 (*aliphatic -C)*. HRMS calc. for $C_9H_{10}N_3O$ $[M+H]^+$: 176.0818; found 176.0818.

4-Methyl-1-(prop-2-yn-1-yl)-*1H*-1,2,3-triazole (54, MPT)

4-Methyl-1-(prop-2-yn-1-yl)-1*H*-1,2,3-triazole (**54**) was synthesised following GP3. Yellow oil, yield: 215 mg, 80%. ^{1}H NMR (500 MHz, $CDCl_3$) δ 7.50 (s, 1H, *triazole-H*), 5.11 (d, *J* = 2.6 Hz, 2H, *aliphatic-H*), 2.54 (t, *J* = 2.6 Hz, 1H, *alkyne-H*), 2.34 (s, 3H, aliphatic-H). ^{13}C NMR (126 MHz, $CDCl_3$) δ 143.7 (*aromatic-C*), 120.8 (*aromatic-C*), 76.1 (broad, 2C, *alkyne-C*), 39.5 (*aliphatic-C*), 10.8 (*aliphatic -C*). HRMS calc. for $C_6H_8N_3$ $[M+H]^+$: 122.0713; found 122.0713.

Allyl 2-bromoacetate [117] (55)

A suspension of allyl alcohol (1.4 mL, 20 mmol) and dipotassium carbonate (5.5 g, 20 mmol) were dissolved in dichloromethane (10 mL) and cooled to 0°C. Bromoacetyl bromide (2.6 mL, 30 mmol) was added dropwise, and the reaction mixture was stirred for 2 hr at room temperature. Water (10 mL) was added to quench the reaction. The organic layer was separated, and the aqueous layer extracted with dichloromethane (2x10 mL). The combined organic layers were dried over sodium sulfate and concentrated *in vacuo*. The crude oil was purified via silica gel flash chromatography (ethyl acetate / petroleum spirits (2:1) to afford allyl 2-bromoacetate (**55**) as a brown oil (1.15 g, 32%). ^{1}H NMR (500 MHz, $CDCl_3$) δ 5.9 (ddt, *J* = 17.1, 10.4, 5.8 Hz, 1H, *vinylic-H*), 5.3 (dq, *J* = 17.1, 1.5 Hz, 1H, 1H, *vinylic-H*), 5.2 (dq, *J* = 10.5, 1.3 Hz, 1H, *vinylic-H*), 4.64 (dt, *J* = 5.8, 1.4 Hz, 2H, *allylic-H*), 3.84 (s, 2H, *aliphatic-H*). ^{13}C NMR (126 MHz, $CDCl_3$) δ 166.8 (*carbonyl-C*), 131.2 (*allylic-C*), 119.1 (*allylic-C*), 66.7 (*aliphatic-C*), 25.7 (*aliphatic-C*). HRMS calc. for $C_5H_8BrO_2$ $[M+H]^+$: 178.9703; found 178.9703.

1-Cyclohexyl-4-methyl-*1H*-1,2,3-triazole (56)

1-Cyclohexyl-4-methyl-*1H*-1,2,3-triazole (**56**) was synthesised following GP3. Colourless crystals, yield: 180 mg, 50%. ^{1}H NMR (500 MHz, $CDCl_3$) δ 7.26 (d, *J* = 1.6 Hz, 1H, *aromatic-H*), 4.40 (tt, *J* = 11.9, 3.8 Hz, 1H, *aliphatic-H*), 2.34 (d, *J* = 0.8 Hz, 3H, *aliphatic-H*), 2.24 – 2.10 (m, 2H, *aliphatic-H*), 1.91 (dt, *J* = 14.2, 3.6 Hz, 2H, *aliphatic-H*), 1.82 – 1.64 (m, 3H, *aliphatic-H*), 1.44 (qt, *J* = 13.0, 3.5 Hz, 2H, *aliphatic-H*), 1.26 (qt, *J* = 12.9, 3.8 Hz, 1H, *aliphatic-H*). ^{13}C NMR (126 MHz, $CDCl_3$) δ 142.8 (*aromatic-C*), 118.7 (*aliphatic -C*), 59.8 (*aliphatic -C*), 33.6 (*aliphatic -C*), 25.2 (*aliphatic -C*), 25.1 (*aliphatic -C*), 10.9 (*aliphatic -C*). HRMS calc. for $C_4H_{16}N_3$ $[M+H]^+$: 165.1399; found 165.1398.

4-Methyl-1-propyl-1*H*-1,2,3-triazole (57)

4-Methyl-1-propyl-1*H*-1,2,3-triazole (**57**) was synthesised following GP3. Yellow oil, yield: 208 mg, 76%. ^{1}H NMR (500 MHz, $CDCl_3$) δ 7.26 (d, *J* = 1.6 Hz, 1H, *aromatic-H*),4.25 (t, *J* = 7.1 Hz, 2H, *aliphatic-H*), 2.32 (d, *J* = 0.8 Hz, 3H, *aliphatic-H*), 1.89 (hep, *J* = 7.4 Hz, 2H, *aliphatic-H*), 0.92 (t, *J* = 7.4 Hz, 3H, *aliphatic-H*). ^{13}C NMR (126 MHz, $CDCl_3$) δ 142.8 (*aromatic-C*), 118.7 (*aliphatic -C*), 59.8 (*aliphatic -C*), 33.6 (*aliphatic -C*), 25.2 (*aliphatic -C*), 25.1 (*aliphatic -C*), 10.9 (*aliphatic -C*). HRMS calc. for $C_6H_{12}N_3$ $[M+H]^+$: 126.1026; found 126.1024.

1-(*tert*-Butyl)-4-methyl-*1H*-1,2,3-triazole (58)

1-(tert-butyl)-4-methyl-1*H*-1,2,3-triazole (**58**) was synthesised following GP3. Yellow oil, yield: 160 mg, 52%. ^{1}H NMR (500 MHz, $CDCl_3$) δ 7.33 (d, *J* = 0.9 Hz, 1H, *aromatic-H*), 2.33 (d, *J* = 0.9 Hz, 3H, *aliphatic-H*), 1.64 (s, 9H, *aliphatic-H*). ^{13}C NMR (126 MHz, $CDCl_3$) δ 142.6 (*aromatic-C*), 118.2 (*aromatic-C*), 58.8 (*aliphatic -C*), 30.0 (*aliphatic -C*), 10.8 (*aliphatic -C*). HRMS calc. for $C_7H_{14}N_3$ $[M+H]^+$: 140.1183; found 140.1183.

1-(Furan-2-ylmethyl)-4-methyl-1*H*-1,2,3-triazole (59)

1-(Furan-2-ylmethyl)-4-methyl-1*H*-1,2,3-triazole (**59**) was synthesised following GP3. Yellow oil, yield: 190 mg, 53%. ^{1}H NMR (500 MHz, $CDCl_3$) δ 7.42 (q, *J* = 1.9 Hz, 1H, *aromatic-H*), 6.66 – 6.05 (m, 2H, *aromatic-H*), 5.48 (d, *J* = 3.0 Hz, 2H, *aliphatic-H*), 2.33 (d, *J* = 3.0 Hz, 3H, *aliphatic-H*). ^{13}C NMR (126 MHz, $CDCl_3$) δ 147.6 (*aromatic-C*), 143.7 (*aromatic-C*), 143.5 (*aromatic-C*), 120.9 (*aromatic-C*), 110.8 (*aromatic-C*), 110.0 (*aromatic-C*), 46.5 (*aliphatic -C*), 10.8 (*aliphatic -C*). HRMS calc. for $C_8H_{10}N_3O$ $[M+H]^+$: 164.081; found 164.081.

2-(But-3-yn-1-ylthio)benzothiazole (60)[119]

To a solution of 2-Mercaptobenzothiazole (8.4 mg, 5 mmol) in 10 mL of THF containing potassium carbonate (0.75 g, 6 mmol) was added propargyl bromide (0.46 mL, 5 mmol). The

reaction mixture was heated under reflux for 1 h. The crude oil was purified via silica gel chromatography (ethyl acetate/petroleum ether 1:2) to afford 2-(but-3-yn-1-ylthio) benzothiazole (**60**) as colourless powder (8.9 mg, 82%). The ^{1}H NMR spectrum is in agreement with literature data.[120] ^{1}H NMR (400 MHz, $CDCl_3$) δ 7.87 (dd, *J* = 8.2, 1.1 Hz, 1H, *aromatic–H*), 7.80 – 7.72 (m, 1H, *aromatic–H*), 7.49 – 7.36 (m, 1H, *aromatic–H*), 7.35 – 7.23 (m, 1H, *aromatic–H*), 3.52 (t, *J* = 7.1 Hz, 2H, *aliphatic-H*), 2.79 (td, *J* = 7.2, 2.7 Hz, 2H, *aliphatic-H*), 2.09 (t, *J* = 2.6 Hz, 1H, *CH, aliphatic-H*). ^{13}C NMR (101 MHz, $CDCl_3$) δ 165.7 (aromatic-C), 153.1 (aromatic-C), 135.2 (aromatic-C), 126.0 (aromatic-C), 124.3 (aromatic-C), 122.1 (aromatic-C), 121.5 (aromatic-C), 81.8 (alkyne-C), 70.1 (alkyne-C), 32.0 (aliphatic-C), 19.5 (aliphatic-C). HRMS calc. for $C_{11}H_9NS_2$ [M+H]+: 220.0250; found 220.0246.

2-(But-3-yn-1-ylsulfonyl) benzothiazole (61)

A solution of periodic acid in acetonitrile (9.7 mg, 2.5 mmol, 0.125 M) was vigorously stirred for 30 min at rt. Chromium trioxide (49 mg, 0.49 mmol) was added, and the stirring was continued for another 5 min. A solution of 2-(but-3-yn-1-ylthio) benzothiazole (**59**) in acetonitrile (0.5 g, 2.5 mmol, 0.1 M) was added dropwise and formation of a precipitate was observed. After 1 hr of stirring, the reaction mixture was filtered, and the solid was washed with acetonitrile. The filtrate was cautiously concentrated under reduced pressure. Ethyl aetate was added to the residue, and the organic layer washed with brine and water. The organic layer was dried over sodium sulfate and evaporated under reduced pressure. The crude oil was purified via silica gel chromatography (ethyl acetate/petroleum ether 2:3) to afford 2-(but-3-yn-1-ylsulfonyl) benzothiazole (**61**) as colourless powder (0.5 g, 80%). NMR spectrum is in agreement with that described in literature.[120] ^{1}H NMR (400 MHz, $CDCl_3$) δ 8.30 – 8.19 (m, 1H, *aromatic–H*), 8.07 – 8.00 (m, 1H, *aromatic–H*), 7.74 – 7.57 (m, 2H,

aromatic–H), 3.73 (dd, *J* = 8.3, 7.1 Hz, 2H, *S–CH*$_2$), 2.83 (td, *J* = 7.7, 2.7 Hz, 2H, *CH*$_2$*–CH*$_2$), 1.93 (t, *J* = 2.7 Hz, 1H, *CH*). ^{13}C NMR (101 MHz, $CDCl_3$) δ 164.9 (aromatic-C), 152.6 (aromatic-C), 136.8 (aromatic-C), 128.2 (aromatic-C), 127.7 (aromatic-C), 125.5 (aromatic-C), 122.3 (aromatic-C), 78.6 (S-C), 70.9 (alkyne-C), 53.1 (alkyne-C), 13.3 (aliphatic-C). HRMS calc. for $C_{11}H_9NS_2$ [M+H]+: 252.0150; found 252.0146.

1,4-Dimethyl-*1H*-1,2,3-triazole (62)

1,4-Dimethyl-*1H*-1,2,3-triazole (**62x**) was synthesised following GP3. Yellow oil, yield: 82 mg, 40%. ^{1}H NMR (500 MHz $CDCl_3$ δ 4.02 (s, 3H, *aliphatic-H*), 2.31 (s, 3H, *aliphatic-H*). ^{13}C NMR (126 MHz, $CDCl_3$) δ 143.5 (*aromatic-C*), 122.1 (*aromatic-C*), 36.46 (*aliphatic-C*), 10.7 (*aliphatic -C*). HRMS calc. for $C_4H_8N_3$ $[M+H]^+$: 98.0713; found 98.0713.

Appendix

```
Query: None Query ID: lcl|Query_17711 Length: 102


>Nitrosospira multiformis strain Nl13 16S ribosomal RNA, partial sequence
Sequence ID: NR_115148.1 Length: 1498
Range 1: 1334 to 1432

Score:152 bits(82), Expect:4e-37,
Identities:95/101(94%),  Gaps:2/101(1%), Strand: Plus/Minus

Query  2     GCGCCCTCCTTGCGGTTAGGCTACCTCGCTTCTGGTGAAACAAACTCCCCATGGTGTGAC  61
             |||||||||||||||||| |||||| |||||||||| |||  |||||| ||||||||||
Sbjct  1432  GCGCCCTCCTTGCGGTTAGACTACCT-GCTTCTGGTGGAACCCACTCCC-ATGGTGTGAC  1375

Query  62    GGGCGGTGTGTACAAGACCCGGGAACGTATTCACCGCGACA  102
             |||||||||||||||||||||||||||||||||||||||||
Sbjct  1374  GGGCGGTGTGTACAAGACCCGGGAACGTATTCACCGCGACA  1334
```

Figure A-1: Proof of purity and identity of *Nitrosospira multiformis via* 16S rRNA sequencing. Data was provided by Australian Research Genome Facility.

REGISTERED OFFICE
Ochrimum Laboratories, Research Road
The University of Queensland, ST LUCIA QLD 4072 Australia
Ph: 61 7 3365 4448 Fax: 61 7 3365 1823
Email: agrf@agrf.org.au
Website: www.agrf.org.au

ABN 63 097 086 292

16S Microbial Screen

Assay:	16S Microbial Screen
Database:	combined_16s
Database Version:	20th Feb 2017
Sample ID:	Ne1
Processed Date:	22-Oct-2021

Rank	Sequence Entry	Hit Length	% Identity	E value
1	251028 Nitrosomonas europaea str. ATCC 19718 AL954747.1 69139..70677	703	100.000	0.0
2	155255 Nitrosomonas europaea str. ATCC 19718 NC_004757.1 69139..70677	703	100.000	0.0
3	82677 Nitrosomonas europaea str. ATCC 19718 BX321856.1 69139..70677	703	100.000	0.0
4	77085 Nitrosomonas europaea str. ATCC19178 AB070983.1 1..1373	703	100.000	0.0
5	76457 Nitrosomonas europaea str. ATCC25978 AB070982.1 1..1373	703	100.000	0.0

Comments:

This report is supplementary to the blast (.bn), chromatogram (.ab1) and fasta (.fa) files. A report will be generated for any sample which produces sequence, including samples which only generate sequence in a single direction; further information is available in the blast file.

Evalue	The Expect value (E) is a parameter that describes the number of hits one can "expect" to see by chance when searching a database of a particular size. It decreases exponentially as the Score (S) of the match increases. Essentially, the E value describes the random background noise. For example, an E value of 1 assigned to a hit can be interpreted as meaning that in a database of the current size one might expect to see 1 match with a similar score simply by chance. The lower the E-value, or the closer it is to zero, the more "significant" the match is. However, keep in mind that virtually identical short alignments have relatively high E values. This is because the calculation of the E value takes into account the length of the query sequence. These high E values make sense because shorter sequences have a higher probability of occurring in the database purely by chance. For additional information on the bit score: http://www.ncbi.nlm.nih.gov/books/NBK21097/#A614

Figure A-2: Proof of purity and identity of *Nitrosomonas europaea*. Data was provided by Australian Research Genome Facility.

Table A-1. Calculated GHG flux rates for CH_4-C in µg g^{-1} soil h^{-1} for soil A days 1-21. The measurements were performed according to Chapter 5.3.2 *CH_4 gas measurements* and flux rates were calculated according to eqn. 1. All fertiliser treatment were at an application rate of $(NH_4)_2SO_4$ 50 mg kg^{-1} soil. [a]

CH_4-C (µg g^{-1} soil h^{-1})[b], [c], [d]

Soil B	Day 1	Day 3	Day 5	Day 7	Day 14	Day 21
Untreated	1.190 ± 0.015	1.233 ± 0.065	1.163 ± 0.047	1.157 ± 0.041	1.210 ± 0.026	1.163 ± 0.043
Fertiliser $(NH_4)_2SO_4$	0.640 ± 0.036	0.533 ± 0.018	0.443 ± 0.003	0.427 ± 0.009	0.543 ± 0.059	0.737 ± 0.024
Fertiliser + DMP 0.5 mol%	0.650 ± 0.050	0.440 ± 0.015	0.453 ± 0.019	0.420 ± 0.030	0.487 ± 0.049	0.570 ± 0.026
Fertiliser + DMP 2.5 mol%	0.607 ± 0.027	0.383 ± 0.050	0.300 ± 0.049	0.337 ± 0.033	0.393 ± 0.066	0.443 ± 0.034 *
Fertiliser + DMP 5 mol% +	0.657 ± 0.071	0.353 ± 0.033	0.203 ± 0.104	0.103 ± 0.052	0.057 ± 0.057 *	0.250 ± 0.126
Fertiliser + MPT 0.5 mol%	0.770 ± 0.058	0.633 ± 0.058	0.393 ± 0.035	0.277 ± 0.024	0.193 ± 0.113*	0.343 ± 0.062
Fertiliser + MPT 2.5 mol%	0.493 ± 0.247	0.310 ± 0.159	0.080 ± 0.080	0.063 ± 0.063	0.043 ± 0.043 *	0.000 ± 0.000 **
Fertiliser + MPT 5 mol%	0.230 ± 0.230	0.120 ± 0.120	0.027 ± 0.027 *	0.043 ± 0.043 *	0.000 ± 0.000*	0.067 ± 0.067 *

b] mean values (n = 3); errors are standard errors of the mean. [c] Statistical significance: $P < .05$ (*) when comparing inhibitor treatments to the control treatment with $(NH_4)_2SO_4$ alone, Statistical analysis were performed on raw GHG flux rates of CH_4-C (µg g^{-1} soil h^{-1}) with GraphPad Prism 9.5.0 (2-way ANOVA) multiple comparison Tuckey HS

Collection of Supporting Information for submitted manuscripts and published chapters

Supporting Information 1 (SI-1)

A Rapid and Inexpensive Assay for Testing the Efficiency of Potential new Synthetic Nitrification Inhibitors

Sibel C. Yildirim,[a] Robert Walker,[b] Michelle Watt,[b] Ute Roessner,[b,c] Uta Wille*[a]

[a]School of Chemistry, Bio21 Institute, The University of Melbourne, Parkville, Victoria 3010, Australia.
[b]School of BioSciences, The University of Melbourne, Parkville, Victoria 3010, Australia.
[c]Research School of Biology, The Australian National University, Acton, Australian Capital Territory 2600, Australia.

Email: uwille@unimelb.edu.au

1. Optimizing the Assay for Water-Insoluble NIs

The lipophilicity of the synthesized potential new inhibitor compounds differed considerably, with some of these being only poorly soluble in the aqueous sodium phospate buffer (NaPB at pH 7.5). Dimethylsulfoxide (DMSO) is a known solubilizing co-solvent for lipophilic compounds at low concentrations (0.01 - 0.1 v/v%).[1, 2] UV/vis spectroscopy was employed to identify the appropriate DMSO/water ratio that solubilises all compounds.

Inhibitor 4 was used as representative for a lipophilic compound, which has a triazole framework with an absorbance in the range 250-290 nm (Figure S1). While the absorbance intensity should follow the Beer-Lambert Law, it is obvious that the signal intensity at the absoption maximun at 282 nm did not increase proportionally with the concentration of the inhibitor compound, when it was dissolved in NaPB containing 1 v/v% of DMSO, suggesting incomplete dissolution.

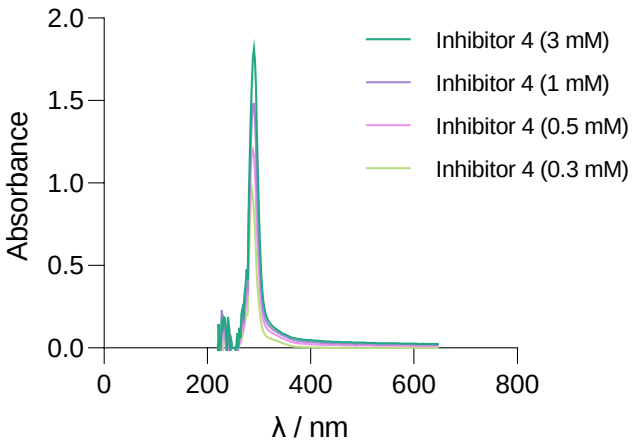

Figure S1. UV/vis absorbance spectra of Inhibitor 4 (0.3 mM, 0.5 mM, 1 mM and 3 mM) in NaPB (pH 7.5) containing 1 v/v% of DMSO. The spectra were corrected by subtracting the spectrum of NaPB containing 1 v/v% of DMSO. [1]

We therefore recorded the absorbance spectra in the 280 - 300 nm range for Inhibitor 4 at a concentration of 0.3 mM, dissolved in NaPB with 0.1 v/v% and 1 v/v% of DMSO, respectively. The absorption spectra were corrected by substracting the 'blank' spectra obtained for the respective solvent mixtures. Figure S2 shows the resulting spectra for three technical replicates obtained for each solvent system. Using 0.1 v/v% of DMSO as co-solvent gave absorption spectra with a standard error of 33.7% for the three replicates (red, blue and green lines). In contrast, with 1 v/v% of DMSO as co-solvent the standard error of the three replicate spectra was only 2.8% (orange, purple and black lines, the latter overlaps with the orange line and is therefore omitted). It should be noted that the higher absolute absorption with 0.1 v/v% of DMSO than with 1 v/v% of DMSO was due to the fact that the inhibitor crushed out of the solution, thereby scattering the light. On the other hand, the high reproducibility of the absorption spectra obtained with 1 v/v% of DMSO as co-solvent indicates complete dissolution of the inhibitor compound at a concentration of 0.3 mM, which was therefore used as standard assay conditions.

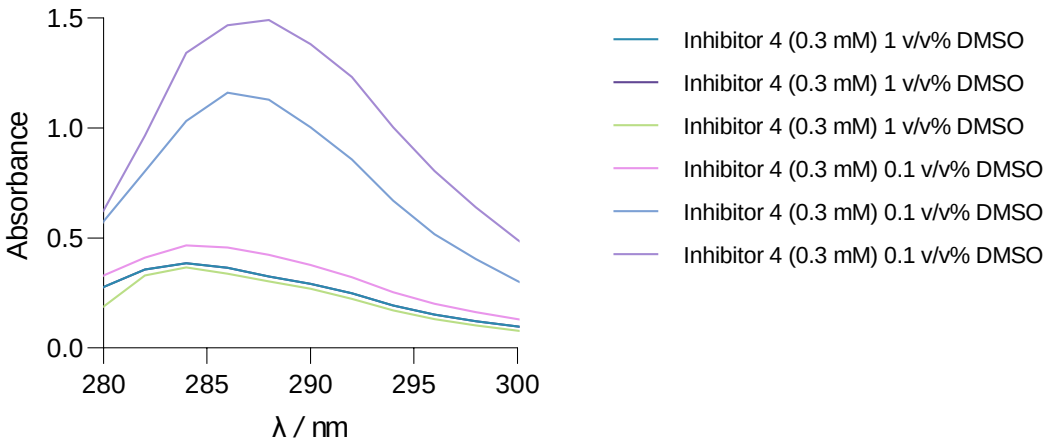

Figure S2. UV/vis absorbance spectra of inhibitor 4 (0.3 mM) in NaPB containing 1 v/v% of DMSO and in NaPB containing 0.1 v/v% of DMSO. The spectra were corrected by subtracting the spectra of NaPB containing 1 v/v% and 0.1 v/v% of DMSO, respectively. Individual spectra represent technical replicates (n = 3). The black line is not shown as it overlaps with the orange line.

2. Additional Supplementary Figures and Tables

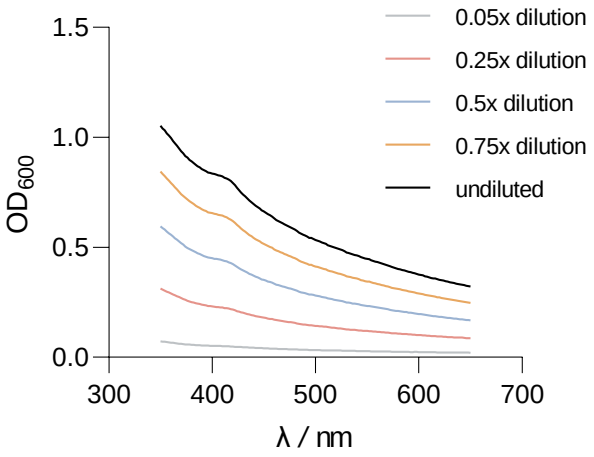

Figure S3. Optical density (350 nm - 650 nm range) of *N. europaea* in NaPB (pH 7.5) at different dilutions of a bacterial subculture (0.75x dilution, 0.5x dilution, 0.25x dilution, 0.05x dilution; see section 1.2(b) in Results and Discussion). All spectra were corrected by subtracting the spectrum of NaPB.

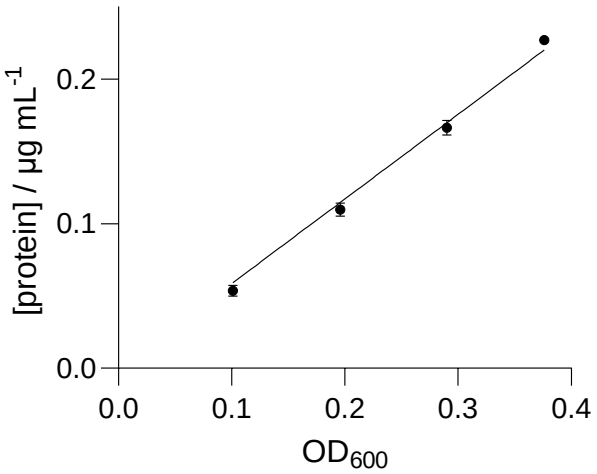

Figure S4. Optical density of *N. europaea* in NaPB (pH 7.5) at 600 nm as a function of protein concentration (determined with a BSA protein assay) using different dilutions of a bacterial subculture: 0.75x dilution, 0.5x dilution, 0.25x dilution, 0.05x dilution; see section 1.2(b) in Results and Discussion). All spectra were corrected by subtracting the spectrum of NaPB. SE are calculated from triplicates.

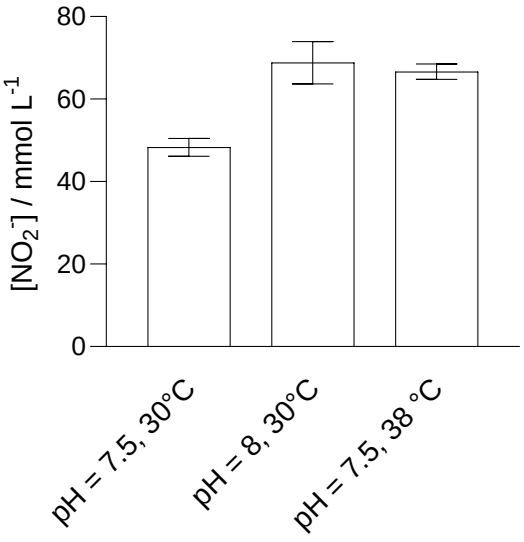

Figure S5. NO_2^- production by *N. europaea* in NaPB at different pH and temperatures, following the *Standard Bioassay Endpoint Procedure* protocol. Standard errors are calculated from triplicates.

Table S1. NO_2^- production after inoculating *N. europaea* (OD_{600} = 0.03) with different $[NH_4^+]$.[a]

$[NH_4^+]$ / mmol L^{-1}	$[NO_2^-]$ / µmol L^{-1}		
	Replicate 1	Replicate 2	Replicate 3
3	41. 6	45.5	41.6
0.3	11.3	11.6	13.0
0.03	7.0	6.3	9.8

[a] According to the *Standard Bioassay Endpoint Procedure* protocol, using $(NH_4)_2SO_4$ as source of NH_4^+.

Table S2. NO_2^- production after inoculating *N. multiformis* (OD_{600} = 0.03) with $[NH_4^+]$.[a]

$[NH_4^+]$ / mmol L^{-1}	$[NO_2^-]$ / µmol L^{-1}		
	Replicate 1	Replicate 2	Replicate 3
3	60.9	60.6	61.5

[a] According to the *Standard Bioassay Endpoint Procedure* protocol, using $(NH_4)_2SO_4$ as source of NH_4^+.

Table S3. Absorbance intensity (at 282 nm) of a solution of Inhibitor 4 (0.3 mmol L^{-1}) in NaPB (pH 7.5) with different amounts of DMSO as co-solvent 0.1 v/v% and 1.0 v.v%.

Solvent System	Absorbance Intensity		
	Replicate 1	Replicate 2	Replicate 3
0.1 v/v% DMSO in NaPB	0.41	0.96	0.80
1 v/v% DMSO in NaPB	0.33	0.35	0.33

Table S4. Correlation between the OD_{600} and formation of NO_2^- during culturing of *N. europaea* in mineral salts media over three days.

Day	OD_{600}	$[NO_2^-]$ / µmol L^{-1}
0	0.00041	20.7
1	0.00272	41.6
2	0.00553	344.0
3	0.01123	807.0

Table S5. Inhibition of NO_2^- formation after inoculating *N. europaea* (OD_{600} = 0.03) with inhibitor compounds 1-16.[a]

Compound	Inhibition / %		
	Replicate 1	Replicate 2	Replicate 3
Inhibitor 1	14.4	10.0	8.8
Inhibitor 2	19.9	9.6	14.9
Inhibitor 3	24.6	41.4	28.9
Inhibitor 4	96.8	84.7	96.8
Inhibitor 5	6.8	7.9	12.5
Inhibitor 6	33.6	35.4	55.5
Inhibitor 7	26.8	46.7	27.8
Inhibitor 8	71.0	58.8	70.2
Inhibitor 9	NI	12.8	9.3
Inhibitor 10	NI	6.9	4.4
Inhibitor 11	95.8	75.0	95.8
Inhibitor 12	84.3	72.8	84.3
Inhibitor 13	NI	17.3	NI
Inhibitor 14	10.4	NI	10.4
Inhibitor 15	27.2	28.1	37.5
Inhibitor 16	35.4	29.7	35.9

[a] Calculated using equation 1; experiment performed according to the *Standard Bioassay Endpoint Procedure* protocol, using $(NH_4)_2SO_4$ as source of NH_4^+. NI: Inhibition < 1%.

Table S6. Inhibition of NO_2^- formation after inoculating *N. multiformis* (OD_{600} = 0.03) with selected inhibitor compounds.[a]

Compound	Inhibition / %		
	Replicate 1	Replicate 2	Replicate 3
Inhibitor 4	28	67	55
Inhibitor 8	29	38	28
Inhibitor 11	27	55	46
Inhibitor 12	6	32	28

[a] Calculated using equation 1; experiment performed according to the *Standard Bioassay Endpoint Procedure* protocol, using $(NH_4)_2SO_4$ as source of NH_4^+.

3. References

1. Li, S.; Yufang, L.; Fangwei, Y.; Herbert, J. K.; Weiming, S. Biological nitrification inhibition by rice root exudates and its relationship with nitrogen-use efficiency. *The New Phytologist* **2016**, *212* (3), 646-656. (acccessed 2022/05/22/).JSTOR.
2. Wright, C. L.; Schatteman, A.; Crombie, A. T.; Murrell, J. C.; Lehtovirta-Morley, L. E.; Stams, A. J. M. Inhibition of Ammonia Monooxygenase from Ammonia-Oxidizing Archaea by Linear and Aromatic Alkynes. *Applied and Environmental Microbiology* **2020**, *86* (9), e02388-02319. DOI: doi:10.1128/AEM.02388-19.

Supporting Information 2 (SI-2)

Assessing the Efficacy, Acute Toxicity and Binding Mode of the Agricultural Nitrification Inhibitors 3,4-Dimethyl Pyrazole (DMP) and Dicyandiamide (DCD) With *Nitrosomonas europaea*

Sibel C. Yildirim,[a] Robert Walker,[b] Ute Roessner,[b,c] Uta Wille*[a]

[a]School of Chemistry, The University of Melbourne, Parkville, Victoria 3010, Australia.
[b]School of BioSciences, The University of Melbourne, Parkville, Victoria 3010, Australia.
[c]Research School of Biology, The Australian National University, Acton, Australian Capital Territory 2600, Australia.

Email: uwille@unimelb.edu.au

1. Additional Supplementary Tables

Table S1. Cumulative NO_2^- production of *N. europaea* with ammonium (NH_4^+) in the absence and presence of DMP and DCD over three cumulative 30-min intervalls (STE n = 3).

Treatment	$[NO_2^-]$ / µM		
	after 30 min	after 60 min	after 90 min
untreated cells[a]	2.3 ± 0.0	2.9 ± 0.1	2.8 ± 0.25
uninhibited cells[b]	17.7 ± 1.0	60.0 ± 1.6	95.9 ± 0.5
DMP 0.3 mM	2.9 ± 0.3	7.0 ± 0.2	9.7 ± 0.3
DMP 0.03 mM	4.9 ± 0.3	17.1 ± 0.4	22.7 ± 0.3
DCD 0.3 mM	8.3 ± 0.7	28.2 ± 1.0	38.6 ± 0.5
DCD 0.03 mM	14.8 ± 0.9	54.3 ± 2.3	85.3 ± 1.7

[a]0% signal; without NH_4^+ and inhibitor. [b] 100% signal; $[NH_4^+]$ = 3 mM, without inhibitor.

Table S2. Cumulative NO_2^- production of *N. europaea* with hydroxylamine (H_2NOH) in the absence and presence of DMP and DCD over three consecutive 30-min intervalls (STE n = 3).

Treatment	$[NO_2^-]$ / µM		
	after 30 min	after 60 min	after 90 min
untreated cells[a]	4.0 ± 0.4	4.7 ± 0.5	4.7 ± 0.5
uninhibited cells[b]	24.3 ± 2.6	74.5 ± 2.8	96.9 ± 3.6
DMP 0.3 mM	21.7 ± 1.0	59.8 ± 2.3	71.4 ± 4.9
DMP 0.03 mM	22.4 ± 1.6	68.2 ± 3.6	90.1 ± 7.2
DCD 0.3 mM	24.6 ± 1.2	75.0 ± 2.3	99.4 ± 4.1
DCD 0.03 mM	24.7 ± 2.0	72.2 ± 1.6	94.0 ± 4.7

[a]0% signal; without NH_4^+ and inhibitor. [b] 100% signal; [H_2NOH] = 3 mM, without inhibitor.

Table S3. Rate coefficients, *k*, for the time-dependent O_2 consumption by *N. europaea* in the absence of [NI]. [a]

k / µmol L^{-1} s^{-1}		
0.142	0.079	0.127
0.155	0.122	0.121
0.158	0.155	0.132
0.180	0.162	0.131
0.256	0.299	0.212
0.256	0.197	0.277
0.238	0.113	0.221
0.291	0.253	0.276

[a]The *k*-value was determined from the linear regression of [O_2] against the time between 15 – 300 s (R^2 > 0.95). The experiment was conducted with [NH_4^+] = 3.0 mM in NaPB (pH = 7.5) at 20°C under constant stirring in the dark.

Table S4. Rate coefficients, *k*, for the time-dependent O_2 consumption by *N. europaea* in the presence of DMP and DCD at different concentrations.[a]

[DMP] / mM	*k* / µmol L^{-1} s^{-1}		
	Replicate 1	Replicate 2	Replicate 3
1.2	0.057	0.054	0.054
0.6	0.069	0.05	0.071
0.12	outlier	0.059	0.035
0.012	0.3003	0.2625	0.3192
[DCD] / mM	***k* / µmol L^{-1} s^{-1}**		
	Replicate 1	Replicate 2	Replicate 3
10	0.037	0.028	0.050
5.0	0.079	0.058	0.065
2.0	0.123	0.120	0.092
1.2	0.119	0.141	0.142

[a]The *k*-value was determined from the linear regression of $[O_2]$ against the time between 315 – 490 s ($R^2 > 0.95$). The experiment was conducted with $[NH_4^+]$ = 3.0 mM in NaPB (pH = 7.5) at 20°C under constant stirring in the dark.

Table S4 Number of cells alive and cells dead of *N. europaea* determined without and with treatment of DMP and DCD at different concentrations determined with a bacterial viability stain.[a]

No inhibitor	**Number of cells alive**	**Number of cells dead**
Image 1	652	23
Image 2	643	29
Image 3	627	35
Image 4	637	51
Image 5	677	38
Image 6	720	12
Image 7	619	71

DMP (10 ppm)		
Image 1	727	222
Image 2	676	222
Image 3	675	49
Image 4	768	7
Image 5	696	51
Image 6	689	29
Image 7	749	12
DMP (100 ppm)		
Image 1	534	89
Image 2	574	255
Image 3	568	277
Image 4	588	297
Image 5	596	319
Image 6	549	253
Image 7	609	134
DMP (1000 ppm)		
Image 1	602	318
Image 2	845	411
Image 3	628	271
Image 4	638	242
Image 5	598	361

Image 6	615	421
Image 7	563	416
DCD (10 ppm)		
Image 1	474	40
Image 2	525	55
Image 3	557	63
Image 4	499	61
Image 5	431	21
Image 6	472	114
Image 7	421	35
DCD (100 ppm)		
Image 1	489	414
Image 2	535	324
Image 3	709	51
Image 4	632	29
Image 5	822	134
Image 6	549	253
Image 7	609	134
DCD (1000 ppm)		
Image 1	450	49
Image 2	446	66
Image 3	403	85

Image 4	462	215
Image 5	412	185
Image 6	408	204
Image 7	429	319

[a]The incubations were performed in NaPB (pH = 7.5) and 30°C with [NH_4^+] = 3 mM, [inhibitor] = 10 ppm (0.015 mM), 100 ppm (0.15 mM) and 1000 ppm (1.5 mM) at 100 rpm for 12 h in the dark. Seven images were taken per treatment with a fluorescent microscope (Leica DM6000, Germany) using the red filter setting to detect dead cells (excitation: 575/30 nm (dichromatic) DC: 600; emission: 635/40 nm) and the green channel to detect live cells using filter setting (excitation: 500/20 nm DC: 515; emission: 535/30 nm).

2. Additional Supplementary Figures

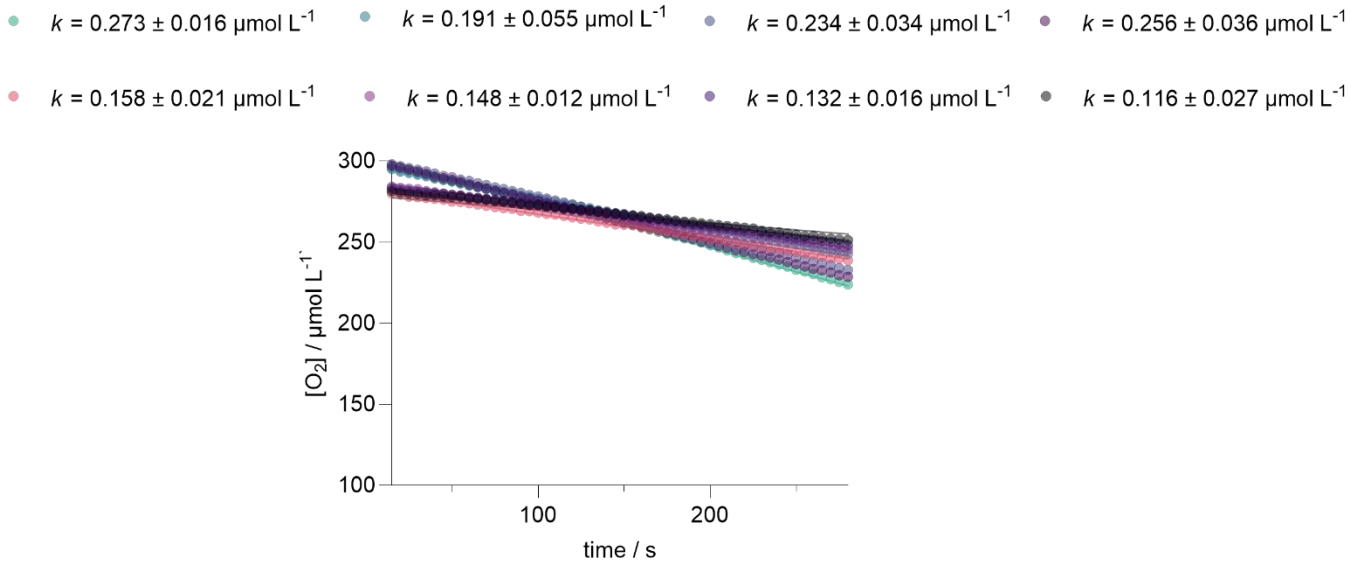

Figure S1. The trace of uninhibited O_2 consumption by *N. europaea* as a function of time after the addition [NH_4^+] = 3.0 mM in NaPB (pH = 7.5) at 20°C under constant stirring in the dark. Note that the average of three measurements were combined in one trace for clarity. Details of the individual *k* values are listed in table S3. The rate coefficient *k* was obained from linear regression of each trace. The mean rate coefficient *k* of 24 measurements was calculated and referred as 'uninhibited rate coefficient'.

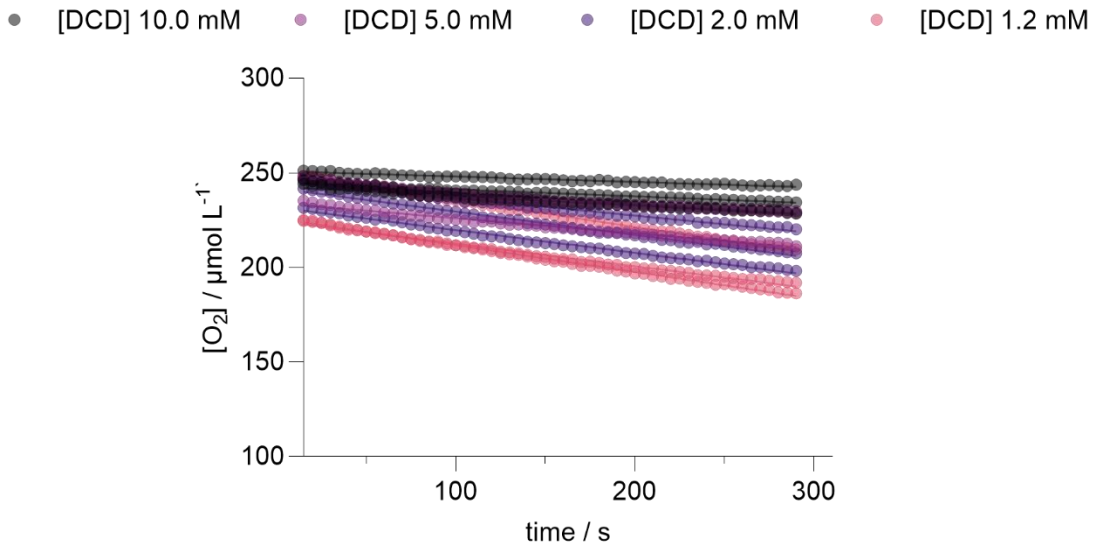

Figure S2. O_2 consumption by *N. europaea* as a function of time after the addition of DMP at different concentrations. Experiments were conducted with [NH_4^+] = 3.0 mM in NaPB (pH = 7.5) at 20°C under constant stirring in the dark. Each treatment was performed with three replicates. The rate coefficient *k* (Table 3 in paper) was obained from the mean value for each treatment.

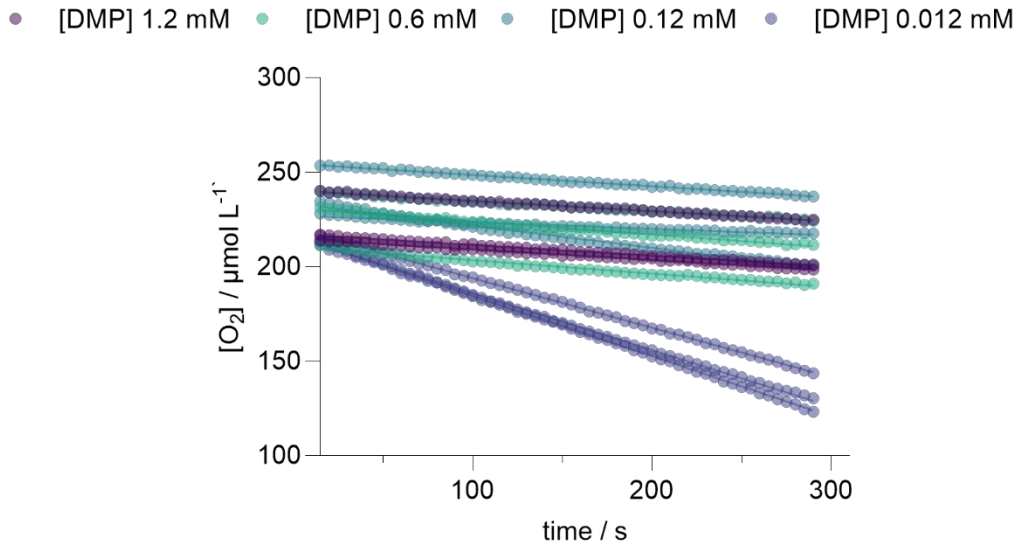

Figure S3. O_2 consumption by *N. europaea* as a function of time after the addition of DMP at different concentrations. Experiments were conducted with [NH_4^+] = 3.0 mM in NaPB (pH = 7.5) at 20°C under constant stirring in the dark. Each treatment was performed with three replicates. The rate coefficient *k* (Table 3 in paper) was obained from the mean value for each treatment.

Supporting Information 3 (SI-3)

Insights into the Efficacy and Binding Mode of 1,4-Substituted 1,2,3-Triazoles - A New Class of Agricultural Nitrification Inhibitors

Sibel C. Yildirim,[a] Bethany I. Taggert, [a] Robert Walker,[b] Michelle Watt,[b] Ute Roessner,[b,c] Uta Wille*[a]

[a]School of Chemistry, The University of Melbourne, Parkville, Victoria 3010, Australia
[b]School of BioSciences, The University of Melbourne, Parkville, Victoria 3010, Australia.
[c]Research School of Biology, The Australian National University, Acton, Australian Capital Territory 2600, Australia.

Email: uwille@unimelb.edu.au

1. Additional Material and Methods

1.1 Cell Preparation

1.1.1 Growing *N. europaea* Protocol

AOB were grown for 3 – 5 d in Duran glass bottles containing 600 mL of mineral salts media (MSM, see below) at 100 rpm and 30°C in the dark. The slightly loose cap was sealed with an O_2 permeable membrane to ensure aeration (Breathe-Easy® sealing membrane, Sigma Aldrich). The MSM constituted the main bulk medium and consisted of dipotassium hydrogen phosphate (K_2HPO_4; 2.27 g L^{-1}), potassium dihydrogen phosphate (KH_2PO_4; 0.95 g L^{-1}) and ammonium sulphate ($(NH_4)_2SO_4$; 0.67 g L^{-1}). The pH was adjusted to 7.0. To 1 L of the bulk medium 2 mL of a filter sterilized (0.2 µm millipore filter) solution of metals was added: disodium ethylenediamine tetraacetate (Na_2EDTA; 6.37 g L^{-1}), zinc sulphate heptahydrate ($ZnSO_4$ x 7 H_2O; 1.0 g L^{-1}), calcium chloride dihydrate ($CaCl_2$ x 2 H_2O; 0.5 g L^{-1}), iron(II) sulphate heptahydrate ($FeSO_4$ x 7 H_2O; 2.5 g L^{-1}), sodium molybdate dihydrate ($NaMoO_4$ x 2 H_2O; 0.1 g L^{-1}), copper(II) sulphate pentahydrate ($CuSO_4$ x 5 H_2O; 0.1 g L^{-1}), cobalt(II) chloride hexahydrate ($CoCl_2$ x 6 H_2O; 0.2 g L^{-1}), manganese(II) sulphate monohydrate ($MnSO_4$ x H_2O;

0.52 g L^{-1}) and magnesium sulphate heptahydrate ($MgSO_4$ x 7 H_2O; 60.0 g L^{-1}). To this media solution 1v/v% of aqueous sodium carbonate (Na_2CO_3; 50 g L^{-1}) was added aseptically as a carbon source.

1.1.2 Harvesting Cells Protocol

After 3 - 5 d of incubation, the turbid cultures were harvested at an OD_{600} of approximately 0.1, which represented the mid-exponential growth phase and an NO_2^- production of approximately 800 µM (determined by Griess assay), cells were harvested by filtration onto 0.2 µm membrane filters (Rowe Scientific, mixed cellulose esters (MCE)). The cells were washed with sodium phosphate buffer (NaPB, pH = 7.5, 0.1 M, 2 x 100 mL) containing $MgSO_4$ (0.2 mM). The filter paper with the cells was transferred into a sterile 50 mL tube, and the cells were washed off by resuspending in NaPB (15 mL), followed by 5 s of vortexing (Ratek, Australia) and 3 s of sonication (Vevor, Australia). The initial inoculum OD_{600}, which was between 0.9 – 1.2, was adjusted to a final OD_{600} of 0.03 and stored at 4°C until used for the assay. Cells could be stored for up to 24 h without losing activity.

1.2 Nitrification Assay and Analysis

1.2.1 Standard Assay Protocol

In a deep 96-well plate (2 mL capacity), 980 µL of the bacterial inoculum (OD_{600} = 0.03 in NaPB at pH 7.5) was added to the inhibitor (10 µL of a 30 mmol L^{-1} or 3 mmol L^{-1} stock solution in DMSO, respectively), the solutions were mixed thoroughly and pre-incubated in the dark for 5 min at 30°C and 100 rpm (Ratek, Australia). $(NH_4)_2SO_4$ (10 µL, 150 mM, from a sterile solution containing 19.8 g L^{-1} of $(NH_4)_2SO_4$ in DMSO) was then added. In experiments in which the NH_2OH-dependent activity was measured, $(NH_4)_2SO_4$ was replaced by equimolar amounts of NH_2OH. The plate was covered with an O_2 permeable membrane to ensure aeration (Breathe-Easy® sealing membrane, Sigma Aldrich) and incubated in the dark for 30, 60 or 90 min at 30°C and 100 rpm. The nitrification process was stopped by adding an excess of DMP (10 µmol L^{-1}, 30 mM; the final concentration of DMP in the solution was 0.27 mM, which was considerably higher than the IC_{50abs} value of 6.6 mM determined previously).[38] An aliquot of the reaction solution (50 µL) was transferred to a 96-well spectrophotometric plate (Greiner Cellstar®, polystyrene) to which 50 µL of Griess reagent was added. The color was allowed to develop for 15 min at room temperature, and the absorbance was measured at

540 nm (Clariostar® BMG Labtech, Australia). Each assay was accompanied by control treatments to determine the 0% and 100% NO_2^- signal. The percentage inhibition was calculated according to eqn. SI-1 from the NO_2^- production of the cells in NaPB with (i) without additive ("untreated cells"; 0% signal), (ii) with $[NH_4^+]$ = 3 mM ("uninhibited cells"; 100% signal) and (iii) with $[NH_4^+]$ = 3 mM and [inhibitor] = 0.3 mM (10 mol% of $[NH_4^+]$; "inhibited cells").

$$\% \text{ Inhibition} = \left[1 - \frac{[NO_2^-]_{\text{inhibited cells}} - [NO_2^-]_{\text{untreated cells}}}{[NO_2^-]_{\text{uninhibited cells}} - [NO_2^-]_{\text{untreated cells}}} \right] \times 100 \quad \text{(eqn. SI-1)}$$

1.2.2 Activity Recovery Assay

Cells were harvested using the 'Harvesting Cells Protocol'. The bacteria solution was adjusted to OD_{600} = 0.8 (~ 468 µg L^{-1} protein), and 980 µL aliquots were transferred to 1.5 mL centrifuge tubes (Eppendorf®, polypropylene). The inhibitor (10 µL of a stock solution of 150 mM in DMSO) was added, and after equilibrating for 5 min $(NH_4)_2SO_4$ (10 µL of a stock solution of 150 mM in Milli-Q water) was added using a multichannel pipette to ensure simultaneous addition in each tube. The tubes were incubated in a temperature-regulated rotary incubator (Ratek, Australia) for 30 min at 30°C and 100 rpm in the dark. A 50 µL aliquot was then transferred to a 96-well plate (Greiner Cellstar®, polystyrene) to which 50 µL of Griess reagent was added and the mixture incubated for 15 min. The absorbance was measured at 540 nm (Clariostar® BMG Labtech, Australia). The remaining cells were subsequently washed (3x) by alternating centrifuging (Boeco, Germany; 10,000 rpm, 10 min) and resuspending the cell pellet in NaPB (1 mL). After the final centrifuging step, the pellet was resuspended in NaPB (990 µL) and re-incubated with $(NH_4)_2SO_4$ (10 µL of an aqueous 150 mM stock solution, see above). The percentage activity ('%activity') was calculated according to eqn. SI-2 from the NO_2^- production of the cells in NaPB with (i) without additive ("untreated cells"; 0% signal), (ii) with $[NH_4^+]$ = 3 mM ("uninhibited cells"; 100% signal) and (iii) with $[NH_4^+]$ = 3 mM and [inhibitor] = 1.5 mM (50 mol% of $[NH_4^+]$; "inhibited cells"). All experiments were performed in triplicate.

$$\% \text{ Activity} = \left[\frac{[NO_2^-]_{\text{inhibited cells}} - [NO_2^-]_{\text{untreated cells}}}{[NO_2^-]_{\text{uninhibited cells}} - [NO_2^-]_{\text{untreated cells}}} \right] \times 100 \quad \text{(eqn. SI-2)}$$

1.2.3 Michaelis-Menten Kinetics

In a deep 96-well plate (2 mL capacity), 980 µL of the bacterial inoculum (OD_{600} = 0.03, ~ 18 µg L^{-1} protein in NaPB at pH 7.5) was added to 1, 2, 4 and 5 (10 µL from 15 mM and 30 mM stock solutions, respectively). The solutions were mixed thoroughly and pre-incubated in the dark for 5 min at 100 rpm and at 30°C (Ratek, Australia). 10 µL of the respective $(NH_4)_2SO_4$ stock solution (0.3 mM, 3 mM, 5mM, 10 mM, 150 mM, 300 mM, 1 M, 1.5 M and 3M) was added to each well (final $[NH_4^+]$ in well: 0.003 mM, 0.03 mM, 0.05 mM, 0.1 mM, 1.5 mM, 3.0 mM, 10 mM, 15 mM, and 30 mM). The plate was covered with an O_2 permeable membrane to ensure aeration (Breathe-Easy® sealing membrane, Sigma Aldrich) and incubated in the dark for 60 min at 30°C and 100 rpm. Termination of the nitrification process and determination of the NO_2^- production was performed as described in 'Standard Assay Protocol'. Data analysis was performed with GraphPad Prism software, using nonlinear regression (curve fit) for Michaelis Menten Kinetics. The results used the best fit values with 95% likelihood.

1.2.4 Acute Toxicity Test

Cells were harvested according to 'Harvesting Cells Protocol'. The bacteria solution was adjusted to OD_{600} = 0.8 (~ 468 µg L^{-1} protein) and divided into 1 mL aliquots. To each well of a 24-well tissue culture plate (Greiner Cellstar®, polystyrene Tissue Culture treated) was added 980 µL of bacterial solution, 10 µL of a 150 mM aqueous $(NH_4)_2SO_4$ solution and 10 µL compound 1 solution with a final concentration in the well of 100 ppm (0.15 mM) and 1000 ppm (1.5 mM), respectively. The well plate was sealed with an O_2 permeable membrane to ensure aeration (Breathe-Easy® sealing membrane, Sigma Aldrich) and incubated in the dark for 4 h at 30°C and 100 rpm. Cells were then transferred into a centrifuge tube and sedimented at 10,000 rpm for 10 minutes. The supernatant was separated, and the cells were re-suspended in NaPB (pH = 7.5, 1 mL). A 5 µL aliquot was transferred into a 96-well plate and the bacterial stain (LIVE/DEAD™ BacLight™ Bacterial Viability Kit for microscopy, ThermoFisher Scientific) was added following the manufacturer's instructions. 10 µL of the solution was transferred onto a microscopic slide (Fisher Scientific, Australia, microscope slides 7.6 cm x 2.5 cm (L x W), thickness 1 - 1.2 mm). Seven images were taken per treatment with a fluorescent microscope (Leica DM6000, Germany) using the red channel to detect dead cells (excitation: 575/30 nm (dichromatic) DC: 600; emission: 635/40 nm) and the green

channel to detect live cells (excitation: 500/20 nm DC: 515; emission: 535/30 nm). The percentage of live and dead cells was calculated via equations SI-3 and SI-4:

$$\% \text{ Live} = \frac{\text{Live cell count}}{\text{total cell count}} \times 100 \qquad \text{(eqn. SI-3)}$$

$$\% \text{ Dead} = \frac{\text{Dead cell count}}{\text{total cell count}} \times 100 \qquad \text{(eqn. SI-4)}$$

1.3 O_2 Consumption Measurements

O_2 consumption rates of cell suspensions of *N. europaea* were measured using a Clark-type oxygen electrode (Rank Brothers, Cambridge, UK) mounted in a water-jacketed electrode chamber (3 mL capacity) that was connected to a recirculating cooler (Lauda, Austria). The data were recorded using a Data-trax™ (World Precision Instruments, UK) sensor data collection system. All measurements were taken at 20°C and 1 mL final reaction solution volume. The polarizing voltage was set to 0.6 V. To calibrate the oxygen signal, an excess (approximately 50 mg) of $Na_2S_2O_4$ was added to 1 mL of Milli-Q water to chemically remove dissolved O_2. Additional O_2 flux was prevented by applying a stopper, and the residual voltage was referred to as "0% O_2". The voltage at saturated O_2 concentration ("100% O_2") was determined by measuring the voltage of the equilibrated aerated reaction system consisting of 1 mL Milli-Q water. Sample measurements were taken as follows: The 1 mL reaction mixture, composed of 980 µL *N. europaea* cell solution in NaPB (OD_{600} = 0.8; corresponding to approximately 468 µg L^{-1} protein) was equilibrated for 5 min in the chamber until the voltage reading was stable. The reaction was then initiated by the addition of $(NH_4)_2SO_4$ (10 µL of an aqueous 150 mM stock solution, the final concentration in the reaction solution was 3 mM) and the chamber immediately sealed with a stopper. After 5 min of oxygen consumption (a linear rate coefficient of approximately 0.24 ± 0.08 µmol O_2 L^{-1} s^{-1} was determined), 10 µL of the inhibitor stock solution of compounds 1, 4 and 5 (150 mM in DMSO) were added via a 10 µL Eppendorf pipette through a capillary opening, ensuring the emergence of the pipette tip in the solution. The voltage was recorded over a period of 5 min in intervals of 5 s. The trace describing the O_2 concentration after addition of $(NH_4)_2SO_4$ against the time (initial 15-300 s) was used as the baseline O_2 consumption for the uninhibited cells, whereas the trace describing the consumption in the presence of the

inhibitor (315-590 s time window) was used to determine the rate of O_2 consumption in the presence of inhibitor. All experiments were conducted in triplicate at 20°C under constant stirring. The voltage was converted to $[O_2]$ according to equation SI-5:[39]

$$[O_2]_t = \frac{\text{voltage (sample)}_t - \text{voltage (0\% } O_2)}{\text{voltage (100\% } O_2) - \text{voltage (0\% } O_2)} \times 280\ \mu M \qquad \text{(eqn. SI-5)}$$

1.4 Determination of $IC_{50(abs)}$ Values

The assay was performed according to the '3.1 Standard Assay Protocol' using *N. europaea* as AMO source. The tested concentration series differed depending on inhibitory efficiency. Compound **1** was tested at concentrations of: 6 mmol L^{-1}, 3 mmol L^{-1}, 3 mmol L^{-1}, 1.5 mmol L^{-1}, 0.75 mmol L^{-1}, 0.6 mmol L^{-1}, 0.15 mmol L^{-1}, 50 µmol L^{-1}, 25 µmol L^{-1} and 2.5 µmol. Compound **2** was tested at concentrations of: 9 mmol L^{-1}, 3 mmol L^{-1}, 1.5 mmol L^{-1}, 0.15 mmol L^{-1}, 50 µmol L^{-1}, 30 µmol L^{-1} and 3 µmol; compound **4** was tested at concentrations of: 9 mmol L^{-1}, 3 mmol L^{-1}, 1.5 mmol L^{-1}, 0.6 mmol L^{-1}, 0.15 mmol L^{-1}, 50 µmol L^{-1}, and 2.5 µmol and compound **5** was tested at concentrations of: 9 mmol L^{-1}, 3 mmol L^{-1}, 1.5 mmol L^{-1}, 0.6 mmol L^{-1}, 0.15 mmol L^{-1}, 50 µmol L^{-1}, and 2.5 µmol. The inhibitor concentration at which the inhibition was 50 % ($IC_{50(abs)}$) was determined by fitting the $\log_{10}$ of the concentration (in µmol L^{-1}) against the response. $IC_{50(abs)}$ was obtained by normalising the response against cells in NaPB with 1v/v% DMSO and $[NH_4^+]$ = 3 mM ('uninhibited' cells; 100% signal) and cells in NaPB with 1v/v% DMSO without additive ('untreated cells'; 0% signal). The curves were plotted with GraphPad prism (version 9.5.0) to determine $IC_{50(abs)}$ via variable slope fit (three parameters).

2. Additional Supplementary Figures and Tables

Table S1. Inhibition of AMO: NO_2^- formation after inoculating *N. europaea* (OD_{600} = 0.03) with inhibitor compounds **1**-**5**.[a]

Compound	Inhibition / %		
	Replicate 1	Replicate 2	Replicate 3
1	96	99	98
2	67	69	65
3	13	14	6
4	80	81	76
5	63	62	69

[a] Calculated using equation SI-1; experiment performed according to the *Standard Assay* protocol, using $(NH_4)_2SO_4$ as N-source.

Table S2. Inhibition of HAO: NO_2^- formation after inoculating *N. europaea* (OD_{600} = 0.03) with inhibitor compounds **1**-**5**.[a]

Compound	Inhibition / %		
	Replicate 1	Replicate 2	Replicate 3
1	25	51	34
2	5	16	11
3	< 1%	< 1%	< 1%
4	8	14	13
5	< 1%	< 1%	3

[a] Calculated using equation SI-1; experiment performed according to the *Standard Assay* protocol, using NH_2OH as N-source.

Table S3. Inhibition of AMO: NO_2^- formation after inoculating *N. europaea* (OD_{600} = 0.03) with inhibitor compounds **1**-**5**.[a]

Compound	Inhibition / %		
	Replicate 1	Replicate 2	Replicate 3
1	28	34	23
2	45	49	46
3	< 1%	< 1%	< 1%
4	41	56	30
5	20	32	14

[a] Calculated using equation SI-1; experiment performed according to the *Standard Assay* protocol, using $(NH_4)_2SO_4$ as N-source.

Table S4. Inhibition of HAO: NO_2^- formation after inoculating *N. europaea* (OD_{600} = 0.03) with inhibitor compounds **1**-**5**.[a]

Compound	Inhibition / %		
	Replicate 1	Replicate 2	Replicate 3
1	38	62	39
2	9	22	16
3	< 1%	< 1%	< 1%
4	12	16	25
5	< 1%	< 1%	18

[a] Calculated using equation SI-1; experiment performed according to the *Standard Assay* protocol, using NH_2OH as N-source.

Table S5. Predicted log $P_{oct/wat}$ values of substituted 1,2,3-triazoles. [1]

Compound	Structure	log $P_{oct/wat}$
1	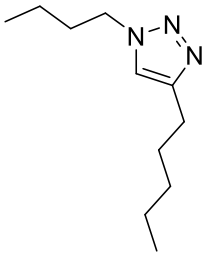	3.5
2	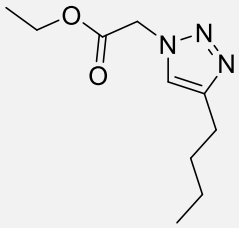	1.7
3	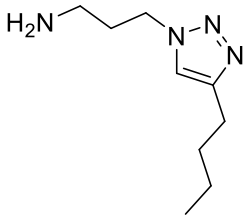	1.2
4	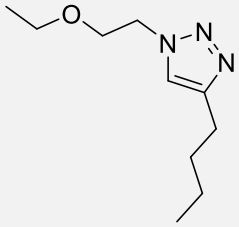	1.8
5	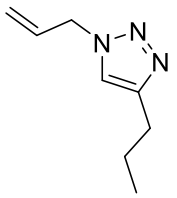	N/A

6	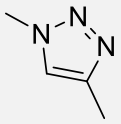	0.2
7	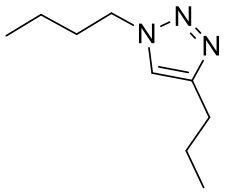	1.8
8	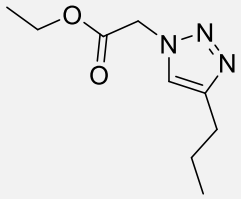	1.1

Table S6. %Inhibition of AMO in dependence of log $P_{oct/wat}$ of inhibitor compounds **6**, **7** and **8** determined via NO_2^- formation using *N. europaea* (OD_{600} = 0.03).[a]

Compound	**Inhibition / %**		
	Replicate 1	Replicate 2	Replicate 3
6	11	2	15
7	56	62	61
8	13	6	4

[a] Calculated using equation SI-1; experiment performed according to the *Standard Assay* protocol, using $(NH_4)_2SO_4$ as N-source.

Table S7. Rate coefficients, k_{obs}, and R^2 values of the linar regression for the O_2 consumption by *N. europaea* in the absence and presence of NI.[a]

Compound		k_{obs} / x 10^{-3} µmol L^{-1} s^{-1} uninhibited	R^2	k_{obs} / x 10^{-3} µmol L^{-1} s^{-1} after inhibition	R^2
1	run 1	143.4	0.96	0.038	0.94
	run 2	118.4	0.98	0.024	0.80
	run 3	129.5	0.97	0.025	0.90
4	run 1	0.333	0.99	0.253	0.99
	run 2	0.359	0.99	0.213	0.99
	run 3	0.193	0.99	0.130	0.99
5	run 1	0.333	0.99	0.178	0.99
	run 2	0.359	0.99	0.209	0.99
	run 3	0.357	0.99	0.193	0.99

Table S8. Fraction of the activity of inhibited AMO, using pure cell cultures of *N*. *europaea*, and after removal of the NI through repeated washing with NaPB.[a]

Compound	% activity inhibited cells	% activity after washing
-		
1	3 ± 1	75 ± 5
2	31 ± 8	82 ± 5
4	10 ± 5	82 ± 2
5	43 ± 7	79 ± 8

[a] The inoculations were performed with [NH_4^+] = 3.0 mM and [NI] = 1.5 mM in NaPB (pH = 7.5) at 30°C and 100 rpm in the dark. The %activity was determined according to eqn. SI-2. Standard errors were calculated from three biological replicates, each performed with three technical replicates

Table S9. Concentration-dependent fraction of the activity of inhibited AMO with compound 1, using pure cell cultures of *N*. *europaea*, and after removal of the NI through repeated washing with NaPB.[a]

Compound	% activity inhibited cells	% activity after washing
1 [0.6 mM]	28 ± 1	100 ± 1
1 [0.75 mM]	20 ± 1	99 ± 4
1 [1.5 mM]	9 ± 1	94 ± 1

[a] The inoculations were performed with [NH_4^+] = 3.0 mM and [NI] = 1.5 mM in NaPB (pH = 7.5) at 30°C and 100 rpm in the dark. Standard errors were calculated from one biological replicates performed with three technical replicates.

Table S10 Number of cells alive and cells dead of *N. europaea* determined without and with treatment of compound **1** at different concentrations determined with a bacterial viability stain.[a]

Conditions	Number of cells alive	Number of cells dead
No inhibitor		
Image 1	605	144
Image 2	687	102
Image 3	680	82
Image 4	774	119
Image 5	775	137
Image 6	752	134
Image 7	758	281
Compound 1 (100 ppm)		
Image 1	584	224
Image 2	574	421
Image 3	443	107
Image 4	583	77
Image 5	704	165
Image 6	536	57
Image 7	653	111
Compound 1 (1000 ppm)		
Image 1	510	100
Image 2	591	160
Image 3	605	198
Image 4	531	144
Image 5	539	119
Image 6	538	157
Image 7	609	290

[a] The incubations were performed in NaPB (pH = 7.5) and 30°C with [NH_4^+] = 3 mM, [inhibitor] = 100 ppm (0.15 mM) and 1000 ppm (1.5 mM) at 100 rpm for 12 h in the dark. Seven images were taken per treatment with a fluorescent microscope (Leica DM6000, Germany) using the red filter setting to detect dead cells (excitation: 575/30 nm (dichromatic) DC: 600; emission: 635/40 nm) and the green channel to detect live cells using filter setting (excitation: 500/20 nm DC: 515; emission: 535/30 nm).

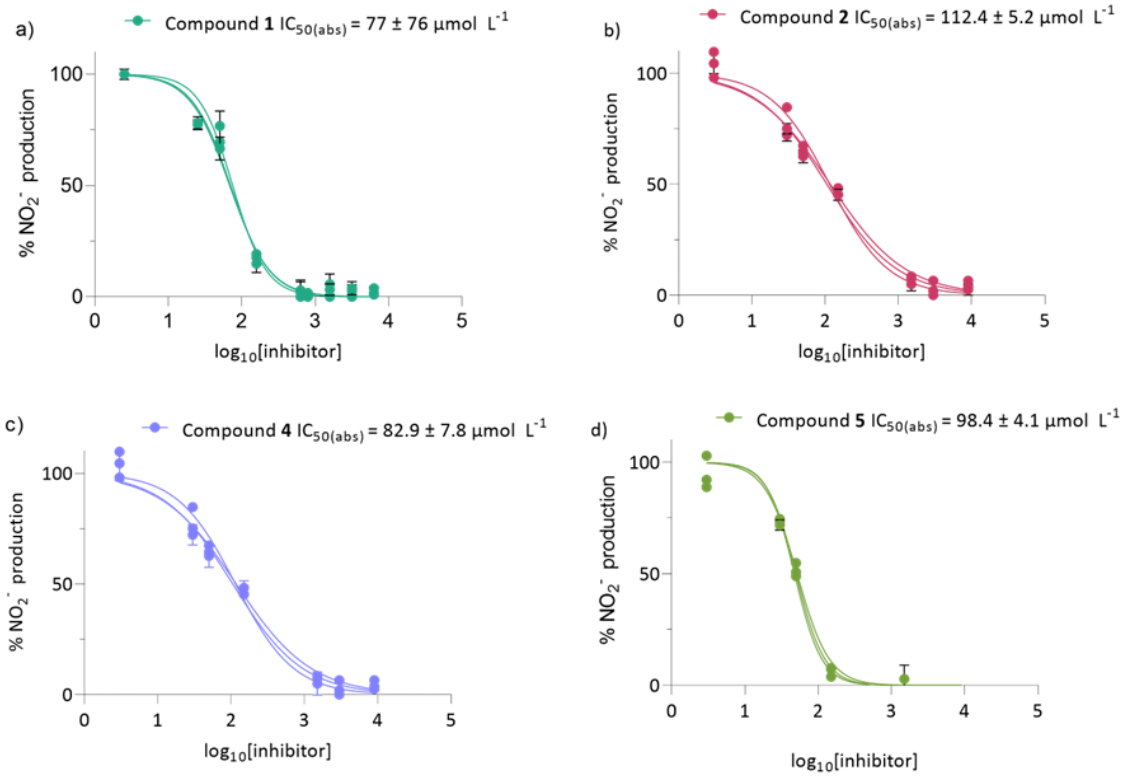

Figure S1. Function of the %NO_2^- production against the logarithmic concentration of compound a) **1**; b) **2**, c) **4**; and d) **5** and the obtained $IC_{50(abs)}$ values. Compounds **1**-**5** were used in the mmol L^{-1} concentration range. Standard errors were determined from three biological with each three technical replicates.

3. References

1. Elsevier *Reaxys,* https://www.reaxys.com, (accessed 24.01.2023).

Supporting Information 4 (SI-4)

4-Methyl-1-(Prop-2-yn-1yl)-1*H*-1,2,3-Triazole (MPT): A Novel, Readily Accessible and Highly Efficient Nitrification Inhibitor for Agriculture

Sibel C. Yildirim,[a,b,c] Joses G. Nathanael,[a] Katharina Frindte,[b] Otávio dos Anjos Leal,[c] Robert M. Walker,[d] Ute Roessner,[d,e] Claudia Knief,[b] Nicolas Brüggemann,[c] Uta Wille*[a]

[a]School of Chemistry, The University of Melbourne, Parkville, Victoria 3010, Australia.

[b]Universität Bonn, Institut für Nutzpflanzenwissenschaften und Ressourcenschutz, 53115 Bonn, Germany

[c]Forschungszentrum Jülich GmbH, Institute of Bio- and Geosciences, Agrosphere, 52428 Jülich, Germany

[d]School of BioSciences, The University of Melbourne, Parkville, Victoria 3010, Australia.

[e]Research School of Biology, The Australian National University, Acton, Australian Capital Territory 2600, Australia.

Corresponding author:

Uta Wille

Email: uwille@unimelb.edu.au

1. Synthesis of MPT and H-MPT

1.1 General Information

The compounds NI-1-3 (Table 1) were provided by Taggert *et al*. [1] and synthesised by copper(I)-catalysed azide alkyne cycloaddition (CuAAC).

Reaction progress was monitored by thin-layer chromatography (TLC) using silica gel 60 aluminium-backed plates coated with fluorescent indicator F254 (Merck). Plates were visualised using a potassium permanganate-based stain. Purification by silica gel chromatography was performed using Davisil Chromatographic Silica Media LC60A 40–63 micron, with solvent systems as specified. All ^{1}H and ^{13}C NMR spectra were recorded on a 500 MHz spectrometer (Agilent, USA) at 500 MHz or 126 MHz, respectively, using solvent resonances as the internal standard (^{1}H NMR: $CDCl_3$ at 7.26 ppm; ^{13}C NMR: $CDCl_3$ at 77.0 ppm). Chemical shifts are reported in parts per million (ppm, δ), with the splitting patterns indicated as follows: s, singlet; d, doublet; t, triplet; q, quartet; p, pentet; h, hextet; m, multiplet; dd, doublet of doublets. The coupling constants, *J*, are reported in Hertz (Hz). Electrospray ionization high resolution mass spectrometry (HRMS) was performed on a Thermo Scientific Exactive Plus Orbitrap mass spectrometer (Thermo, Bremen, Germany) operated in positive mode.

a. Synthesis of 4-methyl-1-(prop-2-yn-1yl)-1*H*-1,2,3-triazole (MPT) [2]

1-Dimethoxypropan-2-one (250 mg, 2.20 mmol, 1.0 equiv.) in methanol (5 mL) and 4-methylbenzenesulfonohydrazide (388 mg, 2.08 mmol, 1 equiv.) were reacted in a 10 mL microwave tube (Biotage®, Sweden). After complete consumption of the starting material, propargylamine (129 mg, 2.29 mmol, 1.1 equiv) and triethylamine (232 mg, 2.30 mmol, 1.1 equiv) were added and the tube sealed. After microwaving for 20 minutes at 120 °C and cooling to room temperature, the reaction mixture was concentrated *in vacuo* to give an orange oil. The crude oil was dissolved in DCM : water (1:1), the phases separated, and the aqueous layer was extracted three times with DCM. The combined organic fractions were washed with brine, dried over Na_2SO_4, concentrated *in vacuo* and purified by flash column chromatography (EtOAc: petroleum spirits (1:1)) to yield MPT as a yellow oil (85%). ^{1}H NMR (500 MHz, $CDCl_3$) δ 7.49 (s, 1H, triazole-H), 5.10 (d, *J* = 2.6 Hz, 2H, aliphatic-H), 2.53 (t, *J* = 2.6 Hz, 1H, alkyne-H), 2.33 (s, 3H, aliphatic-H). ^{13}C {^{1}H} NMR (126 MHz, $CDCl_3$) δ 143.8 (aromatic-

C), 120.9 (aromatic-C), 76.1 (broad, 2C, alkyne-C), 39.6 (aliphatic-C), 10.8 (aliphatic-C). ESI-HRMS calculated for $C_6H_8N_3^+$ ([M+H]$^+$): *m/z* 122.0713; found *m/z* 122.0713.

b. Synthesis of 4-methyl-1-propyl-1*H*-1,2,3-triazole (H-MPT)

(250 mg, 2.20 mmol, 1.0 equiv.) in methanol (5 mL) and 4-methylbenzene sulfonohydrazide (388 mg, 2.08 mmol, 1 equiv.) were reacted in a 10 mL microwave tube (Biotage®, Sweden). After complete consumption of the starting material, propylamine (129 mg, 2.29 mmol, 1.1 equiv.) and triethylamine (232 mg, 2.30 mmol, 1.1 equiv.) were added and the tube sealed. After microwaving for 20 minutes at 120 °C and cooling to room temperature, the reaction mixture was concentrated *in vacuo* to an orange oil. The crude oil was dissolved in DCM : water (1:1), the phases separated, and the aqueous layer was extracted three times with DCM. The combined organic fractions were washed with brine, dried over Na_2SO_4 and concentrated *in vacuo* to yield H-MPT (72%). ^{1}H NMR (500 MHz, $CDCl_3$) δ 7.23 (s, 1H, aromatic-H), 4.22 (t, *J* = 7.1 Hz, 2H, aliphatic-*H*), 2.29 (d, 3H, aliphatic-H), 1.86 (h, *J* = 7.4 Hz, 2H, aliphatic-H), 0.89 (t, *J* = 7.4 Hz, 3H, aliphatic-H). ^{13}C {^{1}H} NMR (126 MHz, $CDCl_3$) δ 142.8 (aromatic-C), 118.7 (aliphatic-C), 59.9 (aliphatic-C), 33.6 (aliphatic-C), 25.2 (aliphatic-C), 25.2 (aliphatic-C), 10.9 (aliphatic-C). ESI-HRMS Calculated for ([M+H]$^+$): *m/z* 126.1026; found *m/z* 126.1026.

2. NMR Spectra

2.1 ^{1}H NMR and ^{13}C NMR Spectra of MPT

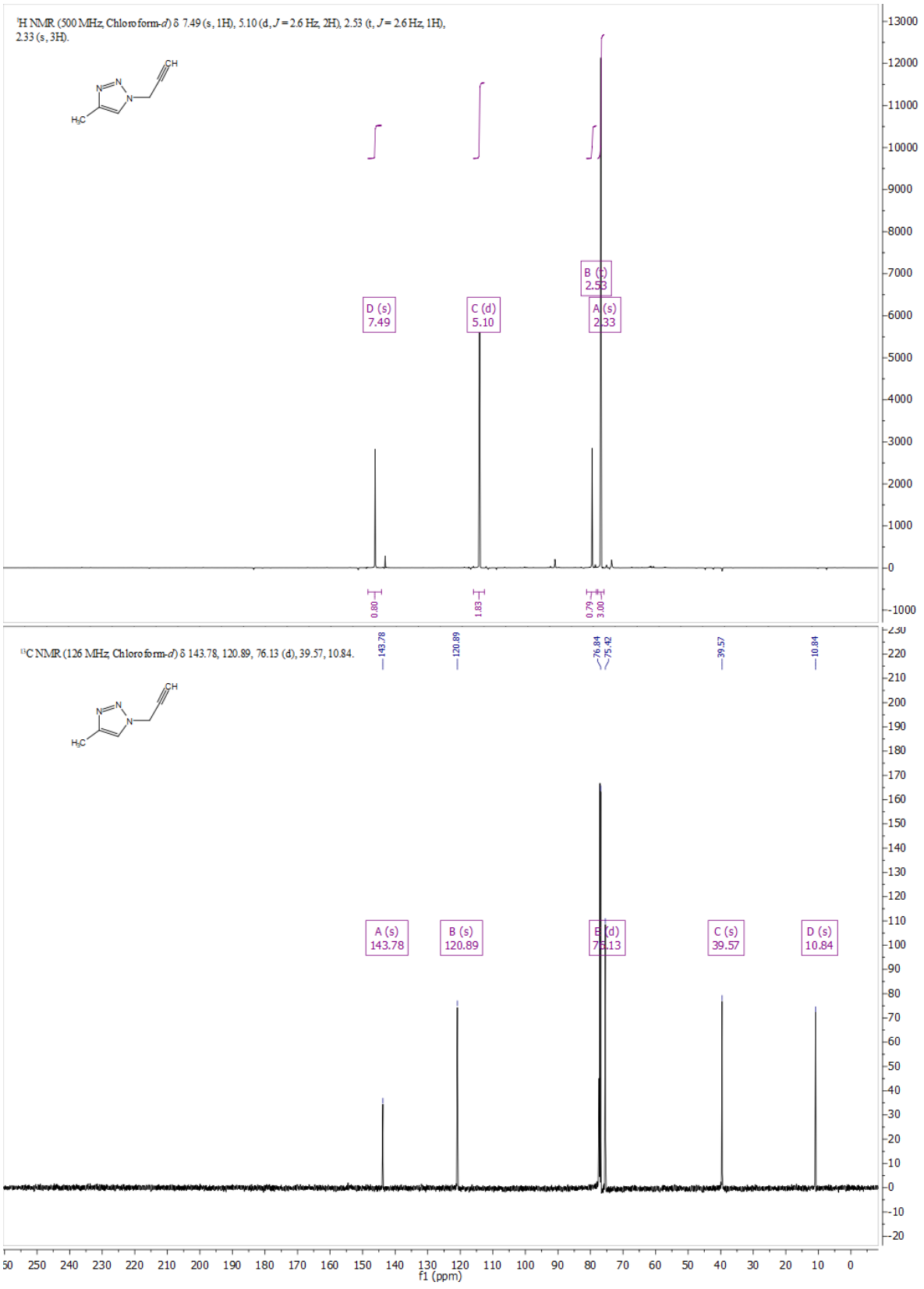

2.2 ^{1}H NMR and ^{13}C NMR Spectra of H-MPT

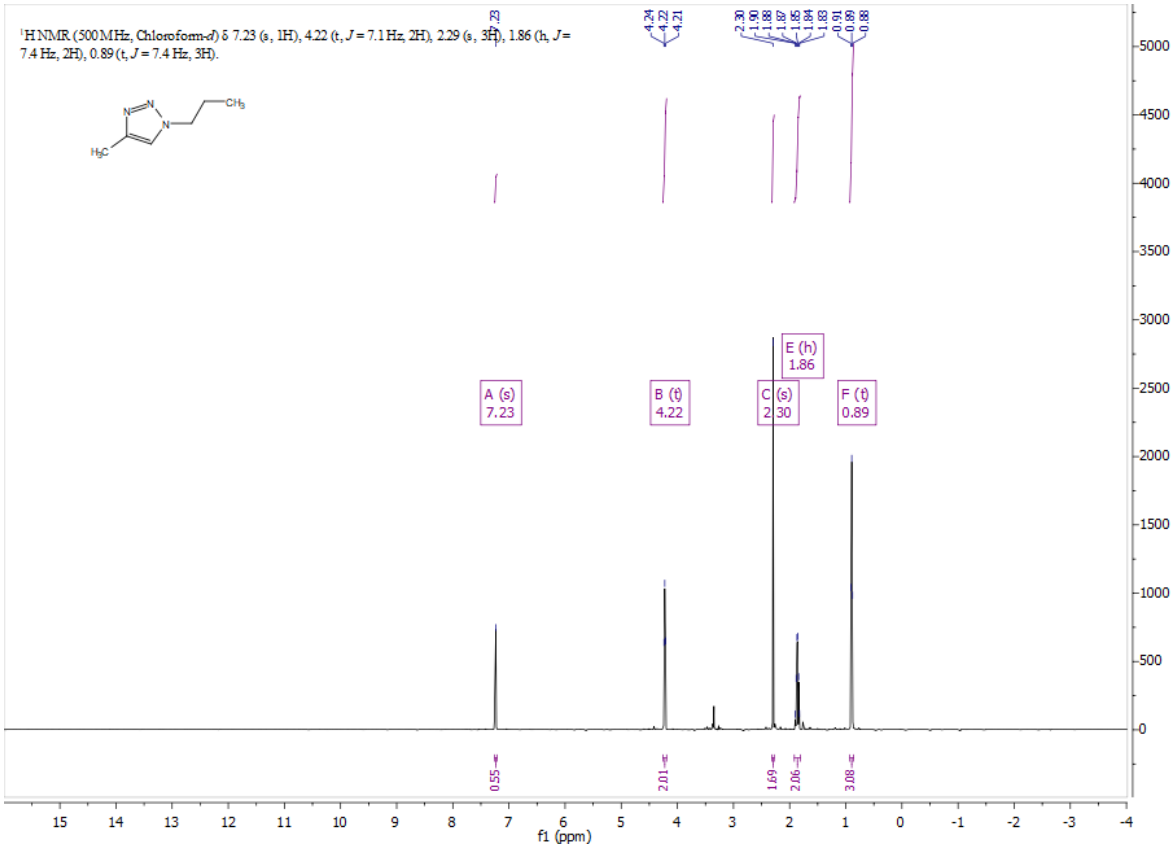

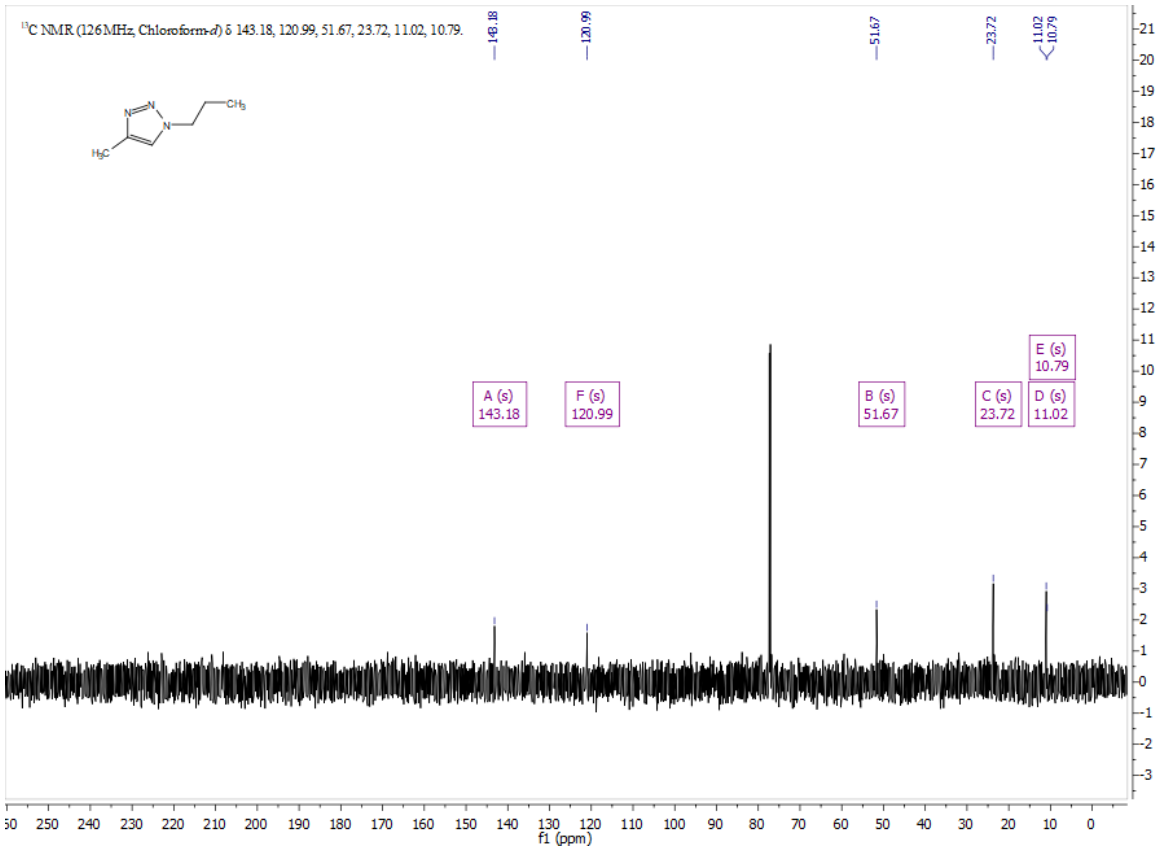

3. Supplementary Materials and Methods

3.1 Isolating Ammonia Oxidizing Bacteria (AOB) [3]

N. multiformis was isolated from an aquarium kit mixture (Aquasonic™, BIO-NATURE STANDARD) through the extinction via dilution method, as reported by Utåker *et al*.[4] Cultures were grown at 26°C and 120 rpm in 12 tubes (polycarbonate) in subsequent dilutions of inoculum:media of 1:1000. Purification of AOB was achieved in liquid ammonium medium (German Collection of Microorganisms and Cell Cultures GmbH (DMSZ), 1583. MEDIUM FOR AMMONIA OXIDIZING BACTERIA) by using the highest dilution level of most probable number tubes, as indicated by acidification (phenol red) and NO_2^- production (determined via Griess reagent).[5] The DMSZ medium contained (per L of Milli-Q water) NH_4Cl (535 mg), KH_2PO_4 (54 mg), KCl (74 mg), $MgSO_4$ x 7 H_2O (49 mg), $CaCl_2$ x 2 H_2O (147 mg) and NaCl (584 mg), to which 1 mL of trace element solution and 2 mL of phenol red solution were added. The trace element solution contained (per 975 mL of Milli-Q water) HCl (1M; 25 mL), $MnSO_4$ x 4 H_2O (45 mg), H_3BO_3 (49 mg), $ZnSO_4$ x 7 H_2O (43 mg), $(NH_4)_6Mo_7O_{24}$ x 4 H_2O (37 mg), $FeSO_4$ x 7 H_2O (973 mg), $CuSO_4$ x 5 H_2O (25 mg). The stock phenol red solution contained 50 mg phenol red in 100 mL water and was used over three months. The pH was adjusted to 7.8 using a sterile aqueous $NaHCO_3$ (10%) solution. The cultures were checked regularly for heterotrophic contamination by inoculation on 100% strength Luria broth (LB) plates containing 15 g L^{-1} technical grade agar (BD Difco™ Agar, Technical, Fisher Scientific). Further contamination through air was prevented by re-inoculation to sealed vessels. After several successful subcultures (at least ten), cells were harvested for analysis by 16S rRNA sequencing.

3.2 Protocol for Growing *N. Europaea* and *N. Multiformis* [3]

AOB were grown for 3 – 5 d in Duran glass bottles containing 600 mL of mineral salts media (MSM, see below) at 100 rpm and 30°C in the dark. The slightly loose cap was sealed with an O_2 permeable membrane to ensure aeration (Breathe-Easy® sealing membrane, Sigma Aldrich). The MSM constituted the main bulk medium and consisted of K_2HPO_4 (2.27 g L^{-1}), KH_2PO_4 (0.95 g L^{-1}) and $(NH_4)_2SO_4$ (0.67 g L^{-1}). The pH was adjusted to 7.0. To 1 L of the bulk medium 2 mL of a filter sterilized (0.2 µm millipore filter) solution of metals was added: Na_2EDTA (6.37 g L^{-1}), $ZnSO_4$ x 7 H_2O (1.0 g L^{-1}), $CaCl_2$ x 2 H_2O (0.5 g L^{-1}), $FeSO_4$ x 7 H_2O (2.5 g L^{-1}), $NaMoO_4$ x 2 H_2O (0.1 g L^{-1}), $CuSO_4$ x 5 H_2O (0.1 g L^{-1}), $CoCl_2$ x 6 H_2O (0.2 g L^{-1}), $MnSO_4$ x

H_2O (0.52 g L^{-1}) and $MgSO_4$ x 7 H_2O (60.0 g L^{-1}). To this media solution 1v/v% of aqueous Na_2CO_3 (50 g L^{-1}) was added aseptically as a carbon source.

3.3 Protocol for Harvesting Cells [3]

After 3 - 5 d of incubation, the turbid cultures were harvested at an OD_{600} (optical density at a wavelength of 600 nm) of approximately 0.1, which represented the mid-exponential growth phase and an NO_2^- production of approximately 800 µM (determined by Griess assay), cells were harvested by filtration onto 0.2 µm membrane filters (Rowe Scientific, mixed cellulose esters (MCE)). The cells were washed with sodium phosphate buffer (NaPB, pH = 7.5, 0.1 M, 2 x 100 mL) containing $MgSO_4$ (0.2 mM). The filter paper with the cells was transferred into a sterile 50 mL tube, and the cells were washed off by resuspending in NaPB (15 mL), followed by 5 s of vortexing (Ratek, Australia) and 3 s of sonication (Vevor, Australia). The initial inoculum OD_{600}, which was between 0.9 – 1.2, was adjusted to a final OD_{600} of 0.03 and stored at 4°C until used for the assay. Cells could be stored for up to 24 h without losing activity.

3.4 Standard Assay Protocol[3]

In a deep 96-well plate (2 mL capacity), 980 µL of the bacterial inoculum (OD_{600} = 0.03 in NaPB at pH 7.5) was added to the inhibitor (10 µL of a 30 mmol L^{-1} or 3 mmol L^{-1} stock solution of the inhibitor in DMSO respectively), the solutions were mixed thoroughly and pre-incubated in the dark for 5 min at 30°C and 100 rpm (Ratek, Australia). $(NH_4)_2SO_4$ (10 µL, 150 mM, from a sterile solution containing 19.8 g L^{-1} of $(NH_4)_2SO_4$ in Milli-Q water) was then added. In experiments in which the NH_2OH-dependent activity was measured, $(NH_4)_2SO_4$ was replaced by equimolar amounts of NH_2OH. The plate was covered with an O_2 permeable membrane to ensure aeration (Breathe-Easy® sealing membrane, Sigma Aldrich) and incubated in the dark for 30, 60 or 90 min at 30°C and 100 rpm. The nitrification process was stopped by adding an excess of DMP (10 µmol L^{-1}, 30 mM; the final concentration of DMP in the solution was 0.27 mM). An aliquot of the reaction solution (50 µL) was transferred to a 96-well spectrophotometric plate (Greiner Cellstar®, polystyrene) to which 50 µL of Griess reagent was added. The colour was allowed to develop for 15 min at room temperature, and the absorbance was measured at 540 nm (Clariostar® BMG Labtech, Australia). Each assay was

accompanied by control treatments to determine the 0% (no N-source) and 100% (with N-source, no inhibitor) NO_2^- signal.

3.5 O_2 Consumption Measurements [6]

O_2 consumption rates of cell suspensions of *N. europaea* were measured using a Clark-type oxygen electrode (Rank Brothers, Cambridge, UK) mounted in a water-jacketed electrode chamber (3 mL capacity) that was connected to a recirculating cooler (Lauda, Austria). The

$$[O_2]_t = \frac{\text{voltage (sample)}_t - \text{voltage (0\% } O_2)}{\text{voltage (100\% } O_2) - \text{voltage (0\% } O_2)} \times 280\ \mu M \qquad \text{(eqn. SI-1)}$$

data were recorded using a Data-trax™ (World Precision Instruments, UK) sensor data collection system. All measurements were taken at 20°C and 1 mL final reaction solution volume. The polarizing voltage was set to 0.6 V. To calibrate the oxygen signal, an excess (approximately 50 mg) of $Na_2S_2O_4$ was added to 1 mL of Milli-Q water to chemically remove dissolved O_2. Additional O_2 flux was prevented by applying a stopper, and the residual voltage was referred to as "0% O_2". The voltage at saturated O_2 concentration ("100% O_2") was determined by measuring the voltage of the equilibrated aerated reaction system consisting of 1 mL Milli-Q water. Sample measurements were taken as follows: The 1 mL reaction mixture, composed of 980 µL *N. europaea* cell solution in NaPB (OD_{600} = 0.8; corresponding to approximately 468 µg L^{-1} protein) was equilibrated for 5 min in the chamber until the voltage reading was stable. The reaction was then initiated by the addition of $(NH_4)_2SO_4$ (10 µL of an aqueous 150 mM stock solution, the final concentration in the reaction solution was 3 mM) and the chamber immediately sealed with a stopper. After 4 min of oxygen consumption (a linear rate coefficient of approximately $k_{obs} = k = 274.7 \pm 20.0$ nmol O_2 L^{-1} s^{-1} was determined), 10 µL of the inhibitor stock solution of MPT in DMSO (1.2 mM and 0.6 mM) were added via a 10-µL Eppendorf pipette through a capillary opening, ensuring the emergence of the pipette tip in the solution. The voltage was recorded over a period of 25 min in intervals of 5 s. The trace describing the O_2 concentration after addition of $(NH_4)_2SO_4$ against the time (initial 15-140 s) was used as the baseline O_2 consumption for the uninhibited cells, whereas the trace describing the consumption in the presence of the inhibitor (255-1740 s time window) was used to determine the rate of O_2 consumption in the presence of inhibitor. All experiments were conducted in triplicate at 20°C under constant stirring. The voltage was converted to $[O_2]$ according to equation SI-1:

Kinetic parameters were determined via GraphPad Prism software, using simple linear regression for uninhibited cells and non-linear fit (curve fit) first order decay with an $R^2 > 0.9$ for inhibited cells.

3.6 Activity Recovery Assay[6]

Cells were harvested using the 'Protocol for Harvesting Cells'. The bacterial suspension was adjusted to OD_{600} = 0.8 (~ 468 µg L^{-1} protein), and 980 µL aliquots were transferred to 1.5-mL centrifuge tubes (Eppendorf®, polypropylene). The inhibitor (10 µL of a stock solution of 150 mM in Milli-Q water) was added, and after equilibrating for 5 min $(NH_4)_2SO_4$ (10 µL of a stock solution of 150 mM in Milli-Q water) was added using a multichannel pipette to ensure simultaneous addition to each tube. The tubes were incubated in a temperature-regulated rotary incubator (Ratek, Australia) for 30 min at 30°C and 100 rpm in the dark. A 50 µL aliquot was then transferred to a 96-well plate (Greiner Cellstar®, polystyrene) to which 50 µL of Griess reagent was added, and the mixture was incubated for 15 min. The absorbance was measured at 540 nm (Clariostar® BMG Labtech, Australia). The remaining cells were subsequently washed (3x) by alternating centrifugation (Boeco, Germany; 10,000 rpm, 10 min) and resuspension of the cell pellet in NaPB (1 mL). After the final centrifuging step, the pellet was resuspended in NaPB (990 µL) and re-incubated with $(NH_4)_2SO_4$ (10 µL of an aqueous 150 mM stock solution, see above), and the NO_2^- concentration was measured under the previously described conditions.

3.7 Michaelis-Menten Kinetics[6]

In a deep 96-well plate (2 mL capacity), 980 µL of the bacterial inoculum (OD_{600} = 0.03, ~ 18 µg L^{-1} protein in NaPB at pH 7.5) was added to MPT (10 µL from 75 µM and 37.5 µM stock solutions of MPT in DMSO, respectively). The solutions were mixed thoroughly and pre-incubated in the dark for 5 min at 100 rpm and at 30°C (Ratek, Australia). 10 µL of the respective $(NH_4)_2SO_4$ stock solution (0.3 mM, 3 mM, 5 mM, 10 mM, 150 mM, 300 mM, 1 M and 3M) was added to each well (final $[NH_4^+]$ in well: 0.003 mM, 0.03 mM, 0.05 mM, 0.1 mM, 1.5 mM, 3.0 mM, 10 mM and 15 mM). The plate was covered with an O_2 permeable membrane to ensure aeration (Breathe-Easy® sealing membrane, Sigma Aldrich) and incubated in the dark for 60 min at 30°C and 100 rpm. Termination of the nitrification process

and determination of the NO_2^- production was performed as described in 'Standard Assay Protocol'. Data analysis was performed with GraphPad Prism software, using nonlinear regression (curve fit) for Michaelis Menten Kinetics. The results used the best fit values with 95% likelihood.

The Michaelis constant, K_m, is the substrate concentration, [S], at which the reaction rate, V, is 50% of the maximal rate, V_{max}, and can be regarded as an inverse measure of the enzyme-substrate affinity (equation SI-2).

$$v = \frac{V_{max}[S]}{K_m + [S]} \qquad \text{(eqn. SI-2)}$$

If the substrate (i.e., NH_3) and MPT are not competing for the same site in the enzyme, a decrease in V_{max} that is independent of [MPT] will characterise non-competitive inhibition of AMO (with no change in K_m). On the other hand, uncompetitive inhibition will result in a decrease in both K_m and V_{max}, whereas competitive inhibition will cause an increase of K_m and no change in V_{max}. [7]

3.8 Determination of $IC_{50(abs)}$ Values[6]

The assay was performed according to the 'Standard Assay Protocol' using *N. europaea* as AMO source. MPT was tested at concentrations of: 1.5 mmol L^{-1}, 0.75 mmol L^{-1}, 0.375 mmol L^{-1}, 0.1875 mmol L^{-1}, 0.0983 mmol L^{-1}, 0.0469 mmol L^{-1}, 0.0234 mmol L^{-1}, 0.011 mmol L^{-1}, 0.0059 mmol L^{-1}). The inhibitor concentration at which the inhibition was 50 % ($IC_{50(abs)}$) was determined by fitting the $\log_{10}$ of the concentration (in mmol L^{-1}) against the response. $IC_{50(abs)}$ was obtained by normalising the response against cells in NaPB with 1 v/v% DMSO and [NH_4^+] = 3 mM ('uninhibited' cells; 100% signal) and cells in NaPB with 1 v/v% DMSO without additive ('untreated cells'; 0% signal). The curves were plotted with GraphPad prism (version 9.0) to determine $IC_{50(abs)}$ via variable slope fit (three parameters). The $IC_{50(abs)}$ value and graph is shown in Supplementary Figure 3.

3.9 Mineral-N Retention in an Australian Soil (Soil A) [1]

Soil A was collected, air-dried, ground and sieved (2 mm) prior to use. Soil microcosm incubations were carried out in polypropylene specimen containers (250 mL, Sarstedt, Germany), containing 20 g of oven dry-weight equivalent of soil. Microcosms were treated

with half the volume of water required to meet the desired WHC of 53% and pre-incubated at 25°C for seven days to revive soil microbial activity. Following pre-incubation, the remaining volume to reach the 53% WHC was applied as one of the treatment solutions: (1) fertiliser ($(NH_4)_2SO_4$,) 100 mg kg^{-1}, (2) fertiliser + 0.5 mol% MPT, (3) fertiliser + 2.5 mol% MPT, (4) fertiliser + 5 mol% MPT or (5) fertiliser + 5 mol% DMP, with three replicates of each treatment per time interval (n = 3). Throughout the incubation period soil microcosms were kept aerated by removing the lid for 10 minutes every 2–3 days to allow gas exchange, and moisture levels were replenished by addition of Milli-Q water as required. At the end of the desired incubation period (i.e., after 0, 3, 7, 14, and 21 days, respectively), soil microcosms were removed and destructively sampled by treating with aqueous potassium chloride solution (KCl, 2M, 100 mL) and shaking for 1 h. Soil-KCl solutions were filtered (Whatman No. 42), and the filtrates were stored at −20 °C until the end of the experiment, when all KCl extracts were analysed for the concentration of soil mineral nitrogen from ammonium (NH_4^+-N) and nitrate (NO_3^--N; the conversion of NO_2^- to NO_3^- in soils is very rapid) after appropriate dilutions using Segmented Flow Analysis (San++, Skalar, Breda, The Netherlands). Results are reported as the mean of three biological replicates, errors reported are standard errors of the mean. Errors associated with raw data were carried through calculations using standard error propagation protocols. The detailed mineral-N data are provided in Supplementary Table 8.

3.10 N_2O Gas Measurements[8,9]

At the day of the measurement (day 1, 3, 5, 7, 14 and 21 after fertilisation) the vials were closed gas-tight with a rubber septum and aluminium lid and opened after each measurement. The N_2O concentrations were analysed using a GC-ECD/FID (Electron Capture Detector/Flame Ionization Detector) (Claurus 580, Perkin Elmer) in intervals of 1, 5.05, 9.1 and 13 h as described previously. [8] A linear regression slope was used to calculate N_2O-N production rates, F, according to equation SI-3,

$$F = \frac{\frac{\Delta C}{\Delta t} V T_0 M}{m T_a V_m} \qquad \text{(eqn. SI-3)}$$

where $\Delta C/\Delta t$ represents the change of the N_2O concentration over the time intervall t in ppbv, V represents the headspace volume in L, M represents the molar mass of N in N_2O, m represents the amount of soil in g dry weight, V_m represents the molar volume of ideal gases (22.414 L mol^{-1}) at 0 °C and 101.325 kPa, corrected for the gas sampler using T_0 (273.15 K) and T_a (air temperature in K). Detailed N_2O production rates are given in Supplementary Table 9.

3. Supplemenary Tables

Supplementary Table 1. NH_4^+-dependent NO_2^- production after supplementing *N. europaea* and *N. multiformis* (OD_{600} = 0.03) with and MPT and H-MPT.[a]

AOB Source	*[NO_2^-] / µM*			
	Untreated	**Uninhibited**	**MPT**	**H-MPT**
N. europaea	8.8 ± 6.5	149.9 ± 46.6	42.1 ± 16.1	135.5 ± 38.6
N. multiformis	2.7 ± 0.3	56.9 ± 4.8	14.7 ± 2.0	54.7 ± 6.0

[a] Incubations were performed in NaPB with 1v/v% DMSO. 'Untreated' = 0% signal; 'uninhibited' = 100% signal with [NH_4^+] = 3 mM; [MPT] and [H-MPT] = 0.3 mM with [NH_4^+] = 3 mM.

Supplementary Table 2. NH_2OH-dependent NO_2^- production after supplementing *N. europaea* and *N. multiformis* with MPT.[a]

AOB Source	*[NO_2^-] / µM*		
	Untreated	**Uninhibited**	**MPT**
N. europaea	9.1 ± 1.9	37.8 ± 1.3	29.7 ± 0.5
N. multiformis	9.8 ± 4.0	40.3 ± 3.3	30.1 ± 2.0

[a] Incubations were performed in NaPB with 1v/v% DMSO. 'Untreated' = 0% signal; 'uninhibited' = 100% signal with [NH_2OH] = 3 mM; [MPT] = 0.3 mM with [NH_2OH] = 3 mM.

Supplementary Table 3. NO_2^- production after supplementing *N. europaea* and *N. multiformis* (OD_{600} = 0.03) with inhibitors NI-1-3. [a]

AOB Source	$[NO_2^-]$ / µM				
	Untreated	**Uninhibited**	**NI-1**	**NI-2**	**NI-3**
N. europaea	3.1 ± 1.3	90.1 ± 2.3	72.4 ± 3.6	47.1 ± 2.4	84.7 ± 3.4
N. multiformis	2.3 ± 0.1	79.3 ± 4.2	48.5 ± 1.6	43.3 ± 1.3	81.9 ± 3.2

[a] Incubations were performed in NaPB with 1v/v% DMSO. 'Untreated' = 0% signal; 'uninhibited' = 100% signal with $[NH_4^+]$ = 3 mM; [MPT] and [H-MPT] = 0.3 mM with $[NH_4^+]$ = 3 mM.

Supplementary Table 4. Rate coefficients, *k*, for the time-dependent O_2 consumption by *N. europaea* in the absence of MPT.[a]

Experiment		***k* / nmol L^{-1} s^{-1}**	***R^2***
before addition of MPT (0.6 mM)	run 1	274.5	0.99
	run 2	256.4	0.99
	run 3	269.3	0.99
before addition of MPT (1.2 mM)	run 4	317.3	0.99
	run 5	270.5	0.99
	run 6	260.4	0.99

[a] The *k*-value was determined from the linear regression of $[O_2]$ vs. time between 15 – 240 s (R^2 > 0.95). The experiment was conducted with $[NH_4^+]$ = 3.0 mM in NaPB (pH = 7.5) with 1v/v% DMSO at 20°C under constant stirring in the dark.

Supplementary Table 5. Rate coefficients, k_{obs}, for the time-dependent O_2 consumption by *N. europaea* in the presence of MPT at different concentrations.[a]

Experiment		***k_{obs}* / s^{-1}**	***R^2***
after addition of MPT (0.6 mM)	run 1	1.82×10^{-3}	0.99
	run 2	2.23×10^{-3}	0.99

	run 3	4.25×10^{-3}	0.99
after addition of MPT (1.2 mM)	run 4	6.40×10^{-3}	0.99
	run 5	3.93×10^{-3}	0.99
	run 6	3.93×10^{-3}	0.98

[a] The observed *k*-value (k_{obs}) was determined from the first oder decay regression of $[O_2]$ against the time between 255 – 1740 s ($R^2 > 0.99$). The experiment was conducted with $[NH_4^+]$ = 3.0 mM in NaPB (pH = 7.5) with 1v/v% DMSO at 20°C under constant stirring in the dark.

Supplementary Table 6. Specifications of the soils studied in this work.[a]

Parameter	Soil A	Soil B	Soil C	Soil D	Soil E
pH ($CaCl_2$)	5.9	6.3	5.5	4.7	7.5
pH (H_2O)	6.4	6.7	6.0	5.4	8.1
Sand (%)	42	8	74	87	5
Slit (%)	35	77	16	8	78
Clay (%)	24	15	10	4	17
TOC (%)	4.86	1.0	2.05	0.47	0.52
TC (%)	5.6	1.0	2.1	0.5	2.12
TN (%)	0.43	0.15	0.04	0.11	0.05
min-N (NH_4^+) / mg kg^{-1} soil	5.6	0.24	0.97	0.63	1.12
min-N (NO_3^-) / mg kg^{-1} soil	70	70.9	39.7	27.7	21.8
WHC / g 100 g^{-1} soil	78	40	51	28	44

[a] Mean values from three replicates; TOC = total organic carbon, TC = total carbon, TN = total nitrogen, min-N = mineral-N, WHC - water holding capacity (WHC). Soil A was collected from an agricultural site in Victoria, Australia; soils B - E were collected from agricultural sites in Germany.

Supplementary Table 7. Experiments with soils B - E. Application rates of DMP and MPT and weight % of total $(NH_4)_2SO_4$ applied.[a]

Treatment	*Application rates mg kg^{-1} soil*	*Weight % of total $(NH_4)_2SO_4$*
Fertiliser + DMP 5 mol%	16.9	7.1
Fertiliser + DMP 2.5 mol%	8.6	3.7
Fertiliser + DMP 0.5 mol%	1.7	0.7
Fertiliser + MPT 5 mol%	21.5	9.1
Fertiliser + MPT 2.5 mol%	10.8	4.6
Fertiliser + MPT 0.5 mol%	2.2	0.9

[a] All samples were treated with $(NH_4)_2SO_4$ at a rate of 50 mg N kg^{-1} soil.

Supplementary Table 8. Soil incubation studies to determine mineral-N conversion in soil A (pH = 5.9) between days 1 and 21.[a]

	[NH_4^+-N] (mg kg^{-1} soil) [b], [c], [d]				*[NO_3^--N] (mg kg^{-1} soil)* [b], [c], [d]			
Soil A	**Day 0**	**Day 7**	**Day 14**	**Day 21**	**Day 0**	**Day 7**	**Day 14**	**Day 21**
Fertiliser only	95.8 ± 0.4	26.3 ± 0.4	9.6 ± 0.1	7.8 ± 0.1	86.5 ± 0.5	167.5 ± 2.3	198.4 ± 1.3	201.5 ± 1.1
Fertiliser + DMP 5 mol%	97.5 ± 0.4	41.4 ± 1.8**	18.7 ± 1.1*	8.2 ± 0.3	84.9 ± 1.4	155.8 ± 1.8	191.4 ± 1.7	203.9 ± 1.9
Fertiliser + MPT 0.5 mol%	97.5 ± 0.4	57.23 ± 1.8**	32.9 ± 1.8**	7.9 ± 0.2	87.6 ± 0.4	140.3 ± 1.1	174.9 ± 2.3*	204.3 ± 1.6
Fertiliser + MPT 2.5 mol%	96.6 ± 0.2	95.6 ± 1.6***###	98.9 ± 1.1***###	91.6 ± 1.4***###	87.8 ± 0.4	101.7 ± 0.5**##	108.0 ± 0.3***###	113.7 ± 3.3***###
Fertiliser + MPT 5 mol%	96.5 ± 0.4	98.9 ± 1.1***###	110.2 ± 1.0***###	110.6 ± 1.7***###	87.3 ± 0.5	94.3 ± 0.6***###	99.2 ± 0.7***###	99.1 ± 2.1***###

[a] The measurements were performed according to section 3.9. All fertiliser treatments were at an application rate of $(NH_4)_2SO_4$ = 100 mg kg^{-1} soil. [b] Mean values (n = 3); errors are standard errors of the mean. [c] Statistical significance: $P < 0.05$ (*), $P < 0.01$ (**), $P < 0.001$ (***) when comparing inhibitor treatments to the control treatment with $(NH_4)_2SO_4$ alone, $P < 0.05$ (#), $P < 0.01$ (##), $P < 0.001$ (###) respectively, when comparing inhibitor treatments to highest concentration of DMP treatment. Statistical analysis were performed with GraphPad Prism 9.5.0 (2-way ANOVA) multiple comparison Tuckey HSD.

Supplementary Table 9. N_2O production rates (in ng g^{-1} soil h^{-1}) for soils B-E between days 1 and 21.[a]

	Day 1	*Day 3*	*Day 5*	*Day 7*	*Day 14*	*Day 21*
			Soil B			
Untreated	0.007 ± 0.007	0.008 ± 0.008	0.000 ± 0.000	-0.021 ± 0.021	0.000 ± 0.000	0.000 ± 0.000
Fertiliser only	0.681 ± 0.044	0.282 ± 0.023	0.204 ± 0.016	0.191 ± 0.009	0.108 ± 0.018	0.048 ± 0.006
Fertiliser + DMP 0.5 mol%	0.318 ± 0.030 *	0.189 ± 0.006	0.151 ± 0.015	0.086 ± 0.043	0.136 ± 0.006	0.019 ± 0.019
Fertiliser + DMP 2.5 mol%	0.224 ± 0.013 *	0.124 ± 0.008	0.060 ± 0.030	0.045 ± 0.023	0.113 ± 0.006	0.127 ± 0.000*
Fertiliser + DMP 5 mol%	0.209 ± 0.054 *	0.067 ± 0.017 *	0.058 ± 0.014 *	0.020 ± 0.010 **	0.052 ± 0.003	0.037 ± 0.019
Fertiliser + MPT 0.5 mol%	0.058 ± 0.004 *	0.009 ± 0.009 *	0.000 ± 0.000 *	-0.013 ± 0.013 **	0.008 ± 0.008	0.011 ±0 .011
Fertiliser + MPT 2.5 mol%	0.007 ± 0.007 *	0.000 ± 0.000 *	-0.007 ± 0.007 *	-0.019 ± 0.019 **	0.000 ± 0.000 #	0.000 ± 0.000
Fertiliser + MPT 5 mol%	0.000 ± 0.000 *	0.000 ± 0.000 *	0.000 ± 0.000 *	-0.048 ± 0.026 **	0.000 ± 0.000#	0.000 ± 0.000

			Soil C			
Untreated	0.013 ± 0.013	0.000 ± 0.000	0.009 ±0.009	0.027 ± 0.014	0.043 ± 0.003	0.052 ± 0.003
Fertiliser only	0.283 ± 0.004	0.198 ± 0.003	0.168 ± 0.003	0.163 ± 0.002	0.243 ± 0.020	0.229 ± 0.008
Fertiliser + DMP 0.5 mol%	0.283 ± 0.008	0.183 ± 0.003	0.081 ± 0.041	0.162 ± 0.037	0.105 ± 0.007	0.101 ± 0.011 **
Fertiliser + DMP 2.5 mol%	0.276 ± 0.006	0.161 ± 0.006	0.133 ± 0.006	0.113 ± 0.005 *	0.086 ± 0.006	0.089 ± 0.005 **
Fertiliser + DMP 5 mol%	0.228 ± 0.017	0.125 ± 0.006 **	0.099 ± 0.008 *	0.098 ± 0.010	0.085 ± 0.009 *	0.095 ± 0.000 *
Fertiliser + MPT 0.5 mol%	0.119 ± 0.011 **	0.062 ± 0.001 ***#	0.059 ± 0.007 **	0.054 ± 0.006 **	0.119 ± 0.010	0.107 ± 0.008 **
Fertiliser + MPT 2.5 mol%	0.042 ± 0.04 ***##	0.000 ± 0.000 ***##	0.011 ± 0.011 *#	0.031 ± 0.003 ***	0.012 ± 0.008 *#	0.019 ± 0.010 ***
Fertiliser + MPT 5 mol%	0.017 ± 0.017 *##	0.000 ± 0.000 ***##	0.000 ± 0.000 ***#	0.024 ± 0.013 *	0.023 ± 0.007 *#	0.000 ± 0.000 **###
			Soil D			
Untreated	0.018 ± 0.018	0.083 ± 0.011	0.049 ± 0.005	0.080 ± 0.006	0.043 ± 0.006	0.067 ± 0.016

Fertiliser only [a]	0.128 ± 0.008	0.144 ± 0.013	0.081 ± 0.011	0.124 ± 0.010	0.076 ± 0.004	0.122 ± 0.010
Fertiliser + DMP 0.5 mol%	0.131 ± 0.001	0.133 ± 0.003	0.063 ± 0.003	0.112 ± 0.008	0.072 ± 0.009	0.098 ± 0.011
Fertiliser + DMP 2.5 mol%	0.073 ± 0.037	0.120 ± 0.005	0.067 ± 0.006	0.115 ± 0.012	0.070 ± 0.006	0.063 ± 0.003
Fertiliser + DMP 5 mol%	0.114 ± 0.015	0.112 ± 0.006	0.039 ± 0.021	0.102 ± 0.014	0.056 ± 0.004	0.069 ± 0.007
Fertiliser + MPT 0.5 mol%	0.029 ± 0.029	0.058 ± 0.009 *	0.004 ± 0.004	0.037 ± 0.021	0.037 ± 0.005 *#	0.045 ± 0.014
Fertiliser + MPT 2.5 mol%	0.015 ± 0.010 *	0.020 ± 0.010 *#	0.000 ± 0.000	0.037 ± 0.018	0.000 ± 0.000 *#	0.000 ± 0.000 *
Fertiliser + MPT 5 mol%	0.000 ± 0.000 *	0.027 ± 0.013 *	0.000 ± 0.000	0.020 ± 0.011 *	0.000 ± 0.000 *#	0.000 ± 0.000 *#

Soil E

Untreated	0.026 ± 0.014	0.000 ± 0.000	0.000 ± 0.000	0.000 ± 0.000	0.000 ± 0.000	0.000 ± 0.000
Fertiliser only	0.207 ± 0.018	0.680 ± 0.069	2.334 ± 0.972	0.059 ± 0.030	0.009 ± 0.009	0.000 ± 0.000
Fertiliser + DMP 0.5 mol%	0.053 ± 0.002 *	0.037 ± 0.006 *	0.015 ± 0.008	0.000 ± 0.000	0.000 ± 0.000	0.000 ± 0.000
Fertiliser + DMP 2.5 mol%	0.080 ± 0.009 *	0.014 ± 0.014 *	0.000 ± 0.000	0.000 ± 0.000	0.008 ± 0.008	0.000 ± 0.000

Fertiliser + DMP 5 mol%	0.045 ± 0.011 *	0.011 ± 0.011 *	0.000 ± 0.000	0.000 ± 0.000	0.007 ± 0.007	0.000 ± 0.000
Fertiliser + MPT 0.5 mol%	0.007 ± 0.007 *	0.011 ± 0.011 *	0.000 ± 0.000	0.000 ± 0.000	0.000 ± 0.000	0.000 ± 0.000
Fertiliser + MPT 2.5 mol%	0.008 ± 0.008 *	0.008 ± 0.008 *	0.000 ± 0.000	0.000 ± 0.000	0.000 ± 0.000	0.000 ± 0.000
Fertiliser + MPT 5 mol%	0.012 ± 0.012 *	0.000 ± 0.000 *	0.000 ± 0.000	0.000 ± 0.000	0.000 ± 0.000	0.000 ± 0.000

[a] The measurements were performed according to section 3.10, and production rates were calculated according to eqn. SI-3. All fertiliser treatments were at an application rate of $(NH_4)_2SO_4$ = 50 mg kg^{-1} soil. Mean values (n = 3); errors are standard errors of the mean of biological replicates. Statistical significance: $P < 0.05$ (*), $P < 0.01$ (**), $P < 0.001$ (***) when comparing inhibitor treatments to the control treatment with $(NH_4)_2SO_4$ alone, $P < 0.05$ (#), $P < 0.01$ (##), $P < 0.001$ (###), respectively, when comparing inhibitor treatments to the highest concentration of the DMP treatment. Statistical analyses were performed on raw N_2O production rates (µg g^{-1} soil h^{-1}) with GraphPad Prism 9.5.0 (2-way ANOVA) multiple comparison Tuckey HSD test.

Supplementary Table 10. Calculated gene abundances (copy g^{-1} soil) of *amoA* from bacteria and archaea after 22 days of incubation.[a]

	Untreated	***Fertiliser only***	***Fertiliser + DMP***	***Fertiliser + MPT***
		***amoA* bacteria**		
soil B	$(5.6 \pm 0.9) \times 10^6$	$(3.7 \pm 0.4) \times 10^6$	$(6.7 \pm 3.0) \times 10^6$	$(4.5 \pm 1.0) \times 10^6$
soil C	$(3.3 \pm 0.8) \times 10^5$	$(4.1 \pm 0.6) \times 10^5$	$(3.0 \pm 0.5) \times 10^5$	$(2.7 \pm 0.1) \times 10^5$
soil D	$(5.1 \pm 2.5) \times 10^6$	$(2.5 \pm 0.2) \times 10^6$	$(2.1 \pm 0.2) \times 10^6$	$(2.7 \pm 0.4) \times 10^6$
soil E	$(5.1 \pm 0.6) \times 10^5$	$(1.6 \pm 0.1) \times 10^6$	$(5.9 \pm 0.1) \times 10^6$ ***	$(5.4 \pm 0.1) \times 10^5$ ***
		***amoA* archaea**		
soil B	$(2.4 \pm 0.6) \times 10^8$	$(1.6 \pm 0.1) \times 10^8$	$(1.2 \pm 0.1) \times 10^8$	$(9.0 \pm 0.3) \times 10^7$ #
soil C	$(1.2 \pm 0.2) \times 10^7$	$(1.4 \pm 0.1) \times 10^7$	$(1.3 \pm 0.1) \times 10^7$	$(1.2 \pm 0.1) \times 10^7$
soil D	$(3.5 \pm 0.6) \times 10^8$	$(2.8 \pm 0.3) \times 10^8$	$(2.0 \pm 0.6) \times 10^8$	$(8.5 \pm 1.5) \times 10^7$ #
soil E	$(1.4 \pm 0.1) \times 10^7$	$(1.8 \pm 0.1) \times 10^7$	$(1.8 \pm 0.1) \times 10^7$	$(2.4 \pm 0.5) \times 10^7$

[a] Detailed soil specifications are listed in Supplementary Table 6; 'untreated' soil contains only deionized water as an 'additive'. The fertiliser treatment contained N fertiliser ($(NH_4)_2SO_4$ at an application rate of 50 mg kg^{-1} soil. Inhibitor treatments were performed with high application rates of 5 mol% of applied fertilizer-N to determine the maximum effect. [b] Mean values (n = 3); errors are standard errors of the mean of biological replicates. [c] Statistical significance: $P < 0.05$ (*), $P < 0.01$ (**), $P < 0.001$ (***) when comparing inhibitor treatments to the control treatment with $(NH_4)_2SO_4$ alone, $P < 0.05$ (#), $P < 0.01$ (##), $P < 0.001$ (###) respectively, when comparing inhibitor treatments with untreated soil. Statistical analyses were performed on gene copy numbers (copy g^{-1} soil) with GraphPad Prism 9.5.0 (ordinary one-way ANOVA) with GraphPad Prism 9.5.0 (2-way ANOVA) multiple comparison Tukey HSD.

4. Supplementary Figures

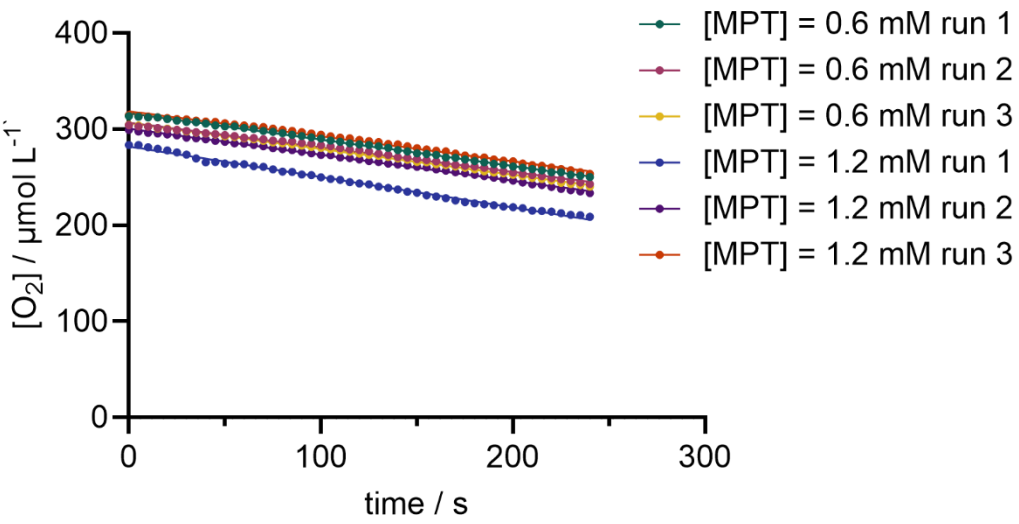

Supplementary Figure 1. O_2 consumption by *N. europaea* as a function of time before the addition of MPT (between 15 – 240 s). Note that time is corrected by -15 s to start at 0 s Experiments were conducted with $[NH_4^+]$ = 3.0 mM in NaPB (pH = 7.5) with 1v/v% DMSO at 20°C under constant stirring in the dark. Each treatment was performed in three replicates (run 1–run 3); the shown O_2 profiles are the average of these. The rate coefficient, *k*, was obtained from linear regression of each individual treatment. The data are provided in Supplementary Table 4.

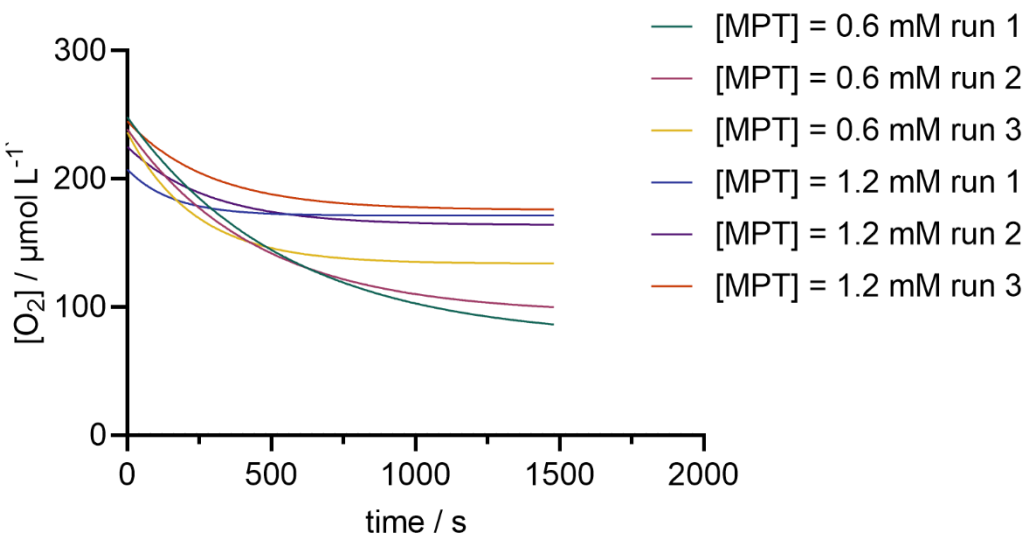

Supplementary Figure 2. Pseudo-first oder decay exponential fit of O_2 consumption by *N. europaea* as a function of time after the addition of MPT (between 255 – 1740 s). Note that time is corrected by -255 s to start at 0 s. Experiments were conducted with $[NH_4^+]$ = 3.0 mM in NaPB (pH = 7.5) with 1v/v% DMSO at 20°C under constant stirring in the dark. Each treatment was performed with three replicates (run 1–run 3); the O_2 profiles shown in the paper are the mean values of these. The pseudo first order rate coefficient, k_{obs}, was obtained from nonlinear regression of a first-order decay fit (via GraphPad Prism 9.5.0 of each individual treatment. The data are provided in Supplementary Table 5.

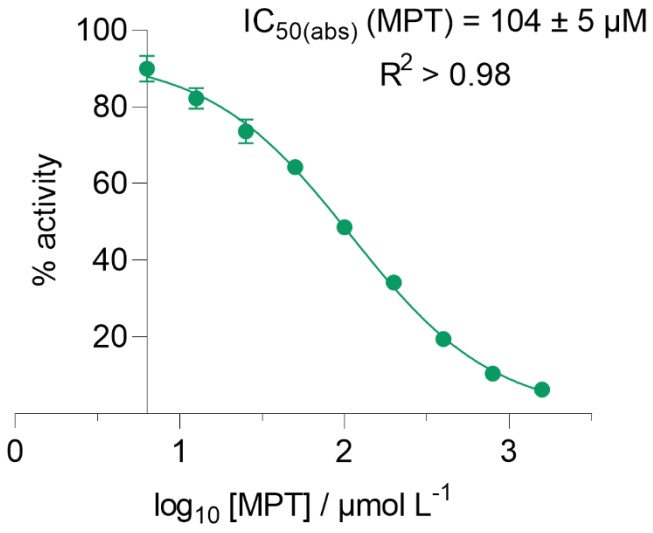

Supplementary Figure 3. Function of the %activity (determined by measuring the NO_2^- production) against the logarithmic concentration of MPT, and the obtained $IC_{50(abs)}$ value. Standard errors were determined from three biological and three technical replicates (n = 3).

5. Supplementary References

1. Taggert, B. I.; Walker, C.; Chen, D.; Wille, U. Substituted 1, 2, 3-Triazoles: A New Class of Nitrification Inhibitors. *Sci. Rep.* **2021**, *11*, 1-12. DOI: 10.1038/s41598-021-94306-1

2. Clark, P. R.; Williams, G. D.; Hayes, J. F.; Tomkinson, N. C. A Scalable Metal-, Azide-, and Halogen-Free Method for the Preparation of Triazoles. *Angewandte Chemie International Edition* **2020**, *59*, 6740-6744. DOI: 10.1002/anie.201915944

3. Yildirim, S. C.; Walker, R. M.; Roessner, U.; Wille, U. Rapid and Inexpensive Assay for Testing the Efficiency of Potential New Synthetic Nitrification Inhibitors. *ACS Agric. Sci. Technol.* **2023**. DOI: 10.1021/acsagscitech.2c00229

4. Utåker, J. B.; Bakken, L.; Jiang, Q. Q.; Nes, I. F. Phylogenetic Analysis of Seven New Isolates of Ammonia-Oxidizing Bacteria Based on 16S rRNA Gene Sequences. *Syst. Appl. Microbiol.* **1995**, *18*, 549-559. DOI: 10.1016/S0723-2020(11)80415-7

5. Naghdi, M.; Cledon, M.; Brar, S. K.; Ramirez, A. A. Nitrification of vegetable waste using nitrifying bacteria. *Ecol. Eng.* **2018**, *121*, 83-88. DOI: 10.1016/j.ecoleng.2017.07.003

6. Yildirim, S. C.; Walker, R. M.; Roessner, U.; Wille, U. Assessing the Efficacy, Acute Toxicity, and Binding Modes of the Agricultural Nitrification Inhibitors 3,4-Dimethyl-1H-pyrazole (DMP) and Dicyandiamide (DCD) with Nitrosomonas europaea. *ACS Agric. Sci. Technol.* **2023**. DOI: 10.1021/acsagscitech.2c00303

7. Delaune, K. P.; Alsayouri, K. *Physiology, Noncompetitive Inhibitor*. In: *StatPearls Publishing [internet]*. StatPearls Publishing 2022. (accessed 2022-10-04).

8. Reichel, R.; Wei, J.; Islam, M. S.; Schmid, C.; Wissel, H.; Schröder, P.; Schloter, M.; Brüggemann, N. Potential of Wheat Straw, Spruce Sawdust, and Lignin as High Organic

Carbon Soil Amendments to Improve Agricultural Nitrogen Retention Capacity: An Incubation Study. *Front. Plant Sci.* **2018**, *9*. DOI: 10.3389/fpls.2018.00900

9. Li, Z.; Reichel, R.; Brüggemann, N. Effect of C:N:P stoichiometry on soil nitrous oxide emission and nitrogen retention. *J. Soil Sci. Plant Nutr.* **2021**, *184*, 520-529. DOI: 10.1002/jpln.202000416

References (excluding manuscripts and publications)

1. Ladha, J. K.; Reddy, C. K.; Padre, A. T.; van Kessel, C. Role of Nitrogen Fertilization in Sustaining Organic Matter in Cultivated Soils. *J. Environ. Qual.* **2011**, *40*, 1756-1766. DOI: 10.2134/jeq2011.0064

2. Chadwick, O. A.; Derry, L. A.; Vitousek, P. M.; Huebert, B. J.; Hedin, L. O. Changing Sources of Nutrients During Four Million Years of Ecosystem Development. *Nature* **1999**, *397*, 491-497. DOI: 10.1038/17276

3. Pospišil, A.; Pospišil, M.; Varga, B.; Svečnjak, Z. Grain Yield and Protein Concentration of Two Amaranth Species (Amaranthus spp.) as Influenced by the Nitrogen Fertilization. *Eur. J. Agron.* **2006**, *25*, 250-253. DOI: 10.1016/j.eja.2006.06.001

4. Newbould, P. The use of nitrogen fertiliser in agriculture. Where do we go practically and ecologically? *Plant and Soil* **1989**, *115*, 297-311. DOI: 10.1007/BF02202596

5. Ladha, J. K.; Tirol-Padre, A.; Reddy, C. K.; Cassman, K. G.; Verma, S.; Powlson, D. S.; van Kessel, C.; de B. Richter, D.; Chakraborty, D.; Pathak, H. Global Nitrogen Budgets in Cereals: A 50-year Assessment For Maize, Rice, and Wheat Production Systems. *Sci. Rep.* **2016**, *6*, 19355. DOI: 10.1038/srep19355

6. Wendeborn, S. The Chemistry, Biology, and Modulation of Ammonium Nitrification in Soil. *Angew. Chem. Int. Ed.* **2020**, *59*, 2182-2202. DOI: 10.1002/anie.201903014

7. Gruber, N.; Galloway, J. N. An Earth-systemPerspective of the Global Nitrogen Cycle. *Nature* **2008**, *451*, 293-296. DOI: 10.1038/nature06592

8. Arp, D. J.; Sayavedra-Soto, L. A.; Hommes, N. G. Molecular Biology and Biochemistry of Ammonia Oxidation by Nitrosomonas europaea. *Arch. Microbiol.* **2002**, *178*, 250-255. DOI: 10.1007/s00203-002-0452-0

9. Lin, B.-L.; Sakoda, A.; Shibasaki, R.; Suzuki, M. A Modelling Approach to Global Nitrate Leaching Caused by Anthropogenic Fertilisation. *Water Research* **2001**, *35*, 1961-1968. DOI: 10.1016/S0043-1354(00)00484-X

10. Coskun, D.; Britto, D. T.; Shi, W.; Kronzucker, H. J. Nitrogen Transformations in Modern Agriculture and the Role of Biological Nitrification Inhibition. *Nat. Plants* **2017**, *3*, 17074. DOI: 10.1038/nplants.2017.74

11. Siljanen, H. M. P.; Alves, R. J. E.; Ronkainen, J. G.; Lamprecht, R. E.; Bhattarai, H. R.; Bagnoud, A.; Marushchak, M. E.; Martikainen, P. J.; Schleper, C.; Biasi, C. Archaeal Nitrification is a Key Driver of High Nitrous Oxide Emissions from Arctic Peatlands. *Soil Biol. Biochem.* **2019**, *137*, 107539. DOI: 10.1016/j.soilbio.2019.107539

12. Fuertes-Mendizábal, T.; Huérfano, X.; Vega-Mas, I.; Torralbo, F.; Menéndez, S.; Ippolito, J. A.; Kammann, C.; Wrage-Mönnig, N.; Cayuela, M. L.; Borchard, N.; et al. Biochar Reduces the Efficiency of Nitrification Inhibitor 3,4-Dimethylpyrazole Phosphate (DMPP) Mitigating N_2O Emissions. *Sci. Rep.* **2019**, *9*, 2346. DOI: 10.1038/s41598-019-38697-2

13. Novoa, R.; Loomis, R. S. Nitrogen and Plant Production. *Plant and Soil* **1981**, *58*, 177-204. DOI: 10.1007/BF02180053

14. Jones, D. L.; Healey, J. R.; Willett, V. B.; Farrar, J. F.; Hodge, A. Dissolved Organic Nitrogen Uptake By Plants—An Important N Uptake Pathway? *Soil Biol. Biochem.* **2005**, *37*, 413-423. DOI: 10.1016/j.soilbio.2004.08.00

15. Hart, M. R.; Brookes, P. C. Soil Microbial Biomass and Mineralisation of Soil Organic Matter after 19 Years of Cumulative Field Applications of Pesticides. *Soil Biol. Biochem.* **1996**, *28*, 1641-1649. DOI: 10.1016/S0038-0717(96)00249-0

16. David, L. C., Girin, T., Fleurisson, E., Phommabouth, E., Mahfoudhi, A., Citerne, S., Ferrario-Méry, S. . Developmental and Physiological Responses of *Brachypodium Distachyon*

to Fluctuating Nitrogen Availability. *Sci. Rep.* **2019**, *9*, 1-17. DOI: 10.1038/s41598-019-40569-8

17. Mobley, A. R.; Slavin, J. L.; Hornick, B. A. The Future of Recommendations on Grain Foods in Dietary Guidance. *J. Nutr.* **2013**, *143*, 1527S-1532S. DOI: 10.3945/jn.113.175737

18. Vojvodic, A.; Medford, A. J.; Studt, F.; Abild-Pedersen, F.; Khan, T. S.; Bligaard, T.; Nørskov, J. K. Exploring the Limits: A Low-Pressure, Low-Temperature Haber–Bosch Process. *Chem. Phys. Lett.* **2014**, *598*, 108-112. DOI: 10.1016/j.cplett.2014.03.003

19. Milton, R. D.; Cai, R.; Abdellaoui, S.; Leech, D.; De Lacey, A. L.; Pita, M.; Minteer, S. D. Bioelectrochemical Haber–Bosch Process: An Ammonia-Producing H_2/N_2 Fuel Cell. *Angew. Chem. Int. Ed.* **2017**, *56*, 2680-2683. DOI: 10.1002/anie.201612500

20. Godfray, H. C. J.; Beddington, J. R.; Crute, I. R.; Haddad, L.; Lawrence, D.; Muir, J. F.; Pretty, J.; Robinson, S.; Thomas, S. M.; Toulmin, C. Food Security: The Challenge of Feeding 9 Billion People. *Science* **2010**, *327*, 812-818. DOI: 10.1126/science.1185383

21. Caffrey, J. M.; Bano, N.; Kalanetra, K.; Hollibaugh, J. T. Ammonia Oxidation and Ammonia-Oxidizing Bacteria and Archaea from Estuaries with Differing Histories of Hypoxia. *The ISME Journal* **2007**, *1*, 660-662. DOI: 10.1038/ismej.2007.79

22. Galloway, J. N. The Global Nitrogen Cycle: Changes and Consequences. *Environmental Pollution* **1998**, *102*, 15-24. DOI: 10.1016/S0269-7491(98)80010-9

23. Jetten, M. S. M. The Microbial Nitrogen Cycle. *Environ. Microbiol.* **2008**, *10*, 2903-2909. DOI: 10.1111/j.1462-2920.2008.01786.x

24. Schimel, D. S. Terrestrial Ecosystems and the Carbon Cycle. *Glob. Chang. Biol.* **1995**, *1*, 77-91. DOI: 10.1111/j.1365-2486.1995.tb00008.x

25. Byrne, M. P.; Tobin, J. T.; Forrestal, P. J.; Danaher, M.; Nkwonta, C. G.; Richards, K.; Cummins, E.; Hogan, S. A.; O'Callaghan, T. F. Urease and Nitrification Inhibitors—As

Mitigation Tools for Greenhouse Gas Emissions in Sustainable Dairy Systems: A Review. *Sustainability* **2020**, *12*, 6018.

26. Kondrat'eva, T. F.; Pivovarova, T. A.; Tsaplina, I. A.; Fomchenko, N. V.; Zhuravleva, A. E.; Murav'ev, M. I.; Melamud, V. S.; Bulayev, A. G. Diversity of the Communities of Acidophilic Chemolithotrophic Microorganisms in Natural and Technogenic Ecosystems. *Microbiology* **2012**, *81*, 1-24. DOI: 10.1134/S0026261712010080

27. Kowalchuk, G. A.; Stephen, J. R. Ammonia-Oxidizing Bacteria: A Model for Molecular Microbial Ecology. *Ann. Rev. Microb.* **2001**, *55*, 485-529. DOI: 10.1146/annurev.micro.55.1.485

28. Bachmeier, K. L.; Williams, A. E.; Warmington, J. R.; Bang, S. S. Urease Activity in Microbiologically-Induced Calcite Precipitation. *J. Biotech.* **2002**, *93*, 171-181. DOI: 10.1016/S0168-1656(01)00393-5

29. Lieberman, R. L.; Rosenzweig, A. C. Crystal structure of a membrane-bound metalloenzyme that catalyses the biological oxidation of methane. *Nature* **2005**, *434*, 177-182. DOI: 10.1038/nature03311

30. Gonzalez-Martinez, A.; Rodriguez-Sanchez, A.; van Loosdrecht, M. C. M.; Gonzalez-Lopez, J.; Vahala, R. Detection of Comammox Bacteria in Full-Scale Wastewater treatment Bioreactors Using Tag-454-Pyrosequencing. *Environ. Sci. Pollut. Res.* **2016**, *23*, 25501-25511. DOI: 10.1007/s11356-016-7914-4

31. Xu, L.; Chen, H.; Xu, J.; Yang, J.; Li, X.; Liu, M.; Jiao, J.; Hu, F.; Li, H. Nitrogen Transformation and Plant Growth in Response to Different Urea-Application Methods and the Addition of DMPP. *J. Plant. Nutr. Soil Sci.* **2014**, *177*, 271-277. DOI: 10.1002/jpln.201100390

32. Ravishankara, A. R.; Daniel, J. S.; Portmann, R. W. Nitrous Oxide (N_2O): The Dominant Ozone-Depleting Substance Emitted in the 21st Century. *Science* **2009**, *326*, 123-125. DOI: 10.1126/science.1176985

33. Chen, H.; Yin, C.; Fan, X.; Ye, M.; Peng, H.; Li, T.; Zhao, Y.; Wakelin, S. A.; Chu, G.; Liang, Y. Reduction of N_2O Emission by Biochar and/or 3,4-Dimethylpyrazole Phosphate (DMPP) is Closely Linked to Soil Ammonia Oxidizing Bacteria and nosZI-N_2O Reducer Populations. *Sci. Total Environ.* **2019**, *694*, 133658. DOI: 10.1016/j.scitotenv.2019.133658

34. Arp, D. J.; Stein, L. Y. Metabolism of Inorganic N Compounds by Ammonia-Oxidizing Bacteria. *Crit. Rev. Biochem. Mol. Biol.* **2003**, *38*, 471-495. DOI: 10.1080/10409230390267446

35. Utåker, J. B.; Bakken, L.; Jiang, Q. Q.; Nes, I. F. Phylogenetic Analysis of Seven New Isolates of Ammonia-Oxidizing Bacteria Based on 16S rRNA Gene Sequences. *Syst. Appl. Microbiol.* **1995**, *18*, 549-559. DOI: 10.1016/S0723-2020(11)80415-7

36. Schmidt, E. L.; Belser, L. W. Autotrophic Nitrifying Bacteria. In: *Meth. Soil An.* **1994**, pp 159-177. DOI 10.2136/sssabookser5.2.c10

37. Di, H. J.; Cameron, K. C.; Shen, J. P.; Winefield, C. S.; O'Callaghan, M.; Bowatte, S.; He, J. Z. Nitrification Driven by Bacteria and Not Archaea in Nitrogen-rich Grassland Soils. *Nature Geoscience* **2009**, *2*, 621-624. DOI: 10.1038/ngeo613

38. Wang, F.; Liang, X.; Ma, S.; Liu, L.; Wang, J. Ammonia-oxidizing Archaea are Dominant Over Comammox in Soil Nitrification under Long-Term Nitrogen Fertilization. *J. Soil Sed.* **2021**, *21*, 1800-1814. DOI: 10.1007/s11368-021-02897-z

39. Ensign, S. A.; Hyman, M. R.; Arp, D. J. *In vitro* Activation of Ammonia Monooxygenase from Nitrosomonas europaea by Copper. *J. Bacteriol.* **1993**, *175*, 1971-1980. DOI: 10.1128/jb.175.7.1971-1980.1993

40. Juliette, L. Y.; Hyman, M. R.; Arp, D. J. Inhibition of Ammonia Oxidation in Nitrosomonas europaea by Sulfur Compounds: Thioethers Are Oxidized to Sulfoxides by Ammonia Monooxygenase. *Appl. Environ. Microbiol.* **1993**, *59*, 3718-3727. DOI: 10.1128/aem.59.11.3718-3727.1993

41. Keener, W. K.; Arp, D. J. Transformations of Aromatic Compounds by *Nitrosomonas europaea*. *Appl. Environ. Microbiol.* **1994**, *60*, 1914-1920. DOI: 10.1128/aem.60.6.1914-1920.1994

42. Sayavedra-Soto, L. A.; Hommes, N. G.; Alzerreca, J. J.; Arp, D. J.; Norton, J. M.; Klotz, M. G. Transcription of the *amo*C, *amo*A and *amo*B Genes in *Nitrosomonas europaea* and *Nitrosospira sp.* NpAV. *FEMS Microbiol. Lett.* **1998**, *167*, 81-88. DOI: 10.1016/S0378-1097(98)00367-X

43. Vajrala, N.; Martens-Habbena, W.; Sayavedra-Soto, L. A.; Schauer, A.; Bottomley, P. J.; Stahl, D. A.; Arp, D. J. Hydroxylamine as an Intermediate in Ammonia Oxidation by Globally Abundant Marine Archaea. *Proc. Natl. Acad. Sci.* **2013**, *110*, 1006-1011. DOI: 10.1073/pnas.1214272110

44. McTavish, H.; Fuchs, J. A.; Hooper, A. B. Sequence of the Gene Coding for Ammonia Monooxygenase in Nitrosomonas europaea. *J. Bacteriol.* **1993**, *175*, 2436. DOI: 10.1128/jb.175.8.2436-2444.1993

45. Norton, J. M.; Alzerreca, J. J.; Suwa, Y.; Klotz, M. G. Diversity of Ammonia Monooxygenase Operon in Autotrophic Ammonia-Oxidizing Bacteria. *Arch. Microbiol.* **2002**, *177*, 139-149. DOI: 10.1007/s00203-001-0369-z

46. Hyman, M. R.; Wood, P. M. Suicidal Inactivation and Labelling of Ammonia Monooxygenase by Acetylene. *Biochem. J.* **1985**, *227*, 719-725. DOI: 10.1042/bj2270719

47. Wright, C. L.; Schatteman, A.; Crombie, A. T.; Murrell, J. C.; Lehtovirta-Morley, L. E.; Stams, A. J. M. Inhibition of Ammonia Monooxygenase from Ammonia-Oxidizing Archaea by Linear and Aromatic Alkynes. *Appl. Environ. Microbiol.* **2020**, *86*, e02388-02319. DOI: doi:10.1128/AEM.02388-19

48. Hooper, A. B.; Vannelli, T.; Bergmann, D. J.; Arciero, D. M. Enzymology of the Oxidation of Ammonia to Nitrite by Bacteria. *Antonie Van Leeuwenhoek* **1997**, *71*, 59-67. DOI: 10.1023/A:1000133919203

49. Fisher, O. S.; Kenney, G. E.; Ross, M. O.; Ro, S. Y.; Lemma, B. E.; Batelu, S.; Thomas, P. M.; Sosnowski, V. C.; DeHart, C. J.; Kelleher, N. L.; et al. Characterization of a Long Overlooked Copper Protein From Methane- and Ammonia-Oxidizing Bacteria. *Nat. Commun.* **2018**, *9*, 4276. DOI: 10.1038/s41467-018-06681-5

50. Christopher, A. F.; Kathryn, J. R.; Beman, J. M.; Alyson, E. S.; Brian, B. O. Ubiquity and Diversity of Ammonia-Oxidizing Archaea in Water Columns and Sediments of the Ocean. *Proc. Natl. Acad. Sci. U. S. A.* **2005**, *102*, 14683-14688.

51. Lawton, T. J.; Ham, J.; Sun, T.; Rosenzweig, A. C. Structural Conservation of the B Subunit in the Ammonia Monooxygenase/Particulate Methane Monooxygenase Superfamily. *Proteins* **2014**, *82*, 2263-2267. DOI: 10.1002/prot.24535

52. Hodgskiss, L. H.; Melcher, M.; Kerou, M.; Chen, W.; Ponce-Toledo, R. I.; Savvides, S. N.; Wienkoop, S.; Hartl, M.; Schleper, C. Unexpected Complexity of the Ammonia Monooxygenase in Archaea. *ISME J.* **2023**. DOI: 10.1038/s41396-023-01367-3

53. Rasche, M. E.; Hyman, M. R.; Arp, D. J. Factors Limiting Aliphatic Chlorocarbon Degradation by Nitrosomonas europaea: Cometabolic Inactivation of Ammonia Monooxygenase and Substrate Specificity. *Appl. Environ. Microbiol.* **1991**, *57*, 2986. DOI: 10.1128/jb.172.9.5368-5373.1990

54. Bédard, C.; Knowles, R. Physiology, Biochemistry, and Specific Inhibitors of CH_4, NH_4^+, and CO Oxidation by Methanotrophs and Nitrifiers. *Microbiol. Rev.* **1989**, *53*, 68-84. DOI: 10.1128/mr.53.1.68-84.1989

55. Hyman, M. R.; Sansome-Smith, A. W.; Shears, J. H.; Wood, P. M. A Kinetic Study of Benzene Oxidation to Phenol By Whole Cells of Nitrosomonas europaea and Evidence For The Further Oxidation of Phenol to Hydroquinone. *Arch. Microbiol.* **1985**, *143*, 302-306. DOI: 10.1007/BF00411254

56. Hyman, M. R.; Russell, S. A.; Ely, R. L.; Williamson, K. J.; Arp, D. J. Inhibition, Inactivation, and Recovery of Ammonia-oxidizing Activity in Cometabolism of Trichloroethylene by Nitrosomonas europaea. *Appl. Environ. Microbiol.* **1995**, *61*, 1480-1487.

57. Ward, B. B.; Courtney, K. J.; Langenheim, J. H. Inhibition of Nitrosomonas Europaea by Monoterpenes from Coastal Redwood (Sequoia sempervirens) in Whole-Cell Studies. *J. Chem. Ecol.* **1997**, *23*, 2583-2598. DOI: 10.1023/B:JOEC.0000006668.48855.b7

58. Lieberman, R. L.; Rosenzweig, A. C. The quest for the particulate methane monooxygenase active site. *Dalton Transactions* **2005**, 3390-3396. DOI: 10.1039/B506651D

59. Holmes, A. J.; Costello, A.; Lidstrom, M. E.; Murrell, J. C. Evidence that Particulate Methane Monooxygenase and Ammonia Monooxygenase May Be Evolutionarily Related. *Microbiol. Lett.* **1995**, *132*, 203-208. DOI: 10.1016/0378-1097(95)00311-R

60. Carlsen, H. N.; Joergensen, L.; Degn, H. Inhibition by ammonia of methane utilization in Methylococcus capsulatus (Bath). *Appl. Microbiol. Biotechnol.* **1991**, *35*, 124-127. DOI: 10.1007/BF00180649

61. Cao, L.; Caldararu, O.; Rosenzweig, A. C.; Ryde, U. Quantum Refinement Does Not Support Dinuclear Copper Sites in Crystal Structures of Particulate Methane Monooxygenase. *Angew. Chem. Int. Ed.* **2018**, *57*, 162-166. DOI: 10.1002/anie.201708977

62. Hooper, A. B.; Terry, K. R. Specific Inhibitors of Ammonia Oxidation in Nitrosomonas *J. Bacteriol.* **1973**, *115*, 480-485. DOI: 10.1128/jb.115.2.480-485.1973

63. Subbarao, G. V.; Ishikawa, T.; Ito, O.; Nakahara, K.; Wang, H. Y.; Berry, W. L. A Bioluminescence Assay to Detect Nitrification Inhibitors Released From Plant Roots: A Case Study with Brachiaria humidicola. *Plant Soil* **2006**, *288*, 101-112. DOI: 10.1007/s11104-006-9094-3

64. Subbarao, G. V.; Nakahara, K.; Ishikawa, T.; Ono, H.; Yoshida, M.; Yoshihashi, T.; Zhu, Y.; Zakir, H. A. K. M.; Deshpande, S. P.; Hash, C. T.; et al. Biological nitrification inhibition (BNI) activity in sorghum and its characterization. *Plant and Soil* **2013**, *366*, 243-259. DOI: 10.1007/s11104-012-1419-9

65. O'Sullivan, C. A.; Duncan, E. G.; Whisson, K.; Treble, K.; Ward, P. R.; Roper, M. M. A Colourimetric Microplate Assay for Simple, High Throughput Assessment of Synthetic and Biological Nitrification Inhibitors. *Plant Soil* **2017**, *413*, 275-287. DOI: 10.1007/s11104-016-3100-1

66. Coskun, D.; Britto, D. T.; Shi, W.; Kronzucker, H. J. How Plant Root Exudates Shape the Nitrogen Cycle. *Trends Plant Sci.* **2017**, *22*, 661-673. DOI: 10.1016/j.tplants.2017.05.004

67. Alam, P.; Parvez, M. K.; Arbab, A. H.; Siddiqui, N. A.; Al-Dosary, M. S.; Al-Rehaily, A. J.; Ahmed, S.; Kalam, M. A.; Ahmad, M. S. Inter-Species Comparative Antioxidant Assay and HPTLC Analysis of Sakuranetin in the Chloroform and Ethanol Extracts of Aerial Parts of Rhus Retinorrhoea and Rhus Tripartita. *Pharm. Biol.* **2017**, *55*, 1450-1457. DOI: 10.1080/13880209.2017.1304428

68. Kodama, O.; Miyakawa, J.; Akatsuka, T.; Kiyosawa, S. Sakuranetin, a Flavanone Phytoalexin from Ultraviolet-Irradiated Rice Leaves. *PhytoChem.* **1992**, *31*, 3807-3809. DOI: 10.1016/S0031-9422(00)97532-0

69. Zhu, Y.; Zeng, H.; Shen, Q.; Ishikawa, T.; Subbarao, G. V. Interplay Among NH_4^+ Uptake, Rhizosphere pH and Plasma Membrane H^+-ATPase Determine the Release of BNIs in Sorghum Roots – Possible Mechanisms and Underlying Hypothesis. *Plant Soil* **2012**, *358*, 131-141. DOI: 10.1007/s11104-012-1151-5

70. Li, S.; Yufang, L.; Fangwei, Y.; Herbert, J. K.; Weiming, S. Biological Nitrification Inhibition by Rice Root Exudates and its Relationship with Nitrogen-Use Efficiency. *New Phytol.* **2016**, *212*, 646-656. DOI: 10.1111/nph.14057

71. Nozari, M.; Addison, A. W.; Reeves, G. T.; Zeller, M.; Jasinski, J. P.; Kaur, M.; Gilbert, J. G.; Hamilton, C. R.; Popovitch, J. M.; Wolf, L. M.; et al. New Pyrazole- and Benzimidazole-derived Ligand Systems. *J. Heterocycl. Chem.* **2018**, *55*, 1291-1307. DOI: 10.1002/jhet.3155

72. Lucchini, J. J.; Corre, J.; Cremieux, A. Antibacterial Activity of Phenolic Compounds and Aromatic Alcohols. *Res. Microbiol.* **1990**, *141*, 499-510. DOI: 10.1016/0923-2508(90)90075-2

73. Zerulla, W.; Barth, T.; Dressel, J.; Erhardt, K.; Horchler von Locquenghien, K.; Pasda, G.; Rädle, M.; Wissemeier, A. 3,4-Dimethylpyrazole Phosphate (DMPP) – A New Nitrification Inhibitor For Agriculture and Horticulture. *Biol. Fertil. Soils* **2001**, *34*, 79-84. DOI: 10.1007/s003740100380

74. Vannelli, T.; Hooper, A. B. Oxidation of Nitrapyrin to 6-Chloropicolinic Acid by the Ammonia-Oxidizing Bacterium Nitrosomonas europaea. *Appl. Environ. Microbiol.* **1992**, *58*, 2321-2325. DOI: 10.1128/aem.58.7.2321-2325.1992

75. Woodward, E. E.; Kolpin, D. W.; Zheng, W.; Holm, N. L.; Meppelink, S. M.; Terrio, P. J.; Hladik, M. L. Fate and Transport of Nitrapyrin in Agroecosystems: Occurrence in Agricultural Soils, Subsurface Drains, and Receiving Streams in the Midwestern US. *Sci. Total Environ.* **2019**, *650*, 2830-2841. DOI: 10.1016/j.scitotenv.2018.09.387

76. Shin, Y.-g. K.; Szalda, D. J.; Brunschwig, B. S.; Creutz, C.; Sutin, N. Electronic and Molecular Structures of Pentaammineruthenium Pyridine and Benzonitrile Complexes as a Function of Oxidation State. *Inorg. Chem.* **1997**, *36*, 3190-3197. DOI: 10.1021/ic9700967

77. Long, G. J.; Clarke, P. J. Crystal and Molecular Structures of Trans-Tetrakis(pyridine)Dichloroiron(II), -Nickel(II), and -Cobalt(II) and Trans-Tetrakis(pyridine)Dichloroiron(II) Monohydrate. *Inorg. Chem.* **1978**, *17*, 1394-1401. DOI: 10.1021/ic50184a002

78. Edema, J. J. H.; Stauthamer, W.; Van Bolhuis, F.; Gambarotta, S.; Smeets, W. J. J.; Spek, A. L. Novel Vanadium(II) Amine Complexes: A Facile Entry in the Chemistry of Divalent Vanadium. Synthesis and Characterization of Mononuclear L4VCl2 [L = Amine, Pyridine]: X-Ray Structures of Trans-(TMEDA)2VCl2 [TMEDA = N,N,N',N'-Tetramethylethylenediamine] and Trans-Mz2V(py)2 [Mz = o-C6H4CH2N(CH3)2, py = Pyridine]. *Inorg. Chem.* **1990**, *29*, 1302-1306. DOI: 10.1021/ic00332a003

79. Casali, L.; Feiler, T.; Heilmann, M.; Braga, D.; Emmerling, F.; Grepioni, F. Too Much Water? Not Enough? In Situ Monitoring of the Mechanochemical Reaction of Copper Salts with Dicyandiamide. *CrystEngComm* **2022**, *24*, 1292-1298. DOI: 10.1039/D1CE01670A

80. Corrochano-Monsalve, M.; González-Murua, C.; Bozal-Leorri, A.; Lezama, L.; Artetxe, B. Mechanism of Action of Nitrification Inhibitors Based on Dimethylpyrazole: A Matter of Chelation. *Sci. Total Environ.* **2021**, *752*, 141885. DOI: 10.1016/j.scitotenv.2020.141885

81. Koci, J.; Nelson, P. N. Tropical Dairy Pasture Yield and Nitrogen Cycling: Effect of Urea Application Rate and A Nitrification Inhibitor, DMPP. *Crop Pasture Sci.* **2016**, *67*, 766-779. DOI: 10.1071/CP15400

82. Dougherty, W. J.; Collins, D.; Van Zwieten, L.; Rowlings, D. W. Nitrification (DMPP) and Urease (NBPT) Inhibitors Had No Effect on Pasture Yield, Nitrous Oxide Emissions, or Nitrate

Leaching under Irrigation in a Hot-Dry Climate. *Soil Res.* **2016**, *54*, 675-683. DOI: 10.1071/SR15330

83. Wilson, M. The Importance of Parent Material in Soil Classification: A Review in a Historical Context. *Catena* **2019**, *182*, 104131.

84. Pasda, G.; Hähndel, R.; Zerulla, W. Effect of Fertilizers With the New Nitrification Inhibitor DMPP (3,4-Dimethylpyrazole phosphate) on Yield and Quality of Agricultural and Horticultural Crops. *Biol. Fertil. Soils* **2001**, *34*, 85-97. DOI: 10.1007/s003740100381

85. Barrena, I.; Menéndez, S.; Correa-Galeote, D.; Vega-Mas, I.; Bedmar, E. J.; González-Murua, C.; Estavillo, J. M. Soil Water Content Modulates the Effect of the Nitrification Inhibitor 3,4-Dimethylpyrazole phosphate (DMPP) on Nitrifying and Denitrifying Bacteria. *Geoderma* **2017**, *303*, 1-8. DOI: 10.1016/j.geoderma.2017.04.022

86. Li, H.; Liang, X.; Chen, Y.; Lian, Y.; Tian, G.; Ni, W. Effect of Nitrification Inhibitor DMPP on Nitrogen Leaching, Nitrifying Organisms, and Enzyme Activities in a Rice-Oilseed Rape Cropping System. *J. Environ. Sci.* **2008**, *20*, 149-155. DOI: 10.1016/S1001-0742(08)60023-6

87. Menéndez, S.; Merino, P.; Pinto, M.; González-Murua, C.; Estavillo, J. M. 3,4-Dimethylpyrazol Phosphate Effect on Nitrous Oxide, Nitric Oxide, Ammonia, and Carbon Dioxide Emissions from Grasslands. *J. Environ. Qual.* **2006**, *35*, 973-981. DOI: 10.2134/jeq2005.0320

88. Menéndez, S.; Barrena, I.; Setien, I.; González-Murua, C.; Estavillo, J. M. Efficiency of Nitrification Inhibitor DMPP to Reduce Nitrous Oxide Emissions Under Different Temperature and Moisture Conditions. *Soil Biol. Biochem.* **2012**, *53*, 82-89. DOI: 10.1016/j.soilbio.2012.04.026

89. Nauer, P. A.; Fest, B. J.; Visser, L.; Arndt, S. K. On-farm Trial on the Effectiveness of the Nitrification Inhibitor DMPP Indicates No Benefits Under Commercial Australian Farming Practices. *Agric. Ecosyst. Environ.* **2018**, *253*, 82-89. DOI: 10.1016/j.agee.2017.10.022

90. Suter, H.; Lam, S. K.; Walker, C.; Chen, D. Benefits from Enhanced-Efficiency Nitrogen Fertilisers in Rainfed Temperate Pastures are Seasonally Driven. *Soil Res.* **2021**, -. DOI: 10.1071/SR21083

91. Yildirim, S. C.; Walker, R. M.; Roessner, U.; Wille, U. Assessing the Efficacy, Acute Toxicity, and Binding Modes of the Agricultural Nitrification Inhibitors 3,4-Dimethyl-1H-pyrazole (DMP) and Dicyandiamide (DCD) with Nitrosomonas europaea. *ACS Agric. Sci. Technol.* **2023**. DOI: 10.1021/acsagscitech.2c00303

92. Lin, X.; Hasi, W.-L.-J.; Lou, X.-T.; Han, S.-q.-g.-w.; Lin, D.-Y.; Lu, Z.-W. Direct and Quantitative Detection of Dicyandiamide (DCD) in Milk Using Surface-Enhanced Raman Spectroscopy. *Anal. Meth.* **2015**, *7*, 3869-3875. DOI: 10.1039/C5AY00313J

93. Wolt, J. D. A Meta-Evaluation of Nitrapyrin Agronomic and Environmental Effectiveness with Emphasis on Corn Production in the Midwestern USA. *Nutr. Cycling Agroecosyst.* **2004**, *69*, 23-41. DOI: 10.1023/B:FRES.0000025287.52565.99

94. Taggert, B. I.; Walker, C.; Chen, D.; Wille, U. Substituted 1, 2, 3-Triazoles: A New Class of Nitrification Inhibitors. *Sci. Rep.* **2021**, *11*, 1-12. DOI: 10.1038/s41598-021-94306-1

95. McCarty, G. W.; Bremner, J. M. Inhibition of nitrification in soil by heterocyclic nitrogen compounds. *Biol. Fertil. Soils* **1989**, *8*, 204-211. DOI: 10.1007/BF00266480

96. Sidhu, P. K.; Taggert, B. I.; Chen, D.; Wille, U. Degradation of the Nitrification Inhibitor 3,4-Dimethylpyrazole Phosphate in Soils: Indication of Chemical Pathways. *ACS Agricult. Sci. & Tech.* **2021**, *1*, 540-549. DOI: 10.1021/acsagscitech.1c00150

97. Hyman, M. R.; Murton, I. B.; Arp, D. J. Interaction of Ammonia Monooxygenase from *Nitrosomonas europaea* with Alkanes, Alkenes, and Alkynes. *Appl. Environ. Microbiol.* **1988**, *54*, 3187-3190. DOI: 10.1128/aem.54.12.3187-3190.1988

98. Clayden, J., Greeves, N., Warren, S. *Organic Chemistry*; Oxford University Press., 2012.

99. Hua, Y.; Flood, A. H. Click Chemistry Generates Privileged CH Hydrogen-Bonding Triazoles: The Latest Addition to Anion Supramolecular Chemistry. *Chem. Soc. Rev.* **2010**, *39*, 1262-1271. DOI: 10.1039/B818033B

100. Chai, H.; Guo, R.; Yin, W.; Cheng, L.; Liu, R.; Chu, C. One-Pot, Three-Component Reaction Using Modified Julia Reagents: A Facile Synthesis of 4,5-Disubstituted 1,2,3-(*NH*)-Triazoles in a Wet Organic Solvent. *ACS Comb. Sci.* **2015**, *17*, 147-151. DOI: 10.1021/co5001597

101. Hussein, W. M.; McGeary, R. P. Use of Ethyl (Benzothiazol-2-ylsulfonyl)acetate for Malonic Ester-type Syntheses of Carboxylic Acids and Ester. *Aust. J. Chem.* **2014**, *67*, 1222-1227. DOI: 10.1071/CH14085

102. Weiske, A.; Benckiser, G.; Ottow, J. C. G. Effect of the New Nitrification Inhibitor DMPP in Comparison to DCD on Nitrous Oxide (N_2O) Emissions and Methane (CH_4) Oxidation During 3 Years of Repeated Applications in Field Experiments. *Nutr. Cycling Agroecosyst.* **2001**, *60*, 57-64. DOI: 10.1023/A:1012669500547

103. Shi, X.; Hu, H.; He, J.; Chen, D.; Suter, H. C. Effects of 3,4-Dimethylpyrazole Phosphate (DMPP) on Nitrification and the Abundance and Community Composition of Soil Ammonia Oxidizers in Three Land Uses. *Biol. Fertil. Soils* **2016**, *52*, 927-939. DOI: 10.1007/s00374-016-1131-7

104. Ryden, J. C.; Skinner, J. H.; Nixon, D. J. Soil Core Incubation System for the Field Measurement of Denitrification Asing Acetylene-Inhibition. *Soil Biol. Biochem.* **1987**, *19*, 753-757. DOI: 10.1016/0038-0717(87)90059-9

105. Clark, P. R.; Williams, G. D.; Hayes, J. F.; Tomkinson, N. C. A Scalable Metal-, Azide-, and Halogen-Free Method for the Preparation of Triazoles. *Angewandte Chemie International Edition* **2020**, *59*, 6740-6744. DOI: 10.1002/anie.201915944

106. Kolb, H. C.; Finn, M. G.; Sharpless, K. B. Click Chemistry: Diverse Chemical Function from a Few Good Reactions. *Angew. Chem. Int. Ed.* **2001**, *40*, 2004-2021. DOI: 10.1002/1521-3773(20010601)

107. Kolb, H. C.; Sharpless, K. B. The Growing Impact of Click Chemistry On Drug Discovery. *Drug Discov.* **2003**, *8*, 1128-1137. DOI: 10.1016/S1359-6446(03)02933-7

108. Lontoh, S.; DiSpirito, A. A.; Krema, C. L.; Whittaker, M. R.; Hooper, A. B.; Semrau, J. D. Differential inhibition in vivo of ammonia monooxygenase, soluble methane monooxygenase and membrane-associated methane monooxygenase by phenylacetylene. *Environ. Microbiol.* **2000**, *2*, 485-494. DOI: 10.1046/j.1462-2920.2000.00130.x

109. Reichel, R.; Wei, J.; Islam, M. S.; Schmid, C.; Wissel, H.; Schröder, P.; Schloter, M.; Brüggemann, N. Potential of Wheat Straw, Spruce Sawdust, and Lignin as High Organic Carbon Soil Amendments to Improve Agricultural Nitrogen Retention Capacity: An Incubation Study. *Front. Plant Sci.* **2018**, *9*. DOI: 10.3389/fpls.2018.00900

110. Bourne, D. G.; McDonald, I. R.; Murrell, J. C. Comparison of *pmo*A PCR Primer Sets as Tools for Investigating Methanotroph Diversity in Three Danish Soils. *Appl. Environ. Microbiol.* **2001**, *67*, 3802-3809. DOI: 10.1128/AEM.67.9.3802-3809.2001

111. Costello, A. M.; Lidstrom, M. E. Molecular Characterization of Functional and Phylogenetic Genes from Natural Populations of Methanotrophs in Lake Sediments. *Appl. Environ. Microbiol.* **1999**, *65*, 5066-5074. DOI: 10.1128/AEM.65.11.5066-5074.1999

112. Maris, S. C.; Teira-Esmatges, M. R.; Arbonés, A.; Rufat, J. Effect of irrigation, nitrogen application, and a nitrification inhibitor on nitrous oxide, carbon dioxide and methane emissions from an olive (Olea europaea L.) orchard. *Sci. Total Environ.* **2015**, *538*, 966-978. DOI: 10.1016/j.scitotenv.2015.08.0

113. Christopher, A. F.; Kathryn, J. R.; Beman, J. M.; Alyson, E. S.; Brian, B. O. Ubiquity and Diversity of Ammonia-Oxidizing Archaea in Water Columns and Sediments of the Ocean. *Proc. Natl. Acad. Sci.* **2005**, *102*, 14683-14688.

114. Wu, G.-L.; Wu, Q.-P. Metal-Free Multicomponent Reaction for Synthesis of 4,5-Disubstituted 1,2,3-(*NH*)-Triazoles. *Adv. Synth. Catal.* **2018**, *360*, 1949-1953. DOI: 10.1002/adsc.201701587

115. Cheng, D. O.; Bowman, T. L.; Legoff, E. Synthesis and Michael Reaction of 3,4-Dimethylpyrrole. *J. Heterocycl. Chem.* **1976**, *13*, 1145-1147. DOI: 10.1002/jhet.5570130549

116. Hu, L.; Mück-Lichtenfeld, C.; Wang, T.; He, G.; Gao, M.; Zhao, J. Reaction between Azidyl Radicals and Alkynes: A Straightforward Approach to *NH*-1,2,3-Triazoles. *Chem. Eur. J.* **2016**, *22*, 911-915. DOI: 10.1002/chem.201504515

117. Nakagawa, Y.; Nakayama, N.; Goto, H.; Fujisawa, I.; Chanthamath, S.; Shibatomi, K.; Iwasa, S. Computational Chemical Analysis of Ru(II)-Pheox–Catalyzed Highly Enantioselective Intramolecular Cyclopropanation Reactions. *Chirality* **2019**, *31*, 52-61. DOI: 10.1002/chir.23033

118. Clarke, A. K.; Lynam, J. M.; Taylor, R. J. K.; Unsworth, W. P. “Back-to-Front” Indole Synthesis Using Silver(I) Catalysis: Unexpected C-3 Pyrrole Activation Mode Supported by DFT. *ACS Catalysis* **2018**, *8*, 6844-6850. DOI: 10.1021/acscatal.8b00745

119. Hou, Y.; Higashiya, S.; Fuchigami, T. Electrolytic Partial Fluorination of Organic Compounds. 24.1 Highly Regioselective Anodic Monofluorination of 2-Benzothiazolyl and 5-Chloro-2-benzothiazolyl Sulfides. *The Journal of Organic Chemistry* **1997**, *62*, 9173-9176. DOI: 10.1021/jo971293q

120. Fu, D.-J.; Li, P.; Wu, B.-W.; Cui, X.-X.; Zhao, C.-B.; Zhang, S.-Y. Molecular Diversity of Trimethoxyphenyl-1,2,3-triazole Hybrids as Novel Colchicine Site Tubulin Polymerization Inhibitors. *Eur. J. Med. Chem.* **2019**, *165*, 309-322. DOI: 10.1016/j.ejmech.2019.01.033